From conception to interpretation; a new angle on smart tags for reef inhabitants

Lloyd William Hopkins

Submitted to Swansea University in fulfilment of the requirements for the Degree of Doctor of Philosophy in Biological Sciences.

Department of Biosciences

Swansea University

2021

Abstract

Length and direction are the two parameters that define animal movement, from the scale of the limbs to whole-body animal navigation through their environment. However, although step lengths have been considered widely, the effect of angles is rarely documented. This thesis considers some of the ways in which directionality operates to define processes within marine communities, particularly reef-based inhabitants, using animal-attached technology. Rapid improvements in device power, size and utility has led to ubiquitous use of such technology in animal movement and behaviour research. Working within a setting of a proposed multi-species, mass tagging effort of a Red Sea coral reef's inhabitants, this thesis works within the context of angles to evaluate the inherent challenges and areas of opportunities in studying both less- and more-mobile species. It begins by describing a novel system for attaching tags to the dorsal fin of elasmobranchs using a magnetic clip. The angles between the clip halves, as well as between fin and clip, determine the external forces applied to the system and, therefore, the ability of the clip to remain on the animal without causing injury. Despite significant progress in development, there is some way to go to finalise the system. In the second chapter the clip, equipped with a tri-axial accelerometer, was deployed on various captive shark species to investigate the behavioural implications of attachment. Negative reactions to attachment were most notable in whole-body roll angle, due to fleeting chafing behaviours, a reaction that would otherwise be missed by other common, non-angular, tag-derived measures. The thesis then examined the hypothesis that energy expenditure can be represented by rotational (and not necessarily dynamic) movements using invertebrates as a model. Static respirometry methods with spider conchs (*Lambis truncata*) showed this was valid, with important implications for our ability to quantify the energy expenditure of free-living, slow-moving animals. The next chapter found that spider conchs, despite being ostensibly relatively simplistic movers, have probabilistic movement rules, including in terms of directionality, predicted by previous movement as well as the ambient environment. Finally, gape angles of free-living giant clams (*Tridacna maxima*) on a Red Sea coral reef were used to infer the effect of anthropogenic noise on their behaviour, suggesting that post-tagging recovery was hindered by boat passes.

Declarations and statements

DECLARATION

This work has not previously been accepted in substance for any degree and is not being concurrently submitted in candidature for any degree.

Signed [redacted] (candidate)

Date **14/03/2021**

STATEMENT 1

This thesis is the result of my own investigations, except where otherwise stated. Where correction services have been used, the extent and nature of the correction is clearly marked in a footnote(s).

Other sources are acknowledged by footnotes giving explicit references. A bibliography is appended.

Signed [redacted] (candidate)

Date **14/03/2021**

STATEMENT 2

I hereby give consent for my thesis, if accepted, to be available for photocopying and for inter-library loan, and for the title and summary to be made available to outside organisations.

Signed [redacted] (candidate)

Date **14/03/2021**

Table of Contents

Ethics statement and approvals

All work described in this thesis was approved by the Swansea University Ethics Committee (references beginning with 'SU'). Experiments conducted in Chapters 2 and 3, where concerning animals in an aquarium, were approved by the Fundacion Oceanografic Animal Care & Welfare Committee (references beginning 'OCE').

The relevant approvals for each chapter are detailed in the table below.

Chapter	Relevant ethics approval number(s)	Notes
2	SU-Ethics-Student-050118/354	Approval for tag deployments on *Rhincodon typus* in the Maldives
	SU-Ethics-Student-250118/459	Approval for the first deployments in Oceanografic aquarium (2018).
	SU-Ethics-Student-070819/1830	Approval for the second deployments in Oceanografic aquarium (2020).
	OCE-11-19	Approval for the second deployments in Oceanografic aquarium (2020).
3	SU-Ethics-Student-070819/1830	Approval for the second deployments in Oceanografic aquarium (2020).
	OCE-11-19	Approval for the second deployments in Oceanografic aquarium (2020).
4	SU-Ethics-Student-220119/1248	Approval for tag deployments on *Lambis truncata* in a laboratory/aquarium environment.
5	SU-Ethics-Student-220119/1248	Approval for tag deployments on *Lambis truncata* in the Red Sea.
6	SU-Ethics-Student-150120/2413	Approval for tag deployments on *Tridacna maxima* in the Red Sea.

List of figures and tables

Acknowledgements

I count myself very lucky that I have had the wealth of opportunities that I have had in the course of my PhD. In this, I cannot thank Prof. Rory Wilson enough for being an outstanding supervisor and mentor. His relentless optimism, calmness in the face of just about everything and boundless wisdom – even when fighting through an illness that would have, understandably, floored anybody else – has gotten me through this PhD breakdown-free. Thank you for taking a chance on me.

Thanks also to Luca Borger and Emily Shepard for your valuable input and, along with Rory, making the SLAM lab a lovely, exciting, enjoyable place to be and work in. Luca also stepped up to fill in as my primary supervisor for a time and I am incredibly grateful for his huge efforts in doing so. Whilst on the subject of the SLAM lab – what a group! James (my partner in crime), Gwen, Hannah, Baptiste, Manos, Will, Holly, Ewan and to everyone else that I've had the pleasure to work alongside and know in Swansea – you're all excellent, excellent people. I look forward to making up for lost pub time post-lockdowns.

To my research partners: Thank you to everyone at KAUST and the Sensor Initiative that I was privileged to get to know, work with and learn from. I sincerely hope that I will continue to have the opportunity to do so. Thank you to the staff at Oceanografic aquarium for their hospitality, relentless hard work and generosity in facilitating my research. Thank you to Brad Norman for hosting me on several eye-opening, once-in-a-lifetime (or, hopefully, not) field trips.

Bryony - thanks for being so, so patient and supportive of me during my weekend panics and late evening writing sessions. I'm looking forward to taking more time over our dog walks.

Last, but certainly not least – thank you to my parents, Jaynie and David, and sister, Siân, for always believing in me and being the reason that I got to where I am today. I will always be grateful.

Funding and Contributing authors

All work reported in this thesis was funded by the King Abdullah University of Science and Technology, Office for Sponsored Research, as part of the KAUST Sensor Initiative.

In addition to the candidate submitting this thesis, the following authors (with their institution; below) assisted in the research and data gathering presented in this thesis.

Name	Institution/Organisation	Chapter(s) contributed to
Rory P. Wilson	Swansea University	1-6
Carlos M. Duarte	KAUST	2-6
Nathan R. Geraldi	KAUST	4-6
Mark D. Holton	Swansea University	2-6
Brad M. Norman	ECOCEAN/ Murdoch University	2-3
Phil Hopkins	Swansea University	2-6
Samantha Reynolds	ECOCEAN/ The University of Queensland	2-3
Edward C. Pope	Swansea University	4
Simon Withers	Swansea University	2
Daniel G. Parraga	Fundacion Oceanografic	2-3
Miguel Lurgi	Swansea University	4
Michelle-Nicole Havlik	KAUST	6
Jerome Hubert	Leiden University	6
Leigh Gaffney	University of British Columbia	6
Lucille Chapuis	University of Exeter	6

List of Abbreviations

Abbreviation term	Full term
DBA	Dynamic Body Acceleration
VeDBA	Vectoral Dynamic Body Acceleration
RocRM	Rate of change of Rotational Movement
LMM	Linear Mixed Model
CLMM	Ordinal Logistic Mixed Model
MVS	Magnetic Vectoral Sum
M-clip	Magneto clip
FAA	Force Assessment Approach
DD	Daily Diary
TBF	Tail beat frequency

Chapter 1:

General Introduction

Angles and life

Living creatures occupy space whereby each individual can be defined as a complex volume made up by the spatial interactions of their various tissues about the 3 orthogonal axes of space (Haldane 1926, Mcmahon 1971, McMahon 1975, Schaeffer and Lindstedt 2013). Importantly, the juxtaposition of the elements that make up the (outside) surface matrix of their bodies is described by the angles between the facets that make up this surface (Fig. 1), which also have a tri-axial (orthogonal) basis (Hutchinson et al. 2008, Alexander 2011). Such angles are not always fixed however, with moving limbs, for example, being responsible for change (An et al. 1984, Hof 2001, Wilson and Liebsch 2003, Ren et al. 2008).

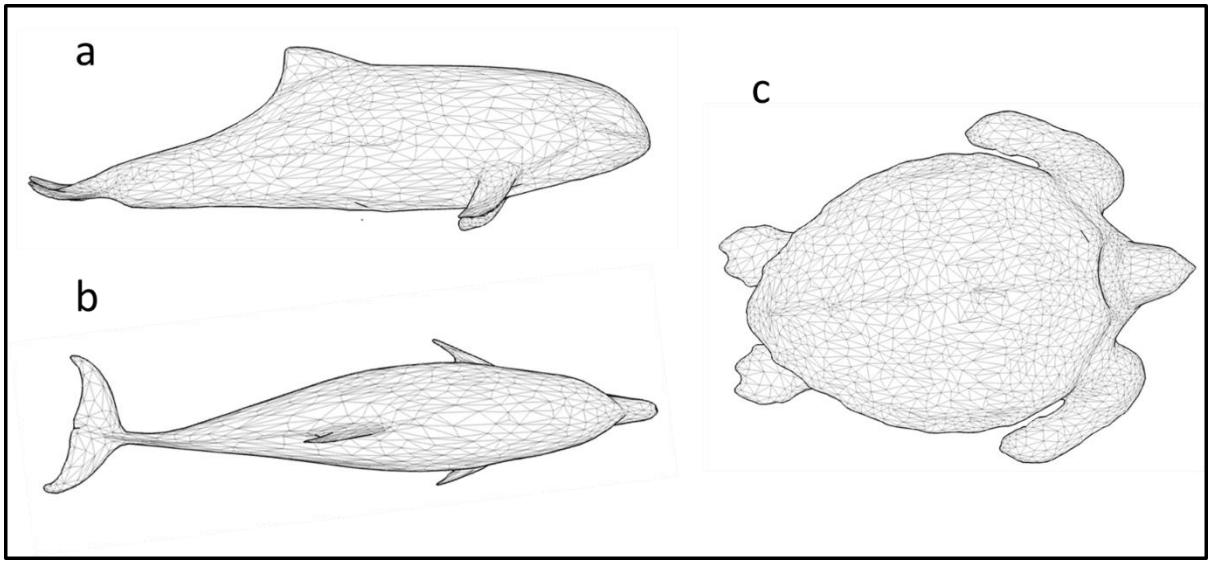

Figure 1.1: The surface area of animal bodies can be represented by facets, whose relative positions define the space occupied by the body. Pictured are triangular meshes, derived from photogrammetry scans taken with an Artec Eva 3D scanner (Artec 3D, Luxembourg) of: (a) a Dall's Porpoise (*Phocoenoides dalli*), from an artificial, to-scale model; (b) a Short-beaked common dolphin (*Delphinus delphis*), from a recently dead specimen; (c) a Loggerhead turtle (*Caretta caretta*), from a living, captive specimen. The scans were processed in Autodesk Fusion 360 software (Autodesk Ltd., Farnborough, UK) and the facet density of the mesh reduced from the raw scan to be more easily seen.

The changing angles between limb elements, such as between the humerus and the radius and ulna in the human arm during a 'bicep curl', not only reflect the changing positions of the tissue, but also the forces required to bring that about (Tözeren 2000, Alexander 2011, Fontana et al. 2018) (see Box 1). These forces are dependent on the angle between the humerus and the radius/ulna at any one time and the moment arms (the perpendicular distance between the muscle's direction of force and the rotational centre within the joint) in the system (Tözeren 2000).

Box 1: Consider a human bending an arm about the pivot point of an elbow, requiring the contraction of the biceps muscle. The changing of the angle (θ) between forearm and humerus depends on torque (τ), provided by the biceps, which varies depending on the range (radius, *r*) and force (*F*) of the movement according to the equation:

$$\tau = r \times F \times sin\theta \quad \textbf{(1)}$$

Accordingly, overall energy expenditure and power at any time also vary as that angle changes (Eisenberg and Hill 1985, Daniel and Tu 1999, Fontana et al. 2018). Such angular changes, and the inherent energetic consequences, are also the drivers behind whole animal body movement through space (displacement), whether it is driven by cilia or muscle contraction, and this feeds up into the diverse behavioural and ecological consequences of animal movement (Nathan et al. 2008). But as with the single limb, the angular velocity (see Box 2) and the angular extent of any turn of the whole animal body (in pitch, roll and yaw terms) profoundly affect energy expenditure (Wilson *et al.*, 2013; Crossley *et al.*, 2018). The instant that an animal adopts a turn angle, it changes its trajectory through the environment. This simple phenomenon, scaled up, has consequences that range from instantaneous energy

Box 2: We can relate changes in an angle between moving elements (and the force required to elicit that move) to speed. In our moving arm example from Box 1, the hand, the furthest point from the pivot point of the elbow, will move faster than the rest of the arm because it travels a greater distance in the same amount of time. The angular velocity (ω), however, will be the same at all points on the moving arm, given by:

$$\omega = \frac{d\theta}{dt} \quad \textbf{(2)}$$

where $d\theta$ is the angular change (i.e. the rotation of the forearm and hand in relation to the humerus) and dt is the length of time taken for the angular change to occur. However, the tangential acceleration, a_t, does change as a function of both angular velocity and distance from the pivot (r) according to:

$$a_t = \omega \times r \quad \textbf{(3)}$$

expenditure to changes in population distributions over time and space (Wilson *et al.*, 2013; Shepard *et al.*, 2013; Amélineau *et al.*, 2014).

All this serves to highlight that the concept of angles is fundamental to the form and functioning of living systems, ranging from defining the occupation of space by animals to their movement within that space, encompassing energy and power as it does so. Exploring the central role that angles have in movement, which has received little attention in the literature, should allow stripping back of a given species' movement and interactions across the body matrix-environment space to more logical, manageable mathematical rules that ground biological processes within physical systems.

Working with angles – a description of the chapters within this thesis

In carrying out my thesis, I 'stumbled' across angles. This thesis started out as an attempt to examine the behavioural ecology of reef inhabitants within the Red Sea, with broad themes being how reef animals moved through and above the reef matrix, and the extent to which this movement might be affected by man. Movement descriptors of course often invoke angles, even if they are only considered to be 'random' elements linking straight-line trajectories, such as in Brownian motion (Horne et al. 2007, Bearup et al. 2016) or Lévy flight (Raposo et al. 2009). However, at the outset I did not realise how angles were to become the major constant theme across chapters, really whether I wanted it or not. As such, as the work developed, I decided to embrace the topic so that, ultimately, the work has now become almost a tribute to angles in the life and function of (a very few of) the reef inhabitants at my main study site in the Red Sea. An overarching question might therefore be: 'How does consideration of angles affect our understanding of reef animals in a changing environment?'. The description of the chapters below will hopefully make the issue clear. What follows in this thesis is a

consideration of how angles, and angular changes, should be considered both in biologging and animal movement and behaviour research generally.

My first research chapter (Chapter 2 - A new approach to minimal impact tagging; the case of a shark fin clip) sought to design a new fin attachment system for smart tags (Ropert-Coudert and Wilson 2005, Wilson et al. 2008) to sharks. The evidence that many conventional (accepted) methods are deleterious is now quite compelling (Hammerschlag et al. 2011, Jewell et al. 2011). As a result, I set out to develop a new attachment system to minimize the detriment that is apparent in the literature. In conceiving this new system, the Magneto-clip (or M-clip), I immediately ran into having to deal with angles. In fact, a proper understanding of forces, angles and torque proved critical for development of the attachment system. I needed to consider the forces externally acting on the fin (e.g. lift, drag and lateral forces) and how these might interact with the attachment, which depends on inwards compression forces of the adherence system. This was theoretically straight-forward as far as physical considerations of forces were concerned. In practice, however, this proved more complex than I thought, due to the complicated inter-relatedness of internal and external (i.e. environmental) forces. Take the force of drag as an example. Whilst drag on the body or tag can be theoretically calculated (see Box 3), the resultant pressures on the fin are dependent on many other factors (such as surface area in contact with the fin). These factors, in turn, are dependent on the compressibility of the materials involved (from both the shark and the attachment mechanism), the frictional hold on the skin, and the internal driving force applied, among others. To facilitate the design process, I incorporated 3D scanning and design - underutilised techniques in biologging - to improve the device fit using a highly-accurate 3D shark fin model. 3D printing allowed rapid prototyping and device development, as well as easy and affordable access to a range of materials. Regular on-animal testing and behavioural observation allowed careful, iterative device testing in both captive and open-water environments, with the M-clip undergoing

carefully considered improvements between deployments. The result is a promising start point for a new elasmobranch attachment device.

Box 3: Animals are profoundly affected by the media through which they move (Biewener and Patek, 2018). The force of drag when moving through water can be of critical importance to aquatic animals and has important implications for bio-telemetry and biologging (Grusha and Patterson 2005, Kay et al. 2019). Devices producing excessive drag can harm the animal directly, such as through skin tearing, or indirectly, such as requiring additional energetic investment. In the case of the shark, the power required to swim (*W)* can be summarised as:

$$W = 0.5 \times C_d \times \rho \times v^3 \times A \quad \textbf{(4)}$$

where C_d is the coefficient of friction, ρ is the water density, v is the velocity and A is the cross-sectional surface area being directly acted upon. Essentially, increasing either surface area or the drag coefficient increases the effort needed for propulsion. This effect therefore increases disproportionately with speed.

Leading from this developmental process, I assessed the reactions to the tag by various shark species within a captive setting (Chapter 3 - On the benefits of captive settings for observing aberrant behaviours due to external tag attachment in sharks). I quantified these reactions using both direct behavioural observations, difficult to do in free-living conditions, and examination of movement data from the attached tag. I found that both methods helped form an understanding of the behavioural and movement consequences of the attachment. Particularly noticeable were full-body angular changes such as rolling of the body about the longitudinal

axis, indicating chafing behaviour as the sharks sought to remove the attachment. In contrast, more simplistic and 'traditional' metrics taken from the data, for example the frequency of tail beats or the vectoral summations of acceleration data, incorrectly suggesting normal behaviour. Such rolling behaviours were particularly well suited to spherical plots of movement data.

As discussed above, body angle changes (in whatever axis, or axes) come with an energetic cost. Although perhaps intuitive when considering larger, faster organisms, this also applies to animals that operate on a much slower scale. Working from this simple assertion, I sought to develop a novel metric for use as a proxy for energy expenditure in slow-moving animals (Chapter 4 - Testing angular velocity as a new metric for metabolic demands of slow-moving marine fauna: a case study with Giant spider conchs *Lambis truncata*). Whilst Dynamic Body Acceleration, or DBA (Wilson *et al.*, 2019), derived from accelerometer data, closely correlates with energetic expenditure in many species (Halsey and White 2010, Elliott et al. 2013, Lyons et al. 2013, Wright et al. 2014) and is therefore a widely-used proxy, it is less useful for species that produce negligible dynamic acceleration signals due to slower, comparatively minimal movement. This is particularly pertinent with regard to benthic marine species, comprising diverse taxa which generally move slowly and therefore exclude the use of DBA metrics. With 'simple' spider conchs I instead explored a new metric, Rate of Change of Rotational Movement (RocRM), which uses the rate of angular changes about each of the three movement axes (pitch, roll, yaw), as measured by accelerometers and magnetometers, within a static respirometry system. This metric was positively correlated with movement where DBA was not, suggesting it should be further tested with other slow-moving animal species.

I then continued with *L. truncata* and, more broadly, the exploration of angular considerations within slow-moving animals (Chapter 5 - Searching for simple rules in a 'simple' animal; movement of the Giant Spider Conch, *Lambis truncata*). Body angle changes are often indicative of turns in tortuous paths, with greater energetic cost than simple straight-line

movement (Wilson et al. 2013, Crossley et al. 2018). I examined activity patterns and the extent to which heading, the angle within the horizontal plane (Edelhoff et al. 2016, Williams et al. 2017), modulates the moving pattern within the context of conditional probability (the probability of an event's occurrence given the occurrence of a preceding event). I found that greater per-movement angle change in a conch's movement path resulted in a correspondingly larger heading change in the successive trajectory. Angular changes might therefore be thought of as integrated within basic rules of an animal's movement.

Thus far, I had applied basic physical concepts to the attachment of a tag to an animal, then to body postural changes, the costs of such postural changes and the ecological consequences of those changes (i.e. changing heading and tortuosity across a reef). Finally, using the giant clam *Tridacna maxima* as a study species, I sought to demonstrate the value of angles as a manifestation of an organism's response to anthropogenic disturbance and therefore the conservation value of such an approach (Chapter 6 - Using biologging to monitor the response of a free-living marine invertebrate to boat noise – a case study with the Maxima clam, *Tridacna maxima*). The shell closing of *T. maxima* was measured as a response to small boat noise in a free-living coral reef setting, with an apparent effect of boat noise on the habituation to the handling process.

Angular thinking

By linking these seemingly disparate studies together, I hope to have demonstrated the potential of considering angles in animal movement and behaviour research, particularly in the fields of bio-logging and biotelemetry where a suite of on-animal sensors are able to record angular changes with great accuracy. I have shown how consideration of angles at some level can lead to insights into questions of tag attachment in high-energy media. I have also considered how

visualisation tools can help highlight and understand tag dislodgement behaviour by looking at changes in animal body angles, have proposed a novel metric for proxies of energy usage in slow-moving animals based on angular change, and have used angles to predict movement in a benthic invertebrate and monitor the reaction of animals to human presence. The diversity of these studies – in methodology, study species and research question – has been enlightening, although conducting all of them simultaneously has been challenging and, as a result, some ideas have some way to go to become mature. Every one of them can almost certainly be taken to a more sophisticated level with further work. I would like to think, though, that this work might have catalysed others to think about the value of angles within their own study systems.

Chapter 2:

A new approach to minimal tagging;

the case of a shark fin clip

Abstract

Elasmobranch tagging commonly employs high-strength clamps or fin-drilling to overcome the difficulties of device attachment in a challenging marine environment. In doing so, these techniques may prioritise tag retention over possible impacts on animal welfare and behaviour. In theory, however, consideration of how externally acting forces, particularly drag, act in conjunction with internally acting tag forces (those acting to keep the tag on the animal) should inform design of a tag which is able to exert the minimal amount of force required for prolonged attachment. Guided by this Force Assessment Approach (FAA) and incorporating advanced manufacturing techniques such as 3D-printing and 3D-laser scanning of animal morphology, we have created the Magneto-clip, or M-clip. The M-clip is a dorsal-mounted attachment for elasmobranchs with a leading hinge and a pair of Neodymium-Iron-Boron magnets facilitating closing of the mechanism whilst serving as internal force-generators. The M-clip underwent an iterative design process, where four different versions were trialled across four sets of deployments – two in a captive setting and two in a free-living setting – on five shark species; the Bowmouth Guitarfish (*Rhina ancylostoma*), the Zebra Shark (*Stegostoma fasciatum*), the Nurse Shark (*Ginglymostoma cirratum*, the Blacktip Reef Shark (*Carcharhinus melanopterus*) and the Whale Shark (*Rhincodon typus*). The system was able to stay attached for several hours consistently and is therefore a promising tool for short-term deployments. However, further refinement of the design is required if long-term deployments are to be possible, with only one deployment in this study lasting at least twenty-four hours. Behavioural reactions to the tagging procedure appear minimal with some sharks returning to the tagging area immediately to resume feeding, although some aberrant behaviours, most notably in the form of tag dislodgement chafing, were recorded. The M-clip has so far shown promise as a minimally invasive, adaptable, and cheap method of tagging elasmobranchs.

1. Introduction

Logging and telemetry using animal-attached tags have allowed detailed insights into the behaviour and movements of free-living animals (e.g. Ropert-Coudert *et al.*, 2001; Myers and Hays, 2006; Liechti *et al.*, 2013; McClune *et al.*, 2014) and the environmental contexts around them (McMahon et al. 2005, Charrassin et al. 2008). However, the value of such tagging methods depends critically on minimal impact on the study animal because, aside from ethical issues (Wilson and McMahon, 2006; McMahon *et al.*, 2011; Field *et al.*, 2012), animals compromised by tags will behave in a manner different to their untagged conspecifics (Vandenabeele et al. 2011, Wilson et al. 2019). For this reason, a number of authors have considered the particular properties that tags should have to minimize deleterious effects on their carriers. These include cognizance of drag (Bannash *et al.* 1994), mass (Bowlin et al. 2010), colour (Wilson et al. 1989) and shape (Jones *et al.*, 2013), but also extend to the specifics of where, precisely, these tags should be placed on the body (e.g. Bannasch et al., 1994; Kay *et al.*, 2019). In this regard, solutions often represent a compromise because appropriate attachment sites do not always concur with minimal physical detriment (Tudorache et al. 2014).

A final element within the physical placement of tags on animals involves the suitability of the specific attachment mechanism. Researchers have advocated a suite of mechanisms depending on the species concerned, ranging from glue (Myers and Hays 2006, Hale et al. 2012) and tape (Wilson and Wilson 1989), through collars (Dickinson et al. 2020) and harnesses (Cliffe et al. 2014, Hoover et al. 2017) to skin- and muscle anchors (Gifford *et al.*, 2007; Baumgartner *et al.*, 2015) and implantation (White et al. 2013), each with its pros and cons.

We advocate that most physical detriment that animals incur from attached tags stems from the associated, additional forces (e.g. longitudinal forces such as drag, vertical forces relating to the mass/upthrust, and lateral forces, possibly due to imbalance, as well as forces that the tag-wearer might put on the system by attempting to remove the unit). In order to keep tags properly attached, such external forces have to be balanced by 'internal' forces that serve to keep the tag in place. It follows, therefore, that if tags (and their attachment systems) are conceived to minimize external forces, then the wearer will be subject to minimal internal forces and correspondingly minimal forces overall. All this should result in minimized physical detriment to the animal.

Consideration of the 'force assessment approach' (FAA) is documented here and highlighted in the particular case of a fin-attached clip for use in sharks. Sharks have been tagged for a number of years using a variety of approaches. These have included; device implantation (Feldheim et al. 2002), transdermal bolts through the dorsal musculature (Whitmore et al. 2016), the use of a dart and tow, such as in a Pop-up Satellite Archival Tag, or PSAT (Musyl, Brill, et al. 2011), and a dorsal fin-mounted stainless steel spring that drives inward forces via two metal arms (Gleiss et al. 2009, Chapple et al. 2015). Any and all methods of attachment are designed to accommodate particular sensors and study interests, therefore bringing some inherent limitations in their use. Bolts or pins through the dorsal musculature, for example, reduce the likelihood of premature release and can secure a device for long-term deployments and have a long history within cetacean research in particular (Irvine et al. 1982). However, they risk physical damage beyond that of the hole inflicted by the bolt, through tissue degradation and/or infection (Hammerschlag et al. 2011, Jewell et al. 2011). This can range from ostensibly no effect to harmful migration of the pins through the fin to the point of exit (Irvine et al. 1982, Heide-Jørgensen et al. 2017).

Towed tags do not require the physical recapture of the animal for device retrieval (Musyl, Domeier, et al. 2011, Neilson et al. 2014), but can have mixed effects on the drag and resultant metabolic demands placed on the animal according to the species and size (Grusha and Patterson 2005, Jepsen et al. 2015, Lynch et al. 2017). These methods do also require, however, bringing the animal out of the water for device attachment.

In developing a tool for shorter tagging durations with minimal handling time of the animal required (application using a long pole rather than bringing the animal out of the water), Gleiss *et al* (2009) describe a frontally located spring-driven clamp on the second dorsal fin of whale sharks, *Rhincodon typus*, using sharpened pins on caudally extending arms. This works for short periods (days) with appreciable success. This was followed by a modified design (Chapple et al. 2015) intended for faster-swimming shark species, using pads in place of pins. This clamp design again provides reliable attachment for several days (Chapple et al. 2015, Andrzejaczek et al. 2019) and the attachment procedure itself is near instantaneous (Chapple et al. 2015). Chapple *et al*'s (2015) clamp currently consists of a metal frame to generate the attachment force. Whilst clearly effective, such materials are nonetheless heavy (density of *ca.* 7900 $kg.m^{-3}$ vs. seawater density of 1030 $kg.m^{-3}$) without additional buoyancy aids. It additionally does not truly conform to the variability of fin dimensions, possibly inviting higher exerted pressures at the front *vs* the rear of the clamp due to the attrition of force resulting from torque effects with distance from the spring. We have sought to build upon this design in its material composition, profile and force generation method.

Generally, two considerations have driven the continued design and development of attachment methods for shark tagging; that the system remains securely on the individual for a given time, and that the system is 'minimally invasive'. For the most part, the former has taken precedence and set the parameters within which the latter is applied. Thus, the problem of large externally-acting forces is often dealt with by using large internal force-generating attachment systems

which, together, may produce unintended and unstable resultant actions and forces. Steel spring clamps, whilst highly effective and successfully used tools, are still some way from a hydrodynamic optimum. What's more, depending on the specific data requirements of a given deployment, they might be loaded with sensors in such a way as to invoke unequal lateral forces. This may result in tag displacement and/or meta-stability. By contrast, the behaviours and morphologies of many marine animals are specifically adapted to overcome external physical forces so as to optimize energy expenditure (Gleiss, Jorgensen, et al. 2011). It is reasonable, then, to seek to avoid altering the profile of subject animals away from a hydrodynamic optimum, reducing detriment to movement (Bouyoucos et al., 2017; Lear et al., 2018) and ensuring recorded data are truly representative of the animal's 'normal' state.

Whereas, previously, development of form-fitting attachment methods might be technically demanding or prohibitively expensive for many researchers, recent technological advancements have begun to break down the cost, accessibility and speed-of-production barriers. 3d imaging can produce ultra-high resolution meshes of an animal's morphology – which might be the entire animal or a single limb – that can be used as a model on which to base attachment designs (e.g. Seminati *et al.*, 2017). Combined with ever-cheaper 3d-printing options that include flexible plastics, including some that are biocompatible (Chia and Wu 2015, Baronio et al. 2016), there is a clear opportunity to modernize the tag design and prototyping process.

In this work, we describe the inception, development, deployment and evaluation of a new attachment method based on a magnetic clamp for shark-mounted archival devices and transmitters. This magneto-clip (M-clip) is a dorsally attached system which uses Neodymium-Iron-Boron (NdFeB) rare-earth magnets as force generators, a hydrodynamic, 3D-printed body and an anterior hinge with simple shaped silicone pads for frictional hold. M-clips were tested on 5 shark species: on the Nurse shark (*Ginglymostoma cirratum),* Zebra shark (*Stegostoma*

fasciatum), Blacktip reef shark (*Carcharhinus melanopterus*) and the Bowmouth Guitarfish (*Rhina ancylostoma*) in an aquarium setting and on the free-living Whale shark (*Rhicodon typus*) in open water. The manner and length of the deployments was increased gradually over time through the M-clip development cycle and was mostly successful, demonstrating the M-clips versality and potential but with clear development still needed to secure deployments of at least 24 hours. In developing the M-clip, we have sought to identify and address many key aspects that should be universal considerations in any attachment system, feeding into a framework for work. This framework is informed by our own experiences in the development and testing process described here, as well as considerations of what is increasingly possible in the near-future with continually advancing technologies that are becoming more accessible, user friendly and necessary for tag design and development.

2. Materials and Methods

See Appendix 2 for details on the step-by-step process of creating version 4 (the final version produced here) of the M-clip within Fusion 360 (Autodesk Ltd., Farnborough, UK) software.

2.1 Tag position

The first step in the design process was to identify the requirements for a shark tag attachment. Tag positioning on marine animals is an important covariate in telemetry and movement studies that can affect movement track accuracy and interpretation of behaviours (Mul et al. 2019). To maximize functionality and versatility, we set out to accommodate tags/devices that would either log data autonomously (e.g. Wilson *et al*., 2008) or transmit to satellites (e.g. Godley *et al.*, 2008), with the latter dependent on an out-of-water period. Since some sharks most commonly only expose the dorsal fin out of the water (e.g. Heithaus *et al.*, 2007; Gubili *et al.*, 2009; Anderson *et al.*, 2011), we chose this as the primary site. In addition, tags that capture fine-scale movement, orientation and energetics (e.g. Wilson *et al*., 2008) must reflect the movement of the body of the animal and so necessitate a fixed mount, rather than a towed option. The first dorsal fin met both these requirements best (particularly the mid- to upper-section).

2.2 Geometry of the attachment site

To minimize any unnecessary forces or pressures imposed by the tag or attachment method, a body-mounted system requires reasonable geometries of the attachment site on which to base a design. Firstly (versions 1-3), we obtained measurements of first dorsal fin cross-sections of two similarly-sized (800 and 870 cm total length) captive whale sharks from the Okinawa Research Center (courtesy of Keiichi Sato, personal comm. with Brad M. Norman) allowing

approximations of scales and dimensions in initial designs of our first iteration of the M-clip. At this stage, dorsal dimensions were assumed to scale linearly with body size, although this is likely to be an oversimplification (Irschick and Hammerschlag 2015).

Following this, for design iteration v4 and beyond, we trialled the use of hand-held structured-light 3D scanning technology for obtaining the point-cloud geometry of various shark dorsal fins. Specifically, we used an Artec Eva scanner (Artec 3D, Luxembourg) to scan the dorsal fins of a dead Blue shark (*Prionace glauca*) - total length 192 cm - at Oceanografic aquarium, Valencia, Spain to produce a digital model accurate to 0.1 mm (Fig 1). Scans were initially processed in Artec Studio 12 software (Artec 3D, Luxembourg). Scans from different angles required stitching together and refinement using the inbuilt software tools. This high-accuracy model was then further refined using Autodesk Fusion 360 (Autodesk Ltd., Farnborough, UK) to a simplified model that could be quickly manipulated during the tag-design stage. A simplified model should also be more amenable to any Computational Fluid Dynamics work, which is computationally demanding when using complex geometries (Kay et al. 2019). A series of measurements was taken digitally at 10 cross sections through the raw fin model to create the new, simpler 3d model (Fig. 1). These measurements provided the basis for scaling for deployments on several different shark species; although again an oversimplification, it was deemed sufficient for these tests (as the inner padding of the M-clip (see below) and the flexibility in the plastic allows variation anyway), although we note the importance of obtaining more scans for a potential library of species (and variability therein) in the future. Measurements (length, height, thickness) of *Ginglymostoma cirratum*, *Carcharinus melanopterus* and *Rhina anclyostoma* first dorsal fins were additionally provided by staff at Oceanografic Aquarium, Valencia, Spain, allowing adjustment of the presumed scaling relationship (see above) to customize the M-clip design to accommodate the size differences.

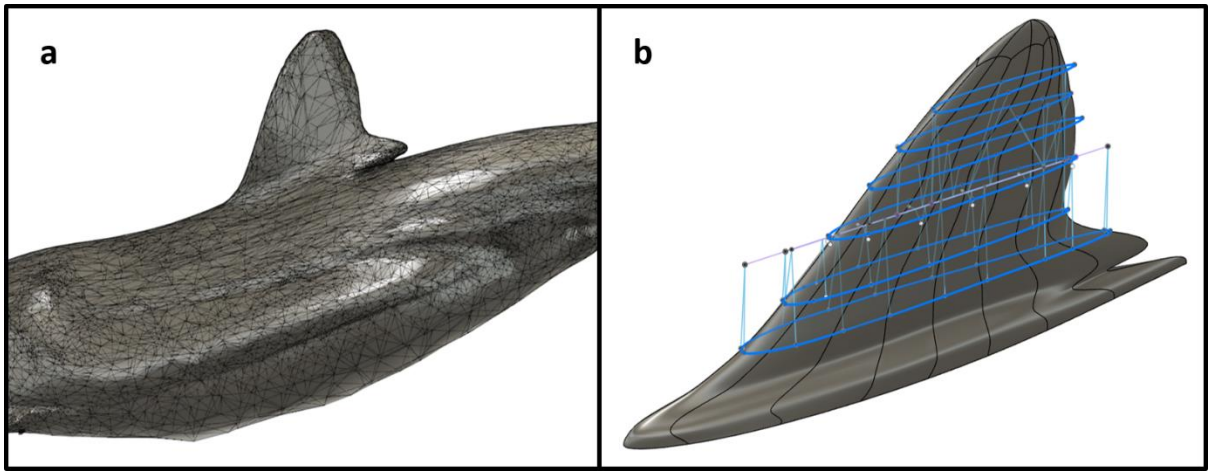

Figure 2.1: a) The initial 3d scan of a dead *P. glauca*, obtained using an Artec Eva (Artec 3D, Luxembourg; hired from Central Scanning Ltd., Bromsgrove, UK) and rendered (following initial refinement through Artec Studio software) using Fusion 360 software (Autodesk Ltd., Farnborough, UK); **b)** Cross-sections of the scan were used to rebuild a simplified fin model for easier manipulation and correction of imperfections (all within Fusion 360) in the original specimen's fin (allowing generalisation of the model). These cross-sections could be scaled accordingly.

2.3 Overview of M-clip design

We projected that the M-clip should consist of a symmetrical two-armed device joined by a hinge, orientated to run longitudinally along the dorsal fin (with the hinge at the leading edge) so as to present a minimum cross-sectional area to the normal flow of the water and reduce negative impacts on swimming and behaviour (Bouyoucos et al. 2017). Neodymium-Iron-Boron (NdFeB) rare-earth magnets mounted to the rear of each arm provided a firm, known force to shut the clip mechanism immediately posterior to the fin (Fig. 2.2). Specifics of this design include 3-d printed arms (made of several plastic variants through development, but finalised with laser-sintered polypropylene), the hinge sitting at an angle of 45^{o} – 55^{o} (depending on the species) to accommodate the sloped profile of the anterior edge of the dorsal fin and held together by a pin through the hinge. In addition, the NdFeB magnets were located within a pocket of the arms, held either *via* small steel pins that allow a swivel motion (version 2) or Tesa tape (versions 1, 3 and 4; Tesa, California, USA).

By locating the closing force at the rear of the unit (Fig. 2.2), the leading edge can be shaped hydrodynamically (compared to, for example, existing spring clamps (Gleiss et al. 2009)). In these tests, the movement tags (Daily Diary (DD) units; Wildbytes Technologies Ltd, UK) themselves were located within custom-made acrylic housing in turn attached to the M-clip. Initially the DD package was attached to the M-clip *via* cable ties but for the final described tests (version 4) it sat within a shallow depression in the plastic and was fixed in place by Velcro (Velcro Ltd., UK) which allowed quick removal and reattachment of the DD. The work described here does not include any float-and-recover capability, which is intended to be implemented at a later date.

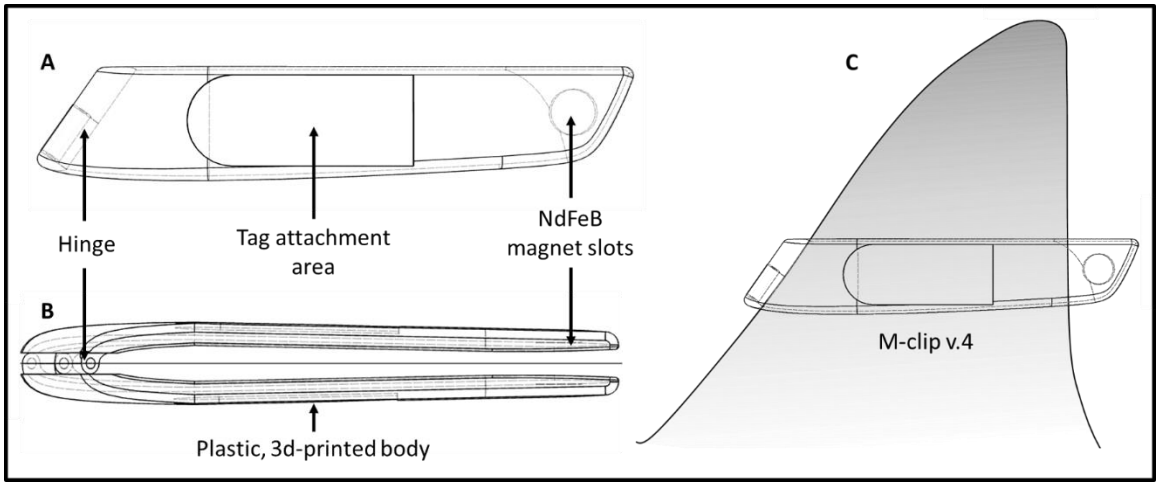

Figure 2.2: An overview of the design for the final M-clip version tested here (version 4), although all designs followed the same basic principles and features. The clip is shown from a side view (**A**), top view (**B**) and as envisaged on a generalised shark fin (**C**). In this version, the tag was fitted onto the M-clip *via* Velcro strips (Velcro Ltd., UK), the magnets were held in place *via* Tesa-tape (Tesa, Norderstedt, Germany) and the body was made from 3d-printed, laser-sintered polypropylene plastic. Note that the position of the magnet slots are shown in A, but the actual recesses for the magnets are on the inside of the arms.

A release system was not tested here. Whilst versions 1-3 used galvanic pins (steel and magnesium) in the hinge (with an intention that the pin degradation would release the internally acting pressure on the fin driven by the magnets) this was changed to simple all-steel pins for testing of version 4. We have thus far sought to validate the use of the basic system (that of an around-the-fin clip with magnets as force generators) with a view to developing the release and recovery mechanisms later.

2.4 Use of Neodymium-Iron-Boron magnets as a closing mechanism

Neodymium-Iron-Boron (NdFeB) rare-earth magnets with Nickel coatings (E-Magnets UK, Hertfordshire, UK) were selected for our system, functioning as force generators to help to

close and align the arms and generating the force necessary for adhesion to the fin. The forces generated by these permanent magnets are substantial and have been used, e.g. in human orthodontics (Noar and Evans 1999) with great success but, importantly, are predictable for known sizes and separation distances. In addition, the magnetic field strength of a magnet generally adheres to the relationship of an inverse square law, such that:

$$I = \frac{1}{d^2}$$

where 'I' is the magnetic field intensity and 'd' is the distance from the magnet. To predict the generated force and therefore the most appropriate magnet size to use for a given deployment (i.e. dependent on species size and therefore the required M-clip size), magnetic pull strength (the minimum perpendicular force (N) required to separate two identical magnets at known distance from each other) was compared for various magnet dimensions across increasing separation distance using an online calculator by Frenergy Magnets (Queensland, Australia). The reliability of this calculator was first validated experimentally. Circular magnet pairs of (individual) dimensions 18 x 5, 22 x 10, 22 x 6, and 25 x 5 mm (diameter x depth) were each separated by distances of 0, 10, 20, 30, 40 and 50 mm using plastic blocks. For each magnet pair size and separation distance, a spring balance was fixed to one of the magnets in a pair and the magnetic pull force recorded (N = 3 for each separation and magnet pair combination).

To ensure that the magnet pairs did not interfere with the magnetometer readings of the DD and could be 'filtered out' – that is, accounted for so that magnetometer data recorded by the tag are unaffected – magnetometer calibrations (Williams et al. 2017) were performed both with and without the magnets present whilst the DD was attached to a 206 mm version 4 M-clip in its deployment position. Calibrations followed the same procedure of rotating the DD and M-clip about the pitch and then the roll (relative to the worker) axes whilst turning 360°

on the spot each time, before repeating the whole process for a second time (Williams et al. 2017). The procedure was conducted in the exact same location for both spheres- in an open space away from any buildings or obvious sources of metal. M-spheres (tri-axial plots of magnetic field intensity from the tri-axial magnetometers within the DDs cf. Williams et al. 2017) were generated within DDMT (Daily Diary Multiple Trace; Wildbyte Technologies, Swansea, UK) following the software's magnetometry correction algorithm.

2.5 Understanding the generation of inwardly acting forces

The combination of rear mounted NdFeB magnets and a hinged leading edge facilitates force generation through the arms of the attachment system. It is effectively a Class II lever (akin to a nutcracker), also known as a force multiplier lever. In a model Class II lever with rigid arms, the resistance to motion (in this case, the fin pushing back against the M-clip arms) sits between the applied effort (the inward force resulting from the closing force, driven by the magnets) and the fulcrum (the hinge). The force applied inward to the fin multiplies through the arms according to the equation:

$$\frac{E}{L} = \frac{b}{a}$$

where *E* is the Effort applied (here the force generated by the NdFeB magnets, at this stage excluding external hydrodynamic loading), *L* is the Load (the resistance to motion from the fin – which effectively translates into a resultant pressure applied to a particular point of the fin surface once the surface area of contact is known), *a* is the effort-fulcrum distance (the distance from the magnet pair to the hinge) and *b* is the load-fulcrum distance (distance from hinge to the point of pressure we wish to measure). The force applied by the NdFeB magnets at the rear therefore increases closer to the hinge and the leading edge of the fin.

The distribution of inwardly acting forces was then used to calculate the maximum frictional forces likely to act on the fin. However, these are critically dependent on the pressure at the points of contact, itself dependent on the force and area of contact since:

$$P = \frac{F}{A}$$

(where P = pressure, F = force applied perpendicular to the surface and A = area over which the force is applied), and on the material in contact with the fin.

This process was informed by maximum friction (F_{max}) measurements. Silastic P100 (Dow Corning, UK), now known as Xiameter 4250, is a silicon rubber material that has been used variously to secure tags to birds (Vandenabeele et al. 2013, Thaxter et al. 2015) and fish (Houghton et al. 2009) through harnesses and to other animals using collars (Halsey et al. 2009). Silastic was a choice material owing to its biological compatibility (it is used within medical implants), flexibility and compressibility (which can be modulated by mixing with silicon oil). It was therefore deemed an appropriate material for padding the inside of the M-clip and to be in contact with the fin. It was critical, however, to understand the frictional relationship the material would have when in contact with the fin and contextualize this by comparing it to some other materials. To do this, the frictional hold of 5 materials was compared by dragging a weighted sledge across a 40 x 40 mm square of skin from the dorsal region of a small-spotted catshark (*Scyliorhinus canicula*) (supplied from accidental bycatch and death in Swansea Bay, Swansea, UK). Materials tested were: P60 Sandpaper, P80 Sandpaper, Dual Lock SJ4575, Dual Lock SJ3550 and Silastic (supplied by Notcutt Ltd., Ripley, UK). Sandpaper was used for comparison due to its obvious high frictional properties, and Dual Lock variations due to their structures of small plastic ‘hairs’ which were

substantially different to the other materials and was theorised might act antagonistically with the denticles of shark skin. Sledges were mounted on to 30 x 30 mm squares of each material and loaded with lead balls to achieve total weights of 100, 200, 500, 1,000, 1,500 and 2,000 g, therefore creating applied downward pressures of 0.061, 0.123, 0.306, 0.613, 0.919 and 1.225 N/cm^2 respectively. The sledges were pulled perpendicularly along the shark skin surface with, against, and perpendicular to the skin denticle direction (as shark denticles are not radial - Dean and Bhushan, 2010) by an attached spring-balance used to take measurements. The horizontal force (N) required to move the sledge from a stationary position was recorded (N = 3 per each material-direction-weight combination) and the coefficient of (static) friction 'μ', calculated according to:

$$\mu = \frac{F_{max}}{R},$$

where F_{max} is the largest frictional force (equivalent to the largest pull force) at the point in time just as the sled begins to slide and 'R' is the magnitude of the vertical force applied to the moving object (the weight of the sled).

2.6 Trial deployments

2.6.1 First open-water trial

For the first on-animal trial and to evaluate the basic principles of the design, one *R. typus* was tagged near the northern Thaa Atoll of the Maldives (approx. 2°17'5.8878"N, 73°19'21.3522"E) using the M-clip version 1 (Fig 2.3). *R. typus* was approached by snorkelers whilst it fed near the surface under the light of a fishing platform. The clip was attached by hand around the first dorsal fin and the reaction of the animal was observed for ~ 30 minutes

until the snorkelers left the water. Version 1 of the M-clip featured a 3d-printed ABS-plastic front hinge and long polypropylene arms cut to size. For subsequent versions, the entire clip body would be 3d-printed – subsequent *R. typus* tagging with the M-clip would therefore use a smaller version targeted to the second dorsal fin instead. Eight resin floats with embedded glass micro-spheres were also used for version 1 to facilitate neutral buoyancy of the clip, but in subsequent versions these were not used. This and all subsequent M-clips were equipped with Daily Diary (DD) archival tags, recording at 40 Hz across accelerometer, magnetometer, temperature and pressure channels, (Wilson et al. 2008) within a housing of size 30 x 75 mm (though with rounded leading edges).

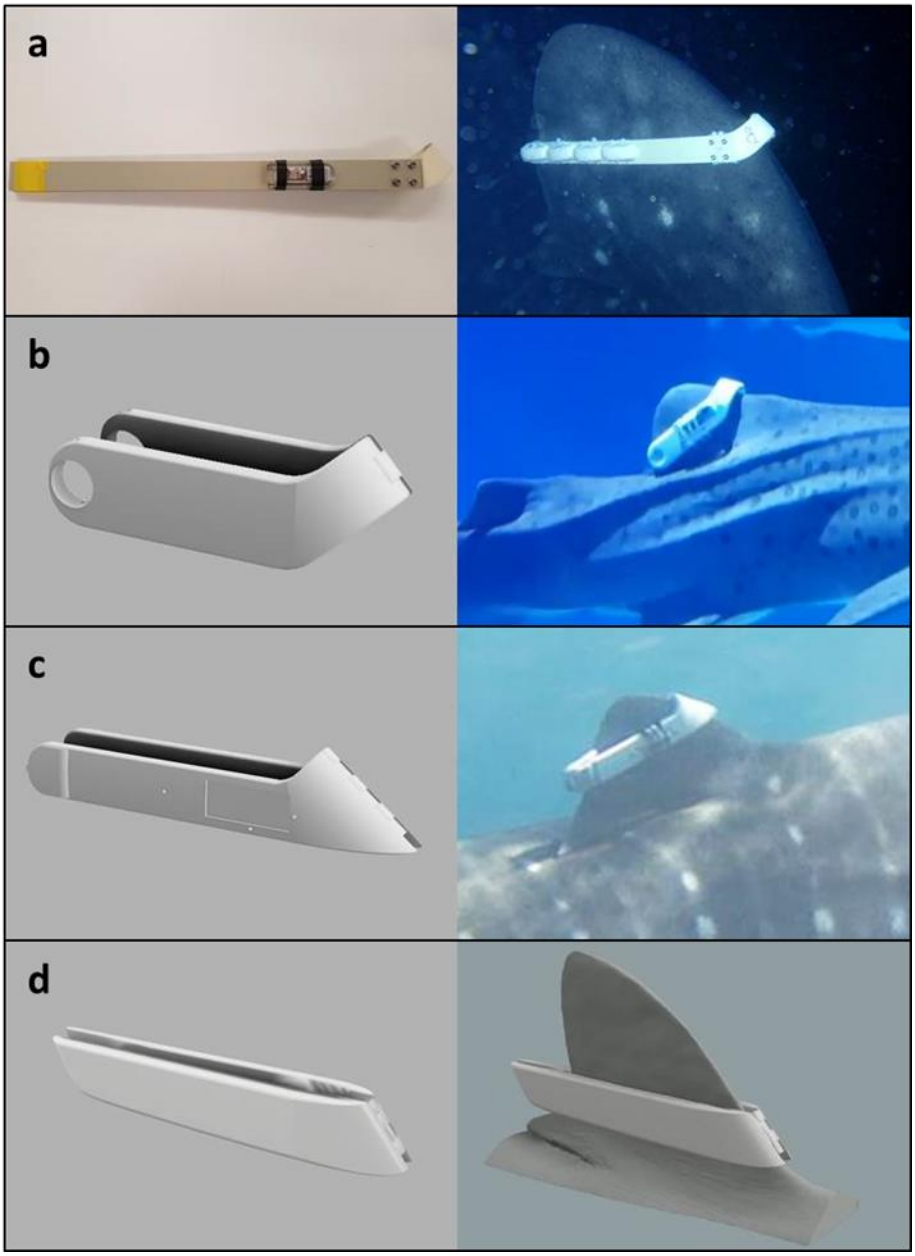

Figure 2.3: Consecutive iterations of M-clip designs/forms and images from their respective trials. **(a)** version 1, combining a 3D printed hinge with machined polyproylene-plastic arms. Deployment on the first dorsal fin of *R. typus* in the Maldives; **(b)** version 2, switching to a fully 3D printed, extruded ABS, body with cut-outs for swivelling magnets (held on steel pins). Deployed on the first dorsal fin of a captive *S. fasciatum* in Oceanografic Aquarium,Valencia, Spain in Jan 2018; **(c)** version 3, with adjustments to the leading edge, a recess for the tag housing attachment and reversion to magnets sat in pockets and secured with Tesa-tape, made from 3D printed laser-sintered Nylon. Deployed on the second dorsal fin of a free-living *R.*

typus at Ningaloo Reef, Australia; **(d)** version 4 with improved hydrodynamic shape, indentations for the DD tag package, silastic padding strips and magnets, and manufactured from 3D printed, laster-sintered polyproylene. Shown fitted to a 3D-scanned *P. glauca* first dorsal fin.

2.6.2 First aquarium trial

Version 2 M-clips were deployed on *Stegostoma fasciatum* (N = 1) and *Ginglymostoma cirratum* (N = 1) in the 'Oceans' tank at Oceanografic aquarium, Valencia, Spain. The *Stegostoma fasciatum* deployment had a 180 mm M-clip attached to the first dorsal fin by hand whilst the individual was restrained by divers at the surface of a quarantine pool for the duration of the attachment procedure (approx. 5 seconds). After approx. 5 minutes the equipped individual was allowed to re-enter the main aquarium tank (approx. dimensions 90 m × 30 m × 5 m L×W×D) by itself, following the raising of the quarantine-pool gate. The M-clip was left attached for 2 hours before being removed within the tank by divers, the removal procedure being a simple, quick grab of the clip by the diver as the shark swam past. The *G. cirratum* deployment had a 220 mm M-clip attached to the first dorsal fin by hand within the main tank by divers, after briefly netting an individual to allow quick attachment. The M-clip was left attached for 1 hour before being removed, again by divers within the tank after briefly restraining the individual with the use of a net. Several adjustments were made to the working M-clip design following these trials (Fig. 2.3), most notably changes to the leading face and hinge area. Specifically, the upturned shape was extended downwards to reduce hydrodynamic forces pushing the M-clip upwards and facilitate water flow around the clip at greater swimming speeds.

2.6.3 Second open-water trial

Four *R. typus* were tagged at Ningaloo Reef, Western Australia (approx. 22º00'S, 113º50'E) in June-July 2018 using version 3 M-clips. Suitable individuals for this trial were considered to be at least 6 metres in length and displaying non-erratic behaviour (i.e. comfortable with approaching snorkelers and maintaining a steady depth in the water column). Snorkelers determined suitability when swimming behind the shark prior to tagging and were also responsible for attachment and detachment of tags. Sharks were double-tagged to allow comparison of behavioural data before and during M-clip attachment and following M-clip detachment. A traditional metal clamp (Gleiss et al. 2009) with a corrosive link and equipped with a DD tag and VEMCO V16 acoustic transmitter (VEMCO, Nova Scotia, Canada) was first attached to the first dorsal fin. The M-clip was attached to the second dorsal fin at the next suitable opportunity. The behavioural reaction to the tag attachment was filmed. The double-tagged shark was followed (at a variable distance but at least a 100 m distance was attempted, dependent on the strength of the acoustic signal) by a boat using a directional hydrophone and VEMCO VR100 (VEMCO, Nova Scotia, Canada). Tags were removed by a snorkeler at a suitable opportunity 1-3 hours after tagging and when the animal was close to the surface. The timing of removal was also dictated by light – visually spotting the shark below the surface became increasingly difficult after 2.30 pm local time. When removing the tags, the M-clip was removed first and then followed by the metal clamp. It should be noted that the Ningaloo Reef area during this time has a high volume of ecotourist boats and snorkelers, and tagged sharks were often followed (at a distance of >10 m) when near the surface by non-research snorkelers prior to and following tag attachment. Following this trial, the M-clip design was made more hydrodynamic, slimmer and made from a more flexible polypropylene plastic as the Nylon material appeared 'cumbersome' and unnecessarily dense (Fig. 2.3).

2.6.4 Second aquarium trial

Following refinement of the M-clip design (Fig. 2.3), informed by the previous aquarium and open-water trials, a 'final' test of the M-clip, version 4, was conducted at Oceanografic Aquarium, Valencia, Spain (Fig. 2.4). N = 4 *Ginglymostoma cirratum*, N = 2 *Carcharhinus limbatus* and N = 1 *Rhina ancylostoma* were tagged in-tank by divers (as in the first aquarium trial) across 8, 3 and 2 separate deployments, respectively, with tagging dependent on how receptive the animals were to tagging on a given day. The dorsal fins were observed before and after tagging to assess any physical impact of the M-clip on the animal, with pictures taken where possible. Behavioural observations were made opportunistically throughout the tagging period, particularly in the first 30-60 minutes and then approx. every hour thereafter (with observations periods of at least 10 continuous minutes). Observations also noted proximity to, and interaction with, other sharks to discern whether the presence of the NdFeB magnets negatively altered behaviours. *G. cirratum*, for example, group together, in close proximity, in inactive groups during the day – avoidance of the tagged individual would therefore suggest a negative effect. M-clips were observed for any movement/migration over the fin for the duration of the attachment period.

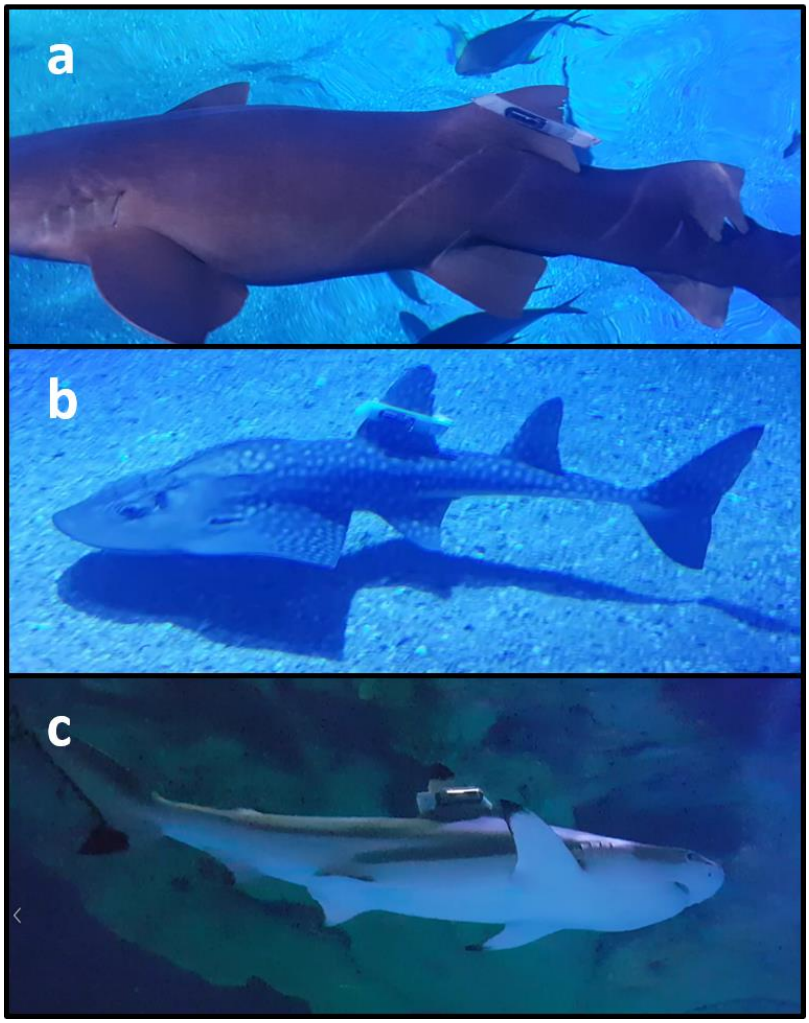

Figure 2.4: Pictures of sharks tagged with the latest (version 4) M-clip design iteration at Oceanografic Aquarium, Valencia, Spain in November 2019. This design used a laser-sintered (3D printed) propylene body, with the DD acrylic housing attached into an indentation with complimentary Velcro. **a)** *Ginglymostoma cirratum*, **b)** *Rhina ancylostoma*, **c)** *Carcharinus melanopterus*. Note that each M-clip pictured here was of a different size, which was tailored for each species using data supplied in advance by Oceanografic aquarium.

2.7 Data handling

In all M-clip tests, DD data were analysed within DDMT software to look for changes in locomotory activity and behaviour profiles (Sundström and Gruber 2002, Gleiss et al. 2009). Locomotory activity was quantified to assess both initial and prolonged disturbance to shark behaviour and movement (Gleiss et al. 2009, Chapple et al. 2015, Bouyoucos et al. 2017).

3. Results

3.1 Magnetic forces

Following calibration of the DDs attached to the M-clip by comparison of M-spheres (cf. Williams et al. 2019), we noted the similarity between the two M-spheres and the lack of distortion from sphericity, indicating that the effect of the magnets can be easily filtered out of the resulting magnetometry data (Fig 2.5).

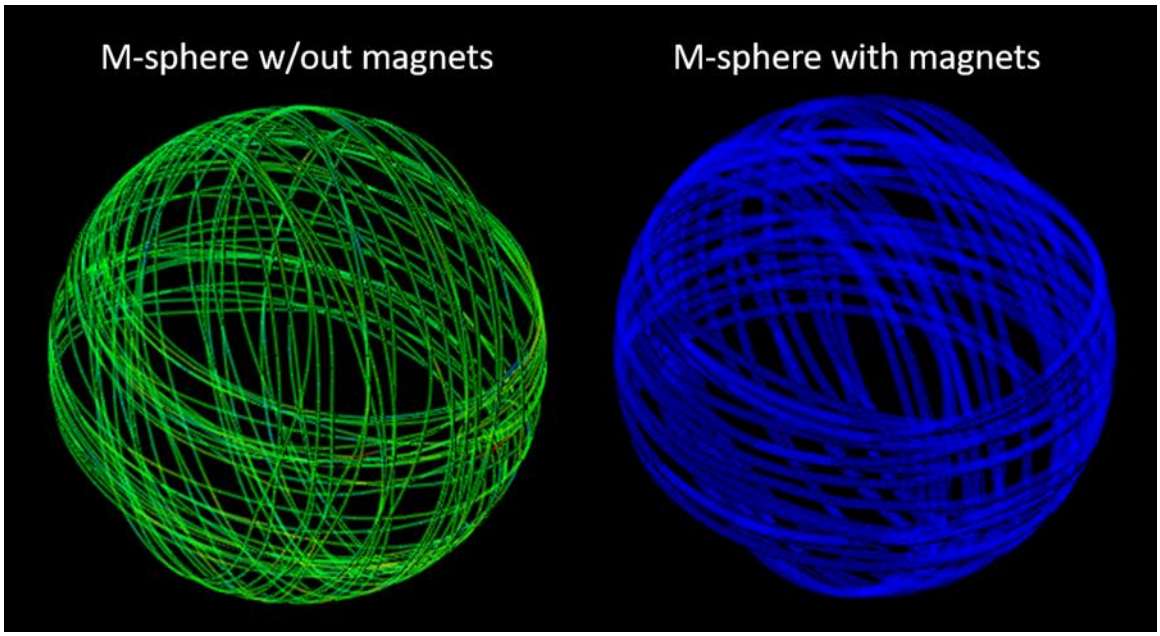

Figure 2.5: M-spheres consisting of tri-axial plots of magnetic field intensity from the tri-axial magnetometers within the DDs (Williams et al., 2017) representing DD calibrations (see methods) made with the DD attached to the M-clip (version 4; length = 206 mm) either with (left, green sphere) or without (right, blue sphere) a pair of magnets (individual magnet dimensions: 22 cm diameter x 5 cm depth) attached to the clip. Note the similarity between both spheres indicating that the magnetic field from the magnets was undetectable by the tag.

Recorded pull/separation strengths of NdFeB were compared to those generated by the Frenergy Magnets online calculator which was found to relate closely to laboratory tested

values (Fig. 2.6). The online calculator was therefore used for any further magnet strength calculations.

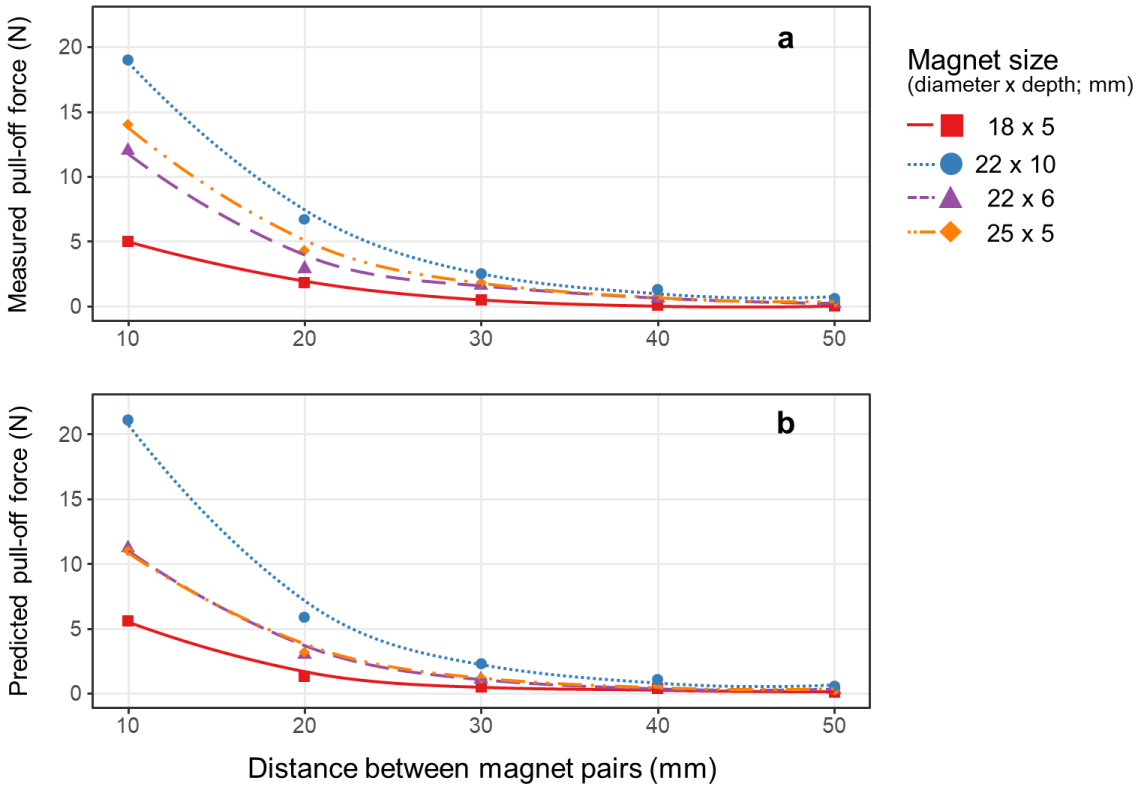

Figure 2.6: The force required (applied perpendicularly to the magnet face and measured by a spring force-metre) to pull-away a Neodymium Iron Boron (NdFeB) magnet from an identical magnet, separated by a plastic block of varying thickness either as (**a**) experimentally validated or (**b**) calculated at 'https://www.frenergy.com.au/flux-calculator.html'. Very similar values led to the use of the online calculator for all further magnet-strength calculations.

3.2 Frictional forces

There were notable differences in the F_{max} required to cause different materials to slide over the shark skin as a function of perpendicularly applied forces (Fig. 2.7). All F_{max} values increased linearly with increasing perpendicular forces. In the direction *with* that of the skin

denticles, silastic and 80-grit sandpaper performed the best. Perpendicular to skin direction, both sandpaper grades had the highest Fmax with silastic comparing reasonably well. When dragging the sled against the direction of the shark skin, Dual Lock SJ4575 (1) was the best performer with similar values between both sandpaper variants and silastic. Dual Lock SJ3550 was the worst-performing material in terms of frictional hold in all three pull directions. Based on this, Silastic P100 was considered to be a suitable frictional material for the M-clip. Although Silastic P100 was not the best performing in all three tests, it performed consistently well, especially in the ‘with’ and ‘perpendicular’ directions that are likely to be most relevant on a swimming shark with water drag forces acting against in the opposite direction. Silastic’s hypoallergenic and mouldable nature further informed the decision to use it as the frictional material in these tests.

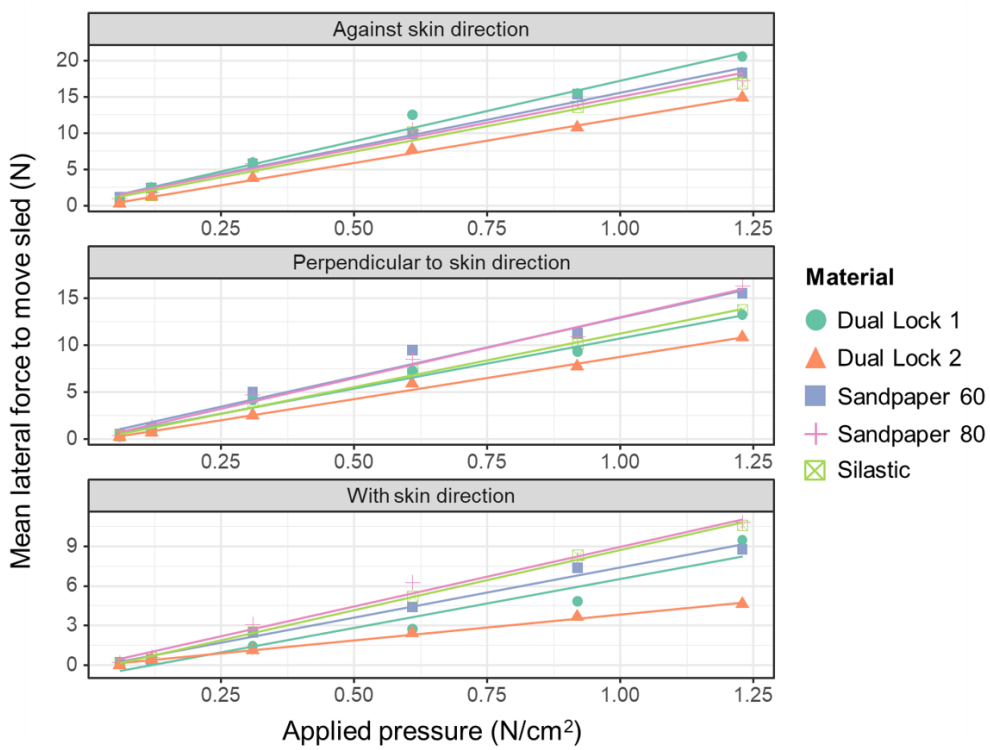

Direction of sled movement	Material	Intercept	Gradient
Against	●	0.56	16.67
	▲	-0.23	12.25
	■	0.72	14.86
	+	0.69	14.29
	⊠	0.38	14.07
Perpendicular	●	0.09	10.67
	▲	-0.26	9.05
	■	0.32	12.61
	+	0.01	12.98
	⊠	-0.10	11.27
With	●	-0.86	7.38
	▲	-0.10	3.93
	■	-0.21	7.62
	+	-0.08	9.05
	⊠	-0.41	9.14

Figure 2.7: *Left:* The minimum lateral force (F_{max}) required to pull a weighted sled across a section of dogfish skin either with, against or perpendicular to the direction of the denticles. The bottom of the sled was fitted with one of 5 test materials. The sled was loaded with increasing weight, which was converted into pressure applied per cm. *Right:* Linear model outputs for regressions. 'Intercept' here refers to the lateral force required to move the sled without any applied pressure. 'Gradient' here refers to the increase in required lateral force to move the sled per N/cm^2 of applied pressure.

3.3 Deployment durations

Of the four open water trials on *R. typus* at Ningaloo, Australia (with M-clip v.3), two had successful deployment and retrieval (with deployment durations of 150 and 180 minutes), one was confirmed still attached after 60 minutes but not sighted thereafter and one was lost having not been resighted following attachment (Table 2.1). In the case of the latter, it was noted that the shark second dorsal fin was misshapen and likely prevented proper closure of the magnet pairing.

Of the thirteen deployments in the second captive trial using the latest M-clip, v.4, seven had durations of over an hour (Table 2.1). Mean duration was 435.46 minutes, with longest and shortest durations (both on *G. cirratum*) of 18 and 1352 minutes, respectively. The longest-duration deployment was also the only instance in the second set of captive trials where the M-clip was removed by workers.

3.4 Behavioural changes caused by the M-clip

During trials of M-clip versions 1, 2 and 3, behavioural reaction to the clip and tagging procedure appeared minimal at most (Table 2.2). In testing v.1, *R. typus* continued feeding at a fishing platform for at least 30 minutes, interspersed by brief dives out of sight. During captive trials testing of v.2, both *S. fasciatum* and *G. cirratum* showed little obvious change in their usual swimming and social behaviour with *G. cirratum* seen resting next to conspecifics. For v.3 testing, again on free-living *R. typus*, the only consistent behavioural reaction was a quick (i.e. several tail beats) burst swim away on tagging, although longer term trends and tag reactions are harder to quantify with only four deployments (Figs. 2.8.1 and 2.8.2).

Table 2.1: Details of each deployment through each of the 4 M-clip iterations. Captive aquarium trials were conducted at Oceanografic Aquarium, Valencia, Spain. Note that 'Sp. ID' gives a new set of ID numbers per species.

M-clip version	Deployment no.	Species	Setting	*Sp.* ID	Deployment length	Reason for finish/method of removal/notes
v1	1	*R. typus*	Free-living (Maldives)	1	At least 25 mins	Unknown outcome. Dived after 25 mins; bad weather in subsequent days stopped follow-up searches. Resighted after 107 days without tag.
v2	2	*S. fasciatum*	Captive (aquarium)	1	187 mins	End of test. Removed by divers.
	3	*G. cirratum*		1	63 mins	End of test. Removed by divers.
v3	4	*R. typus*	Free-living (Ningaloo)	2	150 mins	End of test (resurfaced). Removed by snorkelers.
	5			3	Sighted after 60 mins with M-clip attached. Likely at least 277 mins attached (inferred from moving acoustic tag pings).	Unable to retrieve as shark did not resurface after 60 mins, until bad light halted search. Unable to re-find subsequent days.

	6			4	180 mins	End of test (resurfaced). DD data from M-clip not recoverable (but metal clamp data recovered).
	7			5	Unknown	Unknown. M-clip missing upon shark resurface. Noted that 2nd dorsal fin had an abnormal shape (bent) and prevented ideal magnet closure.
v4	8	*G.cirratum*	Captive (aquarium)	2	31	Fell off whilst swimming normally (observed).
	9			2	1352	End of test/removed to observe state of fin.
	10			3	820	Roll/chafe on sand to remove (inferred from accelerometer data visualization)
	11			3	34	Roll/chafe on sand to remove (inferred from accelerometer data visualization)
	12			3	18	Roll/chafe on sand to remove (observed).
	13			4	458	Roll/chafe on sand to remove (inferred from accelerometer data visualization)

14		5	35	Roll/chafe on sand to remove (inferred from accelerometer data visualization)
15		5	50	Presumed knocked off against aquarium features (inferred from DD data).
16	*C. melanopterus*	1	145	Removed due to shaking of body (inferred from visualization of DD data).
17		1	23	Knocked off by conspecific (observed).
18		2	1308	Removed due to shaking of body (inferred from visualization of DD data).
19	*R. ancylostoma*	1	683	Fell off; unknown reason.
20		1	704	Fell off; unknown reason.

Table 2.2: Observed behavioural reactions of every shark tagged with the M-clip. Note that 'Deployment no.' matches that of Table 2.1 for reference. Behaviours described here do not include DD tag-inferred behaviour.

Deployment no.	**Species**	***Sp.* ID**	**Initial behavioural reaction**
1	*R. typus*	1	***No obvious reaction.*** Continued feeding at fishing platform throughout attachment procedure, as well during several checks of its fit. Dived deeper and returned several times to continue feeding within ~ 30 minutes (workers left the water after this time).
2	*S. fasciatum*	1	***No obvious reaction.*** Swam at steady pace for 109 minutes, before resting at the bottom of the tank for the remaining 78 minutes.
3	*G. cirratum*	1	***Initial burst swim away*** (tagged in-tank by divers). Followed by slow swimming near bottom of the tank.
4	*R. typus*	2	***Initial burst swim away.*** Within 4 minutes returned to steady swimming near surface. Dived and returned to near-surface twice in following 120 mins.
5		3	***Initial burst away.*** Quickly resumed behaviour shown before tagging – quick turns near surface, presumed to be feeding behaviour. Resighted after ~60 mins, followed by a dive.
6		4	***Initial burst swim away.*** Was swimming slowly again within 5 minutes (snorkeler swimming speed).

7		5	***Initial burst swim away, followed by dive*.** Next sighted near surface (~1 m) approx. 60 mins later, slow swimming.
8	*G. cirratum*	2	***No obvious reaction.*** Slow swim away from feeding area. Returned to area immediately for further feeding and returned a further 5 times within 20 minutes.
9		2	***No obvious reaction.*** Slow swim away from feeding area. Returned to area immediately for further feeding and returned a further 5 times within 20 minutes.
10		3	***Some thrashing to get away.*** Swam slowly away from feeding area. Returned to feeding area a further seven times within next 18 minutes.
11		3	***No obvious reaction***. Swam slowly away from feeding area. Returned to feeding area four times in 7 minutes.
12		3	***Some high intensity tail movement to get away.*** Immediately circled back around to the feeding area. Remained near feeding area swimming normally until feeding finished.
13		4	***Some high intensity tail movement to get away.*** Swam slowly away from feeding area. Returned to feeding area within 2 minutes.
14		5	***Some high intensity tail movement to get away.*** Swam slowly away from feeding area. Slight dive. Returned to feeding net three times in 23 minutes.

15		5	***Some high intensity tail movement to get away.*** Swam slowly away from feeding area. Note that this tagging immediately followed a failed attempt – shark returned immediately after anyway.
16	*C. melanopterus*	1	***Sustained burst swimming upon release and dive to tank bottom***. Stayed near bottom for several minutes before gradual return to 'regular' swimming pattern and depth around tank, punctuated by occasional burst swimming.
17		1	***Sustained burst swimming upon release and dive to tank bottom***. Returned to regular swimming and depth within 4 minutes.
18		2	***Sustained burst swimming upon release and dive to tank bottom***. Stayed near bottom for several minutes before gradual return to 'regular' swimming pattern and depth around tank.
19	*R. ancylostoma*	1	***No obvious reaction***. Stayed at bottom of medical pool until release into main tank (approx. 48 minutes later). Slow swimming near bottom of main tank followed.
20		1	***No obvious reaction***. Slow swimming into main tank, where it remained swimming close to the bottom.

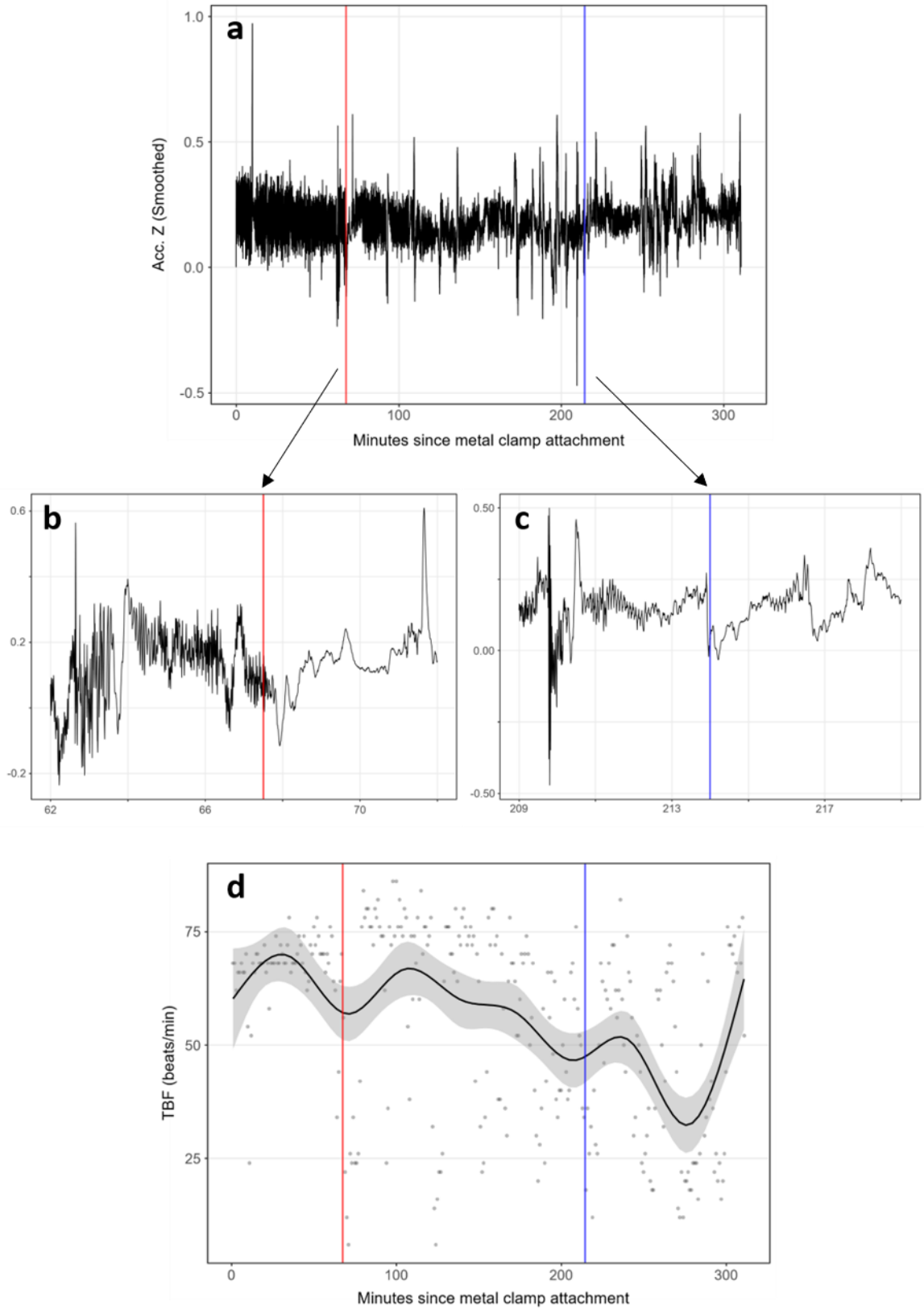
a
Acc. Z (Smoothed)
1.0
0.5
0.0
-0.5
0
100
200
300
Minutes since metal clamp attachment
b
0.6
0.2
-0.2
62
66
70
c
0.50
0.00
-0.50
209
213
217
d
TBF (beats/min)
75
50
25
0
100
200
300
Minutes since metal clamp attachment

Figure 2.8.1: Movement data from *Rhincodon typus* (deployment number 4 – see Table 2.1), from a Daily Diary deployed onto the 1st dorsal fin *via* a 'traditional' metal fin clamp. The M-clip was attached to the 2nd dorsal fin at 67.5 minutes (red vertical lines) and removed at 214 minutes (blue vertical lines). **(a)** Z-axis (sway) acceleration data, smoothed over 0.5 s. Data were originally recorded at 20 Hz and then thinned, for the purpose of this figure, to 10 Hz. The 360 minutes of data were recorded by the 1st dorsal fin clamp. The M-clip attachment and detachment events are shown further in **(a)** and **(b)** respectively. Note the clearly visible tail-beats in (c). The tail-beat frequency (TBF) per minute is shown in **(d)**, with a GAM (plotted using ggplot2 in R; solid black line) and its respective 95% CI's (light grey sections).

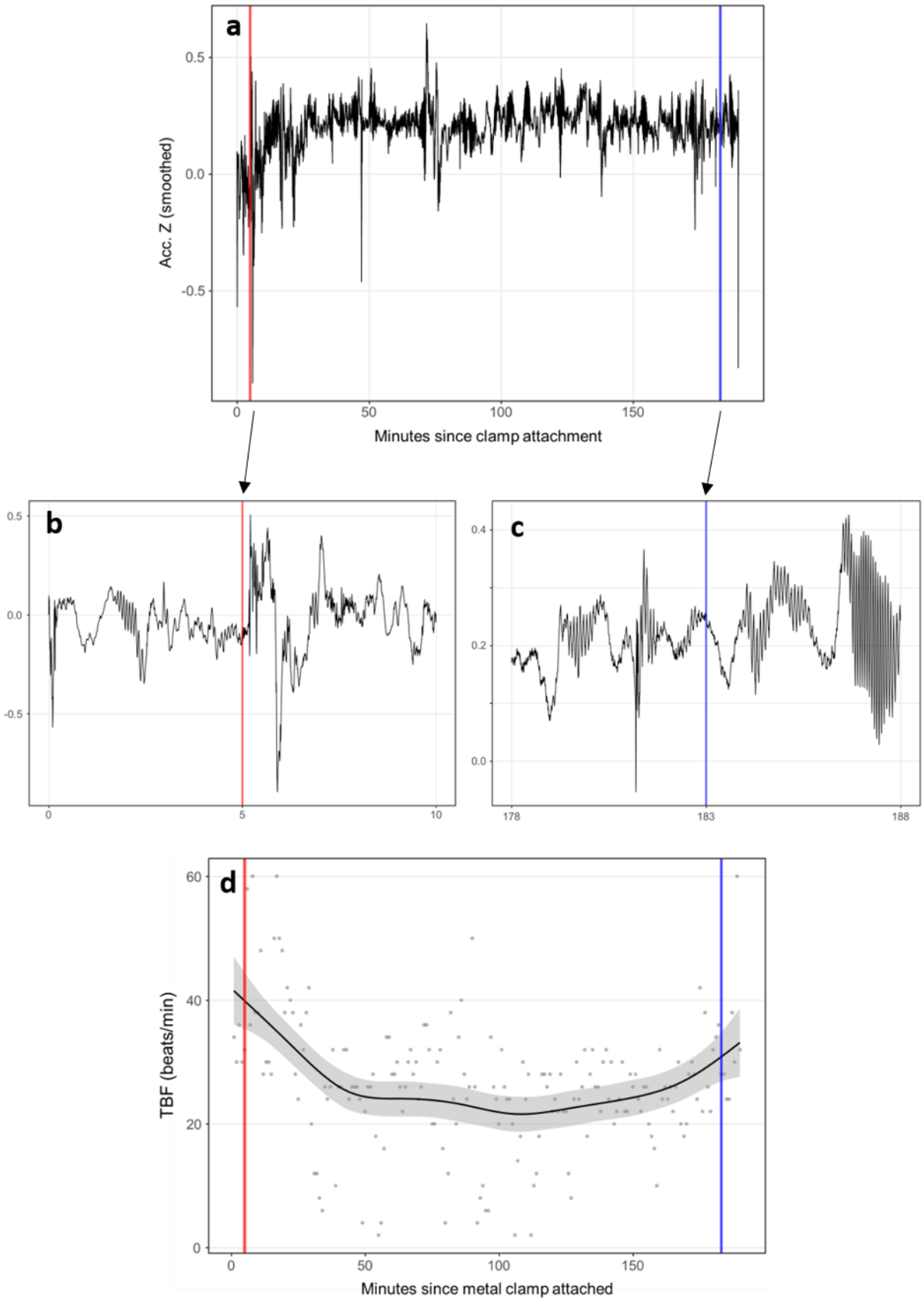
a
Acc. Z (smoothed)
0.5
0.0
-0.5
0
50
100
150
Minutes since clamp attachment
b
0.5
0.0
-0.5
0
5
10
c
0.4
0.2
0.0
178
183
188
d
TBF (beats/min)
60
40
20
0
0
50
100
150
Minutes since metal clamp attached

Figure 2.8.2: Movement data from *Rhincodon typus* (deployment number 6 – see Table 2.1), from a Daily Diary deployed onto the 1st dorsal fin *via* a 'traditional' metal fin clamp. The M-clip was attached to the 2nd dorsal fin at 5 minutes (red vertical lines) and removed at 183 minutes (blue vertical lines). **(a)** Z-axis (sway) acceleration data, smoothed over 0.5 s. Data were originally recorded at 20 Hz and then thinned, for the purpose of this figure, to 10 Hz. The 360 minutes of data were recorded by the 1st dorsal fin clamp. The M-clip attachment and detachment events are shown further in **(a)** and **(b)** respectively. Note the clearly visible tail-beats in (c). The tail-beat frequency (TBF) per minute is shown in **(d)**, with a GAM (plotted using ggplot2 in R; solid black line) and its respective 95% CI's (light grey sections).

During the second aquarium trials, where M-clip v.4 was tested, the tagging procedure did not appear to elicit any response beyond an initial bout of high intensity movement in *G. cirratum* whilst still held in the feeding net, a brief period (i.e. < 5 mins) of burst movement and swimming at greater depth in *C. melanopterus* and slower movement near the bottom of the tank (again < 5 mins) in *R. ancylostoma* (Table 2.2). Every tagged *G. cirratum* returned almost immediately, and repeatedly, to swim through the feeding net – one individual returning 7 times in 18 minutes – as well as returning on successive days.

Notably, however, numerous aberrant behaviours were observed during the M-clip v.4 aquarium trials. Seven instances of chafing behaviour were observed in tagged *G. cirratum*, where the individual would descend to the tank bottom, roll onto its back and 'rub' its dorsal side against the sand. In one instance, this behaviour was seen to remove the tag from the dorsal fin. It is suspected from the accelerometer data, however, that a further 5 deployments were ended by chafing in this way (Table 2.2; also see chapter 3). In addition, there appeared to be several instances of 'side to side' shaking of the whole body in both *C. melanopterus* and *R. ancylostoma* on several occasions, and *C. melanopterus* was even observed to leap from the water in a 'breaching'-style event. Observations of the same individuals when not tagged did not record these behaviours in any of the three species.

3.5 Evidence of physical detriment caused by the M-clip

Observations of *R. typus* dorsal fins (including analysis of video footage) immediately after M-clip removal did not produce any evidence of physical marking or damage. In the tagged aquarium species, marking of the fin was only evident in the longest tagged shark (*G. cirratum*), which had an M-clip attached for 24 hours (Fig 2.9). In this instance, the marks had noticeably faded following 24 hours and had disappeared completely after 1 week.

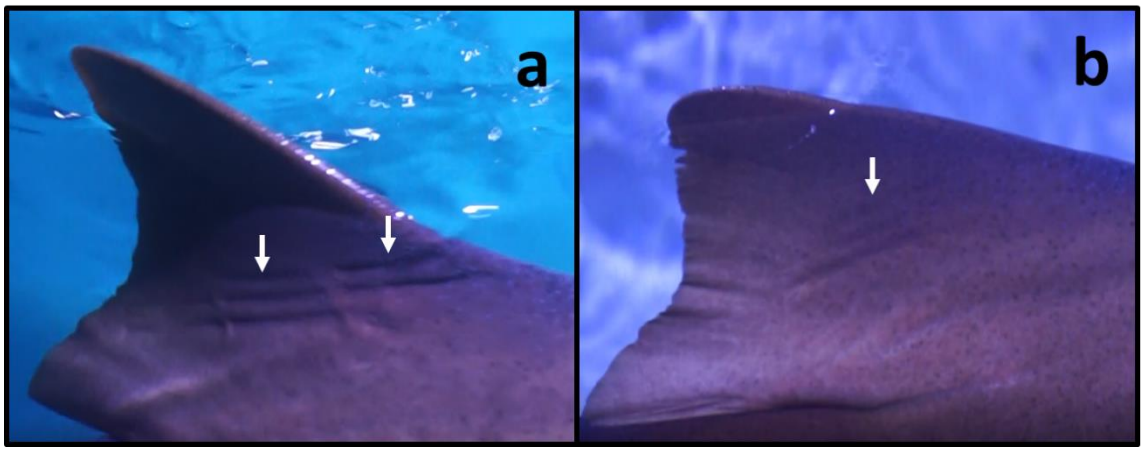

Figure 2.9: Markings left by the M-clip on a captive *G. cirratum* first-dorsal fin (indicated by white arrows) after the longest M-clip deployment (of any version) at 1352 minutes (deployment no. 9), **a)** immediately after removal of the M-clip and **b)** 24 hours after removal of the M-clip. This was the only aquarium-tagged individual with notable markings left behind on the fin following M-clip removal. Note the lined appearance of the marks are due to the silastic padding material being shaped as long strips.

4. Discussion

This report examined the viability of a magnet-based attachment system for deployment of loggers or telemetric devices on sharks (the M-clip) and highlighted the design philosophy within which it was constructed, where modern manufacturing methods (such as 3d printing) were used to allow rapid testing and refinement. From this, we believe that a magnet-based attachment system that encompasses the fin length is a viable method of tagging elasmobranchs for short term deployments where an externally mounted and easily removed attachment is required.

4.1 A call for minimized detriment

Researchers studying shark behaviour and movement are increasingly looking for less-invasive attachment methods (e.g. Fontes et al.'s (2017) harness system) and systems that can be easily attached. The M-clip accords with both these criteria in being minimally-invasive, highly adaptable for elasmobranch tagging, producing minimal reaction to the presence of the tag (at least comparable to those shown during the development of clamp-style attachments (Gleiss et al. 2009, Chapple et al. 2015)), and extremely rapid to deploy. In addition, it is low-cost (the body of the final clip design, seen in Figure 2.7, cost approximately £50 / $63 to produce).

We acknowledge that the M-clip described here, although at an advanced stage of development, still requires improvement and therefore may not be a complete replacement for other tagging methods. Instead, it provides another tool for consideration by researchers dependent on their needs. Further tests, for example, are now needed to assess how it performs on high speed, free-living species over multiple days to test the M-clip under high-drag conditions. Tests of the M-clip's attachment success over even longer periods (at least weeks) are also required

before it can be substituted for more invasive methods typically used to keep tags on sharks in place for extended periods (e.g. Haulsee *et al.*, 2016; Braun, Skomal and Thorrold, 2018). Beyond this, whilst the current M-clip can include a galvanic release mechanism (possibly *via* a degrading bolt in the hinge), we have not yet provided an appropriate float mechanism to help recovery (Lear and Whitney 2016, Whitmore et al. 2016). We note that the combination of fast swimming and a floatation system, which would likely increase the drag, may require increased magnetic forces to hold the system securely on the fin.

Currently, we would advocate that the M-clip seems most relevant to studies on site-faithful sharks such as those species tagged at Oceanografic aquarium in this study (*G. cirratum, C. melanopterus*). The nature of attachment and the ease with which the system can be attached and detached by hand (despite its defined firm hold on the fin) lends itself well to such a scenario. The time taken to deploy this system (a few seconds) is important because it can happen under water on an unrestrained animal with resultant minimized handling stress. Indeed, a large number of sharks could be tagged in a relatively short space of time. This is particularly relevant for controlled lab experiments or aquarium-based studies or monitoring, especially as some aquarium facilities embrace tagging technology for monitoring of animal health and behaviour (e.g. Arkwright *et al.*, 2020). Public-facing aquarium facilities would additionally be keen to avoid physical marks on the animals – as shown, the M-clip marks fade quickly under the current iteration.

4.2 Balancing tag removal forces with tag adherence forces

A central issue in designing tag attachment methods for sharks (and other fish) is how best to minimize the forces that are required to keep the tag in place (the ‘internal’ forces) with the forces that act to remove it (‘external’ forces). Assuming that shark-attached tags have roughly

neutral buoyancy, the external forces take two forms; (i) those forces that result from hydrodynamic pressure (with vertical, horizontal [drag] and lateral components) and will depend on the swim speed of the shark and (ii) forces exerted by the substrate or similar if the equipped shark attempts to rub off the system (see e.g. Table 2.2). In the first case, it is relevant that the drag increases with the square of the swim speed (e.g. Pavlov, Wilson and Lucke, 2007a; Alex Shorter *et al.*, 2014) so the internal forces required to keep the tag in place need to scale accordingly. In this case, assuming that the external forces can be estimated by e.g. CFD models (Kay et al. 2019), the likelihood that these forces result in the loss of the M-clip can be examined. This can be done by effectively combining knowledge of the forces generated by the magnets used and the distances at which they are deployed (Fig. 2.6) and then directly substituting this pull-off force for a push force (generated by their mutual attraction), equivalent to that exerted by the sled and transposed into pressure *versus* the perpendicular force (the putative external force) to cause the contact area to slide over the shark skin (according to direction) (Fig. 2.7). Where the swim speed results in a greater force than that involved in keeping the M-clip in place, the tag is likely to fall off. This can be mitigated by increasing magnet size, reducing the contact area or changing the nature of the contact surfaces within the lever system. The ultimate viability of the system will depend on the likelihood that an equipped shark will swim at speeds that would result in the internal forces not being enough to counteract the external forces. Shark swim speeds range around a norm of 0.09 – 1.06 ms^{-1} (Jacoby et al. 2015) but can regularly exceed that. The mako shark (*Isurus oxyrinchus*), for example, can reach speeds of 20 m/s (Fernandez-Waid et al. 2019) (although some estimates for *I. oxyrinchus* suggest 40 m/s is possible as a maximum speed during burst (Motta et al. 2012)), which would provide a real challenge to any fin-clamp system.

The removal of the M-clip by animals rubbing their fins against the substrate poses a more intractable problem because it is hard to estimate the forces generated. Ultimately though, if

extremely irritated, it is appropriate that sharks should be able to remove tags without damaging themselves and this is the case with the M-clip, in marked contrast to some other systems such as through-the-fin bolt systems (Whitmore et al. 2016). There may be a delicate balance between applying the right amount of retention force by the magnets and allowing the system to drop off, but I do note that the magnet system can be constructed to err on the side of caution with regard to animal well-being.

4.3 Potential effect of magnetism

Many elasmobranch species can detect electric and magnetic fields through a sensory network located in the head (Kalmijn 1973, 1982, Peters et al. 2007, O'Connell et al. 2010) so that the use of a powerful neodymium boron magnet might disrupt navigation and/or detection of prey (O'Connell et al. 2010, Smith and O'Connell 2014, Anderson et al. 2017). However, I believe that deployment of our magnet-based clip is unlikely to adversely affect any of these key behaviours.

Firstly, magnetic field strength diminishes as a squared function of distance from the magnet (Barnothy 1965), so magnetic drop-off will be rapid with increasing distance from the dorsal fin. The largest NdFeB magnets used here (on *R. typus* deployments) measured 25 mm diameter × 5 mm thickness. Even for these, the measurable magnetic field produced would fall to < 0.65 Gauss (the upper limit of the Earth's detectable background magnetic field) at a distance of 0.2 metres and to effectively 0 Gauss at a distance of 1.05 metres. Equivalent distance for the smaller magnets used on the other species scale accordingly so it is thus extremely unlikely that the head-based sensory organs will be interfered by any dorsal fin-associated magnets.

We note that other studies investigating the use of magneto-sensory perception in elasmobranchs have gone so far as to mount much larger (120 × 30 × 30 mm) NdFeB magnets directly on the head of sandbar sharks (*Carcharhinus plumbeus*) (Anderson *et al.*, 2017), reporting that, despite inhibiting location of conditioned magnetic stimuli, normal swimming and feeding behaviour remained. Given this information, alongside observations during my own M-clip aquarium trials, there is good evidence that the magnets will not interfere with behaviour, social interactions or locomotion of sharks. In the aquarium experiments, *G. cirratum*, which often congregates on the substrate, continued to do so with no observable effects on conspecifics. I recommend, however, that researchers employing magnet-based attachment systems keep this in mind when deciding on deployment lengths, magnet sizes (using magnets that are no bigger than they need to be) and in interpretations of behaviour.

4.4 A framework for developing minimally impactive tags for sharks

It is clearly time to stop thinking of tags simply as 'boxes' (Kay et al. 2019). The importance of understanding effects and consequences of hydrodynamic forces, including drag, lift and pressure, on marine animal tag attachments has been extensively discussed (Bannasch et al., 994; Watson and Granger, 1998; Healy et al., 2004; Jones et al., 2013) although recognition of this is not always apparent in field studies. The critical implication is that increased hydrodynamic loading likely leads to increased energy expenditure that will have consequences for efficiency – should long term deployments be considered (and more than the deployments of a few days as in this study), there may well be implications for growth and survival (Thorstad et al., 2001; Ropert-Coudert and Wilson, 2005; Ropert-Coudert et al., 2007; van der Hoop et al., 2014; Lear et al., 2018), as well as compromising the quality, interpretation and extrapolation of the data. To apply these hydrodynamic principles to data-driven tag design,

minimising the need for animal-borne testing through multiple design stages, a number of authors have employed Computational Fluid Dynamics (CFD) (Shorter et al. 2014, Fiore et al. 2017, Kay et al. 2019). CFD is a powerful tool for simulating fluid flow across a modelled surface and can be used to evaluate hydrodynamic loading on tags (Shorter et al. 2014, Fiore et al. 2017, Kay et al. 2019).

It is also important, however, to consider the complete tag-animal profile in these circumstances. The effect of 'unbalanced' forces acting on the tag through a design that is not bilaterally symmetrical for lateral forces, for example, is rarely discussed, particularly for elasmobranch and cetacean tags. Designs might be streamlined to reduce the hydrodynamic force of drag acting on it but may still, however, generate lift (or negative lift) or uneven lateral forces which may impact the animal carrier. This is particularly problematic for high speed animals moving through a fluid (whether air or water), which are strongly selected to reduce the effect of such physical forces on unnecessary energy expenditure (Gleiss, Jorgensen, et al. 2011, Gleiss et al. 2019). Several studies have considered the complete profile when designing cetacean (Pavlov et al., 2007a; Pavlov and Rashad, 2012) and pinniped (Hazekamp *et al.*, 2010; Kyte *et al.*, 2018; Kay *et al.*, 2019) tags. Notably the studies of Pavlov et al. (2007) and Pavlov and Rashad (2012) simulated water-flow forces on dolphin dorsal fin-mounted designs, incorporating an aero foil-style design to secure the tag using fluid negative lift forces so that as animal speed increases, so too do the retention forces (though this strategy relied almost exclusively on the forward motion of the animal). Kay et al. (2019) used a CFD approach to quantify the importance of tag hydrodynamics on seals, noting the substantial effects of tag size and where it is positioned on the animal.

Consideration of unbalanced forces is particularly critical for fin-based attachments to sharks due to the dorsal fin's stabilizing role in locomotion (Lingham-Soliar 2005). Whilst Bouyoucos et al. (2017) did show that double-tagging (i.e. a tag on each side of the fin) altered locomotion

and activity in Lemon Sharks (*Negaprion brevirostris*) more so than just a single dorsal tag, the tag packages themselves were not streamlined so the predominant effect of the double tagging was to double the, presumed appreciable, drag. In fact, the authors do attribute surface area and greater buoyancy as causes of the tag effects. Unbalanced tag forces would demand greater closing/clamping forces from tag attachments, creating a greater risk of fin damage. Therefore, the entire processes of (i) drag and (ii) overcoming this with closing forces should be thought of as an integrated consideration. We also note that the degree to which drag forces should be considered will vary with species (i.e. their average swimming speed) but also variations in water speed (pelagic *vs* coastal, for example). A full comprehension of the target species and deployment conditions are therefore crucial to effective M-clip design and modification.

The technologies used here have been employed previously in animal movement studies, although usually individually, including 3-D printing (Williams et al. 2015, Gleiss et al. 2019), 3-d scanning of animal geometries (Takagi et al., 2013) and CFD (Hazekamp, et al., 2010; Pavlov and Rashad, 2012; Alex Shorter et al., 2014, Kay et al., 2019). However, they have not, to our knowledge, been combined into one design and deployment process of tags. Tagging design should be approached in such a manner that all forces and components are considered equally and as part of one unified process and we suggest a framework that makes the various elements explicit (Fig. 2.10). Combining this with an iterative testing process, with designs refined through a comprehensive combination of controlled tests, open water deployments and computational simulations, should be a priority. Current clamp systems are generally used in a ‘one-size-fits-all’ manner regardless of species shape, size or movement characteristics. The CAD and 3-d printing approach allows alterations of the M-clip tailored to the target species, particularly when combined with accurate 3-d scans of the target area that can be simulated with CFD to create a holistic view of acting forces for that species under particular conditions.

In addition, CAD allows designs to be easily altered to accommodate almost any tag unit or other system such as VHF and acoustic transmitters, or external speed sensors – although care must be taken that any modification which might alter the hydrodynamic profile and internal force distribution is tested and quantified accordingly.

The use of 3-d scanning for this study is limited, with the dorsal fin from just one shark species scanned and digitized here. For future work, it will be important to obtain scans of a range of other species and, within that, individuals of different sizes to fully realise the technology's potential in designing custom-fit tags for different species. However, possession of the *P. glauca* dorsal fin scan alone, and simple assumptions of linear scaling with shark body size, greatly helped the design of the final M-clip iteration as it allowed estimation of fin dimensions through its complete length and will be a model for use in CFD simulations. Indeed, with regard to the latter point, having such a high resolution (state resolution) model allowed us to take as much or as little detail as needed.

We have sought to consolidate the findings, and the design and testing considerations, outlined in this section into a tag-design framework for elasmobranchs (Fig. 2.10) for future work.

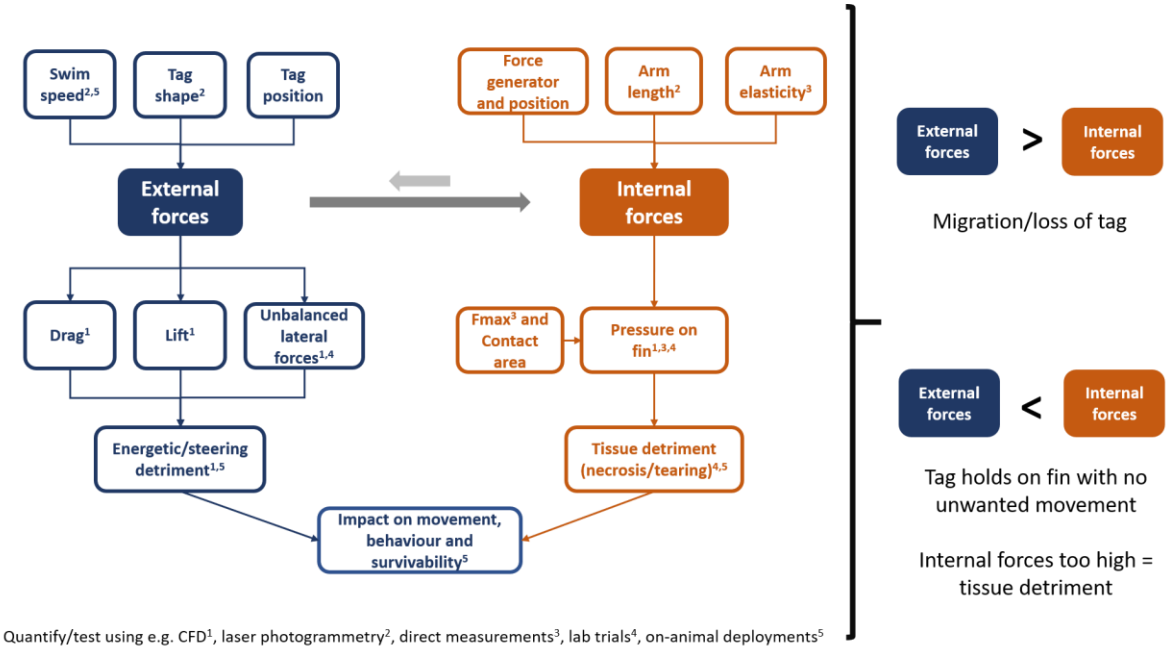

Figure 2.10: Schematic framework to illustrate considerations in tag design (including attachment) for a fin clamp for sharks. The tag shape, tag placement on the fin/body and swim speed all affect the external forces, which can be separated into lift, drag and unbalanced lateral forces. For the system to remain stable on the shark, the 'internal' forces holding the tag in position must be greater than these external forces at all times. The internal forces depend on the force applicator (e.g. spring, magnet) and its position and the arm length. The pressures on the fin depend on the forces and the area in contact with the fin, itself dependent on the Fmax between the material in contact with the fin and the skin. Note that bolts through the fin do not exert lateral pressure in the same way but rather exert longitudinal pressure on the posterior section of the hole as a result of the tag drag and the surface area acting on that posterior surface. External forces can influence the internal forces – for example by drag modulating pressure onto the fin – and, to a lesser extent, *vice versa* – for example by the arm lengths and force generator position influencing tag shape.

4.5 Conclusions

Researchers attaching tags to birds have noted important consequences of tag position, mass and drag on behaviour and survival metrics (e.g. Chivers, Hatch and Elliott, 2015). Such effects

manifest differently and with variable severity according to tag position on the body (Vandenabeele et al. 2014) as well as species (e.g. Thaxter *et al.*, 2016) with consequently a move towards more taxon-specific tags (for example, leg-loop harnesses for raptors (Harel et al. 2016) vs. necklaces for game birds (Hagen et al. 2006), or how flatter, side-mounted tags are better in fusiform fish species compared to saddle-like mountings (Jepsen et al. 2015) that might best suit other fish species). Given that sharks also operate within a fluid medium and are exposed to many of the same types of forces as birds, most notably drag, lift and lateral forces, it would seem time for elasmobranch researchers to move towards this approach also. This would improve animal well-being and, with it, increase the likelihood of meaningful, accurate data (Wilson and McMahon 2006).

Chapter 3:

On the benefits of captive setting for observing aberrant behaviours due to external tag attachment in sharks

Abstract

Externally attached devices on animals are likely to affect their movement and behaviour to some degree. Efforts to mitigate these effects at the design stage are crucial to ensuring the health of the animal and maximizing the usefulness of the data gathered. In the case of marine animals, new devices are often tested on free-living species. This makes observation and contextualisation of any aberrant, tag dislodgement behaviours difficult. We tested a novel tag attachment method on 3 shark species; Nurse sharks (*Ginglymostoma cirratum*), Blacktip reef sharks (*Carcharhinus melanopterus*) and the Bowmouth guitarfish (*Rhina ancylostoma*) in captivity at the Oceanografic Aquarium, Valencia, Spain, and observed them while also recording their tag-recorded responses using commonly employed movement metrics (tail-beat frequency, Vectorial Dynamic Body Acceleration [VeDBA] and dive rate). Although the tag-derived metrics initially suggested little tag detriment, visual observation identified several aberrant, fleeting behaviours assumed to be efforts to remove the tag, notably chafing in Nurse sharks and shaking in Blacktip sharks. Once observed, particular visualisations of the tag data, such as *g*-spheres and the Boolean search functions, found these transient behaviours and indicated their persistence even hours after initial tagging. These tools also identified chafing behaviour in the Guitarfish, although we did not observe it. Captive animals can therefore help identify aberrant behaviour both within captivity as well as providing a template for wild animals.

1. Introduction

Electronic tagging has greatly increased our knowledge of shark movement ecology and behaviour, informing policymaking and conservation decisions world-wide (e.g. Chapman, et al., 2015; Sims, et al., 2005). This tagging is usually achieved *via* externally attached tags, commonly by anchors into the skin (e.g. Musyl, Domeier, et al. 2011) or fin-based clamps (e.g. Chapple et al. 2015). External systems have some advantages over internally implanted tags (e.g. Broell, Burnell, & Taggart, 2016; Feldheim, Gruber, De Marignac, & Ashley, 2002), including that they are less invasive and easier to recover as well as generally necessitating a shorter contact duration with researchers during deployment. Against this, external tag attachments disrupt an animal's hydrodynamic profile (Bouyoucos et al., 2017; Kay et al., 2019) and can alter buoyancy (Bouyoucos et al. 2017, Lynch et al. 2017). This may consequently increase energetic demands by way of decreased swimming efficiency (Lear, Gleiss, & Whitney, 2018; Lynch et al., 2017).

Generally, workers are aware of potential deleterious effects, and, where possible, attempt to quantify tag effects by visual observation and/or the use of behavioural data from the attached sensors noting, for example, the severity of the immediate reaction to tagging. For example, responses can be categorised into 'strong' (e.g. thrashing, immediate movements away from the area), 'mild' (e.g. changes in movement speed or direction) or 'no reaction' (Fontes et al., 2017; Gleiss et al., 2009). The most common tag sensor information used to infer elasmobranch post-tagging reaction is tail-beat frequency (TBF), calculated by peak detection in the 'sway' (side-to-side) acceleration (e.g. Gleiss et al., 2009; Lynch et al., 2017), and the rate and magnitude of vertical movement (e.g. Fontes et al., 2017). These metrics can show an initial post-tagging escape reaction of increased TBF and deeper, faster dives, followed by a gradual 'normalising' where the TBF slows and depth changes are less erratic, with no further

significant change after a given time period (Bullock et al., 2015; Chapple et al., 2015; Gleiss et al., 2009). The normalising in these behaviours would be considered a habituation to the tagging procedure and the tag itself.

Beyond any initial visual observation phase, identification of negative impacts of a tag relies not only on data from tag sensors but, implicitly, on knowledge of what data correspond to aberrant behaviour (Brown et al., 2013). Here, acceleration data can be equivocal. For example, an attempt by a shark to remove a tag might take the form of 'chafing' (scraping the dorsal side against the sand (Myrberg and Gruber 1974, Bullock et al. 2015)) but, without observation, this might be confused with rolling that occurs during mating behaviour (Whitney et al., 2010; c.f. Broell, Burnell, & Taggart, 2016 & Collins et al., 2002;). Metrics such as TBF may indicate short term reactions well (Gleiss et al. 2009) but not always be suitable on their own in identifying aberrant swimming behaviour related to tagging. This is because the complexity of fish swimming may be lost and not necessarily show critical physiological efforts to compensate (Bouyoucos et al. 2017). However, the more extensive (in both quality and quantity) the information on shark behaviour, the more completely we will be able to examine potential tag effects (Hoolihan et al. 2011).

Here, we highlight the benefits of using a captive environment for understanding the behavioural effects associated with tagging elasmobranchs. Three species – *Ginglymostoma cirratum* (Nurse shark), *Carcharhinus melanopterus* (Blacktip reef shark) and *Rhina ancylostoma* (Bowmouth guitarfish) - were tagged during testing of a new fin-mounted attachment system (the M-clip: see chapter 2) on captive sharks at Oceanografic Aquarium, Valencia, Spain. We found that each of the species displayed at least one aberrant behaviour post-tagging, which would otherwise be difficult to discern from recorded tag behaviour alone. We also report that swimming behaviour metrics often used to examine a shark's reaction to tags (i.e. TBF, dive profile) may give a false impression of the animal's apparent acceptance

of the tag, particularly when these metrics are used in isolation without the benefit of visual observation.

2. Materials and Methods

2.1 Subject species, tagging procedure and observation

All visual observation and sensor data were collected during testing of a fin-mounted tag-attachment system for elasmobranchs, called the M-clip (see Chapter 2 for a full description of the M-clip). Data were collected over a period of two weeks in November 2019 at Oceanografic Aquarium, Valencia, Spain.

Three species of shark were tagged; *Ginglymostoma cirratum* (the Nurse Shark), *Carcharhinus melanopterus* (the Blacktip Reef Shark) and *Rhina ancylostoma* (the Bowmouth Guitarfish). They were chosen based on their accessibility in the aquarium- in terms of both the tagging procedure and subsequent observations- and the shape and profile of their fins (i.e. those that seemed most appropriate for a dorsal fin-mounted tag). *G. cirratum* and *R. ancylostoma* were housed in the same primary tank (an oval of approx. 90 m length, 30 m width, 6 m depth, with a circular column each end and an overhead walkway linking the columns, for a total volume of 7 million litres) with various other shark, fish and ray species. *C. melanopterus* were housed in a sectioned-off area of the tank (approx. $1/8^{th}$ the size of the large tank). All attachments were conducted by trained veterinary and aquarium staff. *G. cirratum* had been trained to be equipped with a fin-mounted attachment prior to these experiments by having them swim through a shallow (< 1 m) netted area to receive food whilst being exposed to physical pressure to their fins. Tags were attached to *G. cirratum* during feeding (which took place at approx. 15h each day), requiring brief restraint by holding the fin and body. *G. cirratum* (4 individuals; 2 male and 2 female) were tagged over 7 deployments. *C. melanopterus* (2 individuals; 1 male and 1 female) were tagged across 3 deployments through brief restraint – divers entered the tank and caught the individual to be tagged with a hand net, before bringing the shark to a floating platform where the shark was briefly held (its eyes covered by wetted neoprene) and

the tag attached. *R. ancylostoma* was also tagged (2 deployments on 1 male) by diver capture using hand nets, before being brought to a shallow medical pool adjoining the main aquarium tank. Divers held the *R. ancylostoma* at the water's surface after inducing tonic immobility so that the tag could be attached. The animal was then observed (to ascertain good tag attachment and orientation) for ~30 minutes before being allowed back to the connected, main aquarium. Details of each deployment can be found in Table 3.1. The duration for each deployment lasted for as long as the M-clip remained on the fin before falling off except for *G. cirratum*, individual 1, deployment 2, which was removed by hand.

Table 3.1: Duration of every tag deployment (min) used in this study according to species, individual and deployment number on that individual.

Species	**Individual**	**Deployment number**	**Duration of tag attachment (min)**
Ginglymostoma cirratum (Nurse shark)	1	1	31
		2	1352
	2	1	758
		2	34
	3	1	448
	4	1	35
		2	50
Carcharhinus melanopterus (Blacktip reef shark)	1	1	145
		2	23
	2	3	1308
Rhina ancylostoma (Bowmouth guitarfish)	1	1	683
		2	704

Tagged sharks were directly observed immediately following attachment and then opportunistically between 0800h and 1900h. Shark movements were recorded using voice and/or video recordings, noting any behaviour that might be considered a reaction to the attached tag. Untagged sharks were similarly observed opportunistically, and their behaviours and tail-beat frequencies recorded. Due to limited numbers of individuals available for tagging, all 'untagged' individuals had, at some point, also been tagged during the two-week period. All observations were made from either the walkways directly above the tanks, or from the public visitor viewing areas beneath the water's surface. For tail-beat counts of untagged individuals, only observations of at least 30 continuous seconds were used and lasted until the individual was out of sight. Tail-beat counts were scaled to a per-minute observation. A total of 38.5 (N = 35 separate observations) minutes of untagged observations were collected for *G. cirratum*, as well as 39.1 minutes (N = 24 observations) for *C. melanopterus* and 11 minutes (N = 13 observations) for *R. ancylostoma*.

2.2 Tags and software

The activity of tag-equipped sharks was recorded using Daily Diary ('Elongated' model; Wildbyte Technologies Ltd, UK) archival tags (hereafter 'DD'). Each DD recorded tri-axial acceleration (surge, heave and sway) at 40 Hz and pressure (0-30 bar operating pressure with a 50 mbar accuracy; TE Connectivity). As the aquarium was primarily underground and built with a large amount of ferrous material, tri-axial magnetometry was not used. Each DD and attached battery (750 mAh, 3.6 V; EVE Energy Co., China) was housed within a custom-machined acrylic plastic housing and mounted to the side of the experimental attachment.

Movement data from the DD units was extracted and initially analysed and behaviours determined using DDMT software (Wildbyte Technologies, UK). Subsequent analysis was conducted in R (version 3.6.1).

2.3 Data analysis and behaviour identification

Acceleration data were initially smoothed over 0.5 seconds and pressure by 0.25 seconds, both windows being chosen to eliminate noise in the data. Tag dislodgement behaviours were first identified within DDMT by pairing with observation data, before using characteristics in the data channels to create Boolean-based behaviour classifiers (Wilson, Holton, et al. 2018) to find other likely instances of these behaviours (see Appendix 3 for the exact rules/parameters used). These behaviours were 'rolling' in *G. cirratum* and 'shaking' in *C. melanopterus.* To investigate the utility of rules across species when behaviours were not directly observed, the rolling behaviour rules were also applied to the *R. ancylostoma* data. All data were further examined as *g*-spheres (tri-axial spherical plots of the smoothed acceleration data (Wilson et al. 2016)) to validate the success of rules by looking for characteristic 'fingerprints' for behaviours in the plots – in particular, loops in the case of rolling/chafing, or VeDBA spikes away from the *g*-sphere surface in the case of whole-body shaking. The *g*-sphere visualisations were found, for instance, to help the researcher determine rolling *vs* other unusual swimming movements (e.g. when a shark was trying to enter the feeding net in the case of *G. cirratum*). Data that tested negative or positive against the behavioural rules used in the Boolean algorithms could further be classified as (i) *true* or *false* and, based on whether the behaviour or period was actually observed or only inferred from fingerprints in the data, (ii) *assumed* or *known* (see Table 3.2 for an explanation of the terms). Measures of precision and recall were then calculated according to Reshef *et al* (2014) and Wilson *et al* (2018) using;

(1) $Precision = True\ positives/(True\ positives + False\ positives)$

(2) $Recall = True\ positives/(True\ positives + False\ Negatives)$

Table 3.2: Explanation of classification of periods of data to validate a Boolean behaviour identifier. ‘TP, K’ = True Positive, Known (correctly flagged by the software as the behaviour of interest, verified with observation); ‘FN, K’ = False Negative, Known (not flagged, but known to be one from observation); ‘FP, K’ = False Positive, Known (incorrectly flagged, verified from observation); ‘TP, A’ = True Positive, Assumed (not observed, but flagged and judged correct by manual data inspection); ‘FP, A’ = False Positive, Assumed (not observed, but flagged and judged incorrect by manual data inspection). ‘FN, A’ = False Negative, Assumed (not observed and not flagged, but judged to be the behaviour of interest through manual data inspection). ‘Y’ and ‘N’ denote ‘Yes’ and ‘No’ respectively.

Visually observed period?	**If observed, did the behaviour happen?**	**Did the software flag as positive?**	**Given data inspection, was software correct?**	**Decision**
Y	Y	Y	-	TP, K
Y	Y	N	-	FN, K
Y	N	Y	-	FP, K
N	-	Y	Y	TP, A
N	-	Y	N	FP, A
N	-	N	N	FN, A

TBF, dive rate and VeDBA were calculated for the duration of each deployment, to contextualise the presence, or absence, of aberrant behaviours and determine how well these metrics capture tag effects when used alone. For TBF, a Boolean function was written to identify peak to peak intervals in the sway (side-to-side) acceleration axis. As this peak to peak interval would include two individual tail-beats (i.e. caudal movement to a maximum point on each side of the body midline), the count of identified tail-beats was doubled and then expressed in tail-beats per minute. To compare dive rates, depth readings were thinned to once every 5 seconds and dives were considered to be negative depth changes of at least 0.5 metres. This definition reflects the relatively shallow water depth available to the individual. The mean Vectorial Dynamic Body Acceleration (VeDBA) (Qasem et al. 2012), a proxy of energy expenditure, was calculated per minute using a 3 second acceleration smoothing window to separate the static from dynamic acceleration components (Shepard et al., 2008). As the goal was to infer swimming effort as a result of tag presence, only periods of active swimming were used. As *C. melanopterus* and *R. ancylostoma* trials used only 2 and 1 individuals, respectively, simple means of the data for different time periods (the first 0-5 minutes, the first 5-30 minutes and all data overall) were calculated (since *R. ancylostoma* was initially kept and observed in a small medical pool where movement is limited, minute '0' was considered the time of release into the larger main tank).

Changes in the TBF for *G. cirratum* were assessed for the 30 minutes immediately following tag attachment (because each deployment ran for at least this long) by constructing a Linear Mixed Model (LMM) with the lme4 R package (Bates *et al*., 2015). TBF was included as a response variable, with fixed effects of time and repeat number (i.e. the first or second time the individual had been tagged) and individual as a random effect. The effect of individual was a random slope by time. Both the fixed and random effect instances of time were scaled (using the 'scale( )' function in R) to resolve warnings of non-convergence. A second LMM was also

created to assess the change in the VeDBA over this period, using the same model as for TBF but swapping TBF for VeDBA. For all constructed LMMs, model residuals were examined visually using QQ-plots, histograms and residual plots. Significance of the effect of the fixed factor was determined by log-likelihood ratio test. Marginal R-squared (R^2_m) and conditional R-squared (R^2_c) were calculated in the R MuMIn package.

3. Results

3.1 Common measures of tag reaction

G. cirratum individuals all exhibited similar physical responses to the attachment of the tag – some initial thrashing during the positioning of the tag and an apparent effort to leave the training feeding net. However, all individuals made quick and consistent returns to the feeding area and regularly returned into the feeding net several times. *C. melanopterus* showed the most severe immediate reaction to tagging, diving to the bottom of the tank for a few minutes before spending the rest of the deployment swimming 1-2 metres from the surface. *R. ancylostoma* spent most of the initial deployment period at the bottom of the shallow medical pool and resumed swimming at the bottom of the main tank upon release.

Summary data for TBF, VeDBA and dive rate are presented in Table 3.3 and in Figures 3.1, 3.2 and 3.3. Whilst TBF increased to varying degrees for the first 30 minutes of tag attachment, the mean TBF for all tag data was very close to that of untagged individuals (gleaned from observational data). Despite a significant increase in TBF over the first 30 minutes in *G. cirratum* ($R^2_m = 0.20$, $R^2_c = 0.35$, $p < 0.05$), this increase was small (0.26 beats per min ± 0.09, t = 2.74 check this) and followed by a clear plateau (for the three individuals with enough data) for at least the following 60 minutes (slopes = 0.16, 0.10 and -0.004).

Mean VeDBA changes in the initial tagging period were negligible for all 3 species. Indeed, the LMM for *G. cirratum* showed no significant change in the first 30 minutes ($R^2_m = 0.07$, $R^2_c = 0.26$, $p = 0.73$), with values remaining consistent (for the three individuals with enough data) for the periods of 0 – 5, 5 – 30 and 30 – 90 mins after deployment (mean ± sd = 0.19 ± 0.07, 0.19 ± 0.06 and 0.18 ± 0.06, respectively).

Table 3.3: Summary data of common metrics by which to measure tag effect for each species, separated into time periods. Note that '0-5' and '5-30' minutes refer to time since attachment for *G. cirratum* and *C. melanopterus*, but for *R. ancylostoma* refers to time since release into the main pool. Note that *R. ancylostoma* undertook only a single 'dive' in minutes 0 – 5. Dive data for *C. melanopterus* includes only 2 deployments, both on a female, due to a pressure sensor malfunction for the male deployment.

Species	**Measure**	**Untagged mean (TBF only)**	**Overall mean (all tag data; ± sd)**	**0 – 5 minutes mean (± sd)**	**5 – 30 minutes mean (± sd)**
Ginglymostoma cirratum (nurse shark)	TBF (beats/min)	54.93 ± 4.98	53.14 ± 12.16	55.43 ± 6.05	59.85 ± 6.18
	VeDBA	-	0.19 ± 0.07	0.19 ± 0.06	0.18 ± 0.06
	Dive rate (m/s)	-	0.16 ± 0.08	0.17 ± 0.29	0.14 ± 0.16
Carcharhinus melanopterus (blacktip shark)	TBF (beats/min)	84.62 ± 8.42	85.84 ± 7.83	94.13 ± 13.26	100.18 ± 9.71
	VeDBA	-	0.05 ± 0.03	0.08 ± 0.14	0.05 ± 0.04
	Dive rate (m/s)	-	0.14 ± 0.09	0.21 ± 0.17	0.11 ± 0.01
Rhina ancylostoma (bowmouth guitarfish)	TBF (beats/min)	54.90 ± 6.08	54.94 ± 10.04	60.8 ± 7.96	55.96 ± 6.38
	VeDBA	-	0.13 ± 0.10	0.11 ± 0.04	0.11 ± 0.06
	Dive rate (m/s)	-	0.19 ± 0.08	-	0.19 ± 0.07

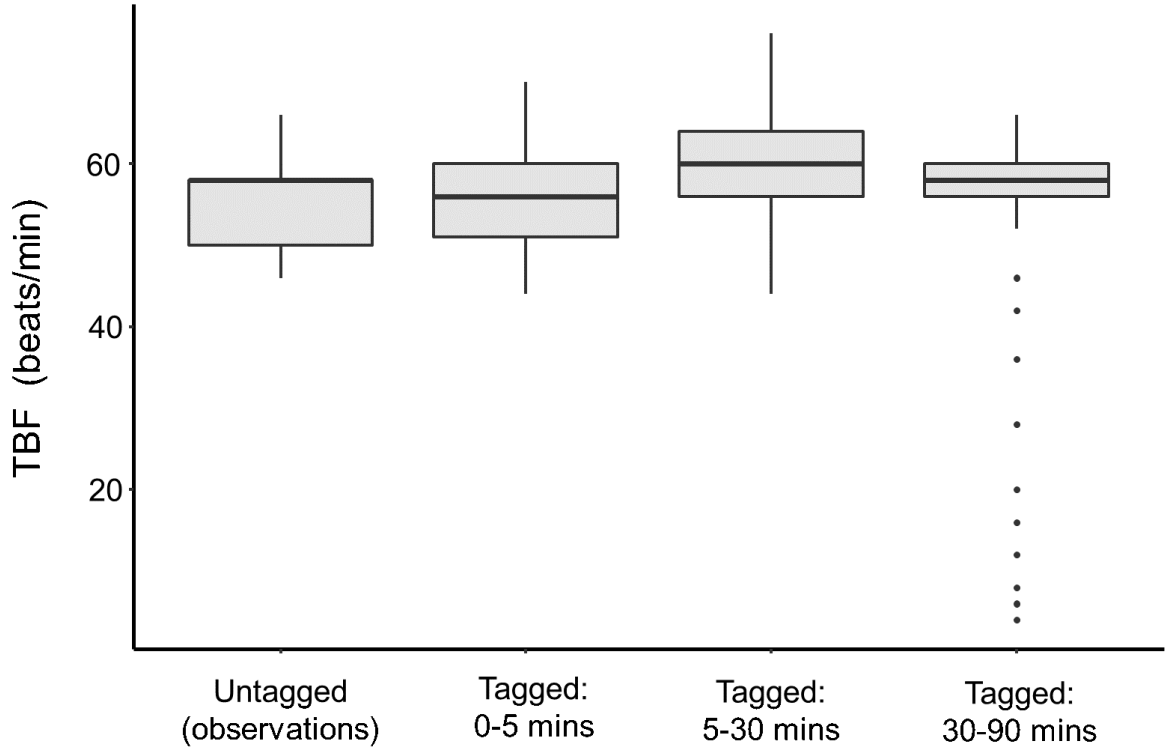

Figure 3.1: Box-whisker plot (bold horizontal lines show the median value, box limits are the 25th and 75th percentiles, whiskers extend to the smallest and highest value to a maximum of 1.5 x the interquartile range and any points beyond the whiskers are outliers) of *G. cirratum* tail-beat frequency (beats/min) for both untagged and tagged individuals, with tagged data further grouped into 0-5 mins, 5-30 mins and 30-90 mins from the time of tag attachment. Untagged counts are taken from individual observations lasting at least 30 seconds (n = 35 observations of 4 individuals). '0-5 mins' and '5-30 mins' data are from N = 7 deployments on four individuals (n = 35 and 175, respectively). '30-90 mins' are from N = 3 deployments on three individuals (n = 170).

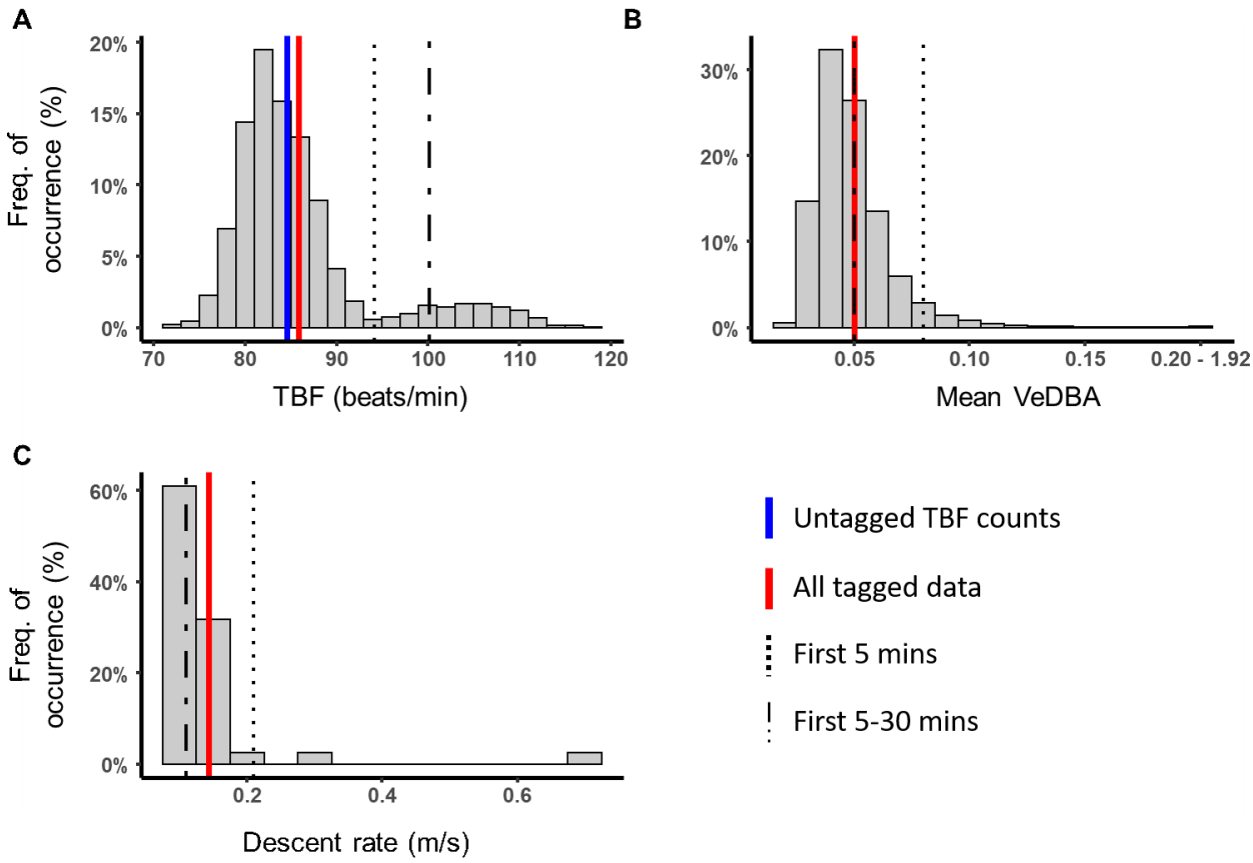

Figure 3.2: Frequency distributions of (A) tail-beat frequency (beats/min), (B) mean VeDBA during swimming (i.e. per tail-beat) and (C) descent rate (metres/second) of two *C. melanopterus* over 3 deployments (1 male, 2 female). Vertical bars indicate mean values for either all gathered data (solid red), the first 5 minutes of tag deployment only (dotted black), the first 5-30 minutes of tag deployment only (dot-dashed black) or untagged TBF counts (blue). Note that in B the dot-dashed line occupies the same value as the red line. Descent rate was only calculated for the female deployments due to a malfunctioning pressure sensor with the male deployment.

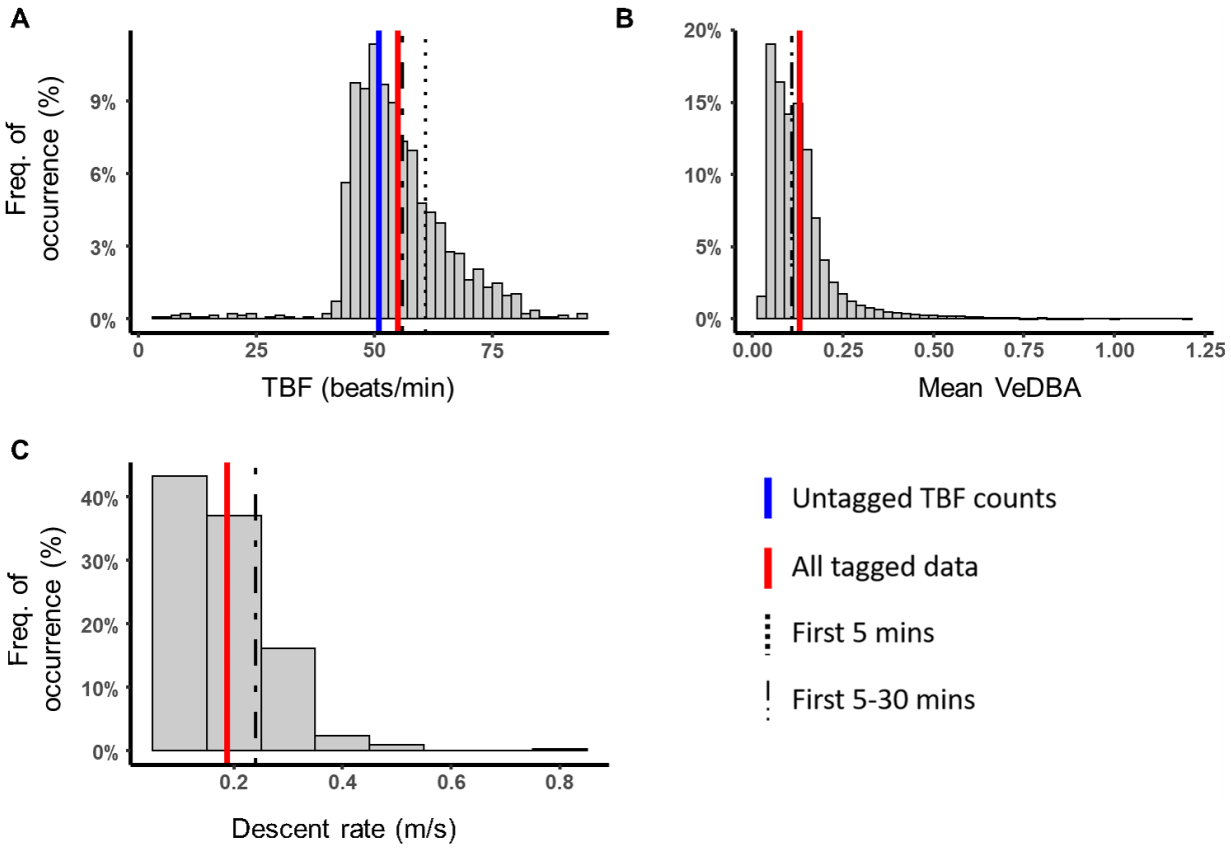

Figure 3.3: Frequency distributions of (A) tail-beat frequency (beats/min), (B) mean VeDBA and (C) descent rate (metres/second) of one Bowmouth guitarfish (*R. ancylostoma*) over 2 deployments. Vertical bars indicate mean values for either all gathered data (solid red), the first 5 minutes of tag deployment only (dotted black), the first 5-30 minutes of tag deployment only (dot-dashed black) or untagged TBF counts (solid blue). Note that the dotted line is absent in C as there was only 1 dive of sufficient depth/rate.

Dive rates similarly remained consistent over time, although blacktip dive rates in the initial 5 minutes were approximately double the overall mean.

3.2 Aberrant behaviours

3.2.1 *G. cirratum* chafing

Thirty-two chafe events by *G. cirratum* across 7 deployments were identified by the DDMT Boolean behaviour function. Visual observations showed these occurred when the fish rolled to scrape their fins along the floor of the tank. *G*-sphere visualisations suggested a characteristic 'loop' about the z (heave) axis, commonly at a depth of ~ 6 m (the depth of most of the main tank, although some areas had a slightly shallower depth) (Fig.3.4). Of the 32 chafing events, 7 were known true positives, 1 was a known false positive, 23 were assumed true positives and 1 was an assumed false positive. An additional 6 chafing events were added manually to the list of counted behaviours (1 known and 6 assumed false negatives) resulting in a total of 36 chafing events across 8 deployments. Thirty-two of these chafe events came from 3 individuals (those with the longest tag attachment duration). Mean duration of the final tally of chafe events was 6.10 seconds (± 2.76 sd). The earliest and latest chafe events occurred 15 mins and 21 hrs 2 mins, respectively, following attachment. Precision and Recall were both 87.50 % for known (observed) events only, rising to 93.75 % and 83.33 % when 'assumed' events were included following manual inspection of the data.

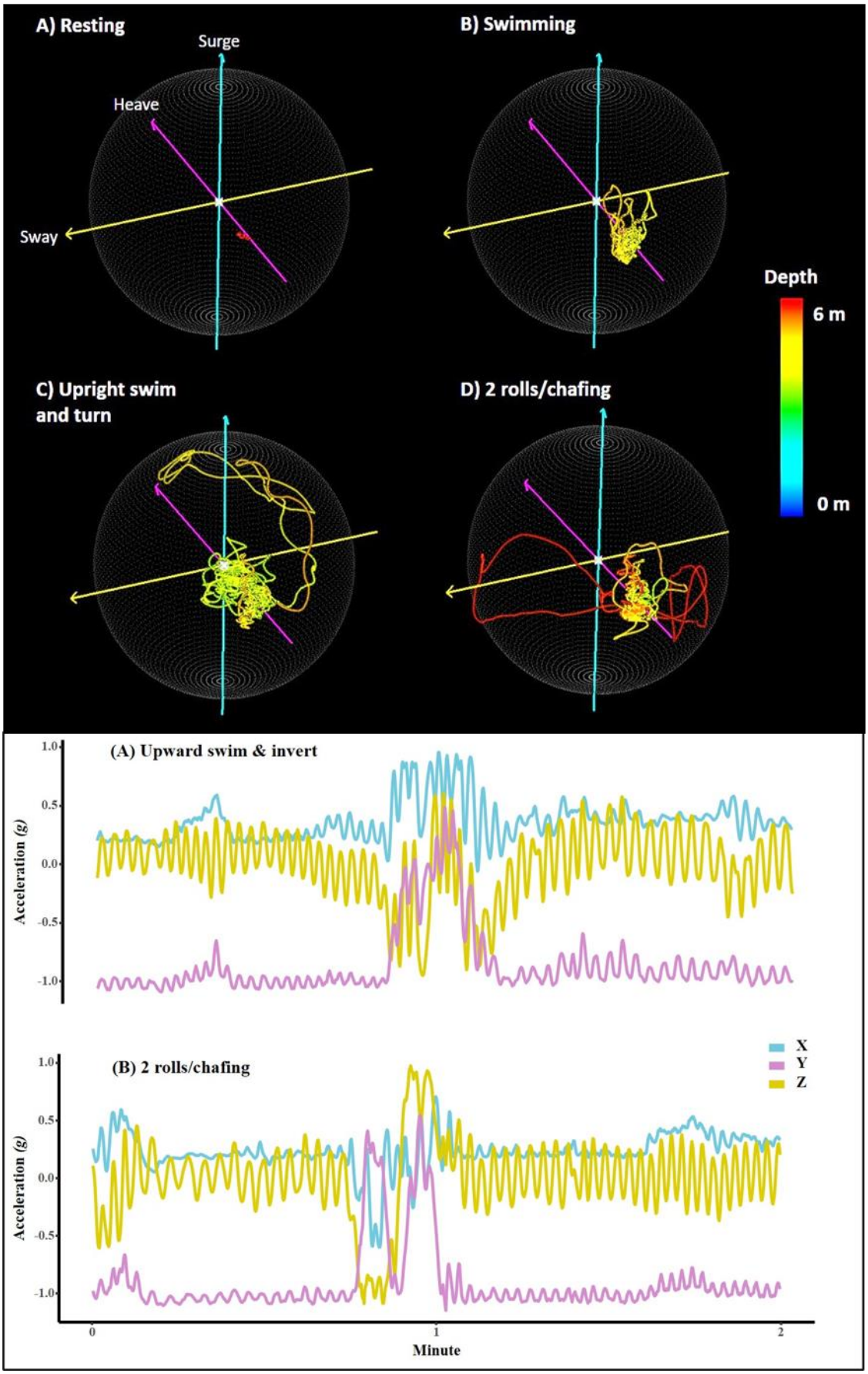
A) Resting
Surge
Heave
Sway
B) Swimming
Depth
6 m
0 m
C) Upright swim and turn
D) 2 rolls/chafing
(A) Upward swim & invert
Acceleration (g)
1.0
0.5
0.0
-0.5
-1.0
(B) 2 rolls/chafing
X
Y
Z
0
1
2
Minute

Figure 3.4: *Top:* G-spheres showing 3-axis acceleration data of *G. cirratum* (projected *via* a tri-axial plot onto a sphere - cf. Wilson et al., 2016 and coloured by depth in the aquarium/water. The sphere surface corresponds to a vectoral sum of the static acceleration (1.0 *g*). All data are taken from the same deployment on the same individual, and each *g*-sphere shows 5 minutes of data. **(A)** Resting at the bottom of the tank (i.e. no dynamic movement), **(B)** Regular, steady swimming, **(C)** A vertical period of swimming after which the shark briefly inverts as it turns away from the tank wall, **(D)** Two (one to the left and one to the right) roll events with chafing (presumed an effort to remove the tag). Note how the rolling clearly occurs at the bottom of the tank (~6 m depth; coloured red).

Bottom: Acceleration data, smoothed using a window of 0.5 seconds, showing the same upward swimming **(A)** and rolling **(B)** behaviours depicted in the last two *g*-spheres (but cut down to 2 minutes of movement data only, to highlight the particular behaviour). Note the similarities in traces between the two (upward spike in the heave axis and a dip in the sway axis) that would make it difficult to distinguish the behaviours relying on visual inspection of the data only. Note that tag orientation for this individual means that the Y (heave) axis is inverted.

3.2.2 *C. melanopterus* body shaking

Twenty-three shaking events by *C. melanopterus* across 3 deployments were identified by the DDMT Boolean behaviour function. Visual observations showed these to be marked by sudden, twisting side-to-side movement and often followed by quick swimming. *G*-sphere visualisations showed that elevated VeDBA was a good marker for these events (Fig. 3.5). Of these 23 events, 7 were known true positives, 15 were assumed true positives and 1 was a known false positive and thus removed – leaving a final total of 22 shaking events. Mean duration of these shaking events was 2.00 seconds (± 0.70 sd). The earliest and latest shaking events occurred 0.03 mins and 21 hrs 48 mins, respectively, following attachment. Precision and Recall were 87.50 % and 100.00 %, respectively, for known (observed) events only and 95.45 % and 100.00 % when 'assumed' events were included.

In addition to burst shaking, the female blacktip was also observed to leap out of the water on one occasion, twisting/rolling upon landing. This is clearly visualised in a *g*-sphere format (Fig. 3.5). No other instances of this behaviour were observed.

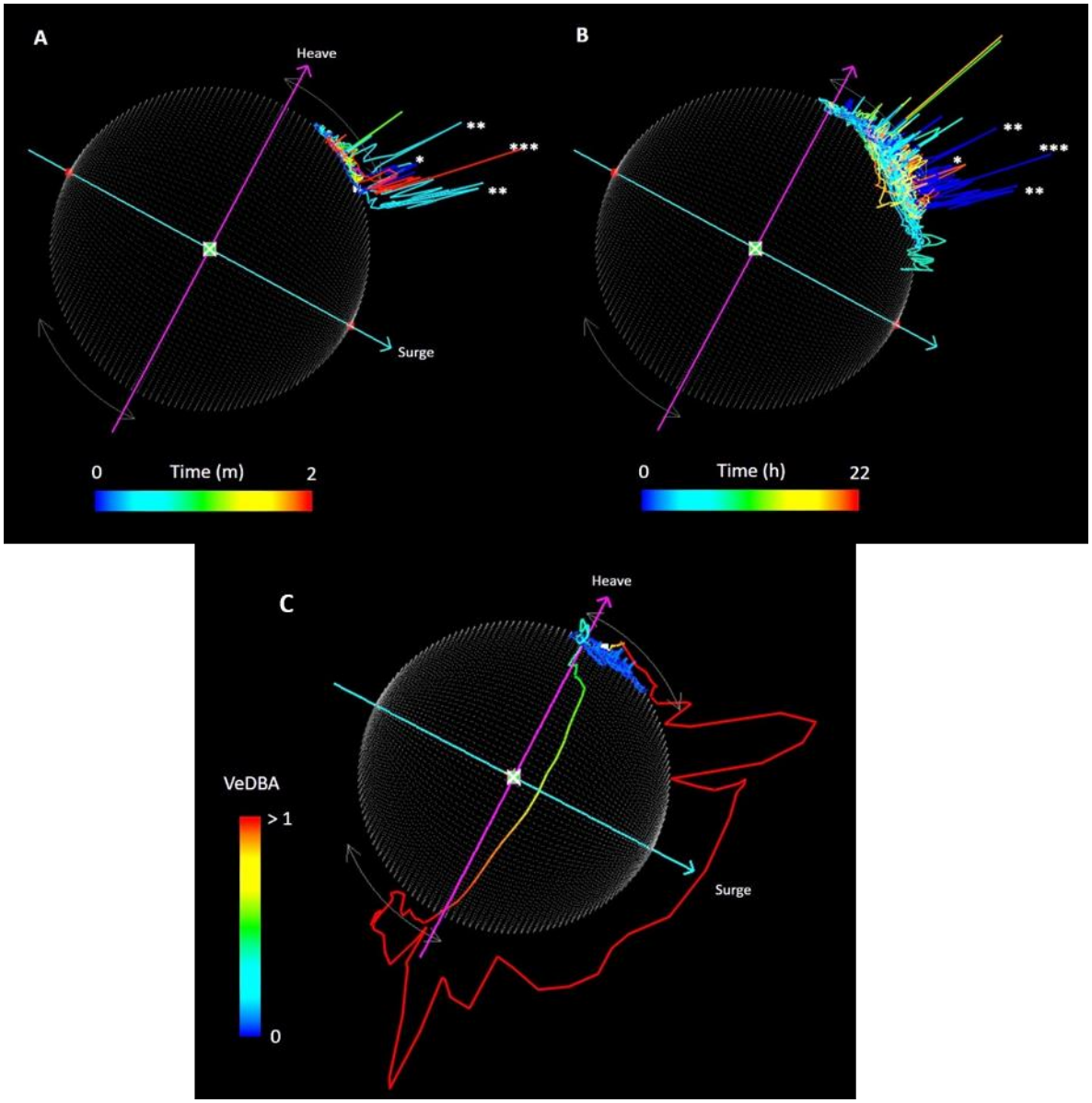

Figure 3.5: G-spheres of smoothed acceleration data from *C. melanopterus*, where distance of the data from the sphere surface corresponds to VeDBA. Colour corresponds to time in **A** and **B**, but to VeDBA in **C**. The sphere surface corresponds to a vectoral sum of the static acceleration (1.0 *g*; VeDBA value of 0). **A** & **B**: the same tag deployment on a male for the first two minutes **(A)** and the full 22 hours **(B)** of deployment time (note the different scales of time). *, ** and *** mark the first three instances of observed shake behaviours. Note how these behaviours, marked by spikes in VeDBA, primarily occur early in the data but can also occur later. **(C)** 2 mins of data from a female showing an observed leap and twist above the water's surface (similar to a 'breaching' style event), marked by a large loop around the heave axis, showing an inversion of the animal and large spikes in VeDBA (perhaps indicating the initial leaving of the water and the subsequent impact on the surface at landing).

3.2.3 *R. ancylostoma* chafing

Forty-six chafing events across 2 deployments were identified by the DDMT Boolean behaviour function. Thirty-two of these matched the characteristic *g*-sphere and acceleration trace signals seen in *G. cirratum* and were assumed to be true positives (Fig. 3.6). However, 3 events were known false positives and a further 11 were discounted due to either (i) the data occurring during feeding time when the individual was known to be swimming in an erratic manner and so unlikely to be related to the tag presence and/or (ii) the pressure reading was too low, indicating looping swimming behaviour near the surface and/or (iii) the *g*-sphere signal was a broad loop as opposed to the identified, characteristic acute loop of a chafing event. For the 32 events, the mean duration was 3.80 s ± 1.26 sd. The earliest and latest chafing events occurred 4 hrs 26 mins and 11 hrs 40 mins, respectively, from release into the main tank. Precision and Recall, using assumed events, were 69.57 % and 100 %, respectively. Specific parameters used in section 3.2 to formulate both rules can be found in Appendix 3.

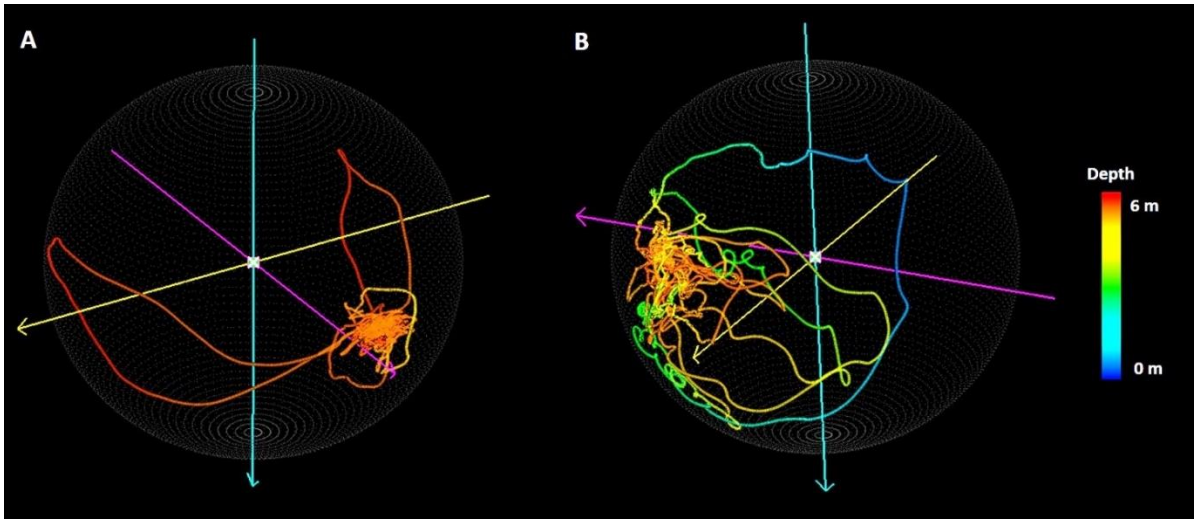

Figure 3.6: *G*-spheres showing 3-axis acceleration data of *R. ancylostoma* and coloured by depth in the aquarium. The sphere surface corresponds to a vectoral sum of the static acceleration (1.0 *g*). All data are taken from the same (second) deployment on the same individual, and each g-sphere shows 5 minutes of data. **(A)** Two (one to the left and one to the right) software-identified (not physically observed) roll events with assumed chafing (based on chafing behaviour rules in *G. cirratum*). Note the similarity between this identified event and the known chafing events of *G.cirratum* shown in Fig. 3.4. **(B)** Data falsely identified as roll events, where the individual was known to be swimming erratically during feeding time. Note how the rolling in **A** can be separated from the activity in **B**, based on depth (true chafing will most likely occur on the sand substrate), acuteness of the loop and the swimming signal surrounding the turn or roll (in **A** the activity is steady and concentrated on the *g*-sphere surface, in **B** the activity is erratic and produces larger loops on the g-sphere).

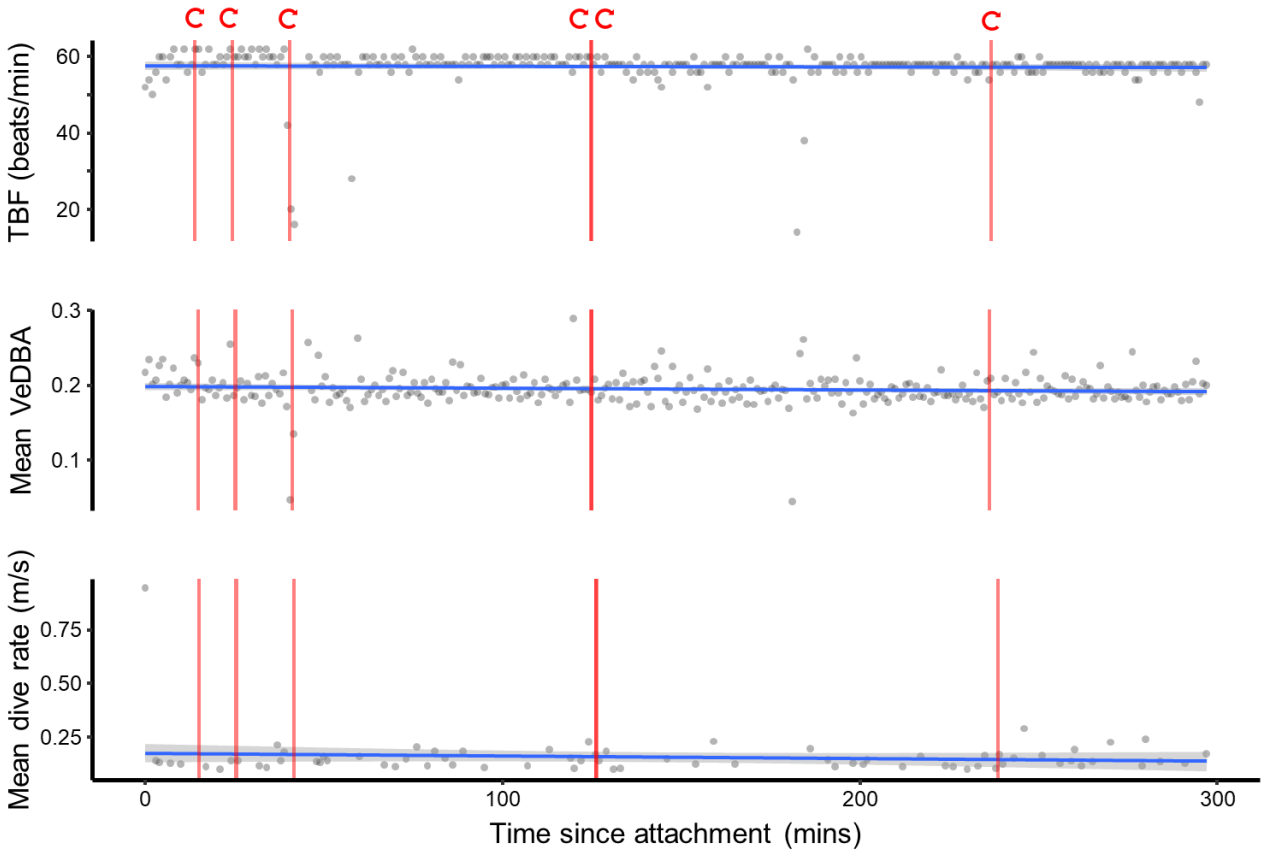

Figure 3.7: Tail-beat frequency (beats/min), mean VeDBA (active swimming periods only) and mean dive rate (metres/second), for the first 300 minutes of tag attachment for one *G. cirratum* individual. Blue lines are fitted GAMs (with respective 95% confidence intervals). Red horizontal lines (marked with circular arrows) show instances of chafing behaviour. Note how tag dislodgement chafing behaviour persists despite little perceptible change in either TBF, VeDBA or dive rate, which, by themselves, would suggest no effect of the tag on behaviour.

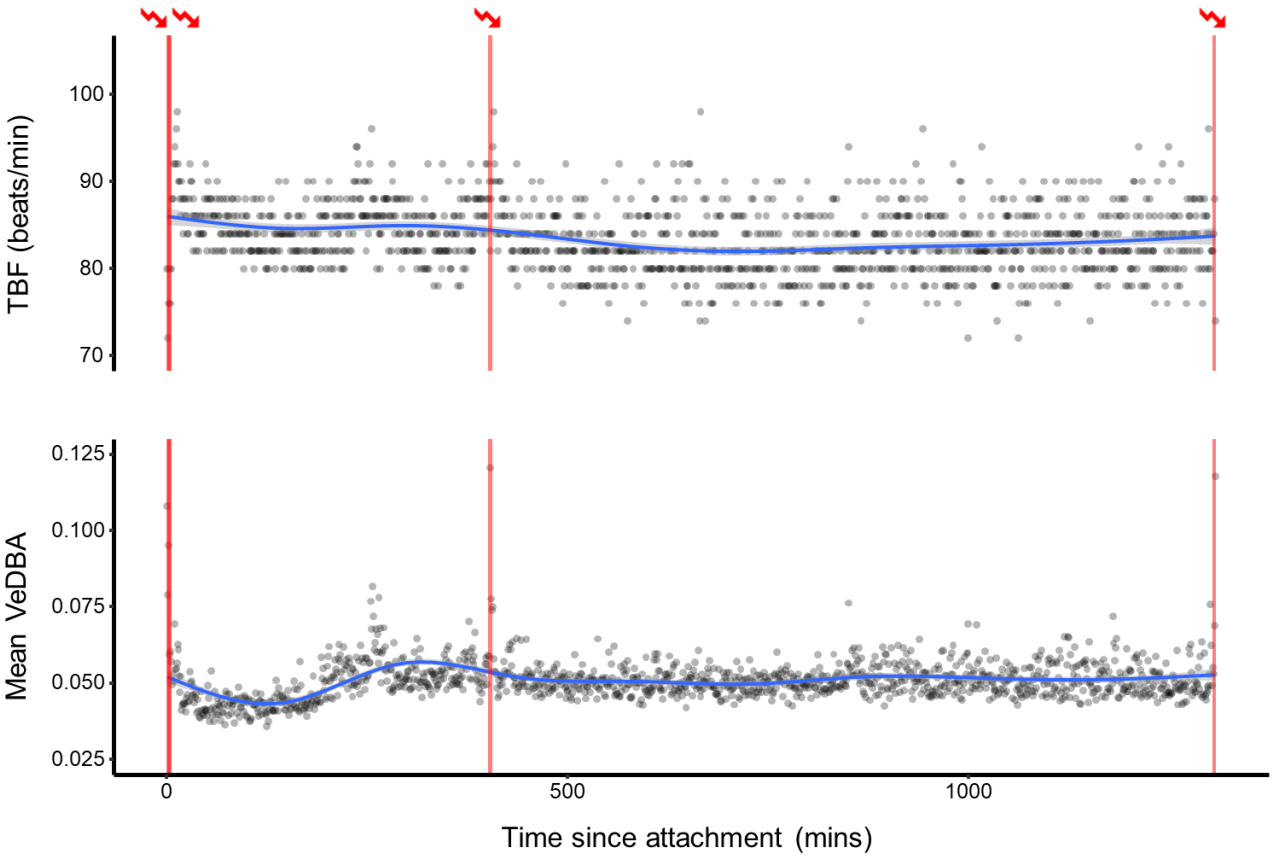

Figure 3.8: Tail-beat frequency (beats/min) and mean VeDBA (active swimming periods only) per minute over the first 300 minutes of tag attachment for one blacktip reef shark (*C. melanopterus*). Blue lines are fitted GAMs (with respective 95% confidence intervals, dark grey). Red horizontal lines (marked with zig-zag arrows) show instances of shake behaviours. Dive data were not included here as the individual's tag suffered a malfunction with the pressure sensor.

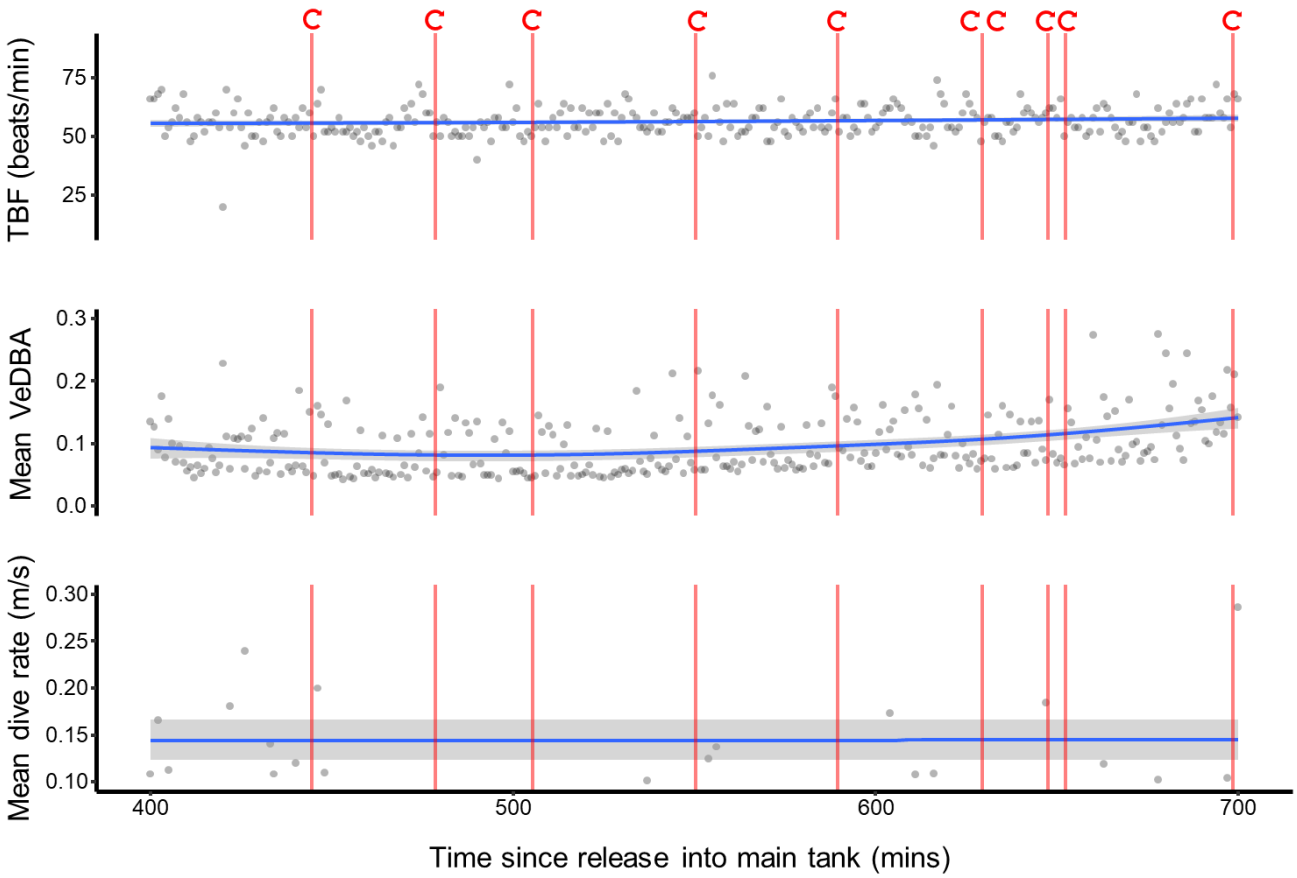

Figure 3.9: Mean tail-beat frequency (beats/min), VeDBA (active swimming periods only) and dive rate (metres/second) per minute over a period of 400 minutes of tag attachment on one Bow-mouth guitarfish (*R. ancylostoma*). Blue lines are fitted GAMs (with respective 95% confidence intervals, dark grey). Red horizontal lines (marked with circular arrows) show instances of identified chafe behaviour.

4. Discussion

4.1 Tagging and changed behaviours

A criticism of externally attached tags to aquatic animals is that they will affect the streamlining (Kay et al. 2019) and thereby cause increased energy expenditure at a given speed due to increased drag. This is particularly germane at high speeds since the power required to swim increases as the cube of the velocity. In this regard, given that overall TBF did not differ between tagged and untagged animals and that reported TBF here are similar to other available data for these species (e.g. Lear et al., 2018; Whitney et al., 2010), it would initially appear that these tags did not have lasting effects on the study animals across these short-term deployments (with any brief change in TBF generally returning to the normal baseline. In addition, neither VeDBA nor dive rate varied much save for a brief time following tagging, so this would seem to indicate that the animals were unaffected by their tags. However, swim speed was not calculated here in order to focus on the most commonly used metrics for measuring tag detriment in the literature, although methods to do so exist (e.g. Shepard et al., 2008; Sundström & Gruber, 2002). We therefore cannot rule out that hydrodynamic inefficiencies arising from the tag are not manifest by slower swim speeds rather than a change in swim power with associated dynamic body acceleration (Gleiss et al., 2010) and TBF (cf. Wilson, Grant, & Duffy, 1986). Finally, the significant negative change in *G. cirratum* TBF over the first 30 mins could be because the tag was attached during feeding time – individuals persisted in the area and would manoeuvre back to the small area in which feeding occurred, requiring slower swimming that would increase again following feeding time. This is supported by visual observations of the tagged individuals regularly returning to, and becoming stationary in, the feeding net, as well as the fact that feeding time generally lasted for these 30 minutes before stopping. Other tagging studies do note, however, an increase in TBF following tagging with

subsequent decreases as the animal returns to a more 'normal' activity pattern, although in these instances the increase tends to be much shorter (less than 1 minute (Gleiss et al. 2009, Chapple et al. 2015)). Across species overall, though, VeDBA and dive rate only manifest notable changes for the initial period of attachment and/or release, if at all. Collectively, these results might suggest that any reaction is simply a response to the handling and attachment procedure itself.

In contrast, consistently occurring transient behaviours such as chafing and shaking would augur otherwise. For instance, tag dislodgement behaviours continued to occur despite TBF, VeDBA and dive rate changing little (Figs 3.7-3.9). Critically, short-term behaviours such as chafing did not noticeably affect overall patterns within e.g. VeDBA or TBF but are clearly indicative of disturbed animals. While it is true that chafing and out-of-water jumps are sometimes observed in the wild, e.g. to remove parasites (Myrberg and Gruber 1974, Ritter 2011), the frequency with which these behaviours were collectively observed during tagging and the absence of them otherwise makes it clear that they are induced by the tags in our study. Chafing has been observed during other tagging studies, with acceleration patterns (such as the 'W' shape in the heave acceleration) matching that found here, although links to the tag itself causing this were not investigated in the studies concerned (Brewster et al., 2018; Lear et al., 2019). Likewise, an assertion that animals returning to, or remaining in, the tagging area indicates little or no negative impact, does not necessarily hold true because our tagged *G. cirratum* returned repeatedly to the feeding net after tagging, both immediately and for days after, while still exhibiting clear chafing behaviour (and even removed the tags this way). This would indicate that researchers should, as far as possible, interrogate their tag data to the full to study tag-induced behaviour - although the ability to do this will depend on the tag's sensor array.

4.2 The case for studies on captive fish

Ideally, behaviours derived from sophisticated tag sensors such as accelerometers to study tag effects should be given context. For example, many species of shark can roll before biting prey (Dudley et al., 2000), during mating (Whitney et al. 2010) or as part of agonistic displays (Ritter and Godknecht 2000), so the specific context of an animal rolling (Figs 3.4 – 3.6) to rub its dorsal fin along the seabed needs confirmation that the action occurred on the bottom and not within another context (e.g. mating). Visual confirmation of the circumstances of e.g. rolling are problematic in free-living sharks due to their mobility, although video-cameras are increasingly being used on elasmobranchs (Moll et al., 2007) so they may provide a basis for confirmation of particular acceleration- or depth-based patterns, even if they only function for a few hours at most (e.g. Andrzejaczek et al., 2019). Against this, a captive setting, such as the one used here, can be particularly valuable in this regard because it provides relatively extensive space for animals to exhibit a range of behaviours while still allowing good observation (including filming) at regular intervals to identify aberrant behaviours. This concept has been adopted by various workers, who have used mesocosms or enclosed waters to investigate tag effects (Bullock et al. 2015, Bouyoucos et al. 2017) or to validate previous findings with follow-up aquarium observations (Payne et al. 2016).

Beyond behavioural observations though, such studies can also help assess the viability of the attachment method and why devices might fail. An example of the latter is the observation that the particularly thin dorsal fin of *R. ancylostoma* over-oscillated side to side during faster swimming (particularly when trying to gain height in the water column). Tags can also be easily retrieved in captive settings, whereas recovery rates of tags deployed on wild sharks can be highly variable (c.f. Dicken, Booth and Smale, 2006; Haulsee *et al.*, 2016); in non-floating systems (e.g. Chapple *et al.*, 2015), this may even be due to the sharks removing the units themselves (cf. Figs 3.8 & 3.9) as was observed in the aquarium.

4.3 Limitations

The clarity with which tag attachment effects can be studied in aquaria (especially if the tag has a suite of sensors) is balanced by appreciable disadvantages of using captive animals. Dart and tow systems (e.g. Musyl *et al.*, 2011), for example, would not be suitable for an enclosed system with potential obstacles and other animals in close proximity, and large species (e.g. Whale Sharks, *Rhincodon typus*) are rarely held in captivity. Even with these limited described trials, data from one *G. cirratum* deployment suggested tag detachment by contact with metal structures (supported by prior visual observation of unusual swimming behaviour), while a *C. melanopterus* tag was observed to be knocked off against a conspecific. The walls themselves further influence behaviour and movement data – many of the false positives identified as chafing in both *G. cirratum* and *R. ancylostoma* were due to vertical swimming and then 'twisting' away from the walls. The relatively shallow tank used here also particularly limited dive profile analysis while captive animals may not necessarily be representative of their wild counterparts and may exhibit different behaviours. Despite the obvious limitations of captivity, however, based on the experiences here it is recommended that the use of captive settings be used where reasonably possible as a supplement to open-water trials, particularly when trialling new attachment methods. Indeed, McMahon *et al.* (2011) recommend that attachment method effects should be systematically studied in controlled conditions such as zoos. The wide-ranging nature of sharks though, and the difficulty of keeping them in captivity repeatedly leads to workers testing new attachment methods in open-water field trials in the first instance, from which swimming metrics such as dive profile and TBF are virtually the only parameters with which to define 'normality' (Gleiss et al. 2009, Chapple et al. 2015, Fontes et al. 2017).

It should be noted that workers are increasingly taking advantage of animal-borne cameras, paired with accelerometers and other sensors, to 'ground-truth' data (Andrzejaczek et al. 2019, Jewell et al. 2019), validate classifications of movement and behaviour and reveal interactions with the surrounding environment that would be otherwise undetected. In the context of measuring response to the tag and tagging procedure itself, cameras would be particularly useful for species that cannot be kept in captivity as well as in determining aberrant behaviour in the wild. However, it should be noted that the addition of cameras would bring additional weight and drag consideration to the tag body. Therefore, data on aberrant behaviours observed with the use of on-board cameras can not necessarily be applied to judgements on tags without cameras.

We note that rules used here to define aberrant behaviours (and stated in Appendix 3) might not necessarily be applicable to free-living species. It is likely, for example, that blacktip sharks will exceed the VeDBA threshold employed here during burst swimming such as chasing prey (Brewster et al. 2018). However, we observed no such movement and so cannot build them into our assessment. Similarly, other factors such as size-linked behaviours will likely also modulate the behaviour. Therefore, workers should seek to verify behaviours through observation and develop their own rules for identification specific to their circumstance and species.

Species will differ in their reactions and behaviours to external tags (Hoolihan et al. 2011) and, therefore, the specific aberrant behaviours noted in the three study species here may not be applicable to others. For example, pelagic species are less likely to interact with the bottom substrate in the same manner and regularity as benthic species and their use of the vertical water space will also differ. The use of the Boolean function for identifying chafing in *R. ancylostoma,* for example, yielded lower precision than for *G. cirratum*. However, this serves

to emphasize that researchers should test across multiple species to identify behaviours they might otherwise have missed before advocating a ‘one size fits all’ philosophy.

Understanding whether aberrant behaviours occur, how frequently and whether these are a result of tagging will have important implications regarding what is deemed acceptable practice for shark tagging. Ultimately, we should be aspiring to minimize detriment, both for the benefit of the animals concerned and the value of the science that they underpin and use of sharks in captive settings seems able to help in this regard.

Chapter 4:

Testing angular velocity as a new metric for metabolic demands of slow-moving marine fauna: a case study with Giant spider conchs, *Lambis truncata*

Since submission of this thesis and viva voce examination, an amended version of this chapter has been published in: *Animal Biotelemetry 9, Article number: 30 (2021)* .

Abstract

Quantifying metabolic rate in free-living animals is invaluable in understanding the costs of behaviour and movement for individuals and communities. Dynamic body acceleration (DBA) metrics, such as vectoral DBA (VeDBA), are commonly used as proxies for the energy expenditure of movement but are of limited applicability for slow-moving species. It has recently been suggested that metrics based on angular velocity might be better suited to characterise their energetics. I investigated whether a novel metric- the 'Rate of change of Rotational Movement (RocRM)', calculated from the vectoral sum of change in the pitch, roll and yaw/heading axes over a given length of time- is a suitable proxy for energy expenditure. It was found that RocRM can be used as an alternative energy expenditure proxy in a slow-moving benthic invertebrate. Eleven Giant spider conchs *Lambis truncata* (collected in the Red Sea) were instrumented with multiple channel (Daily Diary) tags and kept in sealed chambers for 5 hours while their oxygen consumption, $\dot{V}O_2$, was measured. I found RocRM to be positively correlated with $\dot{V}O_2$, this relationship being affected by the time step (i.e. the range of the calculated differential) of the RocRM. Time steps of 1, 5, 10 and 60 seconds yielded an explained variability of between 15 and 31%. The relationship between $\dot{V}O_2$ and VeDBA was not significant, suggesting RocRM to provide more accurate estimations of metabolic rates in *L. truncata*. RocRM proved to be a significant predictor of $\dot{V}O_2$ where VeDBA did not, validating the approach of using angular based metrics over dynamic-movement based ones for slower moving animals. Further work is required to validate the use of RocRM for other species, particularly in animals with minimally dynamic movement, to better understand energetic costs of whole ecosystems. Unexplained variability in the models might be a consequence of the methodology used, but also likely a result of conch activity that does not manifest in movement of the shell. Additionally, density plots of mean RocRM at each time

step suggest differences in movement scales, which may collectively be useful as a species fingerprint of movement going forward.

1. Introduction

Animal movements, behaviours and life processes account for much of an organism's energy demands, with the process-linked metabolism of an individual determining fitness, which in turn can effect ecosystem structure and functioning (Nagy et al. 1999, Brown et al. 2004, Cooke et al. 2004, Anderson and Jetz 2005, Nathan et al. 2008). Accurate determination of energy expenditure in animal species is therefore pivotal to understanding the value and costs of behaviours and how these relate to the ecology of species within ecosystems (Speakman 2005, Tomlinson et al. 2014, Halsey 2016).

However, directly measuring the rate at which an animal expends energy in the field, where it is unrestrained and allowed to exhibit a full suite of behaviours, is challenging (Elliott 2016, Jeanniard-du-Dot et al. 2017). Doubly-labelled water (DLW) - measuring CO_2 over time (Lifson and McClintock 1966, Elliott 2016, Speakman and Hambly 2016) - is the only direct measure, whilst other methods, such as recording heart rate, use proxies for energy expended (Gessaman 1980, Green et al. 2009, Elliott 2016). All such methods have limitations. For example, heart rate monitors are generally intrusive, often requiring implantation, and are less suitable for smaller animals (Green 2011). The doubly-labelled water method, on the other hand, is logistically difficult to conduct and has limited temporal resolution (Butler et al. 2004). A fairly recent approach has used tri-axial accelerometers in externally attached tags to provide a less invasive and high-resolution alternative deriving 'Dynamic Body Acceleration' (DBA) as a proxy for movement-based energy expenditure (Gleiss, Wilson, et al. 2011, Halsey et al. 2011). DBA is calculated from the dynamic acceleration (i.e. the acceleration signal that remains following the subtraction of static acceleration, or the gravitational component (Shepard, Wilson, Halsey, et al. 2008)) summed over all three dimensional axes (x, y, z ; surge, heave, sway) (Wilson et al. 2006, Qasem et al. 2012).

DBA has been repeatedly shown to correlate strongly with the rate of oxygen consumption ($\dot{M}O_2$ and $\dot{V}O_2$) in a diverse range of taxa including, *inter alia*, birds (Wilson et al. 2006), cephalopods (Payne et al. 2011), bivalves (Robson et al. 2016), fish (Wright et al. 2014, Lear et al. 2017) and mammals (Halsey et al. 2008). These laboratory studies have produced statistical relationships between DBA and $\dot{V}O_2$ that can be used to calculate energy expenditure from DBA extracted from accelerometer tags used on wild animals.

Despite the strength of this relationship and its applicability across many taxa, DBA is less likely to be a useful proxy for energy expended for species that move slowly because of their inherently weak dynamic acceleration signals. This limitation is indeed significant, because many marine benthic invertebrates, such as gastropods and crustaceans, move slowly (Dujon et al. 2019, Wilson et al. 2020, Zenone et al. 2020). Indeed, where dynamism occurs, activity and energy expenditure within these periods may be measured by DBA metrics (Dujon et al. 2019) but these may be a small percentage of the overall time budget for these animals. In the American lobster (*Homarus americanus*), for example, it has been shown that DBA correlates with oxygen consumption during the more active periods of movement, but had limited capacity to resolve metabolic rates in periods when movement was slower (Lyons et al. 2013).

Recently, a comprehensive review of DBA highlighted the need for alternative tag-derived metrics to address the problem posed by slow-moving species (Wilson et al. 2020). In particular, the authors suggested that rates of change of rotational axes (pitch, roll and yaw) might offer better insights into the degree of movement - and by proxy energy expenditure (Gleiss, Wilson, et al. 2011) - for such species compared to DBA (*cf.* Wilson *et al.*, 2013). In other words, the movement of, for example, a benthic invertebrate, where dynamic motion is consistently negligible and often only one locomotion type is used, may be manifest most notably in the speed at which it changes its whole-body orientation. Movement along these

rotational axes (assuming no drift or external factors are acting upon the animal), regardless of the speed at which this happens, still requires the exertion of force and, therefore, the expenditure of energy. Indeed, Wilson *et al.* (2020) presented preliminary data showing clearer changes in body angular velocity during movement bouts compared to DBA in the Giant spider conch *Lambis truncata*. Variability in the body roll angle has since been shown to describe slow-moving (walking) activity patterns of the European spiny lobster (*Palinurus elephas*) much better than DBA metrics, due to very smooth acceleration signals (Zenone et al. 2020).

I investigate the validity of a new metric, derived from the rates of change in rotational movement (which we term the 'Rate of Change of Rotational Movement', or 'RocRM'), as an alternative to DBA for estimating energy expenditure in a slow-moving benthic invertebrate, the Giant spider conch, *Lambis truncata*. *L. truncata* is a gastropod of the *Strombidae* family, a family that is commercially important and heavily overexploited in many countries (Leiva and Castilla 2002, Duncan 2003, Tewfik and Guzman 2003). Like many other conch species, it moves mostly via 'jumps' and some rotational (about the yaw axis) 'drifts' (Berg, Jr 1974, Brownscombe et al. 2015, Dujon et al. 2019). In other species of conch, jumps have been shown to accompany increased oxygen consumption (Lefevre et al. 2015). These jumps do produce a notable acceleration signal and the metric of mean ODBA is able to differentiate between leaps and drifts in a movement recognition model (Dujon et al. 2019). Whether DBA is an accurate proxy for oxygen consumption in conchs, however, is unknown. For example, ODBA during a drift is typically much lower than during a leap (Dujon et al. 2019) but might actually demand a considerable energetic commitment in practice (Wilson et al. 2013, Crossley et al. 2018). Here, laboratory-based static respirometry is used to test the hypothesis that RocRM correlates with the rate of oxygen consumption in a slow-moving animal. It is further examined how RocRM compared to VeDBA as a predictor of $\dot{V}O_2$ in this species. It was hypothesised that RocRM would correlate more strongly with $\dot{V}O_2$ than VeDBA.

2. Materials and Methods

2.1 Animal collection and holding facilities

Eleven Giant spider conchs, *Lambis truncata sebae* (Kiener 1843), were collected by snorkellers from areas of rubble and coarse sand on a shallow (<1 m) reef bed near the KAUST campus in the Red Sea during February 2019. Similarly sized conchs were selected (maximum width and length of shells, measured to the nearest cm, are shown in Table 4.1). A GPS fix (using a handheld GPS 73 unit; Garmin, Schaffhausen, Switzerland) was taken of what was deemed to be the most representative of the area where the specimens were collected from (22º17’22.7” N, 39º03’25.5” E), with all individuals being found within a 50 m radius.

Table 4.1: Conch shell measurements. Measurements, to the nearest whole cm, of maximum length and width of conchs used in this study.

Conch	Max. shell width (cm)	Max. shell length (cm)
1	11	17
2	12	19
3	11	14
4	10	14
5	11	15
6	9	14
7	12	16
8	11	16
9	11	16
10	12	17
11	13	17
Mean	11.2 (± 1.1 sd)	15.9 (± 1.6 sd)

Specimens were housed in two separate holding tanks (dimensions 118 x 56 x 46 cm L×W×H) supplied with a continuous flow of raw seawater, with a water level of 40 cm (*ca.* 264 L). Tanks of the same size were used during experiments. Water in both tank types was micro-filtered seawater, pumped directly from the neighbouring Red Sea.

Animals were kept in their holding tanks for 3 days prior to experiments and fed throughout the trial on the algal film that was allowed to coat the tank walls. The shells of the conchs were cleaned with a rigid brush to remove as much biological growth as possible and further cleaning was carried out when deemed necessary throughout the experimental period to minimise the

effect of non-conch oxygen consumption during respirometry. However, conchs were not cleaned within 24 h of being experimentally tested, to reduce the potential stress of handling.

2.2 Respirometry experiments

2.2.1 Overview

The tanks used in the respirometry experiments (see above) were chosen to encourage 'normal' conch movement during the experiments. Before each trial, the water flow into the tank was stopped and the tanks drained to a water level of 20 cm. Flow was restored between experiments and left long enough to completely replace the water. Air was bubbled through the water prior to the start of the experiment to fully oxygenate the water. A water pump was used to circulate the water within the tank to reduce both microbial build-up on the sensor spot and oxygen stratification inside the respirometer (tank), providing more consistent estimates of both background respiration and the $\dot{V}O_2$ of the study animal (Rodgers et al. 2016). MiniDOT O_2 sensor loggers (PME, California, USA) were anchored to the bottom of the tank at the end opposite to the pump (Fig. 4.1), with the sensing face pointing towards the tank centre.

Respirometry trials were conducted using closed chamber/static respirometer techniques (Lighton 2008). For the control/blank runs, initial trials (i.e. when calibrating equipment) and in the experiments themselves, aquaria were sealed with plastic sheeting (similar to those described in Lear *et al.* (2017) and Lear, Gleiss and Whitney (2018)) so as to be gas tight. Four layers of 1 mm thick sheeting were bonded together with duct tape (taking care that the complete material was watertight) to ensure that the final cover had enough weight to rest against the water and push out trapped air. The sheet was sealed to the tank walls as close as possible to the water level using duct tape and the seal inspected for any obvious gaps or unwanted gas exchange. Air bubbles between the water and plastic were pushed out by

smoothing the plastic towards the edges until none remained. Care was taken to seal around the water pump cable in such a way as to also be airtight. The salinity of the water was measured following each experiment and control using a Pro Plus Quatro salinity probe (YSI, Ohio, USA).

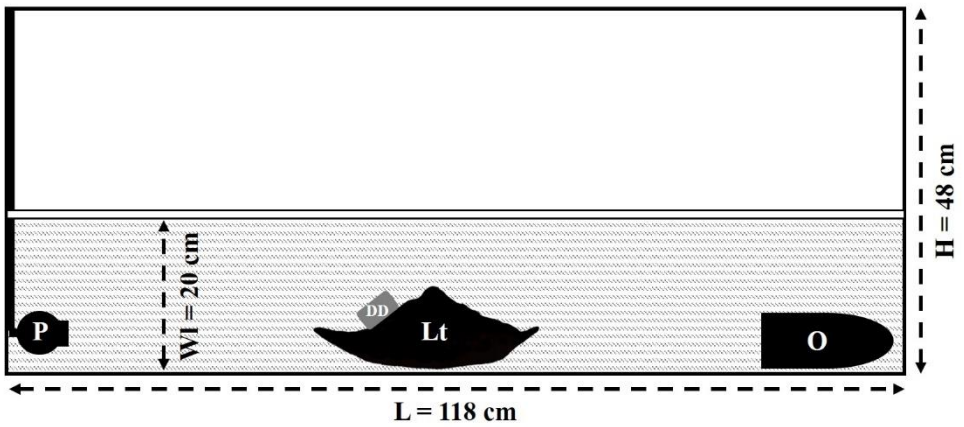

Figure 4.1: Schematic diagram of the static respirometry set-up used in this study. H = the total height of the tank; L = the total length of the tank; P = the water circulation pump, powered externally; Wl = the water level in the tank (shaded area); Lt = *L. truncata* test animal; DD = the Daily Diary tag, positioned on the 'front' of the animal; O = the miniDOT O_2 logger, weighed down to the bottom of the tank. The white rectangle at the top of the water line depicts the plastic sheeting cover used to seal the tank.

2.2.2 Data loggers

Water-dissolved oxygen concentration (mg/L DO) and water temperature were measured with the MiniDOT loggers, with temperature corrections applied automatically by the sensor. Salinity corrections of DO required manual input of salinity using provided 'miniDOT concatenate' software. MiniDOT loggers took one reading of each variable every 30 seconds – the minimum time that O_2 was predicted to take to diffuse through the sensing foil (PME, pers. comm.) and therefore the shortest interval that could be confidently used. The sensing foil was cleaned between each trial.

Conch movement was recorded using an 'elongated' model Daily Diary tag (Wildbyte Technologies Ltd, UK), recording tri-axial acceleration (surge, heave and sway) and tri-axial magnetometry at 20 Hz. Each Daily Diary was powered by a 750 mAh, 3.6 V single-use battery (EVE Energy Co., China). The complete package was enclosed within a vacuform polystyrene plastic housing and sealed using Poly Cement (Humbrol, Hornby Hobbies, UK). The overall maximum package dimensions were 38 × 20 × 13 mm L×W×H with a weight in air of 6 g. Velcro (Velcro BVBA, UK) was glued to the Daily Diary package. All conchs had a 1.5 x 1.5 cm patch of complementary Velcro fixed to their shell using super glue (Loctite Power Flex, Loctite, Germany), at an approximately 25-30^{o} angle on the anterior shell spine (as it was an area conserved between individuals, close to the centre of mass, and relatively flat for ease of attachment). The Daily Diary package was attached to the animal during transfer of the conch from holding to experiment tanks and removed when conchs were returned to holding tanks.

2.2.3 Respirometry experiments

The Daily Diary-equipped conchs were allowed to settle within their testing tanks for at least 30 mins prior to experimentation, with the miniDOT loggers placed in the tank at the same time. Tanks were sealed for 5 h and the DO and conch movement (*via* the Daily Diaries) recorded throughout this time. To increase the number of tests, conchs were tested four times across two general time periods (twice each): (1) 'afternoon' (average start and end times = 11:04 & 15:59, respectively - Saudi Arabia local time = GMT +3) and 'evening' (average start and end times = 17:36 & 22:30, respectively). These times were used as preliminary work had shown *L. truncata* collected from this area appear to slowly increase their movement through the late afternoon and evening (see Chapter 5), therefore giving the best chance of capturing

different ‘levels’ of movement frequency. Conchs were not reused in an experiment for at least 24 hours.

All conchs were released following respirometry experiments and returned as close to their collection location as possible. The Velcro patch and glue were easily removed, leaving only superficial markings.

2.2.4 Calibrations and controls

A control/blank tank, without conchs, was included for both time periods mentioned (3 in the afternoon and 4 in the evening), lasting at least 5 hours each. Blank runs were used to assess microbial (‘background’) $\dot{V}O_2$. The average conch respirometry experiment start and end times informed the times used in calculations of corrections. Two mean control slopes, one for afternoon and one for evening periods, were calculated from linear regression of each control run. Each conch $\dot{V}O_2$ calculation was subsequently corrected for microbial $\dot{V}O_2$ through subtraction of control rates (Rodgers et al. 2016). The lowest recorded DO concentration in any experiment was 5.75 mg / L (87.54 % O_2 saturation).

2.3 Data Analysis

2.3.1 $\dot{V}O_2$

The strength of the relationship of $\dot{V}O_2$ as a function of time (as a linear model) was evaluated immediately after each experiment run, to check that the system was sealed sufficiently and that there was a generally consistent negative correlation. Origin 2019 (Origin Lab Corp., Massachusetts, USA) was used to compute R^2 values for this. Experiment runs were repeated if plots suggested erratic DO readings (potentially due to poor chamber sealing) or a low R^2

value comparing oxygen concentration and time (in the final analysis, all slopes had an R^2 of > 0.87). As a result of the corrections discussed in 2.2.3, three experiments were discounted due to background-corrected slopes turning positive (suggesting breaches in the tank sealing), all of which were in the afternoon period, leaving 41 slopes across 11 conchs (3 conchs with 3 slopes, all others with 4 slopes) to be used in statistical analysis. Of these, 5 experiments did not record for the complete five hours (they recorded for 240, 267, 271, 286 and 295 minutes, respectively) but were included in all analyses.

$\dot{V}O_2$ for a single organism in a static system was calculated as in Lighton (2008):

(1) $\dot{VO_2} = \Delta[O_2].V_{ind}$

where $\Delta[O_2]$ is the regression slope of O_2 in milligrams per litre per hour, V_{ind} is the water volume in litres specific to the tested individual and $\dot{V}O_2$ is the rate of O_2 consumption for that individual in the same time units as the slope (mg ind^{-1} h^{-1}). V_{ind} was calculated as the effective tank volume (132, 160 cm^3) minus the volume of the miniDOT logger (314.16 cm^3), the water pump (179.59 cm^3) and the conch (calculated for each individual).

2.3.2 Movement

Daily Diary data were preliminarily analysed and extracted using DDMT software (Wildbyte Technologies Ltd, UK). Acceleration (1 g = 9.81 m/s^2) was separated into dynamic and static (postural) components using a smoothing window of 3 seconds (the window length informed by Shepard *et al.* (2008) and previously collected data on the movement durations of this species (unpublished data)).

Daily Diary data were used to calculate two movement metrics for each conch experiment run: RocRM and VeDBA.

The RocRM metric was calculated from the vectoral sum of the change (differential) in pitch, roll and heading over a specified time step given by;

$$(2)\ RocRM = \sqrt{Roc_p^2 + Roc_r^2 + Roc_h^2}$$

where Roc_p, Roc_r and Roc_h refer to the rate of change in the angles of pitch, roll and heading, over the given time step, respectively. Pitch and roll angle were derived from postural acceleration data (Robson and Mansfield 2014) while heading is derived from the body orientation data in tandem with the geomagnetic field strength measured in three axes (Williams et al. 2017). There was some magnetic noise within the tanks due to the pump, so heading was smoothed over 5 seconds. For consistency, pitch and roll were also smoothed over 5 seconds. RocRM was subsequently calculated for 4 different time steps (i.e. the vectoral sum of the change in these smoothed channels); over 1 second ($RocRM_1$), 5 seconds ($RocRM_5$), 10 seconds ($RocRM_{10}$) and 60 seconds ($RocRM_{60}$).

The dynamic component of acceleration, used in calculating VeDBA, was calculated as:

$$Dynamic\ Acceleration = Total\ Acceleration - Static\ Acceleration \qquad (3)$$

VeDBA was calculated using the formulation proposed by Qasem *et al*. (2012):

$$VeDBA = \sqrt{A_x^2 + A_y^2 + A_z^2} \qquad (4)$$

where A_x, A_y and A_z are the dynamic accelerations from each of the tri-axial channels at any given time. To be consistent with pitch, roll and heading, VeDBA was also subsequently smoothed over 5 seconds prior to statistical analysis.

Overall means for VeDBA and each RocRM measure were calculated for each experiment run and matched to their corresponding $\dot{V}O_2$ measurement. Each RocRM metric was log-transformed due to a better linear relationship.

2.3.3 Statistical analyses

Statistical analyses were conducted in R (R Core Team 2019) version 3.6.0. Five linear mixed models (LMMs) were constructed to investigate the relationship between $\dot{V}O_2$ and each one of the movement metrics independently, using the lme4 package (Bates et al. 2015) version 1.1.21. Thus, in each model, $\dot{V}O_2$ was the response variable and VeDBA, log(mean $RocRM_1$), log(mean $RocRM_5$), log(mean $RocRM_{10}$) and log(mean $RocRM_{60}$) were included as predictor variables in their respective models (subscript refers to the differential time-step period in seconds). To account for potential dependency of observations obtained from the same individual, 'conch individual' was included as a random effect term in all models. All models included random intercepts only (i.e. only the by-individual intercept, and not the slope, were allowed to vary), as attempts to fit random slopes for the conch ID term had issues with singularity. Mean experiment temperature was initially included as a fixed effect in each model but was removed from all of them through stepwise elimination of insignificant terms (see Supplementary Information), as well as judged on Akaike Information Criterion (AIC) values, starting with the full model (Crawley 2007).

Likelihood ratio tests (R function *anova*, with Maximum Likelihood) were used to determine the validity, effect size and significance of full *versus* null models. Graphical procedures (Q-Q plot, histograms, and residual vs fitted value plots) were used to visually assess the fit of the model and adherence to assumptions of normality and homoscedasticity of residuals (Zuur et al. 2009). Pseudo-R^2 values in the form of marginal (R^2_m) and conditional (R^2_c) values - where the conditional value considers the full model and the marginal value considers the fixed model effects alone relative to the conditional value - were calculated according to Nakagawa & Schielzeth (2013). 95% Confidence Intervals were computed *via* a bootstrapping method using the 'confint' (type = 'percentile', n = 500) function within lme4 (Bates et al. 2015).

3. Results

3.1 Controls

The mean background $\dot{V}O_2$ slopes of the 'afternoon' and 'evening' controls were -2.98 and -4.03 mg hr^{-1}, respectively. Despite the use of micro-filtered water in these experiments, there remained a clear presence of background/microbial respiration, particularly in the evening period, requiring the use of these corrections.

3.2 Differences in movement traces between VeDBA and RocRM

Movement data traces of rotational movement axes, VeDBA and RocRM reveal appreciable differences in the RocRM signal with different movement types (Fig. 4.2). $RocRM_{10}$ movement peaks differed between movements predominantly in the pitch and roll axes, exhibiting split peaks, and those predominantly in the heading/yaw axis, exhibiting peaks that are more singular. VeDBA, in contrast, produced relatively consistent peaks.

3.3 RocRM as a proxy for oxygen consumption

Mean temperature was removed from all five models due to no significant effect of the term on the model (VeDBA model: χ^2 (1) = 0.05, p = 0.82; $RocRM_1$: χ^2 (1) = 0.001, p = 0.97; $RocRM_5$: χ^2 (1) = 0.22, p = 0.63; $RocRM_{10}$: χ^2 (1) = 0.01, p = 0.91; $RocRM_{60}$: χ^2 (1) = 0.09, p = 0.77). See Appendix 4 for further details.

VeDBA was not a significant predictor of $\dot{V}O_2$ mg ind^{-1} h^{-1} with large Confidence Interval bands and an R^2_m of 0.01 (Table 4.2 and Fig. 4.4). In contrast, log-transformed mean RocRM increased significantly with $\dot{V}O_2$ (Table 4.2 and Fig. 4.4) at all time steps, with smaller p-values

for larger time steps. R^2_m values increased with increasing RocRM time-step (0.15, 0.18, 0.23 and 0.31).

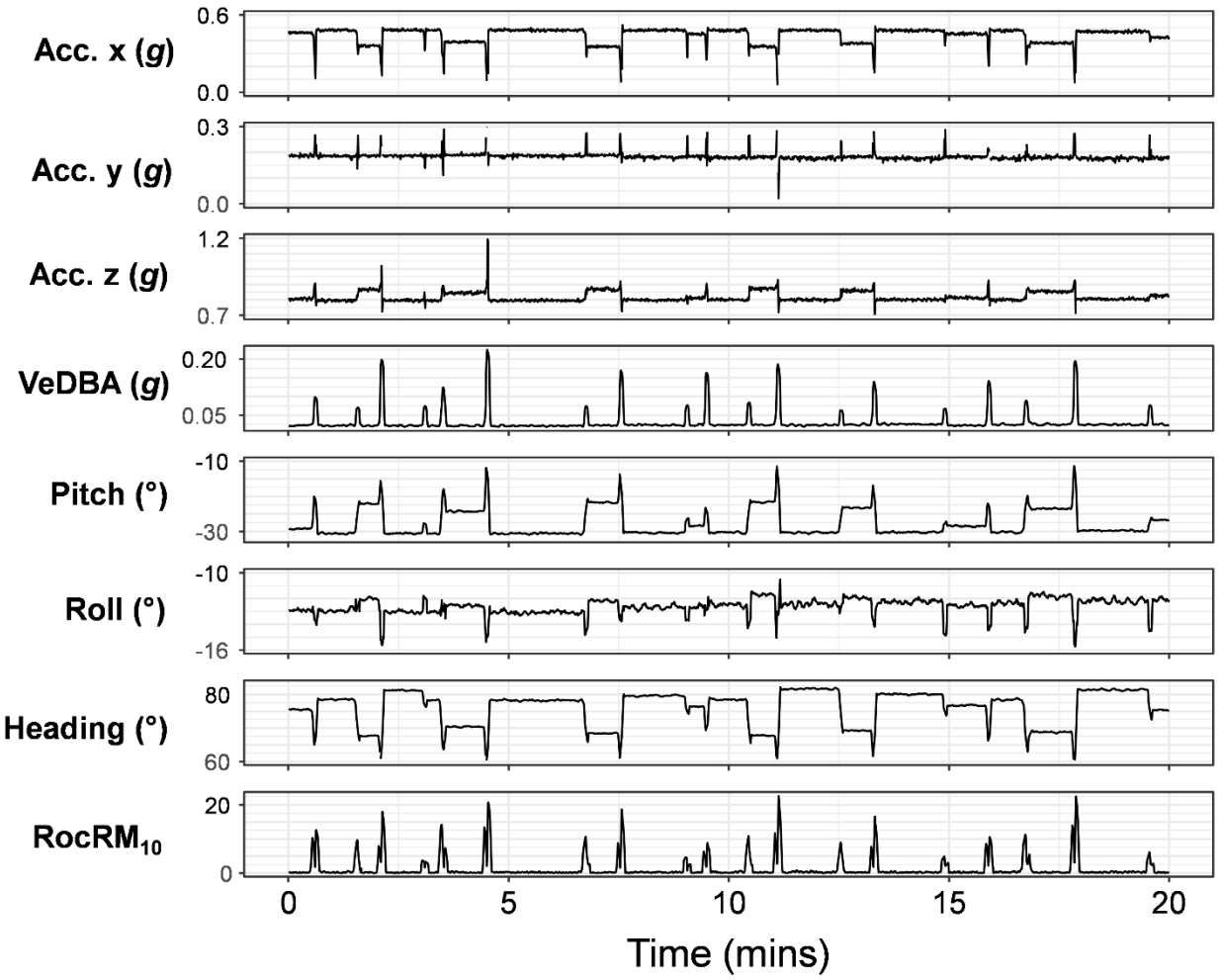

Figure 4.2. Example of the movement of a single conch over 20 minutes with data from the animal-attached tag being recorded at 20 Hz. Nineteen distinct movements are identifiable. Displayed are the three acceleration axes (x, y, z) and components of the VeDBA metric, the three rotational axes components of the RocRM metric (pitch, roll and heading angles), the vectoral sum of the dynamic acceleration (VeDBA) commonly used as a proxy of energy expenditure and the vectoral sum of the rotational axes (RocRM) over a 10 second step length. Pitch, Roll, Heading and VeDBA were subject to a smoothing window of 5 seconds.

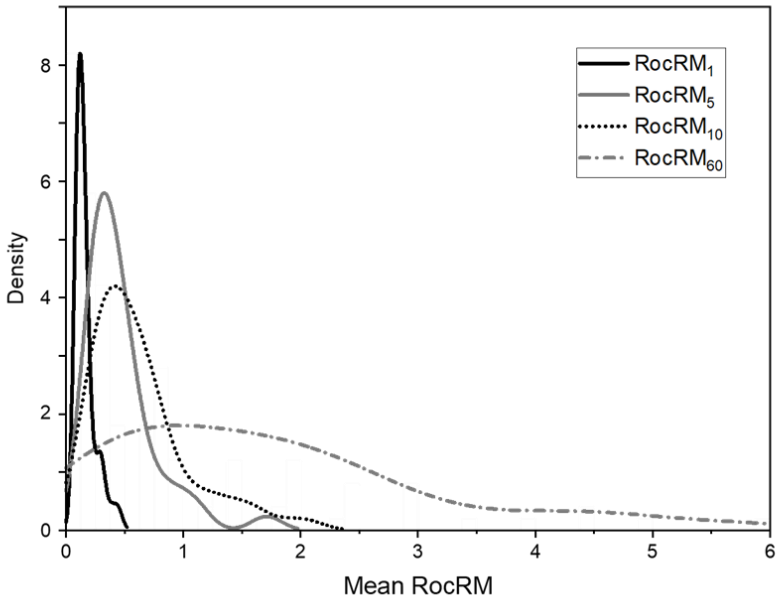

Figure 4.3. Kernel density distributions of the 5-hour mean RocRM values for each time step (where 'time-step' refers to the time interval of the differential that RocRM was calculated over- either 1 second, 5 seconds, 10 seconds or 60 seconds).

Table 4.2: Linear Mixed Model results. Results of the final (following removal of insignificant terms) linear mixed models where VO_2 mg ind^{-1} h^{-1} is predicted by either mean VeDBA or log-transformed mean RocRM (over either 1 second, 5 seconds, 10 seconds or 60 seconds stepping value). '.', '*', '**' and '***' refer to p-values of > 0.05, < 0.05, <0.01 and < 0.001, respectively. 'ΔAIC' refers to the difference between the null and full models, as shown by ANOVA model comparison.

Model	Predictor	Est	CI	t	p	χ^2 (df)	ΔAIC	R^2_m / R^2_c
1	*Intercept*	*7.00*	*1.17 – 12.30*	*2.49*	*			
	Mean VeDBA	-56.08	-259.32 – 158.26	-0.51	.	0.23 (1)	1.77	0.01 / 0.05
2	*Intercept*	*10.54*	*6.74 – 14.27*	*5.82*	***			
	log(mean $RocRM_1$)	2.59	0.73 – 4.28	2.87	*	6.40 (1)	4.4	0.15 / 0.41
3	*Intercept*	*7.61*	*6.10 – 9.19*	*9.27*	***			
	log(mean $RocRM_5$)	2.26	1.01 – 3.55	3.19	**	8.46 (1)	6.46	0.18 / 0.40
4	*Intercept*	*7.06*	*5.67 – 8.22*	*11.00*	***			
	log(mean $RocRM_{10}$)	2.32	1.03 – 3.54	3.84	***	11.79 (1)	9.79	0.23 / 0.46
5	*Intercept*	*5.25*	*4.27 – 6.09*	*10.74*	***			
	log(mean $RocRM_{60}$)	1.68	0.95 – 2.37	4.57	***	16.28 (1)	14.28	0.31 / 0.51

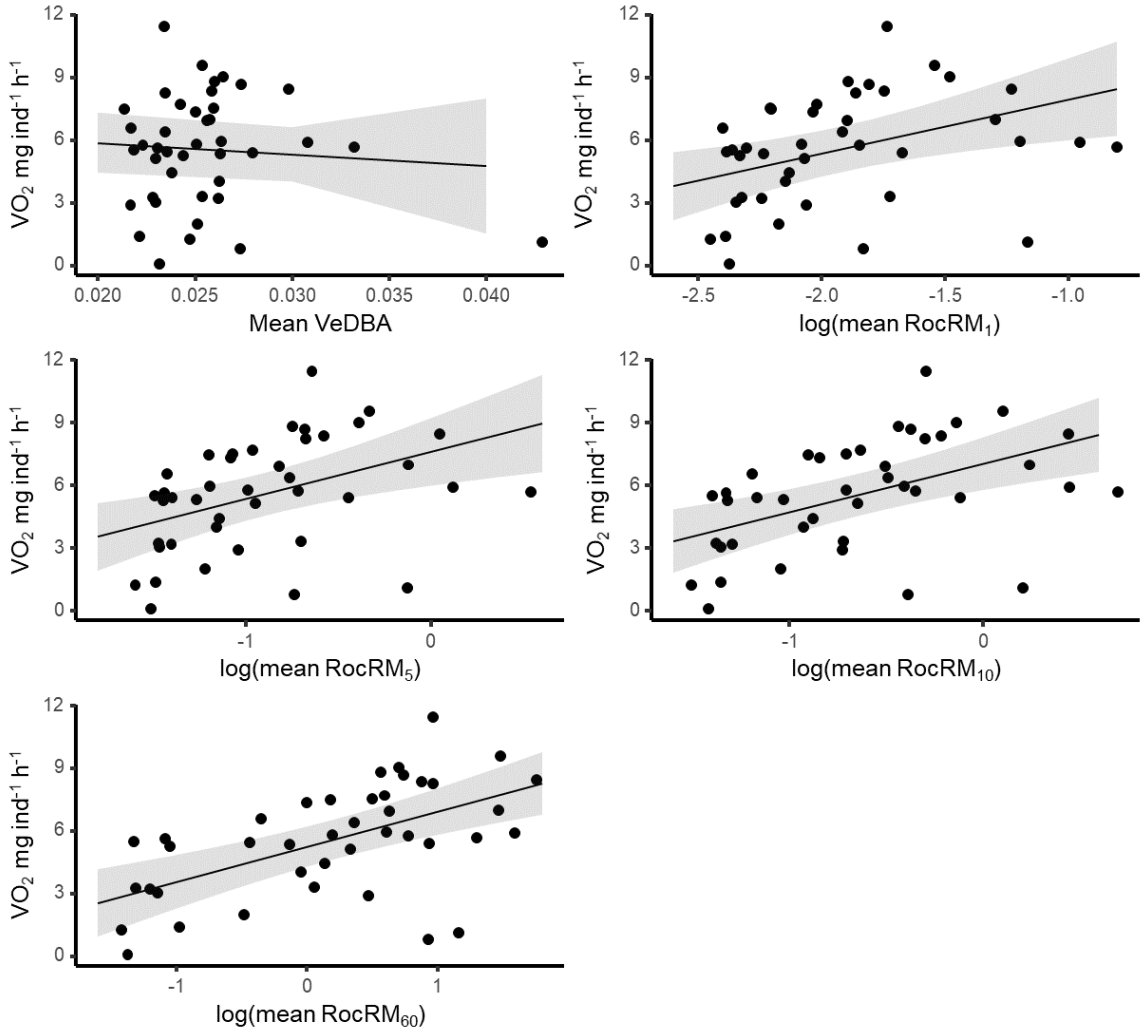

Figure 4.4. Oxygen consumption in *Lambis truncata* is well explained by RocRM but not VeDBA. Relationships between oxygen consumption (VO_2 mg ind^{-1} h^{-1}) and either mean VeDBA or four different time steps of log-transformed mean RocRM (1 second, 5 seconds, 10 seconds or 60 seconds). Trend lines show the fitted relationships calculated from Linear Mixed Models (LMMs) with 95% confidence intervals.

4. Discussion

Dynamic Body Acceleration is the prevalent tag-derived metric by which to quantify energetic expenditure of animal movement. This methodology appears flawed in slow-moving organisms. Alternative ways of assessing movement and their effects on metabolic rates are needed to better understand slow-moving species movements. Here it has been shown that RocRM, a movement metric based on angular velocity about the three rotational axes (pitch, roll, yaw), is a good proxy for estimating energy expenditure in free-living spider conchs. Given the lack of a relationship between $\dot{V}O_2$ and VeDBA in this study, it appears that rotational-based metrics may provide a critical movement-linked energy metric where dynamism-based ones do not. These results support the suggested advantage of rotational metrics from preliminary data on conch movement presented in Wilson *et al* (2020). They also build upon previous studies that show how slow-moving data in the European spiny lobster, *P. elephas,* is best described in terms of pitch and roll metrics (Zenone et al. 2020) and that fine-scale behaviours in diving loggerhead turtles are manifest most noticeably in the angular velocity about the yaw axis (Gunner et al. 2020)

Clearly, however, there is a sizeable source of variation around the predicted relationship not accounted for by RocRM, indicated by the confidence intervals and modest marginal R^2 values for shorter RocRM time steps (particularly 1 and 5 seconds). Firstly, the need to place Daily Diaries on the hard shell of the conch inevitably means that conch activity that does not manifest in the movement of the shell is unaccounted for. For example, conchs feed using their proboscis whilst grazing (Randall 1964, Berg, Jr 1974), which does not result in the movement of the shell (Dujon et al. 2019). The proportion of time, and energetic expenditure, that such movements account for is unknown, but might explain the variance in VO_2 at the lowest RocRM values.

It may also be that the method used here, using an overall mean taken over approximately 5 hours, misses the shorter, more intense bouts of movement that might produce higher RocRM. However, reducing the time period over which $\dot{V}O_2$ is measured is likely to increase the error around $\dot{V}O_2$ estimates derived from the limitations in detecting very small changes in O_2 in a relatively large volume of water, especially as 'high' activity periods are brief. Nonetheless, further tests using more sensitive oxygen sensors may refine this work further or use sensors that directly measure heart rate when such sensors become available. Conversely, reduction of the water volume, which might mitigate some of this problem, will tend to constrain animal movement. This experimental set-up differed from many 'traditional' respirometry studies that use fixed-volume, solid-walled, smaller (relative to the animal's body size) chambers, which would constrain animal movement. The tank volume employed here, approximately 114 times the volume of the conchs, allowed enough room for the animals to move in concentrated bouts. It should be noted that previous studies (Lear et al. 2017, 2018) on blacktip (*Carcharinus limbatus*) and lemon (*Negaprio brevirostris*) sharks encouraged consistent movement by having an animal to chamber volume ratio approximately two times larger than that used here, although these animals are considerably more mobile than the spider conchs tested here. Any tank setup will restrict normal movement, of course. When coming up against a barrier to movement, conchs will often continue to try to move up against it until they can move again (Dujon et al. 2019) – if this happened here, then it is possible that conchs would have expended large amounts of energy for what would appear, from the Daily Diary data, to be limited movement of the shell.

Chamber volume may not be the only factor affecting results. An important consideration when applying this relationship to free-living conchs is how the animal moves in relation to its environment. Specifically, the substrate across which the conch travels will alter the relative

contributions of changes in pitch, roll and yaw/heading and may negate or emphasise the inclusion of one or more rotational axes as part of RocRM. In simple respirometry chambers with flat bottoms as used here, pitch and roll changes are likely to make a smaller contribution towards the overall mean RocRM than if the animal was traversing rocky, uneven substrate such as the coral rubble that many conch species prefer (Brownscombe et al. 2015). Simulating such environments in respirometry conditions poses difficulties in, for example, the proper mixing of water and calculations of water volume when using fixed-volume chambers, as well as providing more substrate for microbes which may affect O_2 measures. As very few, if any, benthic animals move without any change whatsoever in at least two rotational axes, it would seem prudent to include all three axes as part of RocRM predictions of energy expenditure until further work indicates otherwise.

In the frame of slow-moving animals that exhibit little-to-no dynamic acceleration signal (*sensu* Gleiss, Wilson and Shepard (2011)), the actual 'jump' of *L. truncata* is surprisingly dynamic - at least by comparison to the steadier motion of other invertebrates, such as crustaceans or urchins. However, these movements were not sufficiently large or do not occur often enough to result in a relationship between VeDBA and $\dot{V}O_2$. In fact, in many instances, changes of heading were not even accompanied by a discernible change in acceleration in pitch or roll. I suggest that researchers might consider a 'scale' of taxa to compare the competing suitabilities of VeDBA and RocRM according to the types of motion exhibited by the animals, whereby animal movement changes from being mostly described by its dynamic component of acceleration towards predominantly the change in the static component.

Beyond energy expenditure estimations, the use of different timescales (i.e. differentials over varying time-steps) in analysis of animal movement rotations may be a valuable tool in inferring, and in turn describing, scales over which an animal moves. Smaller time steps in RocRM, for example over just a few seconds, can pick up the instantaneous changes that occur

during a jump, where larger time steps (for example, in this instance 60 seconds) might best highlight longer-term changes in body posture (particularly if such body posture changes, relative to the plane of the sea bed, are a summation of slower, gradual, less dynamic movements such as drifts (Dujon et al. 2019)). Indeed, different time scales of yaw-change have been shown to reveal fine-scale movement differences in Loggerhead turtles (*Caretta caretta*) that can be indicative of behaviour types better than DBA metrics alone (Gunner et al. 2020). Visualising these scales of movement, such as through density plots as shown here, may then show movement over different scales simultaneously to produce a *'fingerprint'* for a species, individual or context and potentially be used as a means of comparing these against others. It should be noted, however, that increasing time intervals also allow the animal time to turn back on itself, affecting the angle traversed within the time interval and therefore the estimated angular costs. Researchers concerned about this miscalculation of the differentials might consider instead calculating the integral of each rotational axis over a given time step; comparing the integral to the differentials may well identify instances of the animal turning back on itself.

A natural next step using *L. truncata* would be to derive estimates of energy expenditure-through RocRM in free-living individuals to make ecologically relevant observations and inferences about this and related species. For example, 'energy landscapes' have typically been visualised and described for highly mobile species such as birds (Wilson, Quintana, et al. 2012, Shepard et al. 2013) but, by using RocRM-derived estimates, spatial use and daily movement patterns could be framed more widely within the context of slow-moving benthic invertebrates. Additionally, RocRM may well convey much more information about an animal's movement type than VeDBA when movement data are matched to behavioural observations; here, there are clear differences in the observed peak profiles depending on the relative sizes of change in the pitch, roll and heading axes.

The particular viability of RocRM to predict oxygen consumption ($\dot{V}O_2$) over different time intervals would indicate that it could work for a variety of differentially slow-moving species, even if their angular velocity is appreciably different from that of spider conchs. Further work should be conducted to understand the mechanisms behind the variability around the mean trend of RocRM vs $\dot{V}O_2$. Nonetheless, the evidence presented here suggests that rotational movement metrics better correlate to energetic expenditure in slow moving animals than DBA. Using similar experiments to this on species that will have fewer sources of movement not measured by attached tags would be an obvious first step to validating these results.

Chapter 5:

Searching for simple rules in a ‘simple’ animal; movement of the Giant spider conch, *Lambis truncata*

Abstract

Testament to successful understanding of a system is being able to predict it, which explains why so much research is now invested in movement models and statistical approaches to project animal movement paths. Such efforts typically need to disentangle a complex set of interacting drivers that result from the animal's internal and external situation. Understanding and contextualising these drivers is particularly challenging in large, fast-moving animals that can vary their locomotion styles and speeds and traverse large distances where most predictive effort is currently centred. I advocate that benthic marine invertebrates, with limited slow movement options and relatively simple reactions, may be a valuable place to start and illustrate this using free-living spider conchs, *Lambis truncata*. I tagged 11 animals for 3 days with accelerometer/magnetometer loggers and showed that, despite having a movement style comprising of simple jumps and turns, the frequency and directionality of conch movement changed as a function of (i) the prior movement, (ii) the time of day and, (iii) water temperature. Specifically, I identified a significant positive correlation between the probabilities of magnitude of successive heading changes, modulated by time of day, while successive waiting times between movements were significantly positively correlated. Finally, increasing water temperature reduced the probability of movement, although disentangling this effect from that of the time of day was difficult. I suggest that such a 'simple' moving organism such as *L. truncata* might serve as a good first start for those seeking to understand the rules behind animal movement.

1. Introduction

'Animal movement' is a broad term, being applied over a wide range of temporal and spatial scales, and ranging from 'translocational' (movement across space) to 'on-the-spot', non-translocational (where the body or its parts move but the whole animal does not move through space (e.g. preening, displaying etc.)) (Daanje 1950, Alerstam et al. 2003, Van Moorter et al. 2013). The movement paradigm introduced by Nathan *et al.* (2008) is widely used to frame animal movement across diverse spatio-temporal scales, where it is argued that the overall path taken by a translocating organism is ultimately a product of many smaller processes that can themselves be understood by their own proximate (e.g. physiology) and ultimate (e.g. evolutionary) drivers (Mayr 1961). The paradigm strips investigation down to four key considerations; internal state, motion, navigation, and movement consequences – with all able to affect, and be affected by, one another.

Researchers applying the paradigm of Nathan *et al.* (2008) most regularly do so to animals that are considered to move a lot from the human perspective (although c.f. Ellis *et al.*, 2020), following a longer-running trend in movement research in general (Holyoak et al. 2008). These animals are typically vertebrates and have variable methods by which to move, whether for different forms of locomotion such as walking and flying (Ward et al. 2002), or simply employing one form of locomotion over different speeds, depths or heights (Lovvorn et al. 1999, Grodzinski et al. 2009). The paradigm's consideration of navigation asks *where* the animal is moving towards or from, but also asks *how* the animal moves to do so. Implicit in the latter question, however, is that the animal can indeed vary its form of movement, whether in speed, direction or form. In addition larger, faster organisms are often considered to have a complex, interacting set of drivers within their internal state which Nathan *et al.* (2008) consider to be complicated to contextualise. For these reasons, those seeking to understand

rules and drivers of animal movement of a given species within the Nathan *et al.* (2008) paradigm may benefit by additionally considering simpler animals. The use of more tractable species, whilst not necessarily a substitute, may provide a more easily understood baseline from which to draw inference and comparison. Most particularly, this should help make identification of internal state drivers of movement more straightforward. We propose that many aquatic benthic invertebrates may be considered good candidates in this respect. Although their movement is 'slow', 2-dimensional, ostensibly constrained and often stylized (Perron 1978, Newcomb et al. 2004, Pratchett et al. 2017), they may exhibit variability in movement regularity, speed and heading (e.g. Dujon *et al.*, 2019).

In this chapter, I consider the giant spider conch (*Lambis truncata*), which has limited capacity to move in response to stimuli. *L. truncata* moves primarily by 'hopping', digging its sharpened operculum into the substrate and pushing quickly against it to propel it briefly forward (an illustration of this movement for another member of the *Strombidae* family, *Aporrhais occidentalis*, can be found in Perron, 1978). This action appears essentially binary in that the animal either 'hops' or it is stationary. Conch *spp*. are capable, however, of varying the frequency of their hops and can also change their heading (the compass direction in which they are travelling) during movement (Dujon et al. 2019). Certainly, distinct movement preferences are apparent in other conch species, where movement elicitors have been found to include time of day (Dujon et al. 2019), predator escape (Lefevre et al. 2015), habitat preferences (Brownscombe et al. 2015) and dissolved oxygen concentration (Dujon et al. 2019), which suggests appreciably refined movement control. What is unclear is whether conch movement directions are Brownian (see Codling, Plank and Benhamou (2008) for discussion of this), with animals moving until the movement driver (e.g. oxygen concentration) is no longer pressing, a process that results in an inefficient response to elicitors (e.g. Codling, Plank and Benhamou

(2008) and refs therein), or whether conches can move with appreciable directionality, which implies that they also sense gradients in movement elicitors.

I used tags with accelerometer and magnetometer sensors attached to free-living *L. truncata* to examine the extent to which *L. truncata* movement was graded, rather than binary (i.e. moving *vs* not moving), and directional by examining the incidence of hops, their durations and their contribution to the changing of the conch's trajectory. I also aimed to determine the degree to which these movement parameters were randomly distributed or predicted by that of the previous state – essentially whether the probability of a movement or its directionality could be framed in terms of the probability of that which went before. Lastly, we looked to comment on the drivers of movement by relating movement probability to environmental temperature.

2. Materials and Methods

2.1 Animal collection and holding facilities

In February 2019, snorkellers collected conchs from a section of the 'Abu-sosha' reef a short distance off-shore from the KAUST campus. A GPS fix (using a handheld GPS 73 unit; Garmin, Schaffhausen, Switzerland) was taken of what was deemed to be the most representative position of where the specimens were collected from (22°17'22.7" N, 39°03'25.5" E) with all individuals being found within a 50 m radius from this point. Conchs were taken from an area of the reef where the substrate was largely a mix of coral rubble and coarse sand – their preferred substrate (Brownscombe *et al.*, 2015). Conchs were then housed in holding aquaria for 2 weeks prior to deployment, where the conchs were used in respirometry-based experiments – see Chapter 4) measuring 118 x 56 x 46 cm L×W×H. Holding tanks were supplied with a continuous flow of micro-filtered seawater (pumped directly from the neighbouring Red Sea), with a water level of 40 cm (*ca*. 264, 300 cm^3). Specimens were only collected for use in experiments if they were mature (flared lips on the shell) and approximately 15 cm or more in length.

2.2 Instrumentation and deployment

Each conch was instrumented with an 'elongated' model Daily Diary (DD) tag (Wilson, Shepard and Liebsch, 2008; Wildbyte Technologies Ltd, UK), recording tri-axial acceleration (surge, heave, sway) and tri-axial magnetometry at 20 Hz. The units were each powered by a 750 mAh 3.6 V single-use battery (EVE Energy Co., China). The complete package was enclosed within a vacuform polystyrene plastic housing and sealed using Poly Cement (Humbrol, Hornby Hobbies, UK), giving a final package size of 38 x 20 x 13 mm L×W×H that weighed 6 g in air. The DDs were fixed to the anterior end of the shell at an approximately 30°

angle (a part of the shell that was well conserved between individuals), using Epoxy Adhesive (Alteco, Osaka, Japan). This epoxy was found during a pilot study to be easily removed from the shell without causing more than superficial marking. Tag packages were attached approximately 1 hour prior to release back onto the reef. Each conch had numbered tape attached to several points on their shells for identification purposes.

Eleven instrumented conches were released by snorkellers in the morning, just prior to 11:00 am (Saudi Arabia local time, GMT + 3), back to their home reef at the original GPS-coordinate location recorded upon collection (though with several metres spacing between them). Conchs were recovered by snorkelling after 72 hours. At the end of each trial, all instruments and markings were removed from the shells and the conchs left on the reef. All DDs were successfully retrieved, although the data from one could not be recovered due to hardware issues (leaving a total of 10 individual data sets).

2.3 Data analysis

2.3.1 Identification of movement

Individual conch movements were identified in DDMT software (Walker *et al.*, 2015; Wildbytes Ltd., UK) using the Behaviour Builder function, a Boolean-based decision tree method (Wilson, Holton, et al. 2018), supported by captive (aquarium prior to release) video observations of movement. A movement was identified based on the rate of change in the magnetometry channel, by calculating a differential for each of the 3 magnetometry channels (m_x, m_y, m_z) over a stepping range of 0.5 s. If *any* differential value exceeded 0.03 G, the movement was deemed to have started, ending when the rate of change of *all* 3 differential

channels fell below this value (see Appendix 5). Movements were then filtered so that only those > 0.5 s and < 5 s were carried forward to the analysis stage, as observations indicated that values outside these ranges were not realistic and likely caused by either water disturbance or two successive movements incorrectly identified as one. For each movement identified, the duration (s) of the movement, the time since the previous movement and the change in heading (i.e. angle of direction) was calculated, along with two measures of time – the time of day and the time since deployment (release back onto the reef).

2.3.2 Derivation of heading

Calculation of conch heading involved consolidation of accelerometer and magnetometer outputs following protocols described in Gunner *et al.* (2020).

DDMT calculates magnetic heading- that is, the change in the yaw axis as sensed by the tri-axial magnetometer- *via* the equation detailed in Gunner *et al* (2020) and based on the work of Bidder *et al.* (2015):

$$\textbf{(1)}\ H = mod\left(360 + \left(\text{atan}\left(-m_y, m_x\right) \cdot \left(\frac{180}{\pi}\right), 360\right)\right),$$

where 'mod' is the modulo operator and m_x and m_y are the x and y channels of the DD tri-axial magnetometer, respectively. The heading angle is returned as degrees (i.e. 0° - 360°). Note that m_x and m_y must already have been normalised and the magnetic ellipsoid corrected, i.e. by accounting for differences in local magnetic field disturbances (Bidder et al. 2015) following appropriate data calibrations as discussed in Williams *et al.* (2017) and Gunner *et al* (2020). These axes must also have been corrected according to pitch and roll angles of the DD – correcting for device tilt away from 'level'. Pitch and roll angles, in degrees, were calculated *via*:

$$\text{(2) } Pitch\ angle\ (\beta) = \left(a\tan 2\left(S_x, \sqrt{{S_y}^2 + {S_z}^2} \right) \right) \cdot \frac{180}{\pi}$$

$$\text{(2) } Roll\ angle\ (\gamma) = \left(a\tan 2\left(S_y, \sqrt{{S_x}^2 + {S_z}^2} \right) \right) \cdot \frac{180}{\pi},$$

where S_x, S_y and S_z are the static components of acceleration in the x, y and z axes, or 'surge', 'heave' and 'sway', respectively. The resulting angles can then be used to correct magnetometer data through the equations stated by Bidder *et al.* (2015).

2.3.3 Statistical analysis

Initial data analysis suggested a handling or acclimation effect on the movement of conchs in the first 24 hours compared to the following 48 hours. For this reason, only the last 48 hours of deployment was considered in further analysis – i.e. the analysis presented hereafter. See Appendix 4 for comparison of the first 24 hours to the subsequent recording period.

To determine whether the number of movements differed between night (sunset to sunrise; 18:27 – 06:45) and day (sunrise to sunset; 06:45 – 18:27) periods, a Wilcoxon signed rank test was used (two-sided, paired, with a confidence level of 95 %).

To investigate the effect of ambient temperature on movement, 2 mixed logistic regression models (using the glmm function of the 'lme4' R package (Bates et al. 2015), family = 'binomial') were constructed to determine the probability of observing (i) more than 0 and (ii) more than 10 movements for a given hour. Mean hourly temperature, calculated from per-minute readings from each of the 10 deployed DDs, was included as a predictor in the model. Note that as two models of DDs were used, the temperature sensor resolution was either 0.1 or

0.01°C. Conch ID was included as a random slope (varying by mean temperature) variable. Justification for inclusion of model terms, including the random slope by conch ID, was assessed via log-likelihood ratio tests (*via* the 'anova' function of the lme4 package) and comparison of AIC values.

To investigate whether instances of movement were randomly distributed or could be part of concerted bouts, a Linear Mixed Model was constructed to quantify the relationship between successive between-movement times. That is, the time between two movements t_2 and t_1, the response variable, as a function of the time between t_1 and t_0, the predictor variable. The hour of the day was split into 6-hour periods of '0 – 6', '6 – 12', '12 – 18' and '18 – 0' and was included as an additional predictor variable. Conch individual ('ID') was a random effect, with a random slope term of the between-movement time. Between-movement time as a response, predictor and random slope term were $\log_{10}$-transformed to address the skewed distributions and to meet the assumptions of residual homoskedasticity and normality. Significance of model predictor terms and justification for model inclusion was assessed through log-likelihood ratio tests (r function anova()).

An Ordinal Logistic Mixed Model (CLMM), using the 'ordinal' R package (Christensen 2019), was constructed to investigate predictors of heading change. Hour of the day, split into the 6-hour periods detailed previously, the heading change of the previous movement (t_0) and the duration of the current movement (t_1) were included as predictor variables with an interaction between hour of the day and the t_0 heading change. Both the response and predictor variable of heading change were grouped into 6 ordered intervals so as to be ordinal data: 0° – 10°, 10° – 20°, 20° – 30°, 30° – 40°, 40° – 50° and > 50°. These intervals were informed by inspection of the data (just 0.01 % of movements had a heading change greater than 50°). Conch ID was included as a random intercept. The significance of each term to the model was assessed through stepwise term elimination, including of the interaction term, and likelihood ratio tests

between the full and reduced model/s. The number of quadrature points was set to 10. The ordinal package provides coefficient effects values as log odds; specific probabilities used in the figures were calculated using the ggpredict function within the ggeffects package (Lüdecke 2018).

3. Results

There was a total of 2,698 movements made across 48 hours (1295 in the first of these 24-hour periods, 1403 in the second), with a mean of 269.8 (± 44.7 se, min = 136.0, max = 614.0) movements made per individual. Individual conches moved significantly more at night than during the day ($p < 0.01$; difference in the median = 128; 95 % CIs = 91.5, 181.0).

Temperature had a significant effect on the probability of observing movement, with increasing temperature relating to decreasing incidence of > 0 movements (χ^2 (3) = 50.0, $p < 0.001$) or > 10 (χ^2 (1) = 10.9, $p < 0.001$). A 1°C increase in hourly mean temperature (between the maximum and minimum means of 21.7 °C and 28.2 °C, respectively) was associated with decreases of approximately 38.5% and 69% in the odds of seeing more than n = 0 and n = 10 movements, respectively, per hour (Fig. 5.1).

Individual movement had a mean duration of 1.4 s (± 0.01 se) (Fig. 5.2). The mean and median between-movement interval (in minutes) were 9.6 and 2.5 (± 0.6 se), respectively (Fig. 5.2). The distribution was skewed to the right with many short waits interspersed by few long waits. 28.5 % and 81.2 % of movements occurred after an interval of <1 minute and <10 minutes, respectively, with minimum and maximum times of 0.02 and 508.6 minutes, respectively. The LMM revealed that the ($\log_{10}$-transformed) between-movement interval ($t_2 - t_1$) was significantly ($p < 0.001$) positively correlated (0.28 ± 0.03 se, t = 8.52) with the preceding $\log_{10}$-transformed between-movement interval ($t_1 - t_0$). That is, the interval between two movements had a significant, positive effect on the following interval (Tables 5.1 & 5.2).

A cone-shaped relationship between movement duration and heading change (Fig. 5.3) suggested limits on turning speed so ‘duration’ was included in a later mixed model (CLMM) predicting heading change (see below).

The mean and median per-movement heading changes were 10.3° and 6.2° (0.2 se), respectively (Fig. 5.2). 25.7 % and 62.0 % of values were less than 1° and 10°, respectively, and the minimum and maximum heading changes were 0° and 132°, respectively.

The CLMM revealed that a given movement's heading change was significantly affected by the preceding movement's heading change ($p < 0.001$), the hour of the day ($p < 0.05$), the interaction between these two variables ($p < 0.001$) and the duration of the current movement itself ($p < 0.001$) (Fig. 5.5 and Table 5.3).

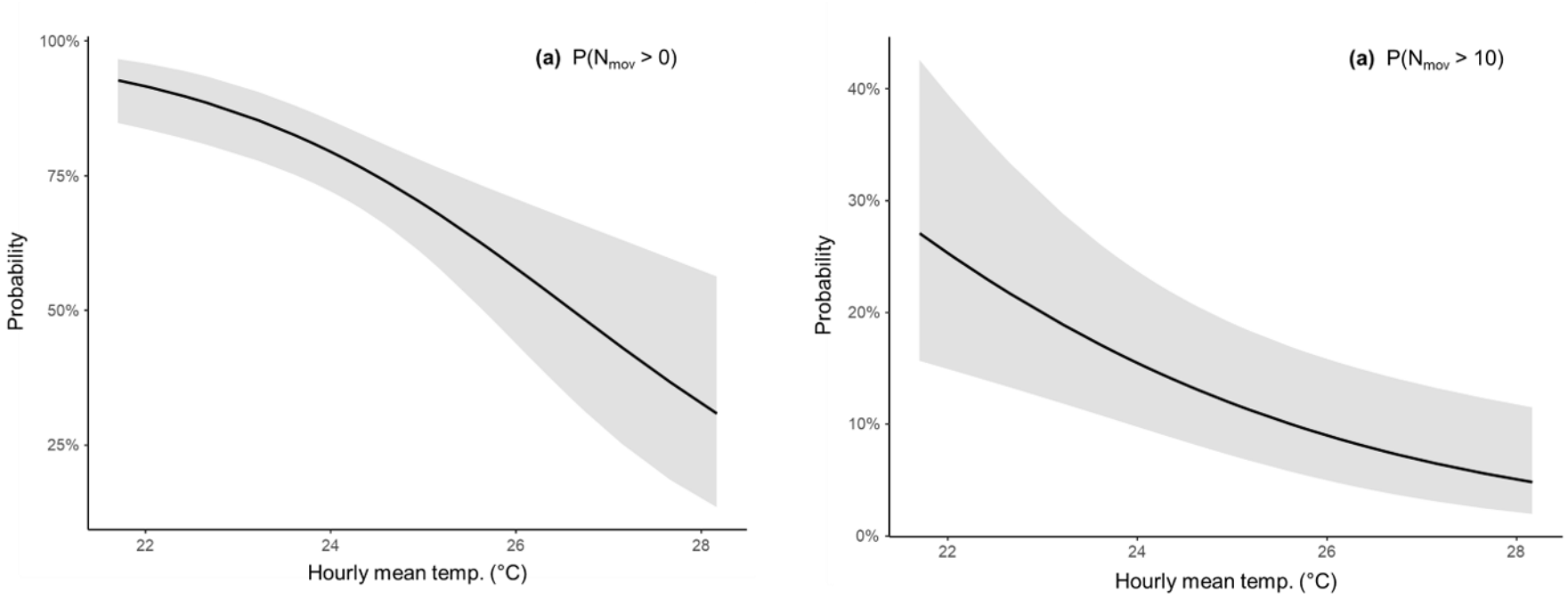

Fig 5.1: Predicted probabilities of seeing (a) n > 0 and (b) n > 10 movements in a given hour as a function of hourly mean temperature, predicted from mixed (repeated measures) logistic regression models. Grey areas represent 95 % CIs.

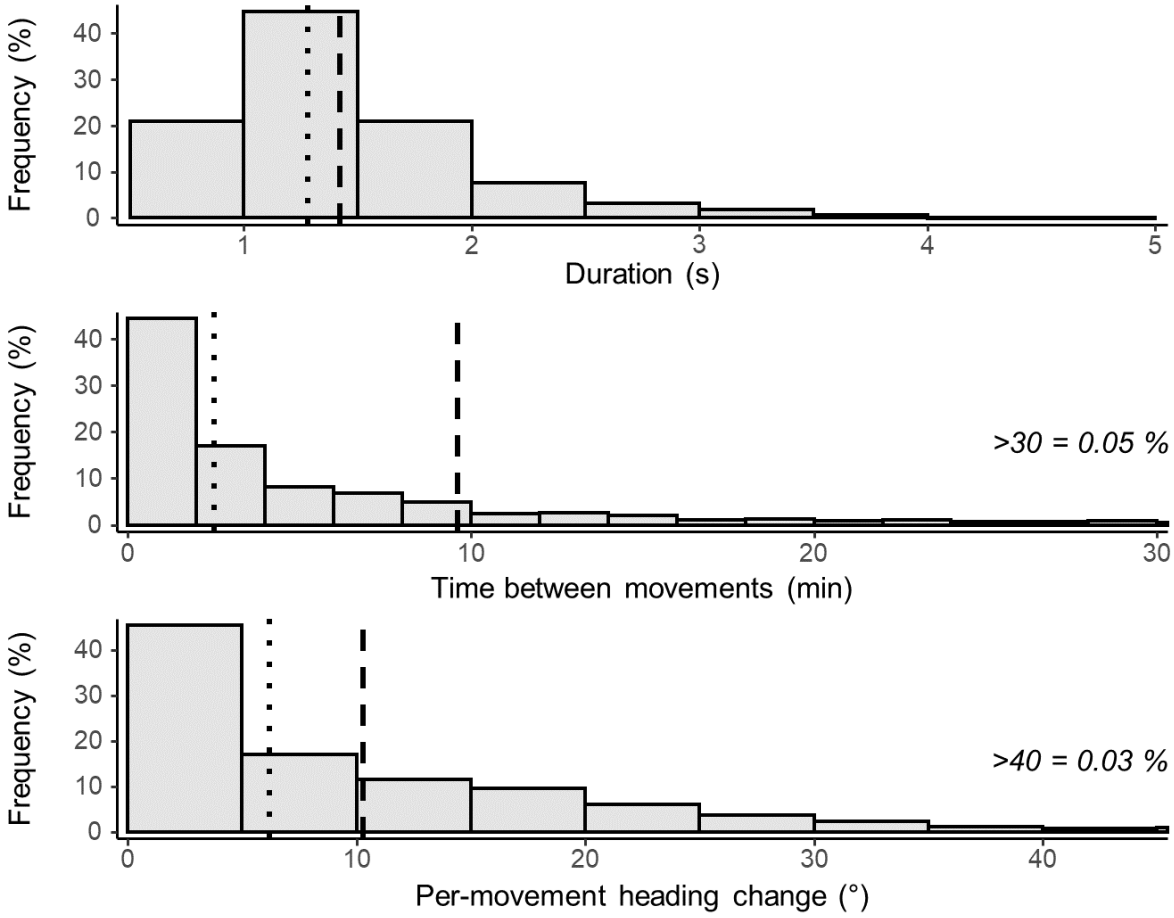

Figure 5.2: Percentage frequency distributions of conch movement: duration of movement, the length of time between successive movements and heading change during movement. Dashed and dotted lines indicate mean and median values, respectively. Note that 'Time between movements' > 30 and 'Per-movement heading change' show up to values of 30 and 40, respectively, to aid visual interpretation.

Table 5.1: Summary output of the LMM describing the effect of the (log_{10} transformed) between-movement interval ($t_1 - t_0$; mins) and hour of the day (binned into 6-hour groups; 'Hr') on the following between-movement interval ($t_2 - t_1$).

Coefficient	**Est. ± s.e.**	**t**
Intercept	*0.42 ± 0.06*	*7.66*
log_{10}(between-movement wait time t_0-t_1)	0.28 ± 0.03	8.52
Hr 18-0	-0.10 ± 0.04	-2.62
Hr 0-6	-0.10 ± 0.04	-2.43
Hr 6-12	-0.20 ± 0.04	-4.02

Table 5.2: Log-likelihood ratio test results (using R function anova()) showing significance of the LMM predictor terms described in Table 5.1. 'ΔAIC' shows the effect of the term's inclusion in the full model vs. a reduced model. 'Hour' refers to hour of the day (binned into 6-hour groups).

Coefficient	**df**	**ΔAIC**	**χ^2**	**p**
log_{10}(between-movement wait time t_0-t_1)	1	-20.30	21.72	**<0.001**
Hr	3	-10.30	16.35	**<0.001**

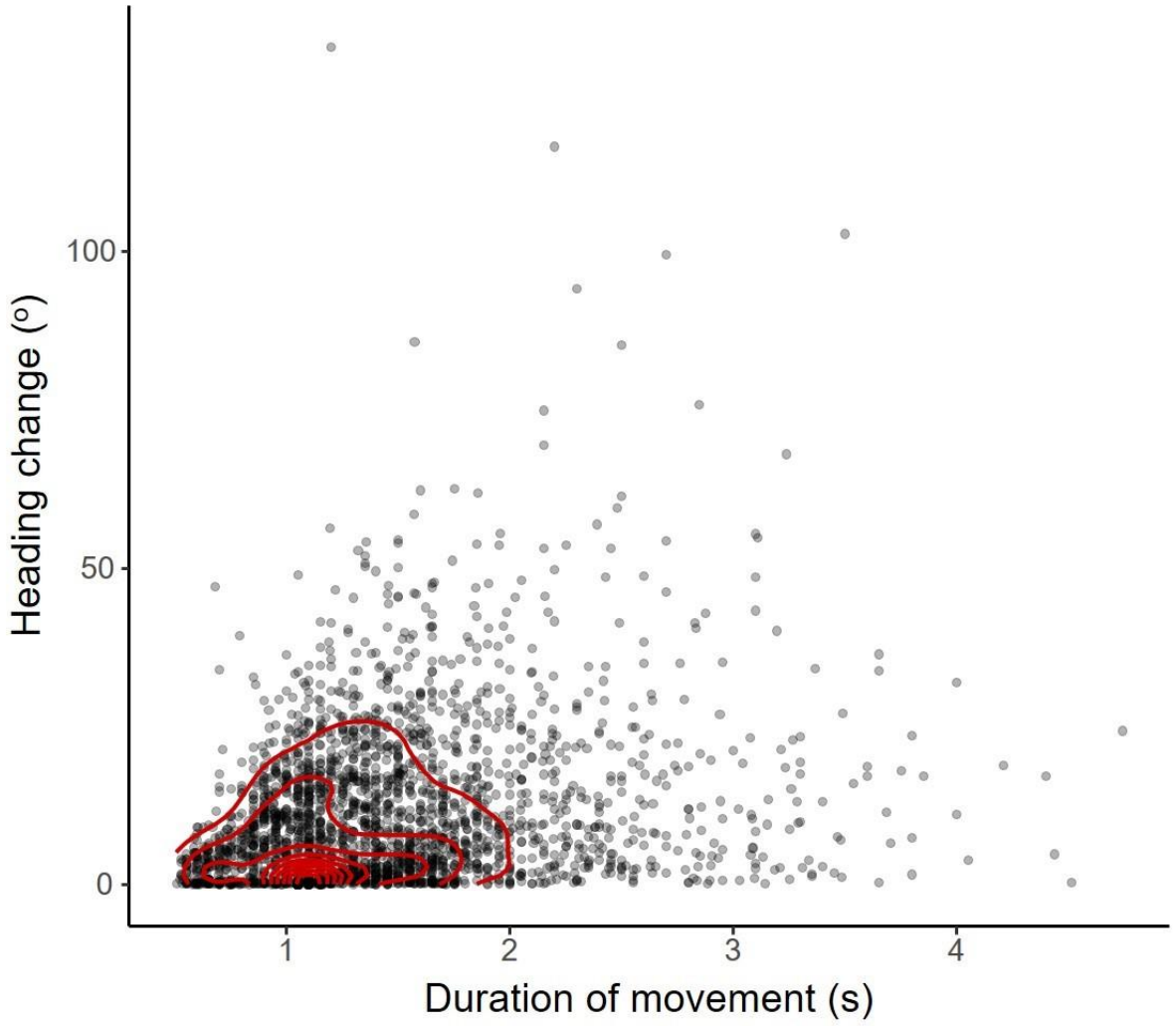

Figure 5.3: The relationship between heading change and duration of conch movements. Contours have a binwidth of 0.01.

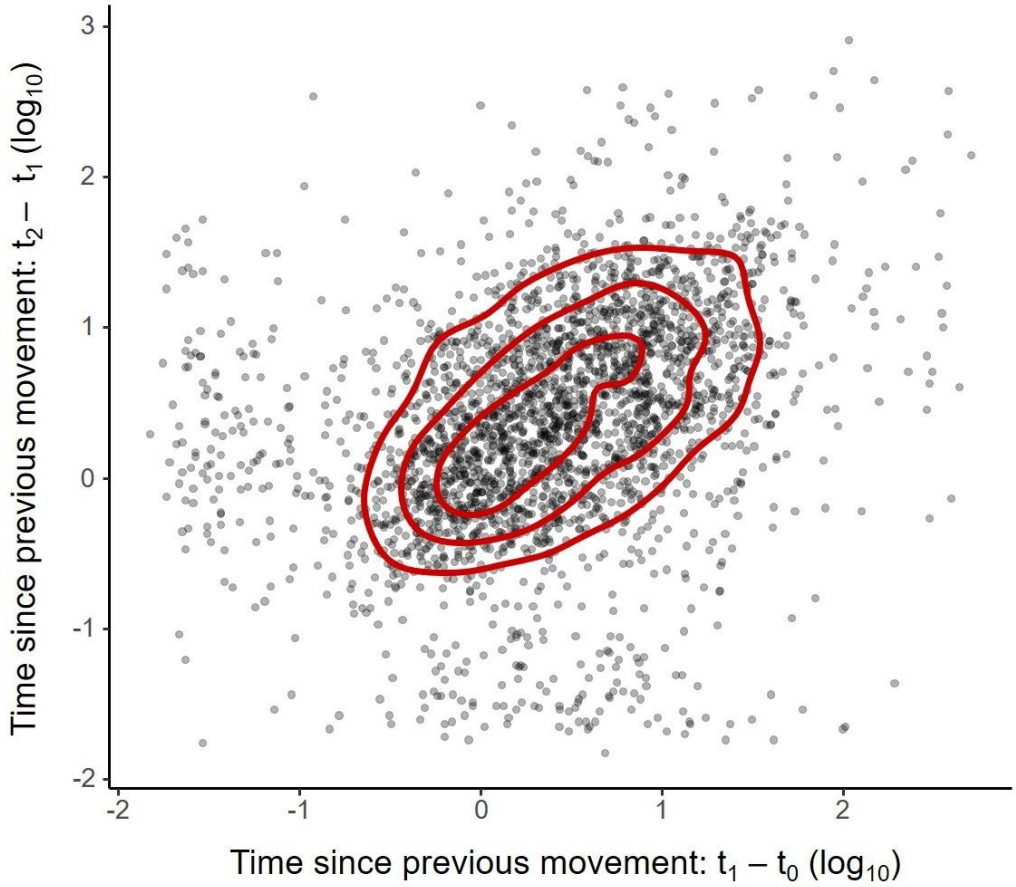

Figure 5.4: The durations between successive movements (i.e. at t_{-1} to t_0 *vs* t_0 to t_1). Both axes are log_{10} transformed. Contours have a bin width of 0.01.

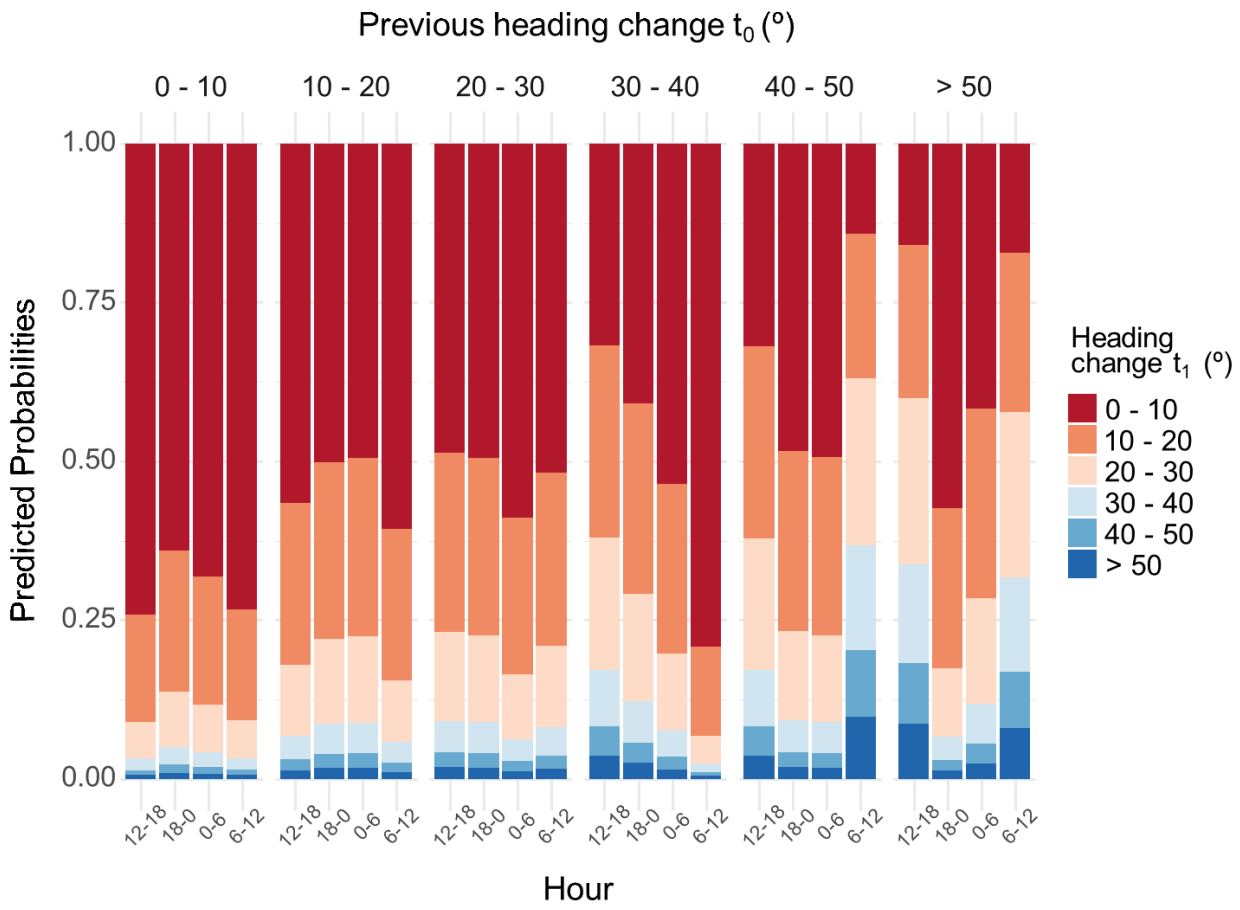

Figure 5.5: CLMM-predicted probabilities of the size of a given (at t_1) per-movement heading change (°) as predicted by an interaction effect between hour of the day (grouped into 6-hour periods) and the heading change (°) of the previous (t_0) movement. Duration of the movement was also a significant predictor term in this model.

Table 5.3: Results of log-likelihood ratio tests of fixed effects for the CLMM model [starting with the full model: $HC(t_1) \sim Hr*HC(t_0) + duration + (1|ID)$], where individual terms were removed and the full model and reduced models were compared. 'Hr' = Hour of the day (6-hour bins); '$HC_{(t0)}$' = Heading change at time t_0 (see Methods for binned increments); 'Duration' = Duration of the movement (secs). 'ΔAIC' = change in AIC values when including the model term; 'LR' = Likelihood Ratio.

Term	**df**	**ΔAIC**	**LR**	**p**
$Hr*HC_{(t0)}$	15	- 5.5	34.511	**0.003**
Duration	1	-102.7	104.68	**<0.001**
Hr	3	-2.60	8.53	**<0.001**
$HC_{(t0)}$	5	-76.4	86.33	**<0.001**

4. Discussion

Several trends emerged in different aspects of the conchs' movements, with time of day, temperature and the preceding heading change and between-movement intervals shown to variously modulate the frequency and gradation of movement. Indeed, These results can be broadly framed within the questions underpinning the framework of animal movement proposed by Nathan *et al.* (2008).

Firstly, the decision of *when* to move is clearly not random, as evidenced by the strong relationship between consecutive waiting times before moving. Rather, that movement occurs in bouts (Fig. 5.4), and these bouts are linked *inter alia* to time of day, with periods that can be broadly described by either concerted movement or waiting – i.e., movement begets movement whilst non-moving periods are unlikely to be broken up by sporadic movement. With conchs able to cover 100's of metres over several months (Bissada-Gooding and Oxenford 2009), but also spending the majority of their time grazing (Dujon et al. 2019), it would seem that movement bouts are most likely associated with feeding, made presumably to access new grazing areas (Dujon et al. 2019) at night. The observation that movement was greater at night differs to the situation observed by Dujon et al. (2019) for Caribbean queen conchs (*Lobatus gigas*) though, which reached a movement peak during late afternoon. In their case, movement was linked to peaks of dissolved oxygen concentration, but this is unlikely to be the dominant driver of movement for the conchs in our study. Dissolved oxygen for a coral reef just 10.5 km away from our study site has been shown to be higher in the day than the night (Giomi et al. 2019), opposite to our observed peaks in movement. In fact, the susceptibility of the Caribbean queen conch to dissolved oxygen is presumed, in the study of Dujon et al. (2019), to be due to it inhabiting a groundwater-fed coastal inlet which likely sees greater variation in dissolved oxygen, in part due to tidal cycles (Stieglitz and Dujon 2017, Dujon et al. 2019). This is a very

different situation to the shallow Red Sea coral reef of our study. Interestingly, it appears that oxygen supersaturation can supply the metabolic demand of marine ectotherms and extend aerobic performance (Giomi et al. 2019), a metabolic mechanism that may help explain why the conch movement periods reported by Dujon *et al*. (2019) differed to those in this study, despite similar daily temperature readings. This oxygen-linked explanation for activity patterns is given further credibility by the results of a study by Brownscombe *et al.* (2015), who noted that Caribbean queen conchs in a different, non-estuarine embayment moved more during the period of late afternoon to midnight – closer to our own results.

Temperature is, however, suggested here to be a factor that influences when our conchs moved and has also been shown in another conch species (Lefevre et al. 2015). Interestingly, Dujon *et al.* (2019) found no such relationship between activity and temperature in the queen conch. This disparity could be down to several factors such as; difference in environment (Caribbean inlet vs. Red Sea coral reef), interactive effects with other environmental parameters (e.g. the relationship between oxygen concentration and movement in the queen conch may override temperature effects, especially when oxygen concentrations are low) or the details of relative timings of movement drivers or inhibitors (e.g. light inhibits movement in the gastropod *Melibe leonine* (Newcomb et al. 2004) and competes for priority with temperature in the gastropod *Radix auricularia* (Rossetti and Cabanac 2006)). We also note that temperature readings were made from the DD onboard sensor. As the DD itself was sealed inside a plastic housing and then covered with a thin layer of black epoxy, the temperature inside will not be truly reflective of the actual ambient water temperature, having significant delays and likely being increased by insulation anyway. Repeating this experiment with a separate environmental sensor probe, which could additionally monitor dissolved oxygen concentration, light and salinity would greatly improve the clarity of the relationships between the internal- and external drivers of conch movement and better contextualise *when* the conchs move. Further experimentation and

measuring of many further parameters, e.g. prey/predator presence would be required to understand the full suite of drivers.

Knowledge of when a conch will be likely to move next, both as a function of its previous movements and time of day and post-handling habituation, can be coupled with the probability of a particular movement trajectory to make predictions on a conch's path and area displacement (the question of '*where to move?*' (Nathan et al. 2008)). The significance of the terms in the full CLMM model shows that the heading change for a given movement can be predicted as a function of (i) its previous movement, (ii) the time of day and (iii) the duration of the movement. There is a clear trend for heading changes to correlate positively with the previous heading change (Fig. 5.5). Thus, a straight movement is very likely to be followed by another straight movement. Beyond that, it is interesting that Fig. 5.5 suggests that the movements following the greatest heading changes – above 40° – vary in their predicted heading based on a night/day basis; large heading changes are much more likely to be followed by straighter movements (low heading changes) at night (between the hours of 18:00 and 6:00) than in the day. Assuming, parsimoniously, a constant advance distance per movement event, the trajectory of conchs following such rules could be visualised by dead-reckoning (Wilson et al. 2007, Bidder et al. 2015, Liu et al. 2015). This process makes apparent the extent to which animals engage in tortuous or more straight-line paths according to circumstance, for example, time of day or environmental parameters such as temperature (Fig. 5.6).

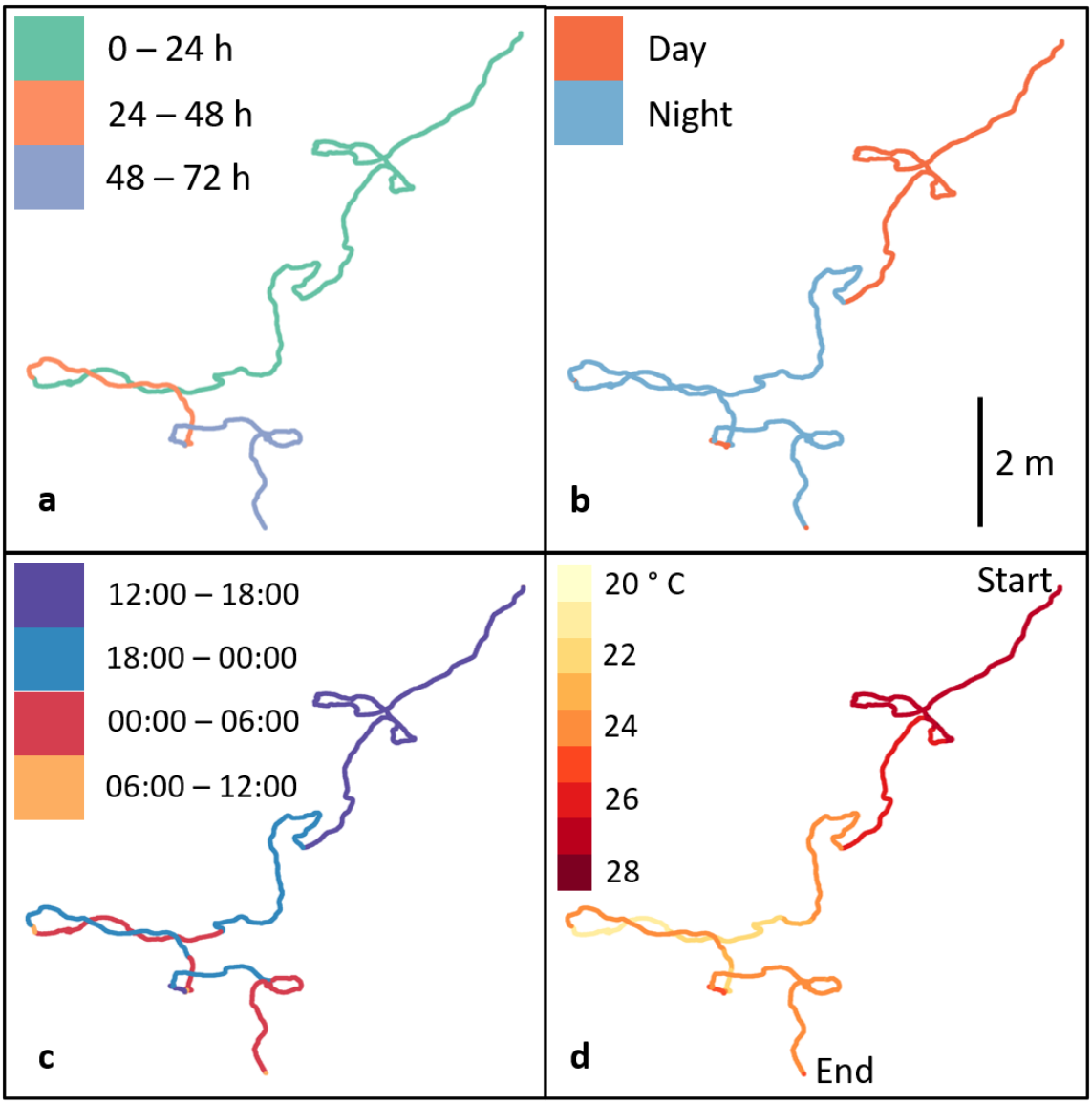

Fig. 5.6: A dead-reckoned track of a single conch's movement over the full 72 hours, coloured according to either **a**) time since release/deployment (as 24-hour periods), **b**) 'Day' or 'Night', defined by periods between sunset and sunrise, **c**) Time of the day, binned into 6-hour periods, or **d**) Temperature (rounded to the nearest whole ° C). The 'start' and 'end' location were marked by GPS and were 8.3 m apart.

Tortuosity is important because it shows energy expenditure for little advance. A prime example of this should occur associated with grazing, where animals stay in a localised spot to take advantage of the enhanced feeding conditions there and Dujon *et al.* (2019) have already noted this phenomenon in the queen conch. Straighter trajectories, such as would appear to typify night movement, may result in animals moving efficiently to new, farther locations prior to grazing, having depleted resources within one patch. Importantly, since the relationships between consecutive heading changes are known probabilistically, as is the frequency of movements, both being modulated by time of day, this study has the beginnings of a model that could be a mathematically driven movement probability function which could be run over multiple steps. To present this properly in 2d space would require knowledge of movement step lengths, however, something that was not done in this study, but it nonetheless would seem a fruitful avenue for quantifying animal movement. This would be most particularly the case if the mathematical descriptors of this movement could be equated to circumstance and fitted into one of the prevailing movement ecology paradigms (Nathan et al. 2008). Certainly, it seems that the probability movement rules deduced here could quite easily form a basis, or at least an additional tool, for understanding the conch's response to stressors in practical terms (e.g. it's response to climate-change), particularly when combined with knowledge such as species' habitat preference (Brownscombe et al. 2015) or interactions with predators (Lefevre et al. 2015).

Overall, our results show that Giant Spider Conchs do not exhibit purely Brownian movement, instead seemingly travelling in a more directed manner. And, since the last heading change modulates the next and this varies with time of day, it would also seem that they do not adhere to the precise mathematical conditions that describe correlated random walks (Codling et al. 2008), although correlated random walks may approximate their movement. It might be that, across even the modest spatial (a few m^2 per conch) and temporal (two days) scale observed in

this study, elements of both strategies are present (Boyer et al. 2006, Plank and James 2008). A better knowledge of the environmental contexts, particularly available food source and physical barriers, would greatly enhance our understanding of how these two models might integrate into an overall movement path (Humphries et al. 2010). A sparse food distribution on this particular coral reef, for example, would likely deter Brownian motion anyway. Nevertheless, it is encouraging that the patterns that have emerged in conch movement have done so relatively easily, perhaps because the species is a 'simple' model organism. It certainly makes a case for continued work on this species in the hope of throwing more clarity onto the rules, drivers and responses that underpin the movement frameworks relating environment to internal state to motion to navigation.

Chapter 6:

Using biologging to monitor the response of a free-living marine invertebrate to boat noise – a case study with the Maxima clam, *Tridacna maxima*

Abstract

Anthropogenic noise is an increasingly prevalent marine ‘pollutant’, with deleterious effects on the behaviour and physiology of many marine animals. Studies detailing such effects have primarily been on vertebrates, with comparatively few studies focusing on invertebrates such as bivalves. However, bivalves have been shown to respond to anthropogenic noise to varying degrees. The use of Hall sensors is an established technique for finely recording gape/opening angle of bivalves as a modulated behavioural response but usually requires a laboratory setting to do so, which hampers extrapolation to free-living individuals. We used autonomous tags with magnetometers on one shell half of free-living *Tridacna maxima*, paired with magnets on the opposing shell half, to monitor opening and closing behaviours in response to small boat noise on Red Sea coral reefs. Playback tracks comprised either of 2 hours of continuous ambient noise (control), or 1 hour of ambient noise followed by 1 hour of intermittent small-boat pass noise. Inspection of the magnetic-vectoral sum (MVS) confirmed gradual profiles of opening and closing of the shell halves over time, similar to that previously reported, with an overall gradual opening following tag attachment punctuated by brief closing events. Counts of these closing events were compared between control and experimental groups *via* permutation tests (comparing mean and medians) and bootstrapping (of 95% confidence intervals). In both treatments, the number of closures decreased from the first to second hours, suggesting an overall habituation effect to the handling and tagging procedure. However, this decrease was significantly greater in the ambient-only control treatment, suggesting this habituation process is compromised under boat-pass noise conditions. These results should help inform the ongoing collation of evidence of the negative impact of anthropogenic noise in the marine environment, particularly regarding bivalves which are understudied despite their ecological and commercial importance globally.

1. Introduction

Anthropogenic noise, ranging from boat engine noise through sonar and seismic surveys to pile-driving, is considered a pollutant in the marine environment (IMO 2014), and one that has increased considerably over the last few decades (McDonald et al. 2006, Frisk 2012). Such sound can interfere with animal communication (Miksis-Olds and Tyack 2009, Putland et al. 2018), orientation and navigation (Simpson et al. 2005, Holles et al. 2013) through masking of, and distraction from, various auditory signals. In addition, high-energy noise, such as pile-driving and seismic surveys, can directly cause physical damage to some marine species (Halvorsen et al. 2012, Casper et al. 2013, Carroll et al. 2017). Certainly, in an environment where sound travels far and is arguably of greater importance than light (Boyd et al. 2011), this has the potential to affect a suite of animal behaviours including, but not limited to, mating (Blom et al. 2019, Ruiz-Ruiz et al. 2019), anti-predator responses (Simpson et al. 2016, Spiga et al. 2017) and recruitment and settlement to coral reefs (Simpson et al. 2005, De Soto et al. 2013, Lecchini et al. 2018).

Unsurprisingly therefore, responses to marine anthropogenic noise have been studied in a broad array of taxa (Duarte et al. 2021). Studies on invertebrates have, however, been few compared to teleosts and mammals despite the importance of invertebrates in marine food webs and ecosystem functions (Shannon et al. 2015, Duarte et al. 2021). There is certainly evidence that many invertebrates are able to detect acoustic stimuli, with resultant changes in behaviour even manifest across sensory modalities (Kunc et al. 2014), although the term ‘hearing’ is judged inappropriate since these animals detect particle motion rather than pressure (Mooney et al. 2010, Carroll et al. 2017, Roberts and Elliott 2017). Such particle motion detection is thought to occur *via* statocysts, mineralised structures used in gravitational detection for orientation (André et al. 2016, Charifi et al. 2017), which have been described in many bivalve molluscs

(Charifi et al. 2017). Importantly though, demonstration that even molluscs can sense sound renders them potentially susceptible to anthropogenic sound *via* disruption of their behaviour (e.g. Wale et al., 2013) and physiology (Celi et al. 2013, Filiciotto et al. 2014).

Bivalves fulfil important ecological functions in water filtration in benthic communities and their sensitivity to, for example, ocean acidification (Waldbusser et al. 2010, Gazeau et al. 2013), salinity (Malone and Dodd 1967, Poulain et al. 2015) and algal concentration (Coquereau et al. 2016) makes them ideal bioindicators of system functioning and wellbeing. Some bivalves have been demonstrated to respond to anthropogenic sound, with siphon retraction and valve closure usually occurring more frequently (Roberts et al., 2015; Solan et al., 2016) and for longer (Roberts et al. 2015) when exposed to anthropogenic noise. Sudden valve closings and openings may be a result of faeces and pseudofaeces expulsion (Robson et al. 2009, 2010). However, the response to anthropogenic noise can vary appreciably. Wale et al. (2019) found that valve gape increased during ship-noise playback despite concurrent DNA damage and reduced O_2 consumption, with the authors hypothesising a 'shock', rather than 'stress', response.

Bivalve opening and closing behaviour can be measured by human observer (e.g. Dehaudt *et al.*, 2019), using video (e.g. Riisgård, Lassen and Kittner, 2014) or by attached sensors (e.g. (Robson et al. 2007, Schwartzmann et al. 2011). One such sensor consists of a Hall sensor/magnet pair. The Hall sensor is attached to one shell half and the magnet to the other (Robson et al. 2007, 2009, Clements and Comeau 2019). The Hall sensor generates a voltage which is proportional to magnetic field strength, which varies with distance between sensor and magnet so that larger gapes are indicated by lower voltage (Wilson et al. 2002, Robson et al. 2009). This system has been used to examine general valve movement patterns and responses to an external stimulus, such as predation (Robson, Wilson & De Leaniz, 2007), time of day (Wilson, Reuter & Wahl, 2005) or CO_2 levels (Clements and Comeau 2019). Similarly,

a pair of electromagnetic coils have been used to the same effect (Jou et al., 2013), for example in measuring the response of shellfish to arsenic levels (Liao et al. 2009). These systems lessen, or even negate, the need for cameras or regular human presence which is itself a disturbance (Robson et al., 2010). However, these systems are wired to an appropriate logging device (in the case of the coils, both sides are wired) and therefore often require a laboratory setting and/or are limited to a few measured individuals at a time, with the wires linking multiple system components together exerting ill-defined forces on the shell halves with water currents (particularly in the intertidal zone where wave action can be considerable). This is not a trivial issue since many bivalves react to variations in pressure on their shell surfaces, including to human touch (Johnson et al. 2017, Dehaudt et al. 2019) as part of their anti-predatory response. To mitigate this, authors have recently used much smaller devices such as accelerometers (e.g. Coquereau et al., 2016) or non-wired magnetometers (e.g. Kaidarova et al., 2018) to measure gape angle.

The study of the effects of anthropogenic noise on bivalves poses challenges though. The norm in such experiments requires tightly controlled conditions (Nedelec et al. 2016, Harding et al. 2019) although it is also accepted that captivity may alter behaviours unless 'normal' free-living conditions are simulated very accurately (Wilson et al., 2005). Indeed, in the field of marine anthropogenic noise, there is some debate as to the degree to which the acoustic environment can be properly represented in a laboratory setting (Slabbekoorn 2016). This process is enhanced by the many available sensor-recording systems, which can now be found in the form of autonomous tags that are able to last for many months (depending on recording frequency and size), and operate in open water experiments (e.g. Johnson and Tyack, 2003; Wilson, Shepard and Liebsch, 2008).

Here, we use autonomous tags to study the gaping behaviour of free-living Maxima clams, *Tridacna maxima*, in response to anthropogenic noise. Giant clams are the largest living

bivalves, providing substrate complexity to the benefit of reef fish assemblages (Cabaitan et al. 2008). Animals were located on three Red Sea coral reefs (Saudi Arabia) and were subjected to either small boat noise or ambient reef sounds. Small boat noise is particularly relevant to this area, and coral reefs in general, because such craft are commonly used for fishing, transport and recreation. Indeed, given that bivalves are capable of detecting differences in particle motion and have a hearing range including that of typical boat noise frequencies (Duarte et al. 2021), we hypothesized that exposure to their noise would result in reduced valve movements as a protective response as the shell would remain closed more often under boat playback conditions.

2. Materials and Methods

2.1 Site selection, study subjects and tags

Trials were conducted over three separate reefs just offshore from King Abdullah University of Science and Technology (KAUST), Saudi Arabia: Abu Shosha (22°18’13.74” N, 39°2’51.79” E), Tahla North (22°16’44.97” N, 22°15’24.77” E) and Quita al-qirsch (22°25’50.18” N, 38°59’42.58” E). Each location was dictated by clam presence – sites within each reef were selected if a clam was 2-6 m deep and had a nearby patch of sand onto which we could anchor the speaker (with the consequence that all trial sites were at the reef edges). Each study animal and each study site were used only once (i.e. for either an ambient control trial or a boat treatment trial). Daily Diary tags [DD’s] (Wilson et al. 2008) and magnets were attached to the clams underwater using epoxy putty (Epo Putty, Alteco, Osaka, Japan) with the tag and magnet attached to opposing shell-halves, close to the lip but no closer than 2 cm from each other when the clam was closed. The DDs were powered by 3.6 V 420 mAh batteries (EVE Energy Co., China) and were housed within custom-made vacuum-formed acrylic boxes (maximum package dimensions = 38 x 20 x 13 mm L×W×H; weight in air = 6 g) that were sealed with polystyrene cement. DDs recorded tri-axial (orthogonal) magnetic field intensity (range ± G at 0.73 mG/LSb) and tri-axial (orthogonal) acceleration (range -8 to 8 *g*) at a frequency of 20 Hz with 12 bit resolution (shown to be an optimised sampling frequency by Robson *et al.*, (2009). A total of 44 clams were tagged in this manner.

2.2 Sound exposure and experimental design

Each individual clam was monitored for two hours subsequent to being equipped with the valve-gape measuring system. Clams were grouped into one of two categories; (i) the group that was only exposed to ambient environmental noise for the full two hours and (ii) the group

that was exposed to ambient environmental noise for the first hour and then boat noise for the second hour.

For the ambient noise track, five 1-hour control ambient playback tracks were constructed using five 1 m 15 s recordings taken at the Abu Shosha reef. For boat noise, three 1-hour tracks with multiple boat passes were constructed using three 1 m 15 s recordings, each of a single boat pass (where the boat approached from a distance and passed the recorder in a straight trajectory, continuing on for a suitable distance). For each ambient track, two ambient clips were concatenated and looped. For each boat track, a boat pass clip and an ambient clip were alternated – resulting in 25 boat passes per 1-hour track. All tracks were band-passed with 15-2,000 Hz filters, anticipating the speaker limitations and the expected hearing range of the study species (Charifi et al. 2017) and then normalised to give the same levels.

In each trial, a stationary hydrophone (SoundTrap, Ocean Instruments) and underwater speaker (UW30, Lubell) were anchored at the site, positioned so that each study animal and the hydrophone were 2-3 m from the speaker (tracks were played back from a recorder (TASCAM) through an amplifier (M033N, Kemo)). Each trial was recorded using a hydrophone at similar distances from the speakers to the study subjects. The sound field during three trials with boat exposures was also measured using an acceleration sensor (M20, Geospectrum). Comparisons of control and experimental sound pressure levels and power spectral densities can be found in Appendix 6 (Figs 5.1 – 5.2).

In each trial, study animals were subjected to two hours of playback sound – either two hours of ambient (control) sound, or one hour of ambient sound immediately followed by one hour of boat pass sound. Two trials could be conducted simultaneously at the same reef provided that enough distance was maintained between the two sites in use so that each playback was not audible at the other site (verified using hydrophone recordings). Upon completion of the

full playback period at each study site, tags and magnets were recovered by simply twisting them free from the clam shells. Care was taken not to leave any putty on the shells. The general deployment set-up described here is illustrated in Fig. 6.1.

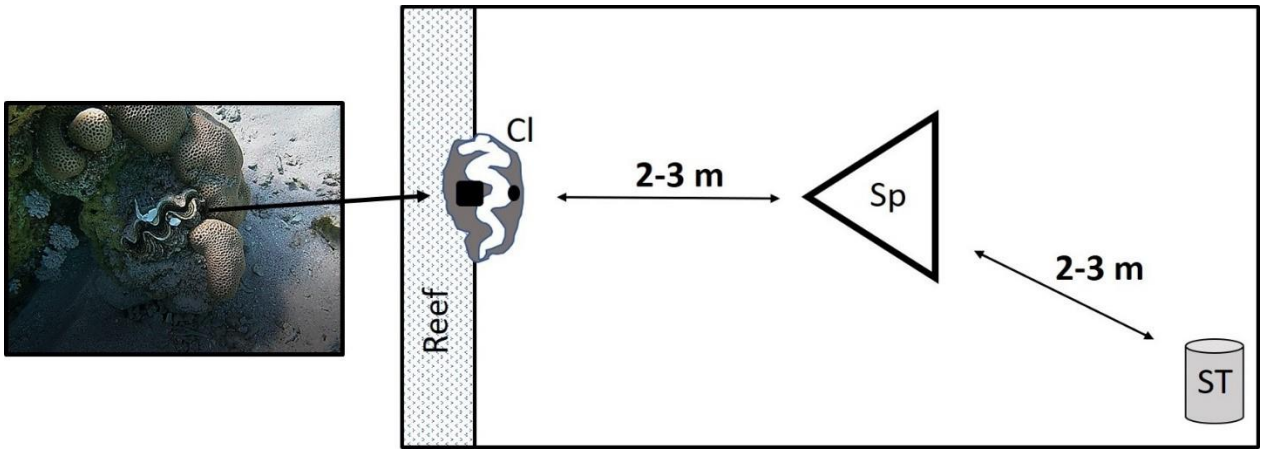

Figure 6.1: Left: A giant clam with a DD and magnet attached. Right: A schematic of the typical experimental set-up, where Cl = a tagged clam; Sp = Speaker, with direction of sound towards the clam; ST = the SoundTrap hydrophone for checking the playback track. The ST is positioned off-centre to indicate that it was not positioned behind the speaker, but to the side to allow better capture of the speaker sound. The playback device, wired to the speaker, was set in an inflatable ring at the water's surface. Both the speaker and SoundTrap were anchored to the sand bottom.

2.3 Identifying movement

Behavioural data was initially inspected using DDMT software (Wildbytes, UK). To determine magnetic field strength as a function of the proximity of the magnet to the DD, the magnetic vectorial sum (hereafter 'MVS') was calculated from the 3 magnetometry axes. The vectorial sum of the dynamic body acceleration (VeDBA) values (derived from all three acceleration axes as defined by) was obtained using a 2 second smoothing window (Shepard, Wilson, Halsey, et al. 2008) to separate static from dynamic acceleration (Qasem et al. 2012). The static acceleration from this exercise was also used to calculate pitch and roll according to:

(1) Pitch $(\beta) = (atan2(S_y, \sqrt{{S_x}^2 + {S_z}^2} \cdot \frac{180}{\pi}$

(2) Roll $(\gamma) = (atan2(S_X, \sqrt{{S_y}^2 + {S_z}^2} \cdot \frac{180}{\pi}$

Where S_x, S_y and S_z are the static component of acceleration in the x, y and z axis, respectively (Bidder et al. 2015). However, since examination of pitch, roll and VeDBA values showed limited sensitivity to clam shell movements (Fig. 6.2), they were subsequently discarded in favour of MVS where visualised data of shell movements were comparable to those reported in other bivalve studies (e.g. Robson, Wilson and De Leaniz, 2007; Schwartzmann *et al.*, 2011; Kaidarova *et al.*, 2018), showing clear sudden closing movements followed by slower opening movements (Fig. 6.2). As a first step, these movements in the MVS data were identified and marked manually with DDMT. Valve closure was dramatic and obvious with high rate increases in MVS (cf. Robson, Wilson and De Leaniz, 2007). As the opening movements typically took the form of an exponential decay, however, the 95% level of opening was used to define the opening period, with the 100% end-point defined as either the start of another closing movement or the point at which there was no change in readings for a period of 10 s or more.

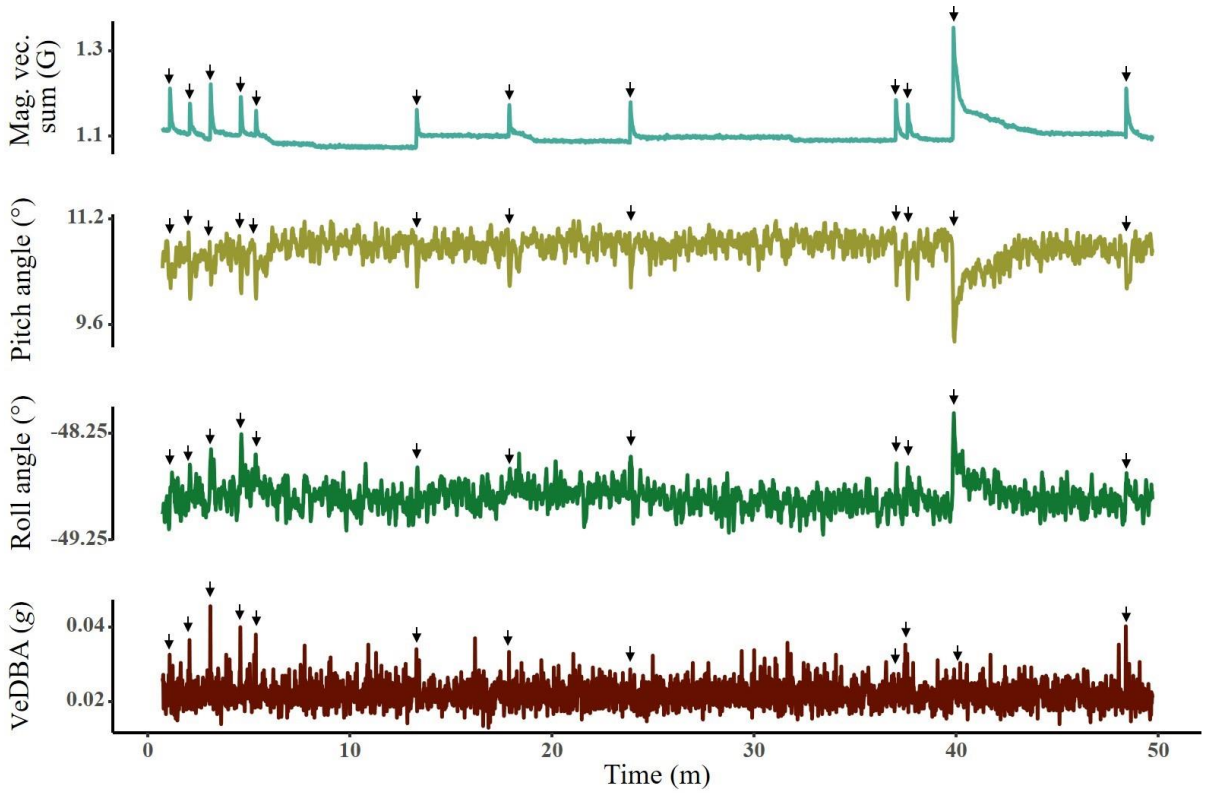

Figure 6.2: Movement data from a single giant clam over 50 minutes, showing the magnetic vectoral sum (derived from the 3 magnetometry channels), the pitch and roll angles of the tag and VeDBA (the vectoral sum of dynamic tri-axial acceleration). Black arrows show the times, in each channel, of reductions in gape angle (i.e. closing movements). The movements of the giant clam (sudden closures followed by slower openings) were most clearly discerned using the vectoral sum of the magnetometry data, where larger values show the magnet as being closer to the magnetometer (and thus indicate reduced gape angle). Although some movement can be seen in the pitch and roll data, it is generally lost to signal noise even with appropriate channel smoothing (due to very little change in the angle itself) while peaks were rarely apparent in the VeDBA signal.

Whilst the closing of clams is driven by adductor muscles, the opening is thought to be a passive process where the muscles relax (Maynard and Burke 1971). To determine whether it was worthwhile examining the metrics describing the full extent of the movement (both opening and closing over time), graphical plots of these movements for each individual were superimposed. This suggested very conserved rates of opening, except for instances for when the MVS was particularly intense (i.e. when the preceding maximum closing extent was greatest), when opening rates appeared to differ somewhat (Fig 6.3). Overall, however, comparison of these movements seemed to support the assumption that opening was indeed passive and examination of rates of opening would not be fruitful. In any event, since each individual clam had a different MVS vs valve gape relationship (because the magnets and DDs could not be fixed to the shells in an identical manner) and we had no independent, individual calibration for gape extent, comparison between individuals would have been problematic. Against this, MVS allowed easy recognition of valve closure as binary events and this was therefore used as a primary metric in further analysis.

2.4 Statistical Analysis

All statistical analysis was conducted in R v3.6.1 (R Core Team 2019). The change in the number of closing movements between hour 1 (ambient noise) and hour 2 (treatment – either ambient noise or boat noise) was compared. The control treatment group in the count data had a non-normal distribution (assessed by a Shapiro-Wilk test and also visually by QQ-plots) but groups were found to be homogenous in variance (assessed by a Levene's test). Given the non-normality and that both groups were small in sample size (N = 11 and 19 for control and treatment groups, respectively), resampling methods, which make few assumptions about underlying distributions and work well with small datasets (Good 2013), were employed.

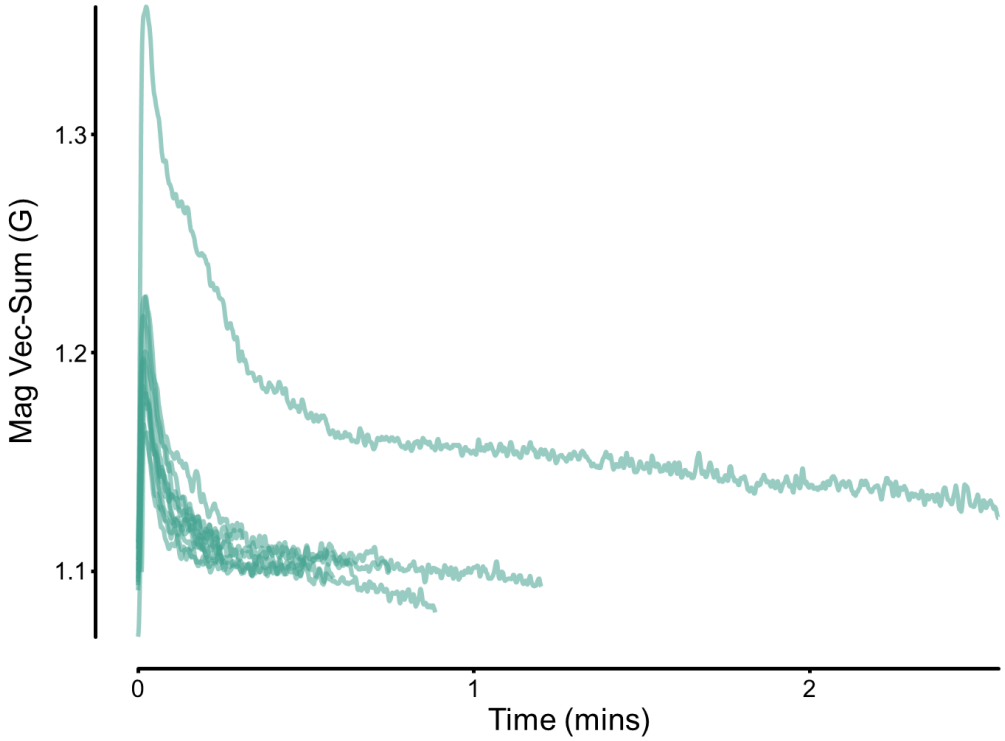

Figure 6.3: The magnetic vectoral sum for the same 12 valve closure and opening movements (sudden closures followed by openings) depicted in Figure 6.2 superimposed onto each other. Note the conserved opening rate, with the exception of the opening following the extreme (>1.3 G on the y axis) closure.

Permutation tests were conducted to compare differences in the means and medians, and a bootstrapping approach (using a percentile method) was used to estimate 95% confidence intervals for the differences in means and medians between the two treatment groups. In both test types, 10,000 iterations of random sampling were conducted. Because there were relatively few numbers of movements overall and because overall movement count per hour had already been investigated, analysis of frequency of closures over shorter temporal scales was not attempted – summing these movement counts was thought to be the most parsimonious way with which to interpret this data.

An attempt was also made to investigate the change in MVS over time between groups. As specific opening angle measurements were not taken during these experiments, changes were quantified within individuals only and linear models for each clam produced (where there were more than 2 data points (closing events) for an individual). The sample size, both of clams and movement counts, complicated this however (see *3.2*).

3. Results

Of the 44 tagged clams, 30 were used in the analysis. Reasons for omission were either; (i) water ingress into the tag housing making data retrieval impossible, (ii) clearly incorrect magnetometry data suggesting a malfunctioning magnetometer/tag, or (iii) interruption of the experiment, so that the trial was either cut short or the data deemed unusable for extraneous reasons (e.g. due to the presence of another boat). Of these 30, 11 were of the control group that was played only ambient reef noise and 19 were of the group that was played boat noise in the second hour of the trial.

3.1 Basic patterns in valve closure

A total of 184 closing (i.e. reduction in gape angle) movements were recorded, the duration of which was very conserved (mean = 1.4 s ± 0.6 sd; Fig. 6.4). These movements followed the same general pattern – a quick reduction in gape angle, followed by a slower opening. On average, clams first moved 8.1 minutes (± 8.1 sd, min = 0.8, max = 34.5) following beginning of sound playback in hour 1. The first movements following the start of the boat noise occurred after a mean of 16.2 minutes (± 17.02 sd, min = 4.2, max = 58.3). Mean time between movements was 9.8 minutes (± 1.6 sd, min = 0.02, max = 87.8) with a generally left-skewed distribution per individual (a higher incidence of shorter times interspersed with longer waits), but with some variation across clams (Fig. 6.5). The extent of closure varied within individuals, though usually with the earliest closures resulting in the smallest mean gape angle (Fig. 6.6).

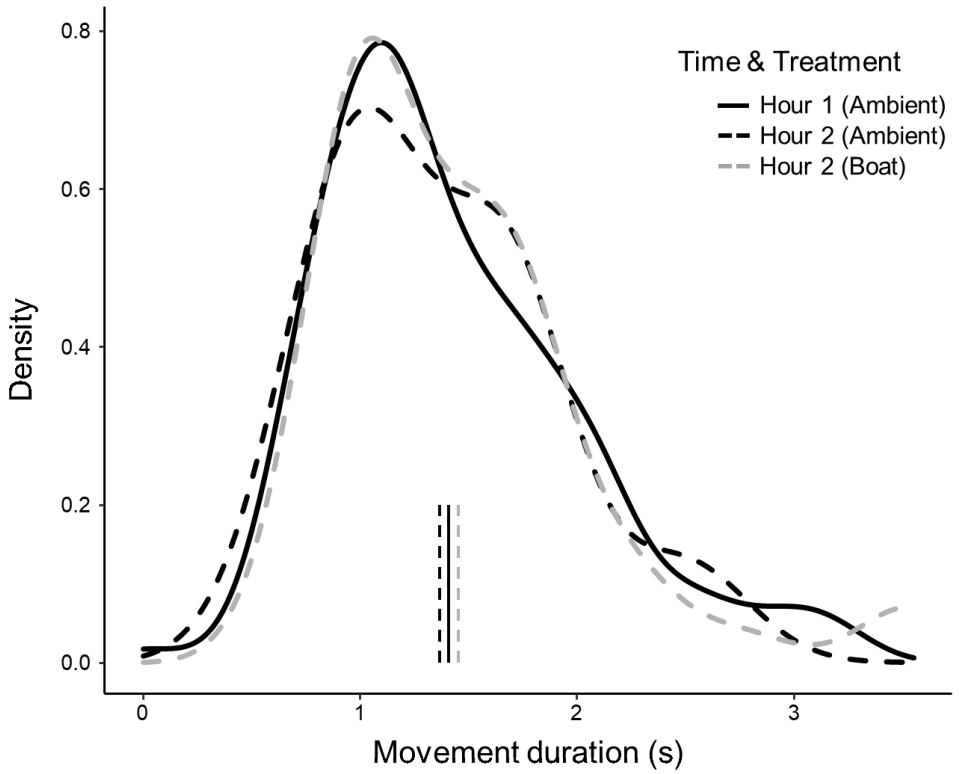

Figure 6.4: Density distributions of durations (seconds) of closing (i.e. reducing gape angle) movements for N = 30 clams (N = 184 movements), presented by either the first hour of the experiment (N = 123 movements) or the second and, for the second hour, ambient (N = 11 movements) or boat (N = 50 movements) noise treatment. Vertical lines represent the mean values for the corresponding three groups.

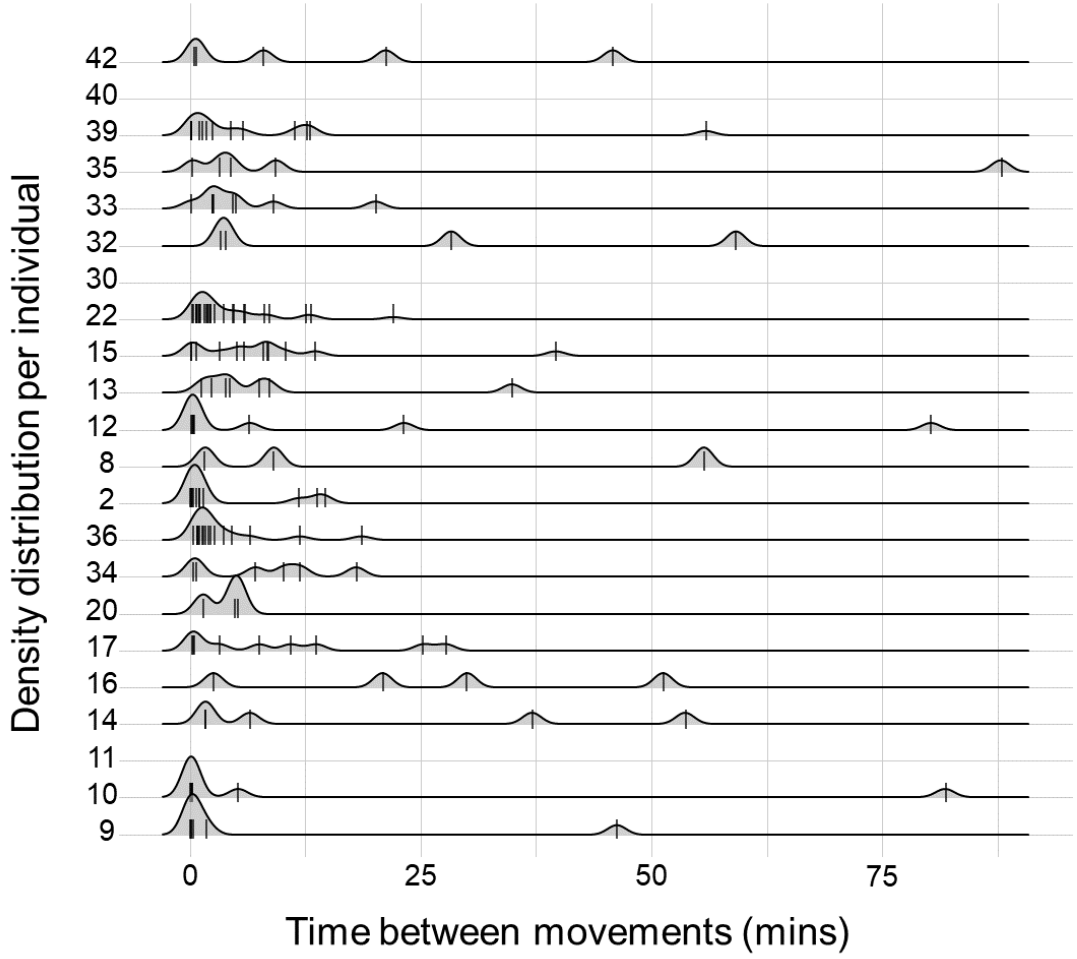

Figure 6.5: Density distributions for time (minutes) between successive closing movements for each clam (numbered y axis). Vertical lines in rugs represent individual data points. Note that the heights of density curves are relative within each individual.

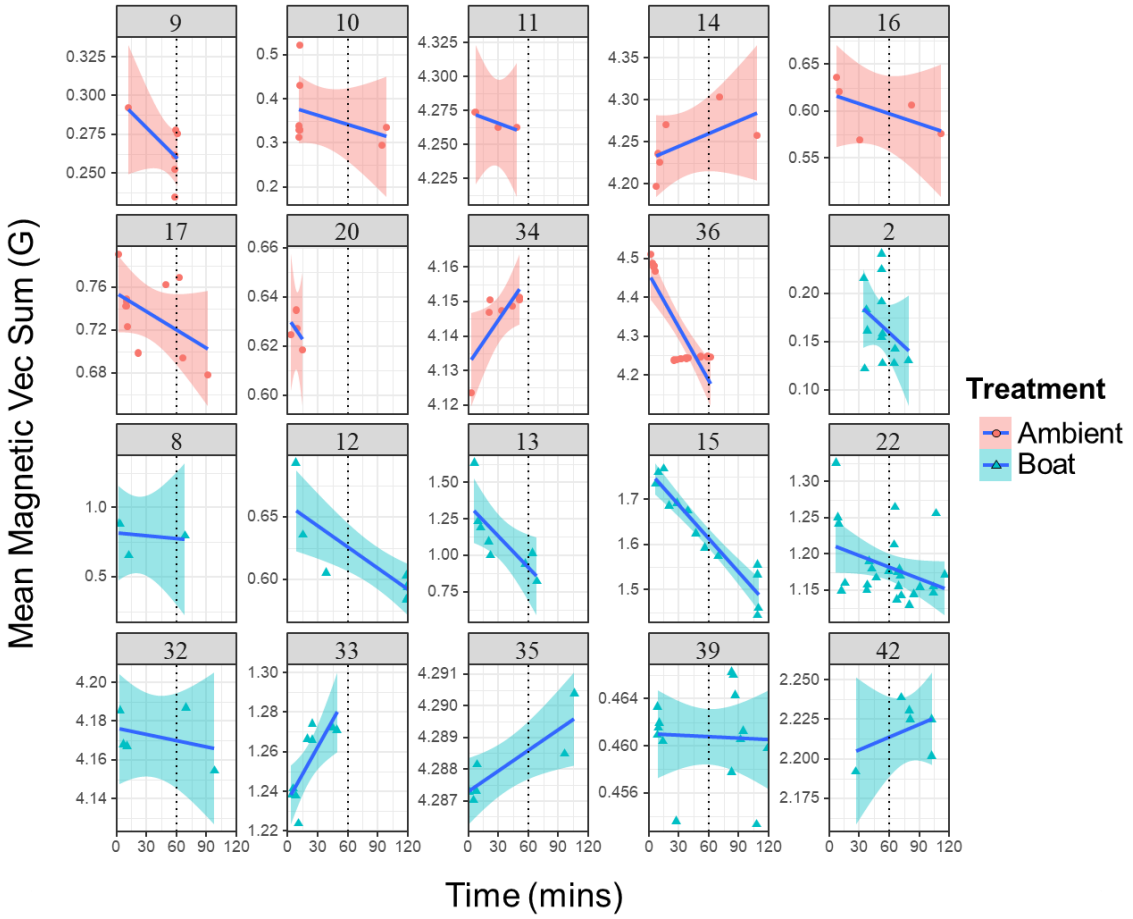

Figure 6.6: Mean magnetic vectoral sum per closing movement over time (minutes since the respective trial start), per individual (by panel and numbered by clam ID) and coloured by treatment (ambient noise: first 9 panels, red CIs and points, circular points; boat noise: last 11 panels, blue CIs and points, triangular points). Each individual has been fitted with a linear model trend line and 95% CIs. The vertical dotted line in each panel (at a time of 60 mins) denotes the start of the second hour (when noise treatment either stayed as ambient control noise or switched to boat noise). Note the dramatically different y-axis scales resulting from small differences in magnet placement and magnet distance from the sensor, limiting inter-individual comparisons.

3.2 Change in movement count

Across all animals, there was an overall decrease in the number of valve closures from the first to the second experiment hours (mean change = -2.1 ± 3.9 sd, median change = -1.5; Fig. 6.7). Of the 30 clams, 8 (27%) did not move at all over 2 hours. 17 clams (57%) moved less in the second hour of their trial and 4 (13%) moved more in the second hour. All clams that moved more in the second hour were from the boat noise treatment group. The overall decrease in each of the groups was, on average, greater for the ambient noise treatment group (mean change = -4.1 ± 4.2 sd, median change = -4) compared to the boat noise treatment group (mean change = -0.9 ± 3.3 sd, median change = 0).

Permutation tests showed that the difference between treatment group averages for changes in movement count was statistically significant, for both the mean and median (absolute difference in group means = 3.2, absolute difference in group medians = 4, both $p < 0.03$). Bootstrap sampling found 95% CIs around the difference in group mean of 0.6 and 6.2 and around the median of 0.0 and 5.0.

3.3 Closing extent and rate

The mean MVS during a closing movement generally decreased with time (4 positive linear slopes *vs* 16 negative, following removal of two clams with only 2 data points (experiments 30 and 40) and 8 with no movements at all). Linear model coefficients and R^2 values can be found in Appendix 6. Attempts to further discern a relationship of MVS with time, or between treatments, however, were discontinued for two main reasons. Firstly, the distribution of points depends on the number of times that the individual closed; numerous clams either did not move at all, did not move at all during the second (treatment) hour, or only moved during the second hour within the first few minutes. Secondly, due to the non-linear relationship of magnetic

force with distance (magnetic field strength decreases with distance approximately according to an inverse square law), scales of MVS vary widely by individual and should likely not be analysed with an assumption of linearity. Any analysis must, therefore, look at changes within individuals only, although our experimental protocol provided too few data points (valve closures) to either discern any non-linear change or draw comparisons between treatment groups. By the same token, because rate of change of MVS is subject to the same errors with regard to magnetic strength and distance, this line of analysis was also discontinued (Appendix 6).

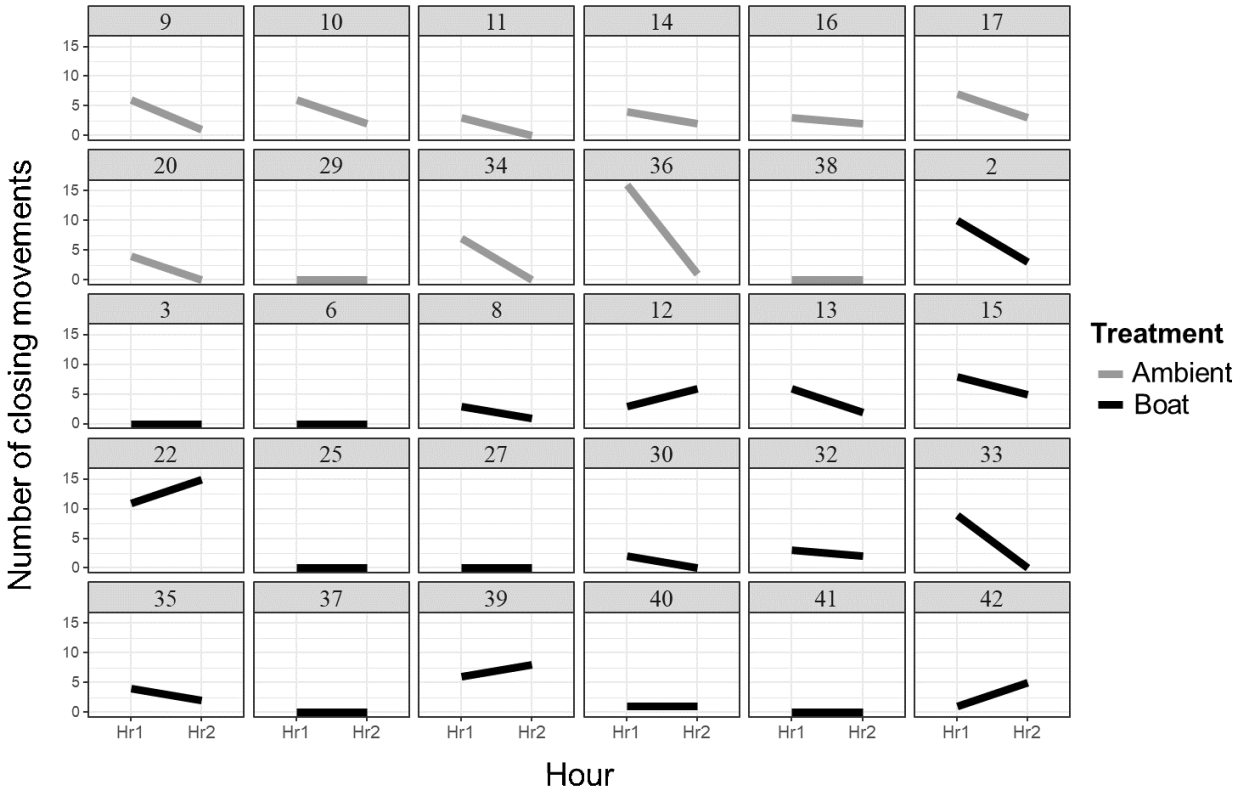

Figure 6.7: The change in the count of movement (closing) events between hour 1 and hour 2. Results are shown for each individual (numbered) and coloured according to treatment of either 2 hours of ambient reef noise (grey) or 1 hour of ambient reef noise followed by 1 hour of boat noise (black).

4. Discussion

4.1 Comparisons with similar studies

The movement signature of clams seen here - a rapid closing typified by a sharp spike in MVS (varying with closure extent), followed by a much slower opening - mirrors that in other bivalve studies including clams (e.g. Kaidarova *et al.*, 2018), mussels (Robson et al. 2009) and oysters (Charifi et al. 2017). Giant clams feed by both autotrophic (*via* zooxanthellae within the mantle) and filtration methods, both reliant on wider valve gape angles that most commonly occur when the animals are undisturbed (Soo and Todd 2014). Gape angles, dictated by valve movements, will often change when the animals remove waste such as pseudofaeces and faeces (Newell 2004, Soo and Todd 2014), with times of day - most commonly closing at night (Morton 1978, Schwartzmann et al. 2011) - or as an anti-predatory response (Johnson et al. 2017, Dehaudt et al. 2019). Their movement, as described here and elsewhere, is brought about by the contraction of the adductor muscle (Maynard and Burke 1971) which reduces gape angle when stimulated while relaxation allows gradual reopening.

4.2 Habituation to the tag attachment protocol

The general decline in peak magnetic strength over sequential valve closures, representing less severe closing extents over time, suggests that there is a habituation effect, even in the animals exposed just to ambient noise. It is certainly expected that the clams would close during the fixation of the measuring apparatus, which might be likened to a typical predatory stimulus and, following this, habituation seems likely given that other bivalves have shown similar trends to that observed by us following disturbance by predators (Wilson, Arnott, et al. 2012),

humans (Robson et al. 2016, Dehaudt et al. 2019), and tagging procedures (C. D. Wilson *et al*., 2011).

Despite the fact that extreme disturbance of bivalves can lead to valve closure anomalies for periods of up to 16 hours (C. D. Wilson *et al.*, 2011), it was still unexpected that the likely length of habituation to be more than a few minutes because the handling of the animals was minimal, with the attachment of the tag and magnet carried about by applying gentle pressure to epoxy putty followed by immediate removal of the worker from the water. This is in contrast to the experiments of, for example, Robson et al. (2016), where human presence was regular and sustained, or C. D. Wilson et al (2011), where mussels were removed from the water for over 40 minutes. We note, however, that Dehaudt *et al*. (2019) showed that *T. maxima* habituate somewhat to touching of the shell and mantle, with time taken to reopen following closure decreasing slightly with each consecutive touch at 2 minute intervals, whilst Johnson *et al.* (2017) found that *T. maxima*'s post-disturbance (a tap with a pole) closed duration declined over 4 non-consecutive days. Neither of these studies looked at habituation over a single, sustained simulated disturbance event so it was uncertain how long any habituation, if observed, would last. Ideally, the experiment detailed here would have benefitted from a much longer period of observation but the short protocol was specifically chosen to minimize the probability of experimental disruption through genuine boat noise invalidating results (which did occur twice during our data collection anyway).

4.3 The effect of boat noise on *T. maxima* behaviour

Despite this being a preliminary study with a small sample size, there is an apparent effect of boat noise on the movement of *T. maxima* which ties in with a few studies that have shown the ability of bivalves to perceive anthropogenically-generated noise, examples being mussels

(Roberts et al. 2015) and oysters (Charifi et al. 2017, Shi et al. 2019). Specifically, the between-hour change in closure events saw a significantly smaller decrease in closing events under the boat noise treatment, which suggests that the boat noise hinders the habituation process that occurs following handling. This process is similar to that seen when *Tridacna squamosa* is exposed to sediment stress (Elfwing et al. 2001) – the general high rates of shell closure reducing sediment build-up in the mantle cavity. In fact, valve closures are often associated as part of the general bivalve stress response, with wider angles typically being taken as a positive welfare indicator (Elfwing et al. 2001, Schwartzmann et al. 2011, Soo and Todd 2014, Charifi et al. 2017). Certainly, repeated valve adduction above the norm interrupts both photosynthetic- and filtration- based feeding which rely on larger gape angles, with potential implications for growth that are further confounded by the energy used to close the valve repeatedly (Livingstone et al. 1981, Robson et al. 2012, Soo and Todd 2014). This helps explain why the Pacific oyster *Magallana gigas* has been shown to suffer lower growth rates when exposed to shipping noise, having also spent more time closed (Charifi et al. 2018). In our experiment, it may well be the case that the handling and noise acted as co-stressors, with the attachment protocol rendering the clams more sensitive to further disturbance. In this regard, it is notable that in the Elfwing *et al.* (2001) study the increased instances of shell contraction in response to water sedimentation was further pronounced if clams had also previously been exposed to copper. Either way, there are clear survival implications in over-active valve closure behaviour for clams, which expend energy in order to activate their adductor muscles and, confounding this energy loss, reduce the time spent fully open, presumably compromising their feeding ability.

We believe that it is highly relevant that our hypothesis, that the clams would not be disturbed by boat noise because they live in an environment with regular boat traffic, is incorrect. In essence, our results imply that the animals do not habituate to the boat noise to which they are

normally exposed. Specifically, with relatively more closing movements in the second hour when exposed to boat, rather than ambient, noise, they simply appear to be more disrupted. This equates to more time closed and greater energy expenditure. The exact reason for them eliciting this movement is difficult to discern without further work – sudden closures (i.e. just several seconds), as seen here, might be part of a protection response (Dehaudt et al. 2019) or an attempt to remove waste (Soo and Todd 2014). The argument for the former is perhaps more intuitive, given that other bivalves have been shown to close suddenly in response to sudden sound treatments (Charifi, et al., 2017; Roberts et al., 2015) and predator cues (Wilson, Arnott, et al. 2012). Given that the response of shellfish to anthropogenic noise, and specifically that from boats, seems to be ubiquitous, it is reasonable to want further clarification. What level noise induces what level of closure and over what length of time? What are the energetic and feeding consequences of this? Can we extrapolate from our test animals to the whole population and, if so, what do the changes invoked in the filtering and growth capacities mean for the environment? Given the increases in boat traffic across the world (Duarte et al. 2021), it would seem germane to begin to answer these questions rapidly.

4.4 Conclusions

Whilst we tentatively infer from this limited sample size that boat noise affects *T. maxima*, we need to examine the effect of the treatment over a longer time period. It may also be that what we observed was due to the co-stimulus of attaching the recording device and the boat noise, which longer term studies could also preclude. Differences in the time of day or night (e.g. Jou et al., 2013; Liao et al., 2009) may also modulate how any effect is manifested, as may the precise type of boat noise. Longer-term experiments should be set up to deal with these issues

and could use several randomised cycles of ambient and boat noise to elucidate the true relationship between closing behaviours and boat noise.

Synopsis

Biologging- collecting data on an animal's movement, physiology, behaviour and/or their environment, using attached tag technology (Cooke 2008, Rutz and Hays 2009, Fehlmann and King 2016)- is a constantly evolving field, or more accurately an approach. This approach is changing in many ways, developing with respect to animal wellbeing, tag size, tag battery longevity, data recording capacity and speeds and more. The research presented here is part of the King Abdullah University of Science and Technology (KAUST) 'Coupled Animal and Artificial Sensing of the Environment (CAASE)' project. CAASE is a collaborative effort between biologists, sensor scientists and engineers to develop and deploy novel sensing technology in the marine environment with a particular focus on animal-attached devices.

At the very start of this PhD research, I was presented with the opportunity to test and deploy some of this new technology on the coral reef inhabitants of the Red Sea and in other tropical areas of the world. I was given a wide topic area to choose from, and could have attempted to look at, for example, predator/prey interactions, niche competition, or group-level coordination and behaviour using 'conventional' (available) tags coupled with more recently developed magnet-sensing speed and limb sensors (Kaidarova et al. 2018). Indeed, the remit was so broad that I could even have looked to use these technologies to use tagged animals as living environmental probes, returning temperature or salinity data as they moved around the Red Sea wearing thin gel-like sensor pads (Nassar et al. 2018). I even had the possibility of using implantable sensors to match context-dependent behavioural changes to hormonal ones (Lee et al. 2018). Confusingly, and unexpectedly, I was subject to the 'child in the sweet shop' syndrome: too much choice made settling on a specific topic difficult. I quickly appreciated, however, that there were fundamental limitations and challenges that I would need to overcome. It is naïve to assume that one simply has to attach a tag to an animal, especially a species that has not been tagged before, and wait for meaningful data to come rolling in.

At the very beginning of the project, for example, wanting to look at movement in teleost fish, I spent time designing novel attachment methods for these animals. Specifically, I sought to use 3d design and printing technologies to produce an animal-friendly, streamlined, cheap, flexible system to accommodate any of the array of tags and sensors that might be made available to me. This attachment was also born from the need to easily attach and detach tags and in a way that was amenable to larger scale deployments. The more I worked on this, the more I became aware of the taxon-specific problems (highly sensitive and thin skin, lateral line operation, mucous-covered external surfaces etc.), the more I found myself wanting to start with a more robust fish group where these problems are minimized and even considering other animals with which to address some of the seemingly near-infinite windows of insight that biologging offers. In its real-world application, biologging is more problematic. In a nutshell, how do you move beyond simply sticking a piece of remarkably powerful technology onto an animal and instead be sure to do it responsibly?

To help facilitate simpler questions that could be applied more widely, I turned to other systems, particularly invertebrates. I was looking to resolve some of the simpler, yet nonetheless important, questions that might arise in the CAASE project's application. For example, how might we better examine slow-moving animals when many biologging methods are more geared to fast-paced and dynamic species (Shepard, Wilson, Liebsch, et al. 2008, Watanabe and Takahashi 2012, Kays et al. 2015, Taylor et al. 2016, Wilmers et al. 2017), particularly when it comes to estimating free-living energy expenditure (Wilson et al. 2006, 2020, Wright et al. 2014). Furthermore, might slow-moving animals even be excellent candidates for understanding movement rules, especially within a probabilistic context? After all, many marine invertebrates do things comparatively slowly e.g. Lyons *et al.*, 2013; Fossette *et al.*, 2015; Dujon *et al.*, 2019, manifesting a response that would seem a 'considered' synoptic manifestation of multiple movement inciters into one action, rather than the fast-paced, quickly

changing responses of many vertebrates to a rapidly changing environment (not least because they move through their environment rapidly and thereby change their local conditions).

As I pursued these efforts, the difficulties of designing a teleost tag attachment system morphed into working on a fin-mounted elasmobranch attachment. However, given the apparent 'ease' with which elasmobranchs could be tagged compared to teleosts, the methods used not only varied widely - ranging from clamps (Chapple et al. 2015) to harness loops (Fontes et al. 2017) to towed systems (Marshall et al. 2015) and bolts through the fin (Jewell et al. 2011) - but also appeared rather cumbersome and onerous to apply, and certainly did not match the 'high-tech' descriptor of the sensor-laden tags that they carried. Indeed, given that many of the sensors that we take for granted in biotelemetry and biologging were originally introduced to, or developed for, aquatic animals (e.g. accelerometers (Yoda et al. 2001), heart rate (Butler et al. 1995, Woakes AJ et al. 1995), hall sensors (Wilson and Liebsch 2003), pressure sensors (Kooyman 1965, Watanuki et al. 2003), critter cam (Williams et al. 1991)), it is surprising that the way we attach these sensors to these animals has not developed at the same pace (Jewell et al. 2011, Musyl, Domeier, et al. 2011, Jepsen et al. 2015).

So, in contemplating the best short-term attachment system of high-tech to sharks while still considering what, exactly, I was going to study when I had achieved my proximate aim, I was forced into the hugely important, but generally underestimated, consideration of 'angles for animals'. This began with having to grapple with moment arms and angles and their role in modulating the forces applied by magnets on fish fins but ended with recognition that animals have choice in the way they change their own body angles (pitch roll and yaw) at varying rates and that this not only constitutes a behavioural response (Noda et al. 2014, Payne et al. 2016, Gunner et al. 2020) that can be quantified but also determines the energy they are expending in their responses (Wilson et al. 2013, Crossley et al. 2018). Identifying this theme helped lay the foundations for the diverse projects that I undertook, but I was subsequently also led down

serendipitous roads, some dead-ends and some fortuitous, as I worked on the various challenges presenting themselves from working with diverse taxa. This made me aware of the value of serendipity in science (Roberts 1989) but also of real-world problems that might not allow such 'distracted' thinking. Whilst I am pleased with where I have taken each thread, I am aware of how much further each could be taken and the steps that I wish I might have taken myself.

The development of the M-clip, discussed in Chapters 2 and 3, is, for me, the most obvious candidate for continued development. Having spent so much time exploring technologies, materials and methods, the attachment system now needs 'finishing'. It would particularly benefit now from continuation of the early Computational Fluid Dynamics work that is shown in the Chapter 2 supplementary information (Appendix 1). Refinement of the M-clip shape and understanding how it interacts with water flow around a shark and the resultant forces (and how this varies with the angle between the body and water flow) would greatly enhance its ability to remain attached to the shark fin for longer periods and with minimal detriment to the animal. By taking advantage of the ease of the CAD process, a worker with groundings in engineering should be able to implement a suite of features for the M-clip such as Venturi channels (Fiore et al. 2017), stabilising fins, integrated electronics within the plastic body or refinement of the leading edge to reduce its current protrusion from the fin. The two features that are clearly required are; 1) improved padding/frictional material on the inner arms and 2) a workable retrieval method. Both needs are perhaps trivial with focused development but, frustratingly, I am out of time. More form fitting materials, such as Neoprene foam or a non-air-filled equivalent, might do better at accommodating the inter-species, and inter-individual, differences in dorsal fin form. For the retrieval method, the Polypropylene plastic used here is already buoyant on its own (although less so when magnets and tag packages are attached) and the leading hinge pin could be galvanic to provide a drop-off system (Gleiss et al. 2009, Whitmore et al. 2016).

In deploying the M-clip in a captive setting, I was able to appreciate the importance of angular changes in identifying aberrant behaviours that might otherwise not be obvious. However, whilst the aquarium setting was an excellent way to monitor the sharks post-tagging in detail, it would be invaluable to expand this work to open water species or, at the least, a semi-open captive setting such as in Bullock *et al.* (2015). The aquarium that hosted the work of chapter 3 (Oceanografic Aquarium, Valencia, Spain), whilst excellently equipped, was primarily underground in an environment with multiple iron beams so magnetometry could not be employed (Williams et al. 2017). Magnetometry would provide additional insights into space use and angular changes in swimming path following tag attachment through dead-reckoning (Wilson et al. 2007, Bidder et al. 2015) and may highlight some behaviours where accelerometry alone does not (Fig. 7.1) (Williams et al. 2017). Where Chapter 2 advocates that researchers should take greater care in attachment of tags, Chapter 3 suggest that others should consider carefully how tag effects might be manifest on the animal and how we can identify such effects, including *via* visualisation.

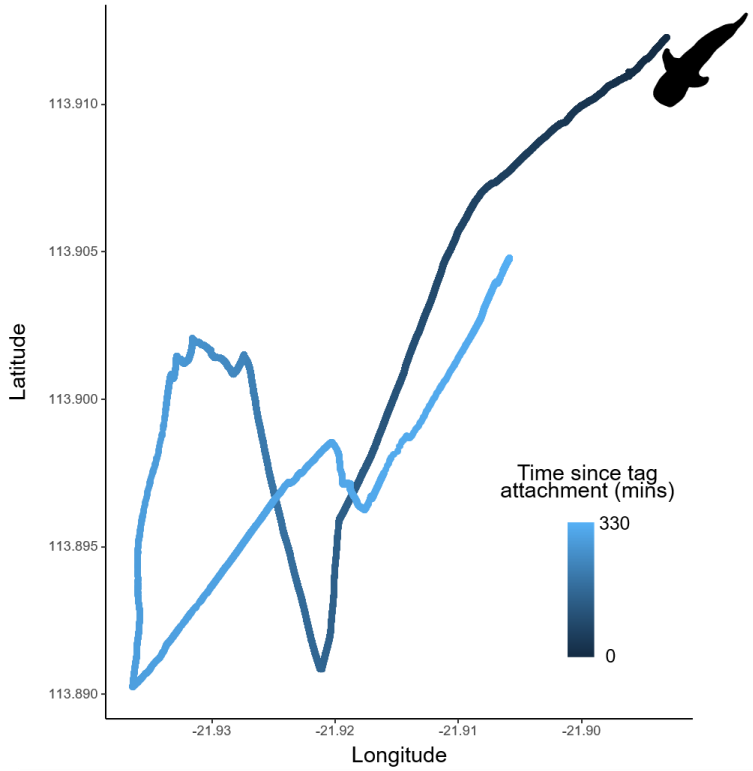

Figure 7.1. A 330-minute dead-reckoned track of a tagged Whale shark, *R. typus*. Dead-reckoning (Bidder et al. 2015) provides high-resolution behavioural data across large special scales and can be supplemented with extra data dimensions. Here, the track is coloured according to time since logger attachment (mins) and emphasises the change in turn angle distribution as a function of logger attachment time (suggestive of an attachment effect).

The use of angular changes as an energy proxy, described in Chapter 4, opens the door to quantifying energy expenditure for hugely diverse and ecologically important, though under-represented, taxa. While the results, that rate of change of body angle (RocRM) relate to energy expenditure, are bound in Newtonian physics (Wilson et al. 2020), it is critical that a much wider selection of species, not just invertebrates, are tested under similar conditions. Such work would identify the extent to which identified relationships between RocRM and VO_2 are valid, particularly as the level of dynamic movement increases *sensu* 'dynamic body acceleration' (Wilson et al. 2020) and DBA is considered the most valuable proxy of VO_2. Indeed, I predict

that there will be species for which a combination of DBA and RocRM are the most important predictors of VO_2 and a sliding scale of the relative importance of each metric will be apparent as we progress to studying more or less dynamic animals (Fig. 7.2). Improvements to the methodology will help this effort greatly though. The static respirometry methods employed in Chapter 3 were clearly not ideal, but a product of limitations of the animal (a slow-moving invertebrate), the nature of the experiment (requiring enough space to 'properly' move) and the facilities and equipment available. A much higher resolution oxygen sensor would allow researchers to measure shorter movement instances, perhaps even to one or a few 'jumps' of the conch, thus lessening the restriction of the tank size and its walls. This would also better facilitate flow-through respirometry as opposed to static methods, which would be particularly necessary for more dynamic animals. At the very least, this work complements the recent interest in angular-based metrics creeping into animal movement studies – whether lobsters (Zenone et al. 2020), snakes (Whitney et al. 2021), conchs (Wilson et al. 2020) or turtles (Gunner et al. 2020) – and encourages the continuation of framing movement in this way as a powerful tool for monitoring the energetics of free-living animals.

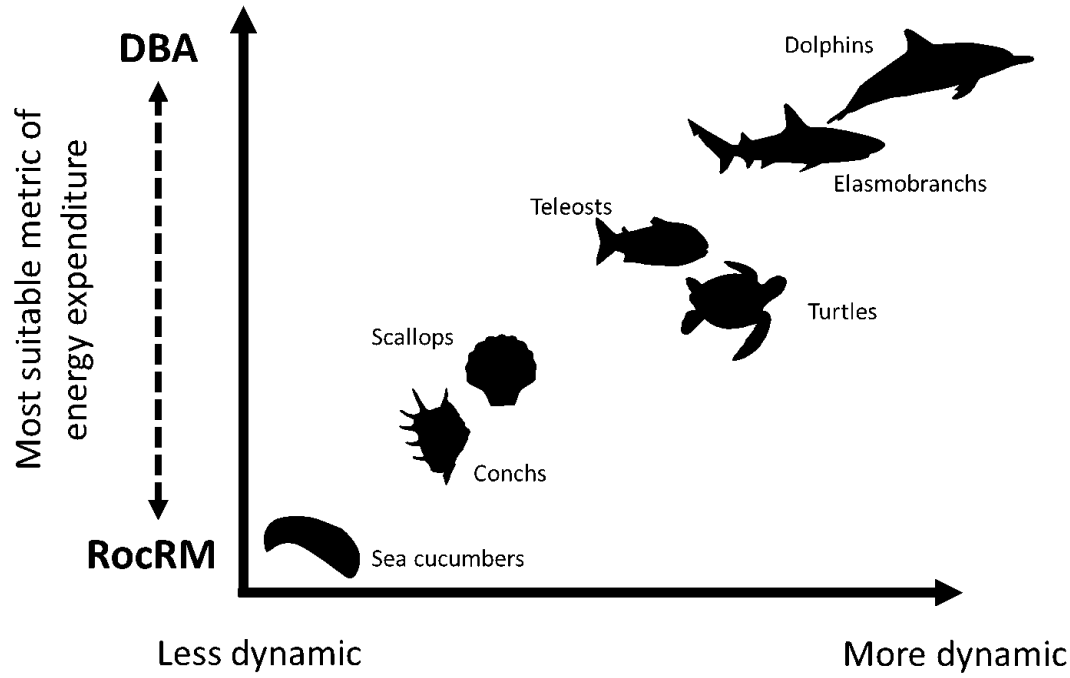

Figure 7.2. Schematic representation of a hypothetical scale showing the relative value of proxy metrics of energetic expenditure, specifically Dynamic Body Acceleration (DBA) vs. Rate of Change of Rotational Movement (RocRM), as a function of how dynamic an animal's movement is. RocRM would serve as a better proxy for energetic expenditure in animals that move slowly and more gradually with a lower dynamic component of acceleration, whereas DBA would be a more suitable proxy for faster moving animals with higher dynamic acceleration. The suitability of one metric over another would not necessarily be absolute, with a combination of both metrics applicable for different movement types. For example a regular turtle swimming signal would be well described by dynamic acceleration signals and DBA, but RocRM may be more apt during the bottom phases of dives when movement is slower and smoother (Gunner et al. 2020).

Extension of the RocRM approach to other taxa offers a tantalising prospect to examine the 'energy landscape' (Wilson, Quintana, et al. 2012, Shepard et al. 2013) at the 'micro' scales.

Coral reefs, for example, host a multitude of site-attached species, including a host of slow-moving invertebrates. Researchers therefore have an opportunity to map fine-scale, overlapping (in the 3d environment) energy landscapes to make inferences into space-time-species interactions far beyond that which has gone before.

Such prospects go hand-in-hand with the work described in chapters 5 (where conch movement was expressed in terms of conditional probabilities) and chapter 6 (where *Tridacna maxima* clams were shown to alter their opening and closing behaviour in response to anthropogenic noise). Continuing with the coral reef example, building a picture of energetic costs and gains as a function of inter- and intra- species interactions, reef topology, environmental conditions (whether natural ambient, such as temperature or salinity, or anthropogenic in origin e.g. Nickel *et al.* (2021)) requires understanding of angular movements – ranging from the movement of the whole animal (as in chapter 5) or the relative movement of limbs or muscles (as in chapter 6).

There is now an appreciable body of literature into the effects of anthropogenic noise on the behaviour of various marine animals. However I believe the work in chapter 6 is unique in its dedication to an open-water experimental setup, which avoids many arguable shortcomings with lab-based procedures (Slabbekoorn 2016). Whilst there is promising evidence of an effect of anthropogenic noise on 'recovery' times post-tag deployment, this study in particular would have benefitted from a greater sample size as well as a more absolute measure of the closing angles of the clams (requiring the measurement of opening and closing angle for each tagged clam for calibration purposes). Unfortunately, whilst the open-water nature of the experiment is a boon to real-world translation of results, it also limited our ability to adequately control for other factors. We contended with boat traffic, the shutting down of the waterways at unpredictable times, and weather, which collectively demanded that we be fast and concise

with what we were doing and regrettably had to discard some data. Plans to gather further data were, sadly, hampered by the global COVID-19 pandemic. Nevertheless, I would be keen to restart this study in the future, not only to refine the methodology and clarify the data gathered, but also to expand (and take advantage of) the open-water approach and tie it into the aforementioned space-time-species interactions in terms of the energetic landscape.

The field of biologging has made mammoth strides in the previous decade alone. I hope that by considering some of the more fundamental aspects of the field- for example attachment methods, probabilistic thinking and measures of aberrant behaviour- and using an overarching thread of thinking about angles, I have provided useful thought for other researchers preparing their own animal tagging studies. Certainly, yaw angles in trajectories across taxa covered in this thesis alone highlight that animal trajectories have been considered time and time again on the basis of step lengths alone (Humphries et al. 2010, Sims et al. 2012, Technitis et al. 2015), assuming that turn angles are random (Sims et al. 2008) despite the existence of many movement models that do incorporate turn angle (Patterson et al. 2017). The simple fact that increasing angular extent of a turn translates into correspondingly greater energy expenditure (Wilson *et al.*, 2013; Crossley *et al.*, 2018; Chapter 4), makes the concept of random turns seem singularly inefficient in a world where natural selection should root out inefficiencies. Additional work should provide further quantification of the link between energy expenditure and turn angle across taxa and re-insert it into a framework that considers optimality in movement patterns. These should be considered on the basis of the conventional elements such as rate of energy acquisition during foraging (Costa 1991, Ropert-coudert et al. 2004, Wilson, Neate, et al. 2018) but bind it with proper energetics, by considering energy landscapes (Shepard et al. 2013, Halsey 2016), step lengths (Codling et al. 2008) and turn angles (Wilson et al. 2013, Crossley et al. 2018) in wild animals (especially the ‘simple’ ones). For my own part, I must submit this thesis and so close-down this avenue of exploration which seems so

fresh and open to new ideas and investigations. Despite any misgivings about not being able to go further, it has been a pleasure to explore such a diverse and fascinating array of life and to offer my own opinions and musings into how biologging might proceed into the future to maximise its potential.

Appendix 1

Supplementary Information for 'Chapter 2 - A new approach to minimal impact tagging; the case of a shark fin clip'.

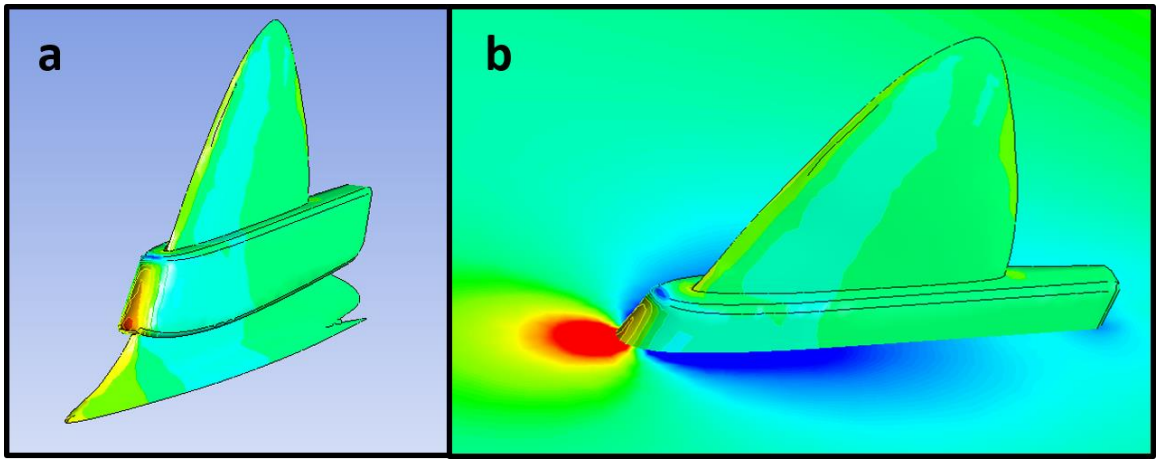

Figure A1.1: Preliminary Computational Fluid Dynamics (CFD) simulations through Ansys Fluent (version R15.0; ANSYS Inc., Pennsylvania, USA) following the step-by-guide from (Kay et al. 2019). Preliminary CFD was conducted to inform the design process. The colour scale of red-blue corresponds to highest–lowest pressure areas.

Calculation of Tail-beat Frequency for Rhincodon typus data

Individual tail beats of *R. typus* were first identified using DDMT's Behaviour Builder function (Wilson, Holton, et al. 2018). Acceleration data were first smoothed over 0.5 seconds. A differential over a rolling 0.5 second interval, of Z-axis acceleration was calculated and this channel passed to behaviour builder. As the signal of the Z-axis differential (Diff Z) oscillates above and below a 0 value with tail-beats, three consecutive conditions had to be met to identify

two tail beats (i.e. the movement of the tail from one extreme, through the body midline and then to the opposite extreme):

1) If Diff Z > 0.005 *g*/s for at 0.125 seconds,

   followed by…

2) If Diff Z < 0.005 *g*/s for at least 0.125 seconds,

   followed by…

3) If Diff Z < 0.005 *g*/s.

Because this approach (where essentially the consecutive peaks of oscillating signal are considered the start and end points) actually classifies two consecutive tail-beats as one 'bookmark', the number of tail beats for a given time period was doubled during further analysis to give the true number of individual beats. Note that, for each rule, there was an additional 'flexibility' of 3 seconds – i.e., once a condition was met, the function was allowed to classify the start of the next condition up to 3 seconds from that point.

Appendix 2

Supporting document: Guide for the construction of the M-clip (version 4) CAD model in Autodesk Fusion 360.

This document accompanies 'Chapter 2 - A new approach to minimal impact tagging; the case of a shark fin clip'.

This is a step-by-step guide on how the M-clip v.4 was created within Autodesk Fusion 360 software (Autodesk Ltd., Farnborough, UK). Before following this guide, it is important to obtain basic measurements of the (1^{st} or 2^{nd}) dorsal fin of the shark species of interest. This guide assumes a basic knowledge of the Fusion 360 software and its toolset.

1) Draw circles representing known widths of the fin through a cross section. Inner circle = actual width of the fin; outer circle = extra leeway given to accommodate tag and fin deviance from standard (here = 1 mm extra).

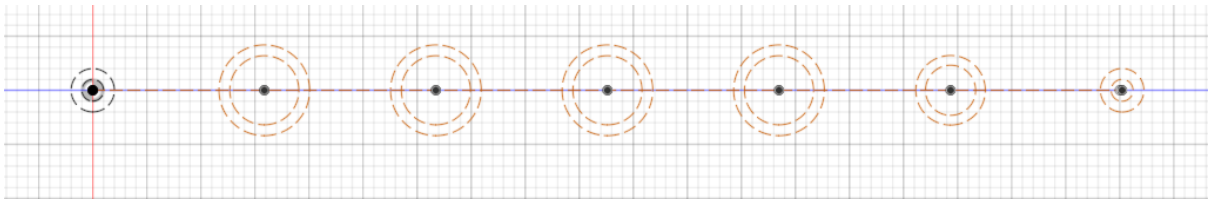

2) Draw the basic fin shape using the outermost circles as a guide. The front circle serves as the leading radius.

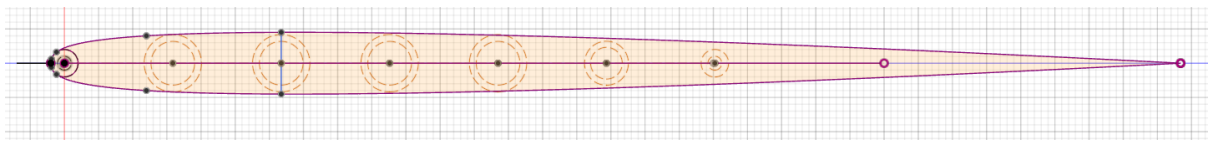

3) ‘Create’ > ‘Sweep’ tool to create a body along the first sketch curve. Here = 22mm width, 5 mm thickness.

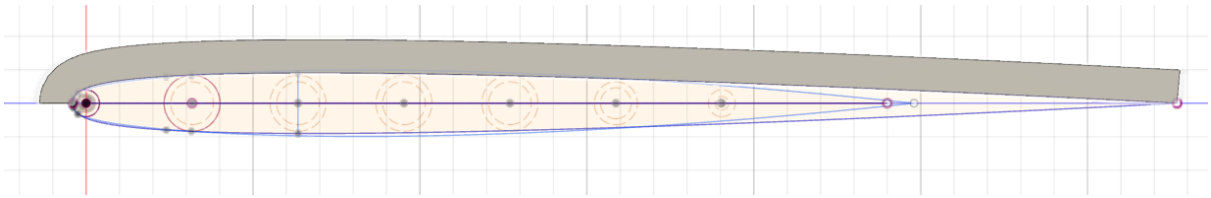

4) Use the ‘mirror plane’ to create a mirrored curved body, using the centre line. Then use the ‘Combine’ tool to join the two into one body.

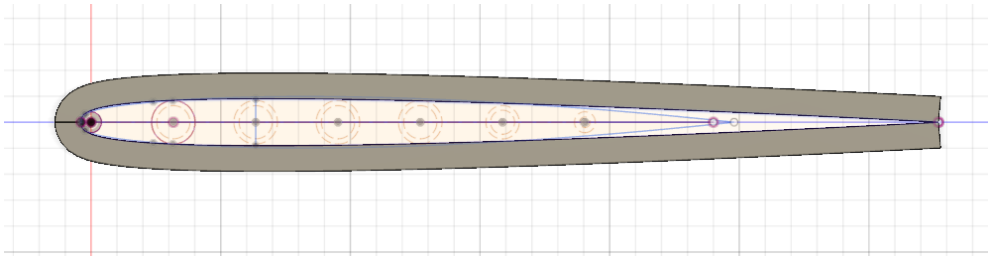

5) Split the body along the marked (blue) line into part A and part B. This will allow a different angle for the leading hinge.

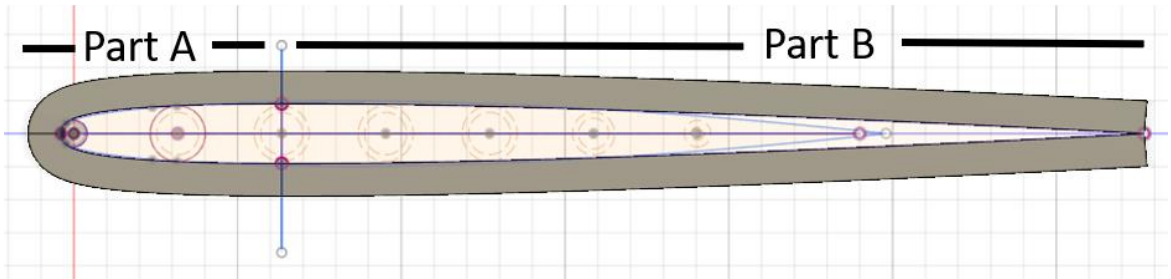

6) Duplicate part A into part A1 and A2 (i.e. copy Part A; we will use Part A2 in step 7). Next, draw a semi-circle as shown*, using the thickness as the diameter of the circle. ‘Split Body’ of part A1 using this semi-circle line, then remove the newly generated part highlighted below (former part of Part A1).

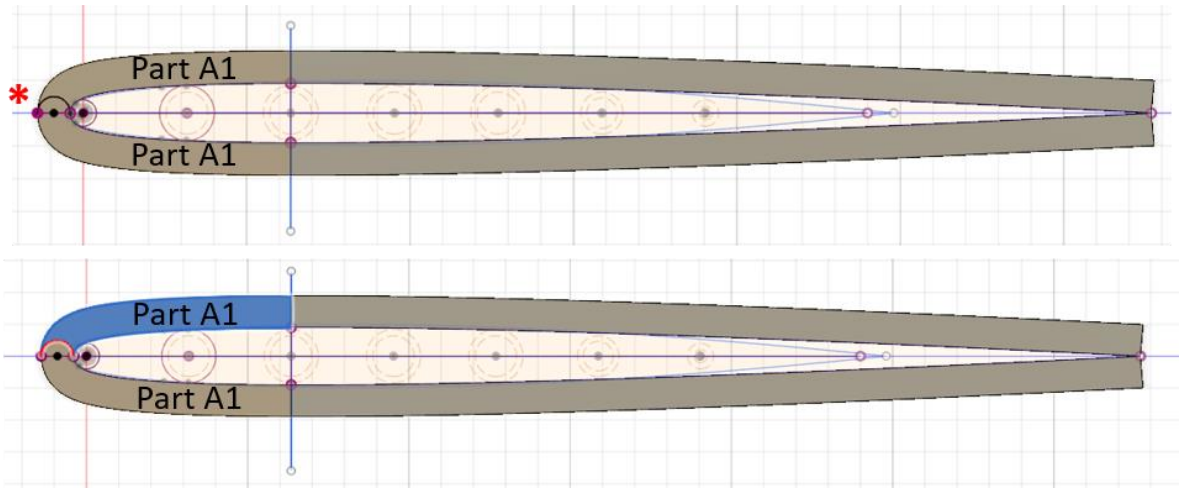

7) Sketch the other half of the leading/hinge circle onto *Part A2*. Split the body Part A2 using this new semi-circle. Remove the newly created section highlighted below.

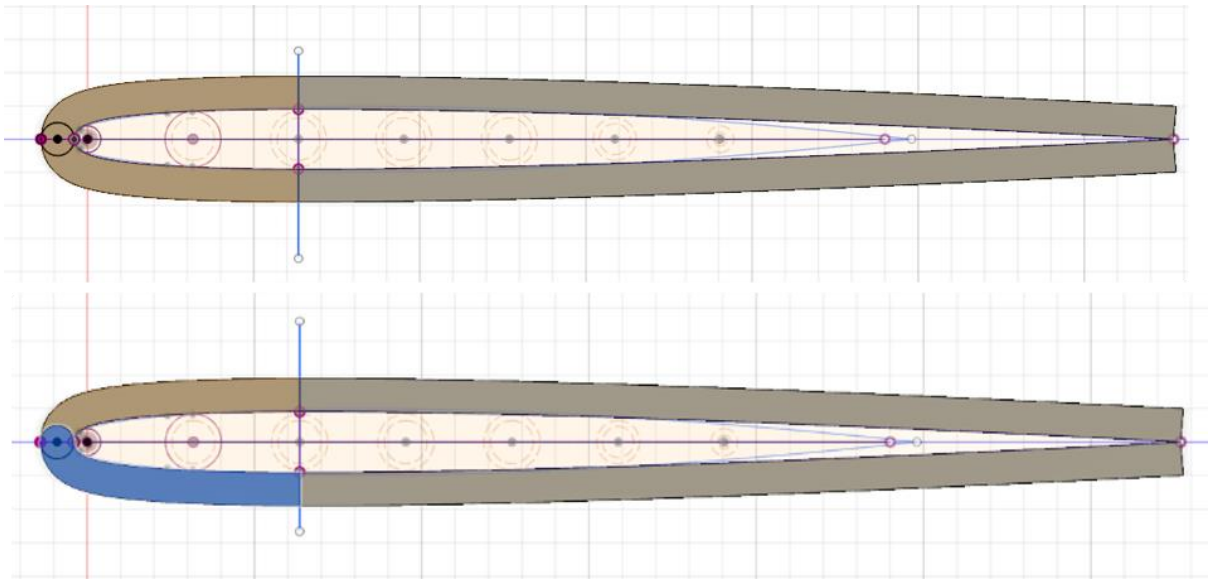

8) You should now have three bodies, as shown by highlighted sections below. The last two highlighted bodies overlap currently but are separate bodies.

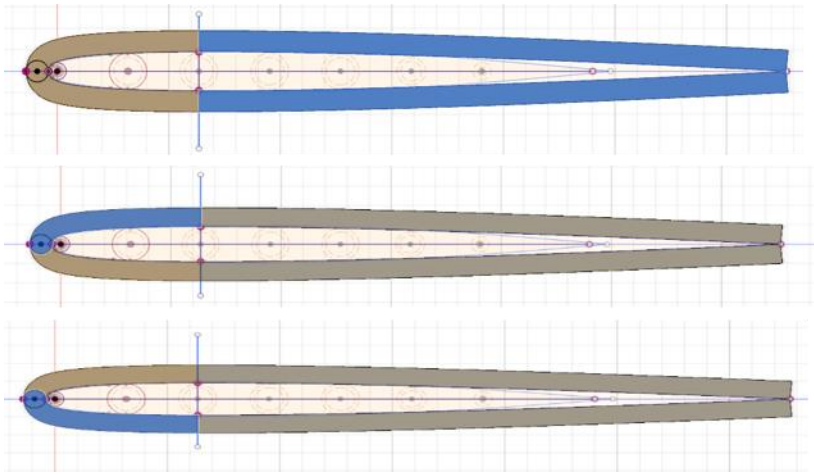

9) Sketch the indicated blue guideline, running tangent to the leading circle and parallel to the mid-plane. This will help inform where to draw the hinge locks in the following steps.

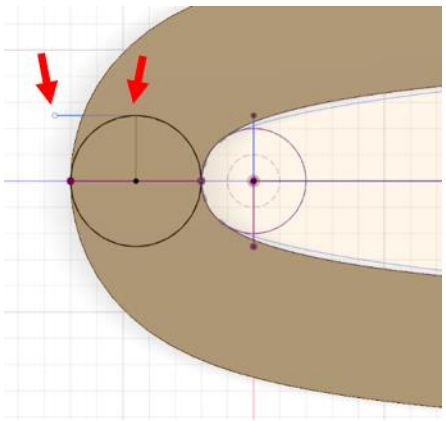

10) Sketch the hinge, drawing on the plane when looking at the hinge from the frontal direction (as shown below). This should be the width of the main circle (the circle drawn across the thickness, drawn in steps 6 & 7). N.B. here, a four-lock hinge is drawn - however, this design was later changed (for deployment) to just two. Here, the teeth are approx. 5 mm wide and 5.5 mm long (relative to the view in the below picture).

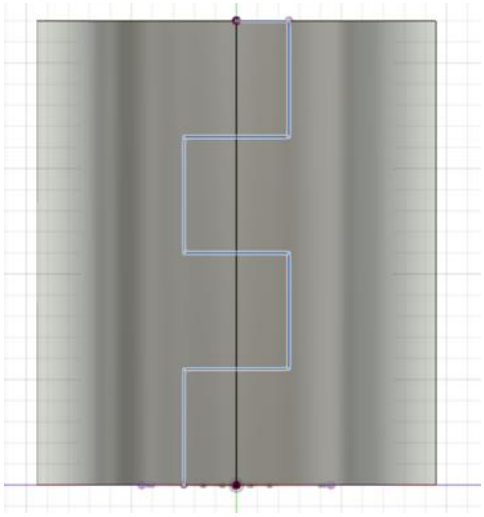

11) Use the hinge teeth sketch to split the relevant body (i.e. in this drawing, split the body on the left). A section should be created as shown.

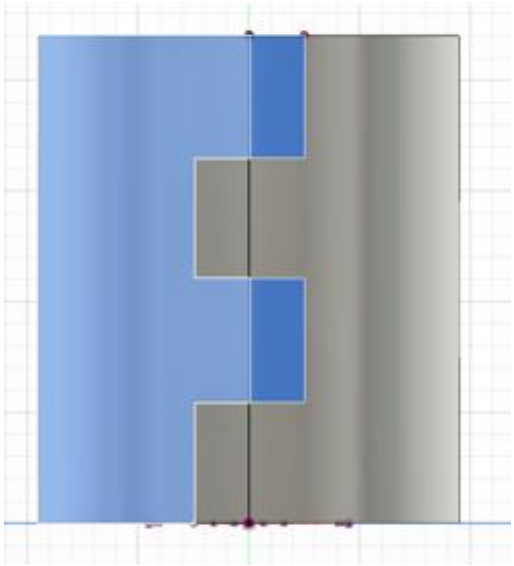

12) Extra, redundant sections will be created (highlighted below). Remove these bodies.

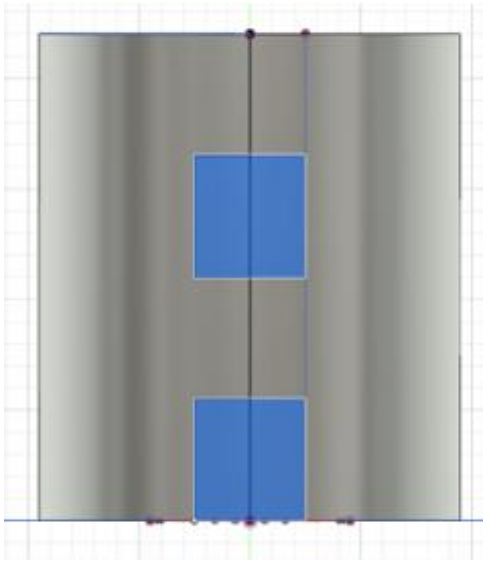

13) Repeat the previous steps, cutting the other body with the sketched teeth. Delete the extra ‘blocks’ as in the previous step.

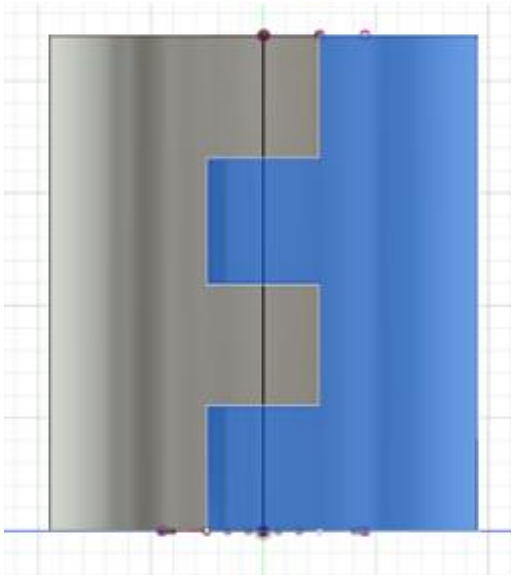

14) You should be left with these two shapes (below picture). Using the semi-circle sketches and the cut body tool, trim away any excess form the hinge (including trimming back to allow room for the hinge to move and deleting any overlapping points). Do this by sketching further lines a short (~ 1 mm) distance from the original sketches and cutting.

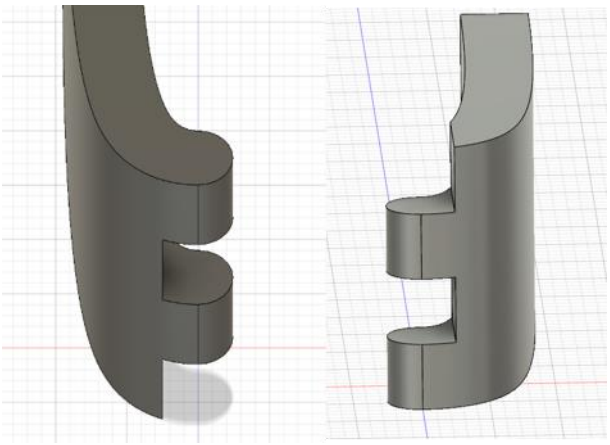

15) Cut the teeth sections away from the main bodies using two lines. We will reattach these later, but for now we must be able to manipulate the teeth independently from the main bodies.

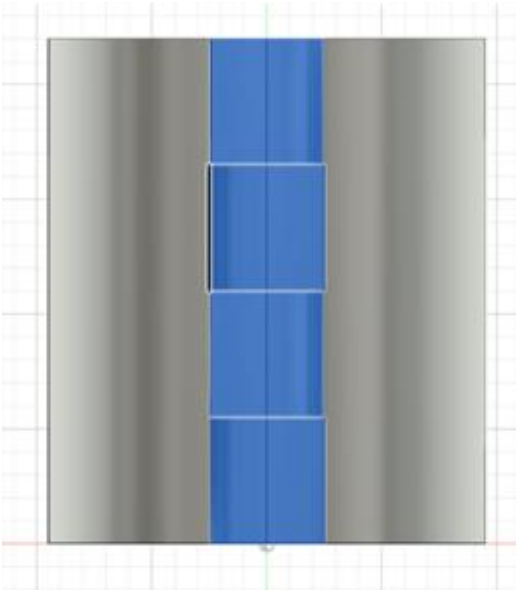

16) Rotate the front section (the two large bodies and the smaller teeth bodies) to the desired angle (dependant on the target fin and species). Here, I used an angle of 50° from upright.

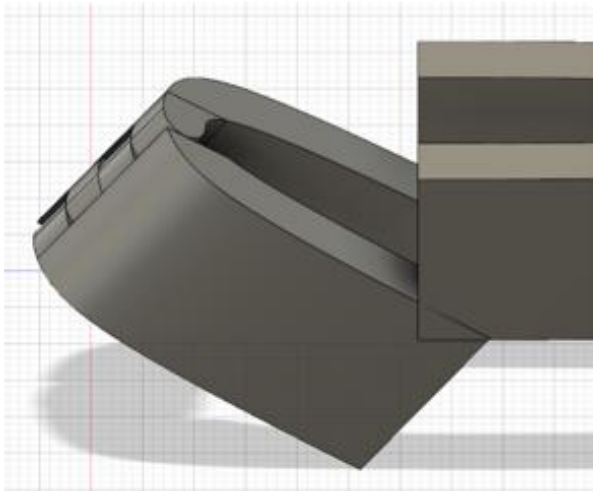

17) ‘Offset’ or ‘Pull’ the top faces of the large front bodies only. Extend the top of these two sections a long way. The precise distance doesn’t matter, but you will need a large enough body to make cuts through in the following steps.

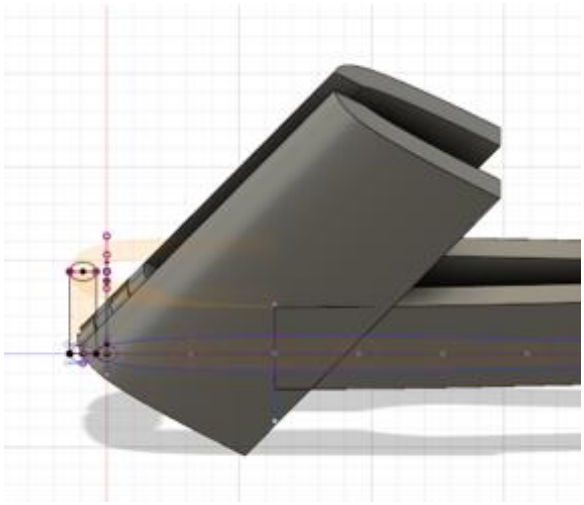

18) Make two horizontal cuts (using the sketch interface and 'Cut Body') parallel to one another and the ground plane. The distance between the two cuts should equal the desired height of the final clip and the long body arms. Keep the middle section and delete the extra sections (not the hinge teeth).

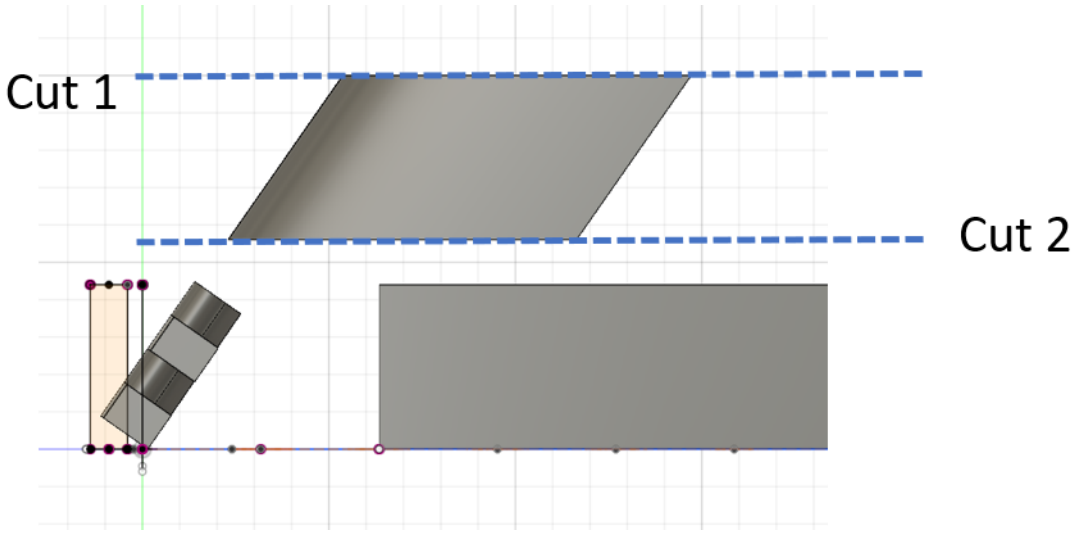

19) Rotate the hinge sections so the hinge teeth are vertical again. Select the teeth and move them upwards, so that they sit back in between the other bodies.

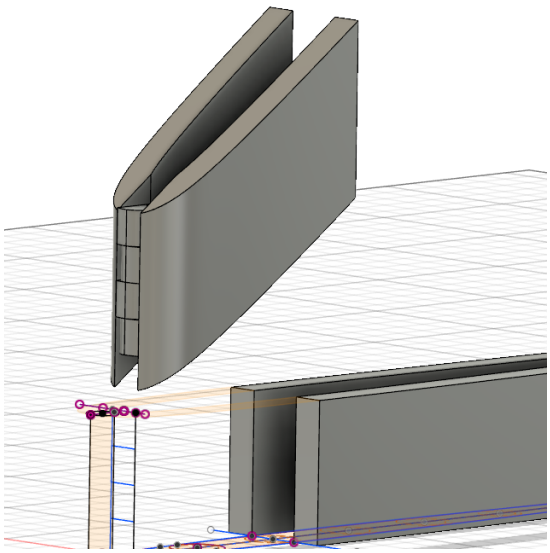

20) From a top-down perspective, sketch a circle and cut a hole into the centre of the hinge section (going through all of the teeth). This is where the front pin will go. The size of the circle depends on the size of your pin, but be aware that too-thin a hinge wall will be more likely to break – consult your 3d printer documentation, or manufacturer advice if outsourcing, on the recommended minimum thickness for your desired material.

Use ‘Combine’ to fuse the hinge teeth back with their original main bodies. You may need to trim the teeth down slightly further (using sketch and ‘Remove’) to get a flat, perfect fit. Note that here the final pin hole was 2.5 mm in diameter.

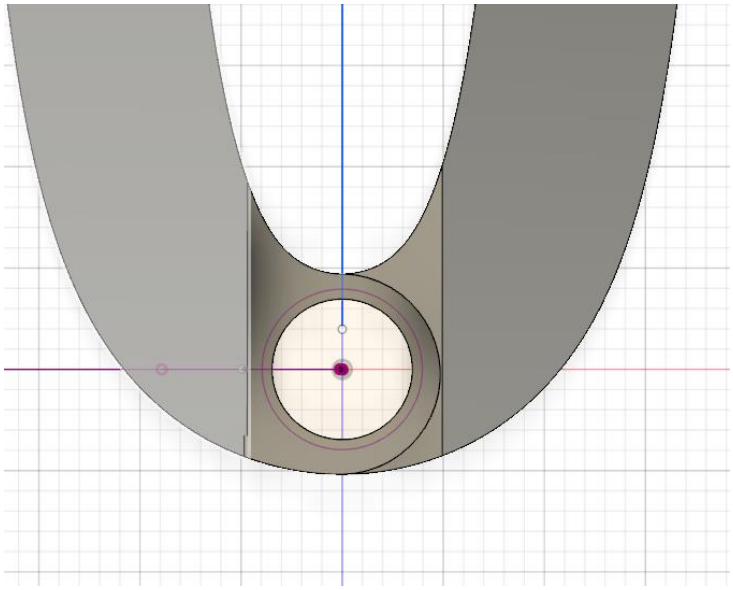

21) Rotate the front section (i.e. the complete hinge segments) back to the desired angle that it will be at in the final product. Align it with the original fin profile (Step 2) to ensure it has kept the desired shape and fit.

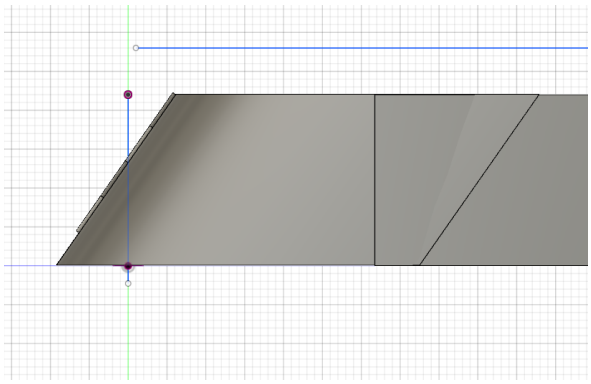

22) Cut the front hinge section (using sketch and 'Cut body') to eliminate the protruding sloped section, as shown below. You can now delete the two arm bodies (indicated below; dark grey section) that are not part of the hinge.

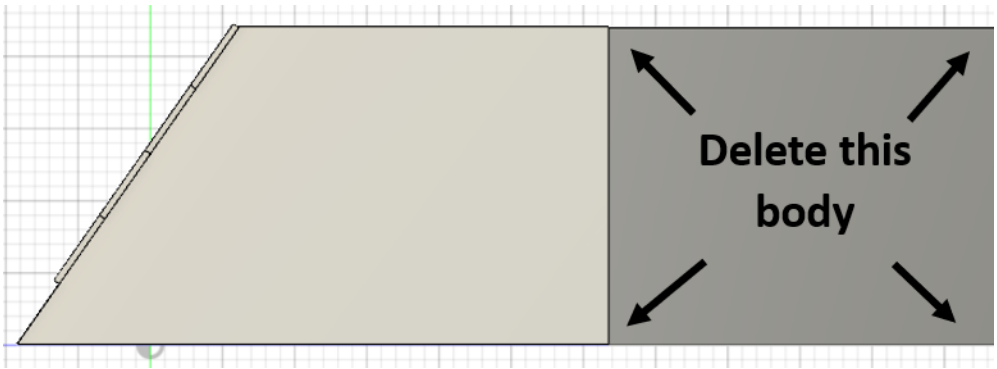

23) Draw (using the sketch tools) an extra guideline that extends beyond the fin profile drawn in Step 3, starting from the point at which the hinge section ends. This is the line that the M-clip will actually follow, so that the arms will meet one another behind the fin.

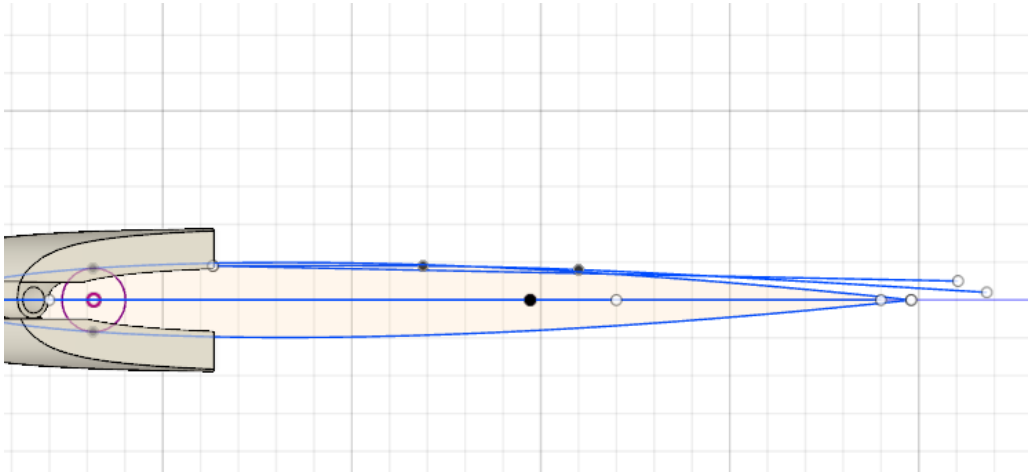

24) Select the rectangular face of one of the hinge sections. Use ‘Sweep’ to extend one arm along the newly created guideline.

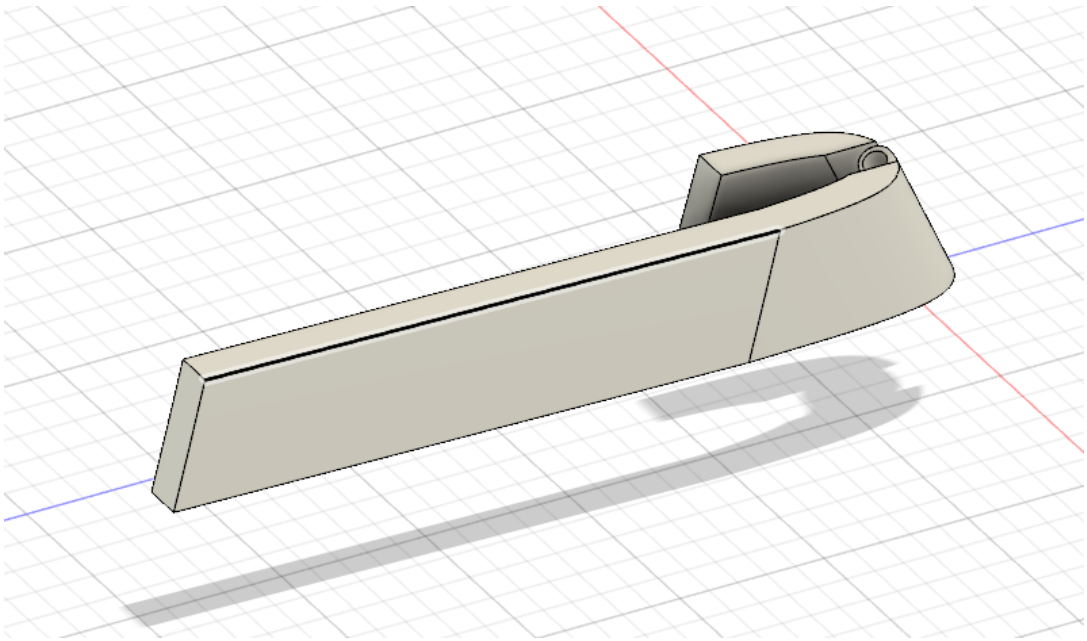

25) Split the front section (again using sketch tools and ‘Cut body’) from the extended arm again, where the break was previously. Use ‘Offset faces’ to extend the bottom faces (the ‘underneath’ faces of both hinge section and the already drawn arm) down. This is to create extra room for the curved underside.

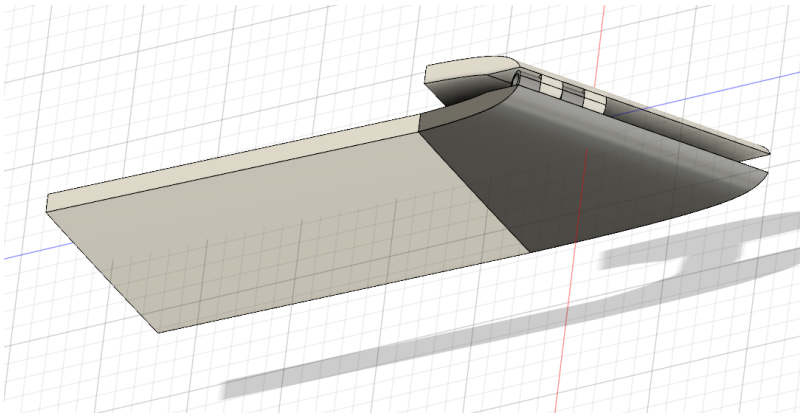

26) Draw (using sketch tools) the desired curve (making sure to accommodate the hinge segments and the space for the magnets at the rear of the arms). Use ‘Cut body’ and ‘Remove’ tools to delete the excess bodies created (below the blue curved line in the picture below).

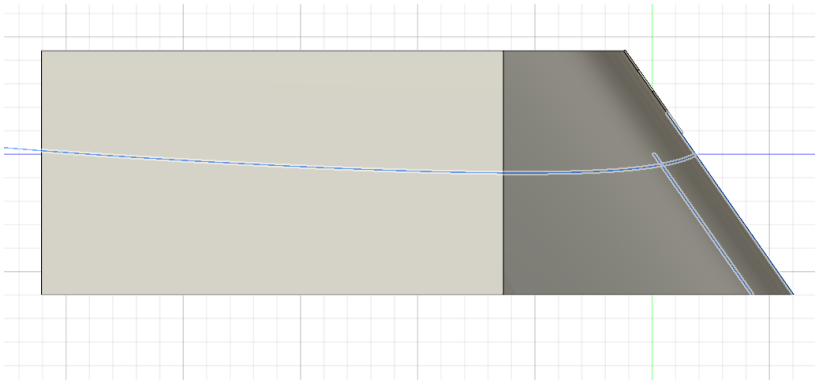

27) Cut the rear of the body to form a new curve. A large fillet or chamfer might achieve the same effect. Delete the small excess body that was created.

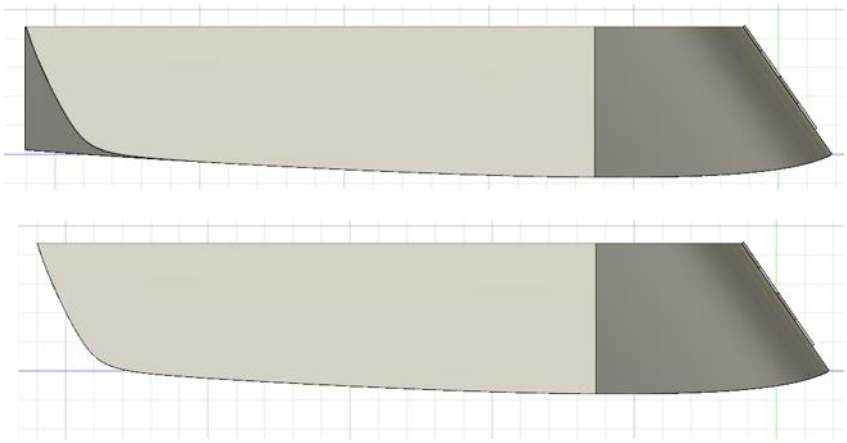

28) Optional – cut into the arm (using a top-down view and sketch tools) to create a shape to allow closer closing of the hinge so that the corners of the two arms don't hit each other when coming together (depending on the magnet depth size).

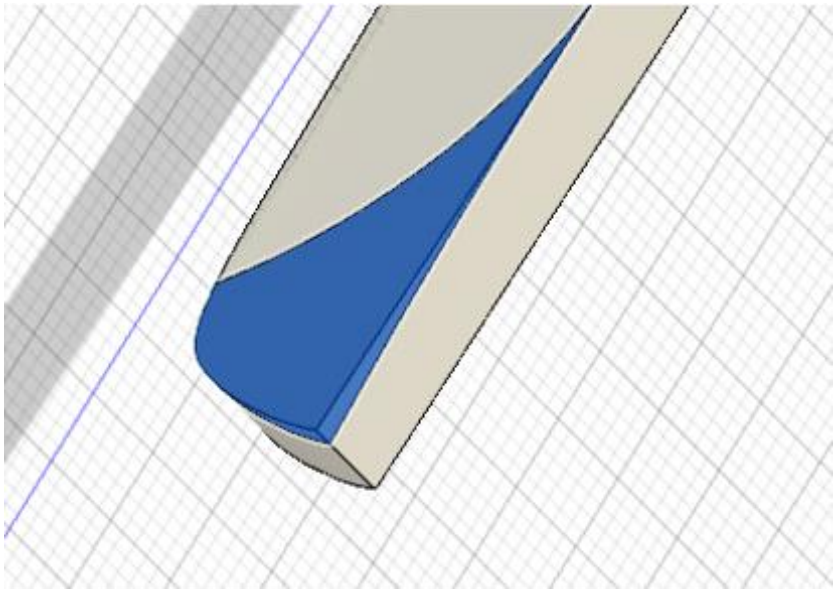

29) Use ‘Fillet’ and ‘Chamfer’ tools on the remaining bodies’ edges to your desired specifications. Here, fillets were usually 0.5 – 1 mm.

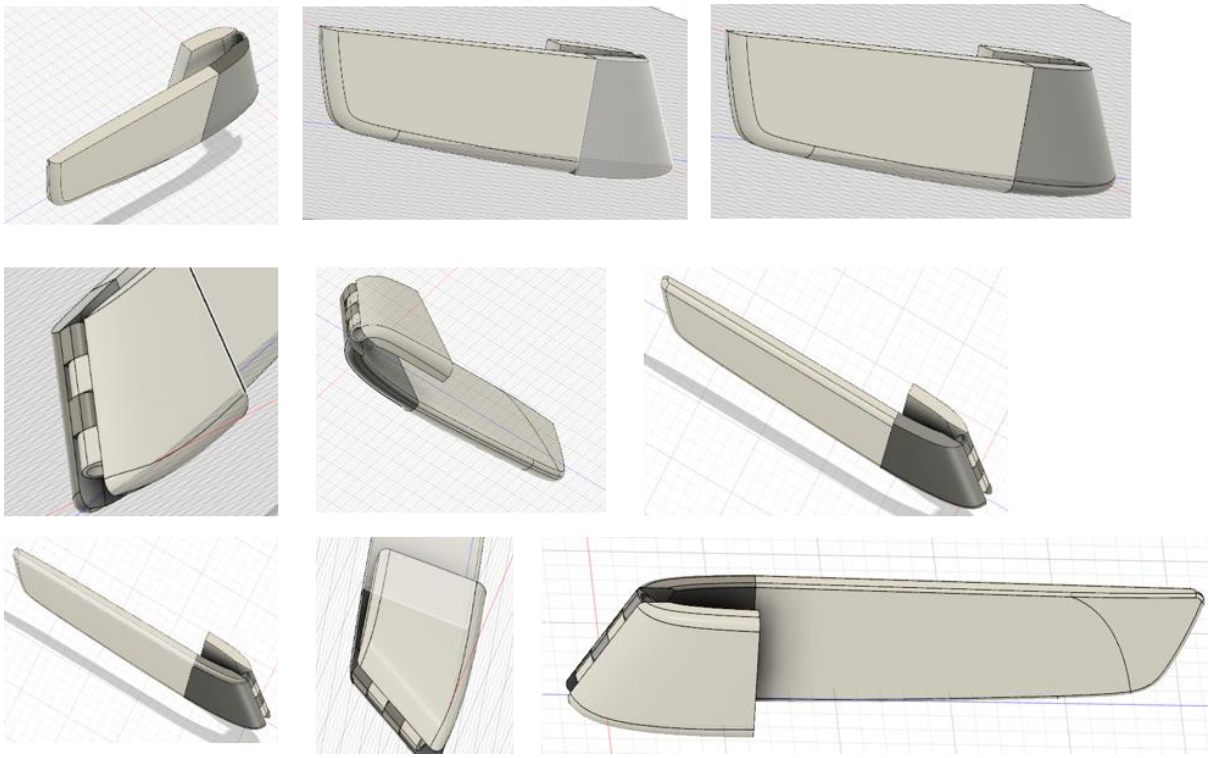

30) ‘Mirror’ the existing arm (i.e. not the hinge) section to create the second arm with already-created fillets and chamfers.

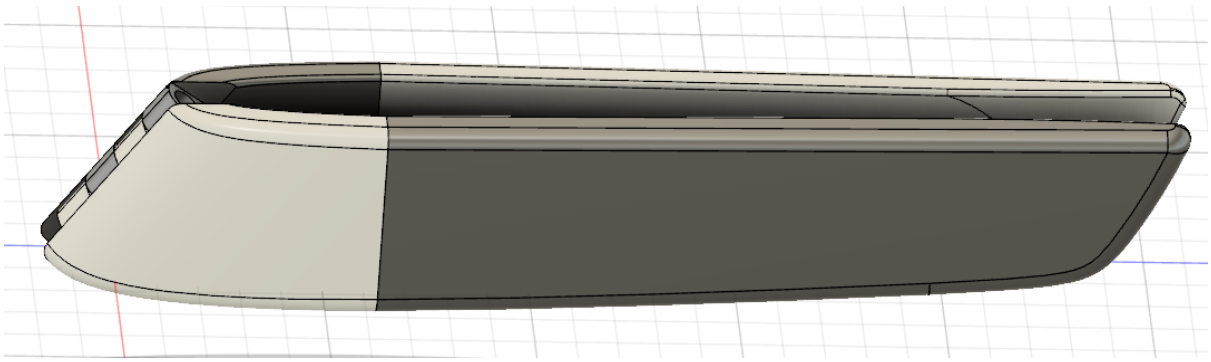

31) Use ‘Combine’ to fuse the arm sections to their hinge sections, creating two bodies that can fit together *via* the hinge.

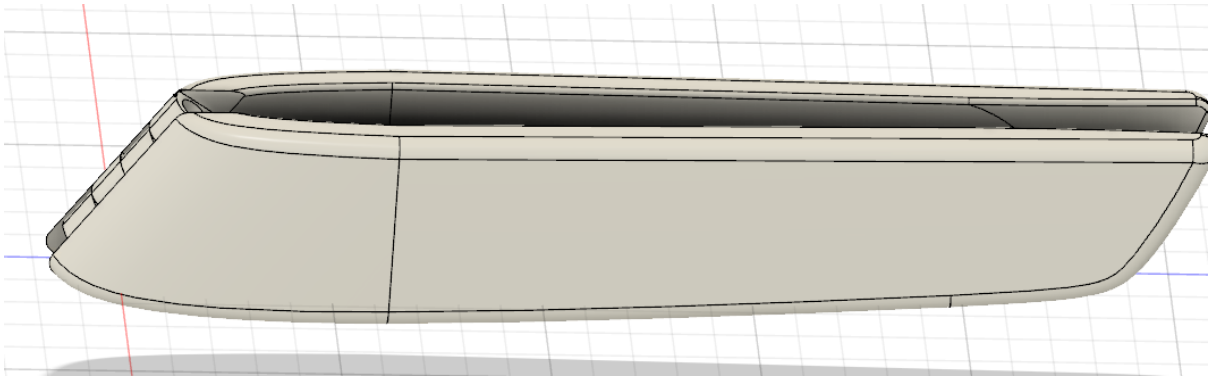

32) If required, cut holes for the magnets using a circle drawn (using sketch tools) on the central plane. Either cut (by extending the circle faces outward and setting the operation to ‘Cut’) all the way through (e.g. to then make complementary swivel disks), or cut only part way for a pocket (e.g. if securing the magnets with something like tape or glue).

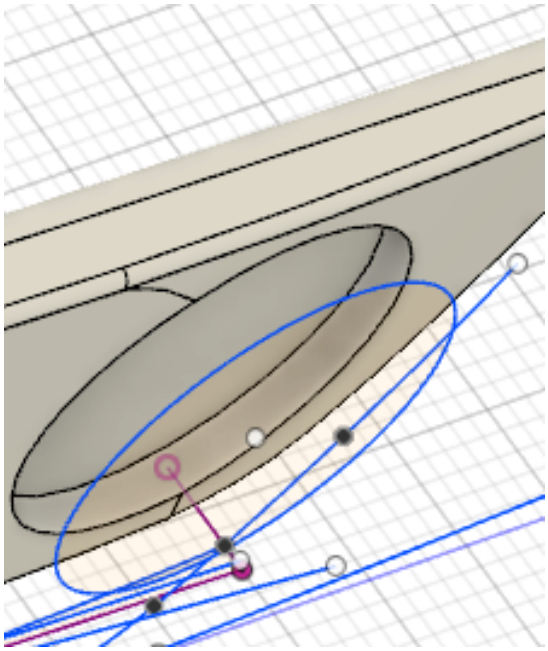

Appendix 3

Supplementary Information for Chapter 3 – 'On the benefits of captive settings for observing aberrant behaviours due to external tag attachment in sharks'

A3.1: Behaviour identification 1: Ginglymostoma cirratum chafing

Nurse shark chafing behaviour was identified using two rules – the first identifying the start of the roll and the second identifying the end. Both were required to be true and happen sequentially (i.e. 'b' following, at some point, 'a') to be true. These rules (assuming that (i) the tag's X axis represents the anterior-posterior/surge direction, the Y axis represents the side to side/sway direction and the Z axis represents the dorso-ventral/heave direction, (ii) the tag is level to the shark body, or that appropriate corrections are applied to the acceleration data) were;

a) If ((Sm. X < 0.6 *g*) AND (Sm. Y > 0.7 *g*) AND (Sm. Z < 0 *g*),

and then, at any point following this,

b) If ((Sm. X < 0.6 *g*) AND (Sm. Y < 0.7 *g*) AND (Sm. Z > 0 *g*),

then mark the complete period of a to b as chafing behaviour.

…where Sm. X, Sm. Y and Sm. Z represent the X, Y and Z accelerometer axes data smoothed over 2 seconds to separate dynamic from static acceleration (Shepard, Wilson, Halsey, et al. 2008).

These rules were selected to emphasise the movement that happens across the fish roll/XZ axes whilst avoiding false positives occurring during erratic swimming, such as when *G. cirratum*

were observed to swim upright and make sharp twisting movements when attempting to enter the feeding net or rising up the tank walls. Therefore, it was required that; (i) the tag and shark did not enter a large upwards angle, indicative of direct upward swimming and represented in the X axis, (ii) the Y axis acceleration force was sufficiently larger than that experienced during regular swimming speeds, but declining to regular levels upon completion of the chafe and (iii) the tag and shark rotated at least 90^{o} from the regular swimming position, and returned to within 90^{o} of the regular swimming position upon completion of the roll.

A3.2: Behaviour identification 2: <u>Carcharhinus melanopterus</u> shaking

Blacktip shark shaking was identified using a simple threshold value of VeDBA (the Vector of Dynamic Body Acceleration (Wilson et al. 2006), as the whole body of the shark moves in a sudden, erratic manner and thus manifests through all three acceleration channels in elevated dynamic acceleration. Two rules - the first identifying the start (c) of the shake and the second identifying the end (d) - were required to be true:

c) If (VeDBA > 0.4),

and then, at any point following this,

d) If (VeDBA < 0.4),

then mark the complete period from c to d as shaking behaviour.

Note that, following Shepard et al. (2008), a smoothing window of 2 seconds was used to separate dynamic from static behaviour.

All periods of data identified with the above rules are listed in Table A3.1.

Table A3.1: All individual aberrant behaviours identified by the Boolean behaviour function and those that were included manually and the decision (as explained in Chapter 3, Table 3.2) on classification of the flagged data.

Species	Aberrant behaviour	Deployment number	Individual	Minutes since tag attachment	Decision
G. cirratum	Chafing	2	1	4.85	FP, K
				15.03	TP, K
				25.50	TP, A
				41.68	TP, A
				125.10	TP, A
				125.28	TP, A
				288.05	TP, A
				580.02	TP, A
				597.68	TP, A
				597.87	TP, A
				601.32	TP, A
				661.62	TP, A
				693.13	TP, A
				780.52	TP, A
				820.57	TP, A
		3	2	39.67	TP, K
				39.80	TP, K
				40.10	TP, K
				46.62	TP, K
				46.75	TP, K
				115.30	TP, A
				444.63	TP, A
				450.53	TP, A

				458.50	TP, A
				458.60	TP, A
		4	3	160.48	FN, A
				160.90	FN, A
				568.10	TP, A
				626.97	FN, A
				1015.97	FN, A
				1250.25	TP, A
				1250.38	FN, A
				1262.37	TP, A
		5	1	28.03	TP, A
		6	4	19.18	TP, A
		6		35.48	TP, A
		7	1	17.47	FN, K
		8	4	45.05	FP, A
R. ancylostoma	Chafing	1	1	131.63	FP, A
				81.30	FP, A
				220.46	FP, A
				225.64	FP, A
				236.84	FP, A
				341.0	FP, A
				341.3	FP, A
				342.8	FP, K
				344.8	FP, K
				397.6	TP, A
				445.7	TP, A
				480.0	TP, A
				506.4	TP, A
				550.4	TP, A
				589.8	TP, A

			630.1	TP, A
			634.1	TP, A
			647.2	TP, A
			652.9	TP, A
			699.9	TP, A
	2	1	169.0	FP, A
			179.9	FP, A
			200.6	FP, A
			212.1	FP, A
			218.8	FP, K
			266.1	TP, A
			266.3	TP, A
			288.2	TP, A
			311.6	TP, A
			311.8	TP, A
			340.6	TP, A
			350.5	TP, A
			364.9	TP, A
			376.2	TP, A
			421.2	TP, A
			424.6	TP, A
			424.7	TP, A
			460.4	TP, A
			460.5	TP, A
			529.7	TP, A
			570.7	TP, A
			585.9	TP, A
			604.6	TP, A
			651.1	TP, A
			686.3	TP, A

				689.6	TP, A
C. melanopterus	Shaking	2	1	0.03	TP, A
				0.2	TP, A
				0.5	TP, K
				1.7	TP, K
				4.3	TP, A
				4.7	TP, A
				16.7	TP, K
				45.9	TP, A
				81.0	TP, A
				85.8	FP, K
				102.9	TP, A
				106.5	TP, A
				116.6	TP, A
				123.0	TP, A
				129.9	TP, A
				139.9	TP, K
				142.3	TP, A
		3	2	0.6	TP, A
				0.8	TP, K
		1	1	0.9	TP, K
				2.4	TP, K
				403.3	TP, A
				1307.9	TP, A

Appendix 4

Supplementary Information for Chapter 4 – 'Testing angular velocity as a new metric for metabolic demands of slow-moving marine fauna: a case study with Giant spider conchs *Lambis truncata*'

A4.1: General information and water salinity and temperature

Mean conch $\dot{V}O_2$ was 5.57 mg ind^{-1} h^{-1} (± 2.66 sd, range = 11.35) and was greater in the evening period (7.11 ± 1.99 sd) than the afternoon (3.96 ± 2.3 sd).

Average daily salinity was 41.69. The overall mean experimental temperature was 23.56 °C (± 0.98 sd), with similar afternoon (23.68 °C ± 0.98 sd) and evening (23.46 ± 1) mean temperatures. The overall mean temperature change during experiments was -0.27 °C (± 0.63 sd), with mean afternoon change of + 0.02 °C (± 0.42 sd) and mean evening change of -0.55 °C (± 0.67 sd).

A4.2: Movement differences across time periods

Mean VeDBA was 0.025 (± 0.004 sd), with no observable difference between afternoon (0.03 ± 0.005 sd) and evening (0.03 ± 0.002 sd) periods.

Mean (± sd) RocRM was 0.16 (± 0.01), 0.46 (± 0.05), 0.62 (± 0.06) and 1.72 (± 0.21) for time steps of 1, 5, 10 and 60 seconds, respectively. In all cases, the mean (± sd) was greater in the evening period than the afternoon (0.17 ± 0.10 vs 0.15 ± 0.10, 0.50 ± 0.21 vs 0.43 ± 0.38, 0.70 ± 0.31 vs 0.54 ± 0.49, 2.14 ± 1.30 vs 1.28 ± 1.33; for $RocRM_1$, $RocRM_5$, $RocRM_{10}$ and $RocRM_{60}$, respectively).

A4.3: Model selection

Table A4.1: Criteria for model selection during stepwise removal of insignificant terms in linear mixed models. Models with and without the fixed effect term 'mean temperature' were compared by ANOVA with maximum likelihood to produce the final models shown in Chapter 4, Table 4.2.

Model	**df**	**AICc**	**ΔAIC**	**logLik**	**ChiSq**	**p**
$\dot{V}O_2$ ~ VeDBA	4	202.97	-	-97.49	-	-
… + mean temperature	5	204.92	0.03	-97.46	0.05	0.82
$\dot{V}O_2$ ~ log(mean $RocRM_1$)	4	196.8	-	-94.40	-	-
… + mean temperature	5	198.8	2	-94.40	0.002	0.97
$\dot{V}O_2$ ~ log(mean $RocRM_5$)	4	194.74	-	-93.37	-	-
… + mean temperature	5	196.52	1.78	-93.26	0.22	0.64
$\dot{V}O_2$ ~ log(mean $RocRM_{10}$)	4	191.41	-	-91.71	-	-
…+ mean temperature	5	193.40	1.99	-91.70	0.01	0.91
$\dot{V}O_2$ ~ log(mean $RocRM_{60}$)	4	186.92	-	-89.46	-	-
… + mean temperature	5	188.83	1.91	-89.42	0.09	0.77

Appendix 5

Supplementary Information for Chapter 5 – 'Searching for simple rules in a 'simple' animal; movement of the Giant Spider Conch, Lambis truncata'

A5.1: Comparison of first 24 hours to the following 48 hours – evidence of handling effect

A5.1.1: Methods - Statistical analysis

To simplify analysis, 'hour of the day' was grouped into 6-hour blocks of '00:00 - 6:00', '6:00 - 12:00', '12:00 - 18:00' and '18:00 - 00:00', informed by preliminary visualisation of typical movement periods. 'Time since deployment' was grouped into 24-hour periods ('0 – 24 h', '24 – 48 h' and '48 – 72 h') starting from the time the Daily Diary-equipped conches were released back onto the reef.

Cumulative link mixed models (CLMMs), using the R package 'ordinal' (Christensen 2019), were used to determine the effect of '24-hour period' on the probability of movement and size of per-movement heading change in two separate models. CLMMs are regression models for ordinal data that allow random predictor terms, thus accounting for individual conchs and avoiding pseudo-replication. 'Hour of the day' and '24-hour period' were included as predictors with an interaction term between them, with individual ID as the random (intercept) effect term. The response variables 'per-hour movement count' and 'heading-change per movement', were each partitioned into incremental bins to facilitate easier interpretation and meet the implicit requirements of CLMM models. 'Per-hour movement count' was binned into '0-25', '25-50', '50-75', '75-100', '100-125' and '>125' movements and 'heading change per movement' was binned into '0-10', '10-20', '20-30', '30-40', '40-50' and '> 50' degrees. The ordinal package returns coefficient effects values as log odds; specific probabilities used in the

figures were calculated using the ggpredict function within the ggeffects package (Lüdecke 2018). Full models were compared to reduced and null models through log-likelihood ratio tests (using the 'anova' function) and comparison of AIC values, to confirm that the model terms (including interaction terms) warranted inclusion.

A5.1.2: Results

Both the mean and the variability of number of movements per hour was greater during the first 24 hours (mean = 6.5, sd = 14.43, range = 116) compared to either of the following 24 hour periods (24 – 48 h: mean = 5.4, sd = 8.61, range = 62; 48 – 72 h: mean = 5.85, sd = 6.8, range = 35). Similarly, both the mean and the variability of heading change per movement was greater during the first 24 hours (mean = 15.36, sd = 18.52, range = 178.8) compared to either of the following 24 hour periods (24 – 48 h: mean = 9.09, sd = 12.14, range = 132.3; 48 – 72 h: mean = 11.41, sd = 12.55, range = 116.6).

In CLMM models, the interaction term of hour (as 6-hour blocks) and 24-hour period since deployment was found to have a significant effect ($p < 0.001$) on movement frequency: Compared to the first 24 h, the periods of 24 – 48 h and 48 – 72 h both saw significant ($p < 0.001$ and < 0.01, respectively) decreasing probability of movement (decreases of 3.99 and 2.89 on the log odds scale, respectively), suggesting that movement frequency varied by 24 hour period but to differing levels depending on the time of day (Fig. A5.2). Similarly, the interaction term of hour (as 6-hour blocks) and 24-hour period had a significant effect ($p < 0.001$) on heading change. Compared to the first 24 h, the periods of 24 – 48 h and 48 – 72 h both saw significant ($p < 0.001$ and < 0.05, respectively) decreasing probability of large heading changes (decreases of 0.49 and 0.2 on the log odds scale, respectively) (Fig A5.3).

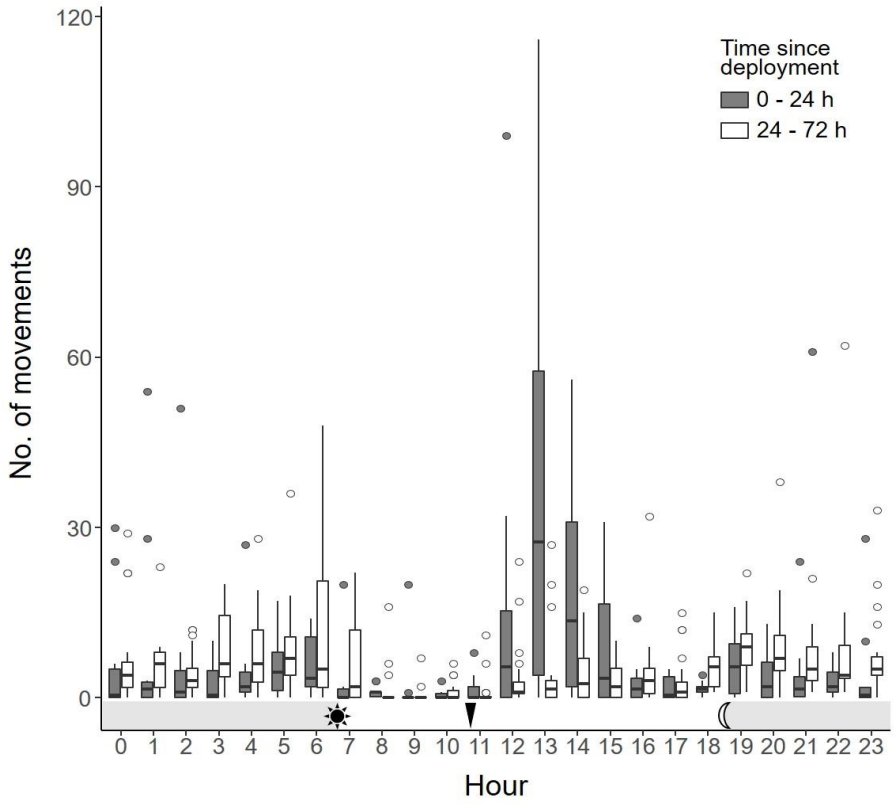

Figure A5.1: The number of movements (where boxes show the 25th, 50th and 75th percentiles) made per hour by 10 *L. truncata* over 72 hours, grouped into either the initial 24 hours of deployment (grey) or the subsequent 48 hours (white). The sun and moon represent sunrise (06:45 am) and sunset (18:27) respectively (times taken from timeanddate.com for Jeddah, Saudi Arabia on 1st March 2019). The horizontal grey bars represent 'night', between sunset and sunrise. The black triangle signifies the release time of the DD-equipped animals to the field site. NB. the hour '0' refers to the period from midnight until 1 am.

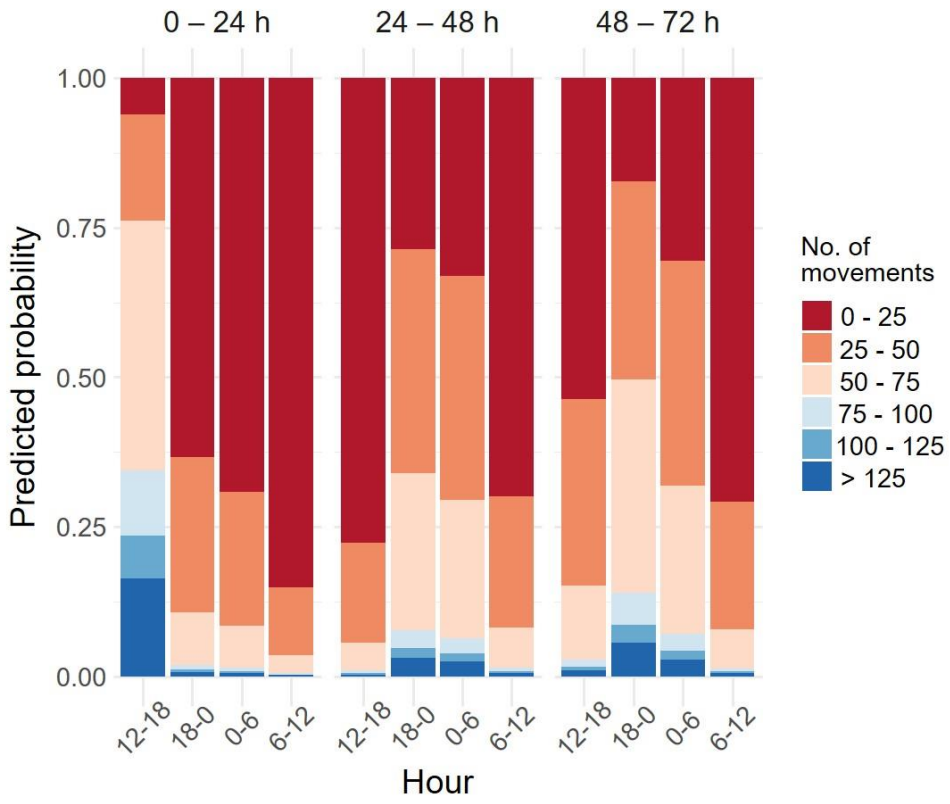

Figure A5.2: CLMM-predicted probabilities of the number of movement events per individual across a day, comparing the first 24 hours of deployment to the subsequent 48 hours. The interactive term between ‘hour block’ and ‘24-hour period’ has a statistically significant effect on movement count probabilities.

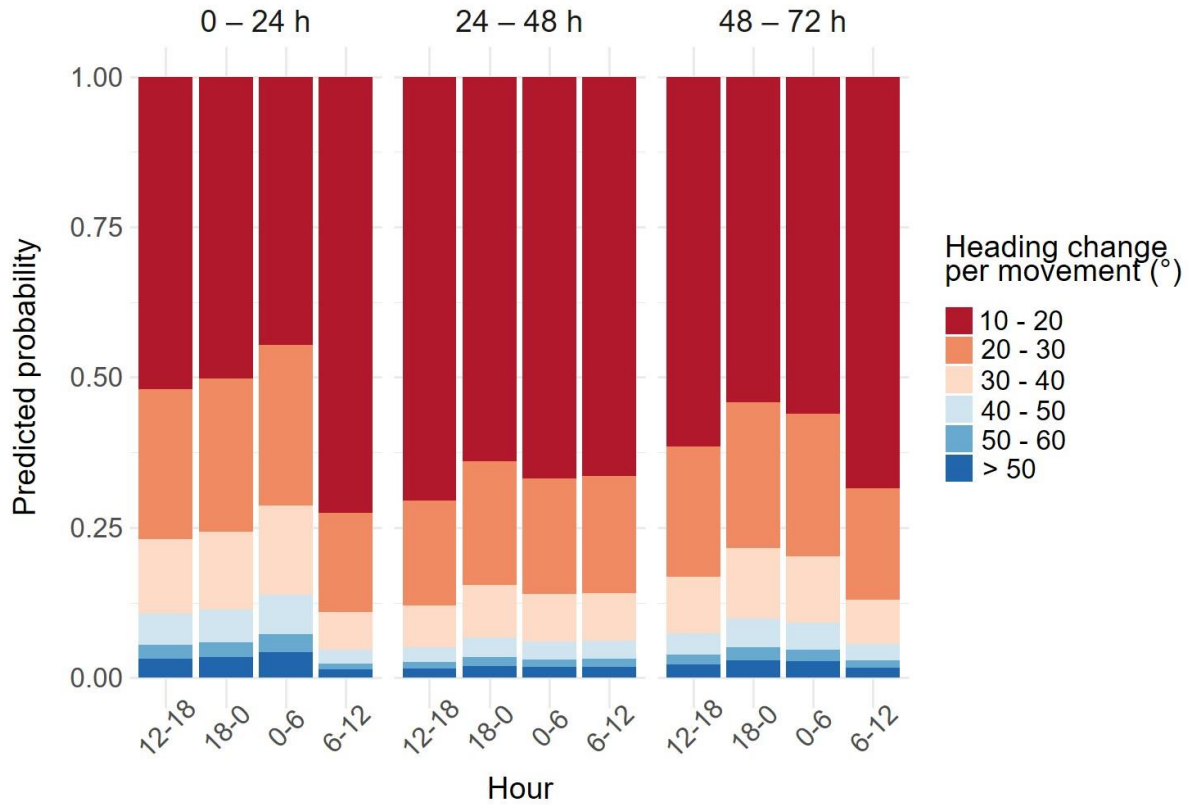

Figure A5.3: CLMM-predicted probabilities of the size of per-movement heading change across a day, comparing the first 24 hours of deployment to the subsequent 48 hours. The term '24-hour period' was found to have a statistically significant effect on predicted probability.

Table A5.1: Summary outputs of coefficients in the CLMM shown in Chapter 5, Figure A5.5 and Chapter 5, Table 5.1 [full model: $HC_{(t1)}$ ~ Hr*$HC_{(t0)}$ + duration + (1|ID)]. '$HC_{(t0)}$' = Heading change at time t_0 (see Chapter 5 - Methods section for binned increments); 'Duration' = Duration of the movement (secs).

Coefficients	**Estimate (± se)**	**z**	**p**
Hr 18-0	0.48 ± 0.17	2.85	**<0.01**
Hr 0-6	0.29 ± 0.17	1.72	0.08
Hr 6-12	0.04 ± 0.21	0.18	0.86
$HC_{(t0)}$ 10-20	0.81 ± 0.24	2.38	**<0.001**
$HC_{(t0)}$ 20-30	1.13 ± 0.31	3.60	**<0.001**
$HC_{(t0)}$ 30-40	1.87 ± 0.40	4.68	**<0.001**
$HC_{(t0)}$ 40-50	1.86 ± 1.05	1.77	0.08
$HC_{(t0)}$ >50	2.79 ± 0.68	4.09	**<0.001**
Duration	0.72 ±0.07	10.18	**<0.001**
Hr 18-0 * $HC_{(t0)}$ 10-20	-0.22 ±0.29	-0.76	0.45
Hr 0-6 * $HC_{(t0)}$ 10-20	-0.004 ± 0.29	-0.015	0.99
Hr 6-12 * $HC_{(t0)}$ 10-20	-0.21 ±0.38	-0.56	0.58
Hr 18-0 * $HC_{(t0)}$ 20-30	-0.51 ± 0.37	-1.37	0.17
Hr 0-6 * $HC_{(t0)}$ 20-30	-0.72 ± 0.39	-1.84	0.07
Hr 6-12 * $HC_{(t0)}$ 20-30	-0.17 ± 0.46	-0.36	0.72
Hr 18-0 * $HC_{(t0)}$ 30-40	-0.89 ± 0.52	-1.73	0.08
Hr 0-6 * $HC_{(t0)}$ 30-40	-1.23 ± 0.55	-2.25	**0.02**
Hr 6-12 * $HC_{(t0)}$ 30-40	-2.20 ± 0.72	-3.06	**<0.01**
Hr 18-0 * $HC_{(t0)}$ 40-50	-1.20 ± 1.13	-1.06	0.29
Hr 0-6 * $HC_{(t0)}$ 40-50	-1.05 ± 1.16	-0.90	0.37
Hr 6-12 * $HC_{(t0)}$ 40-50	1.02 ± 1.24	0.83	0.41
Hr 18-0 * $HC_{(t0)}$ >50	-2.50 ± 0.90	-2.78	**<0.01**
Hr 0-6 * $HC_{(t0)}$ >50	-1.66 ±0.88	-1.89	0.06
Hr 6-12 * $HC_{(t0)}$ >50	-0.13 ± 1.07	-0.13	0.9

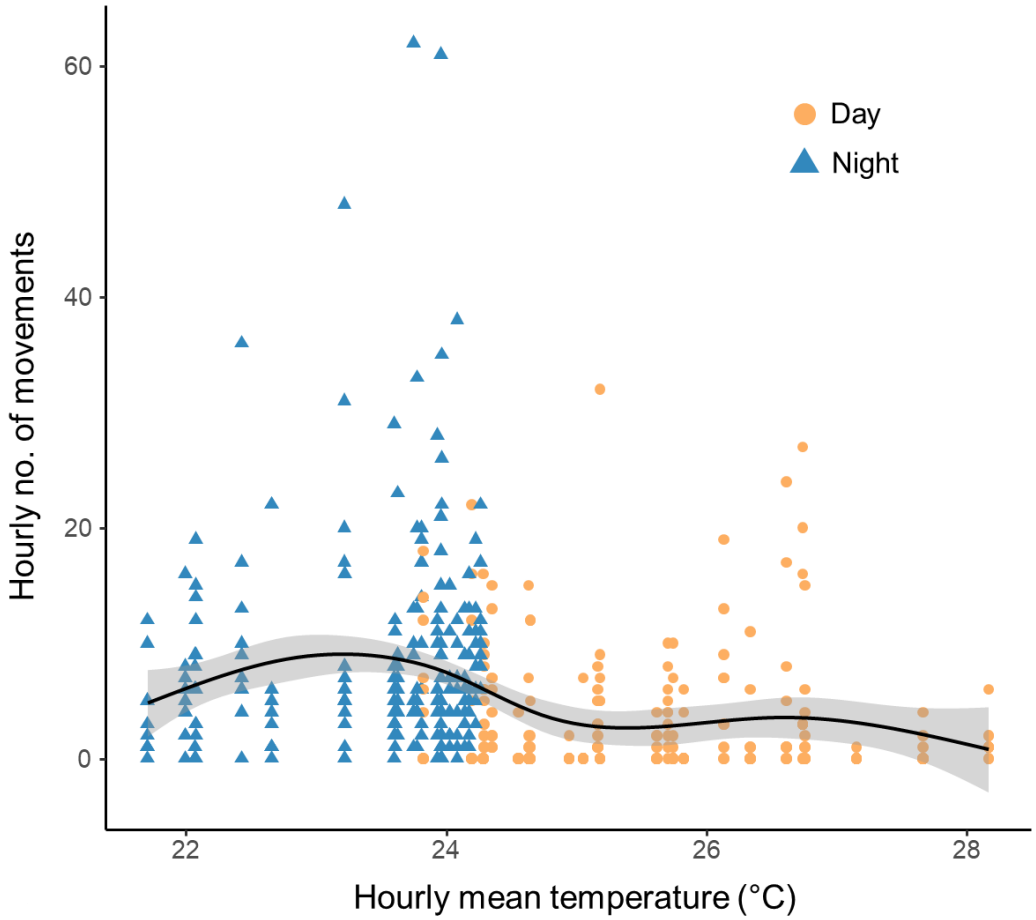

Figure A5.4: The number of movements made per hour (n = 10 conchs) over 48 hours, as a function of the mean temperature for that hour. Orange circles show day-time hours (between sun rise and sun set) and blue triangles show night-time hours (between sunset and sunrise). A fitted GAM model with 95% CIs is overlaid.

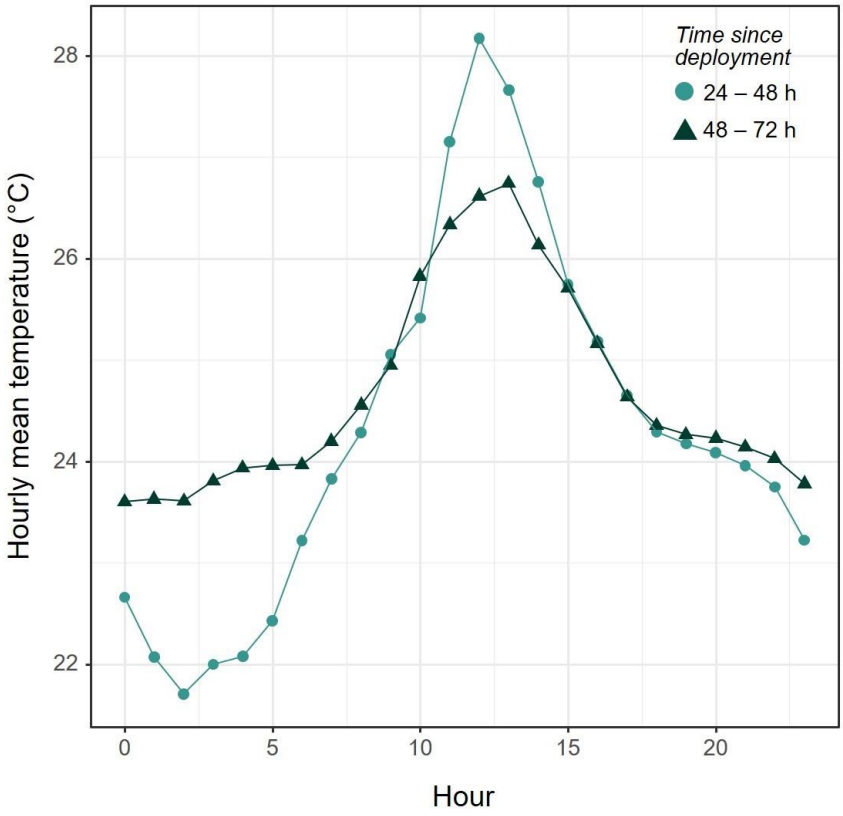

Figure A5.5: The mean temperature per hour of the day for the 2nd (circles and light blue) and 3rd (triangles, dark blue) 24-hour period. Means were calculated from per-second temperature readings from all 10 Daily Diaries.

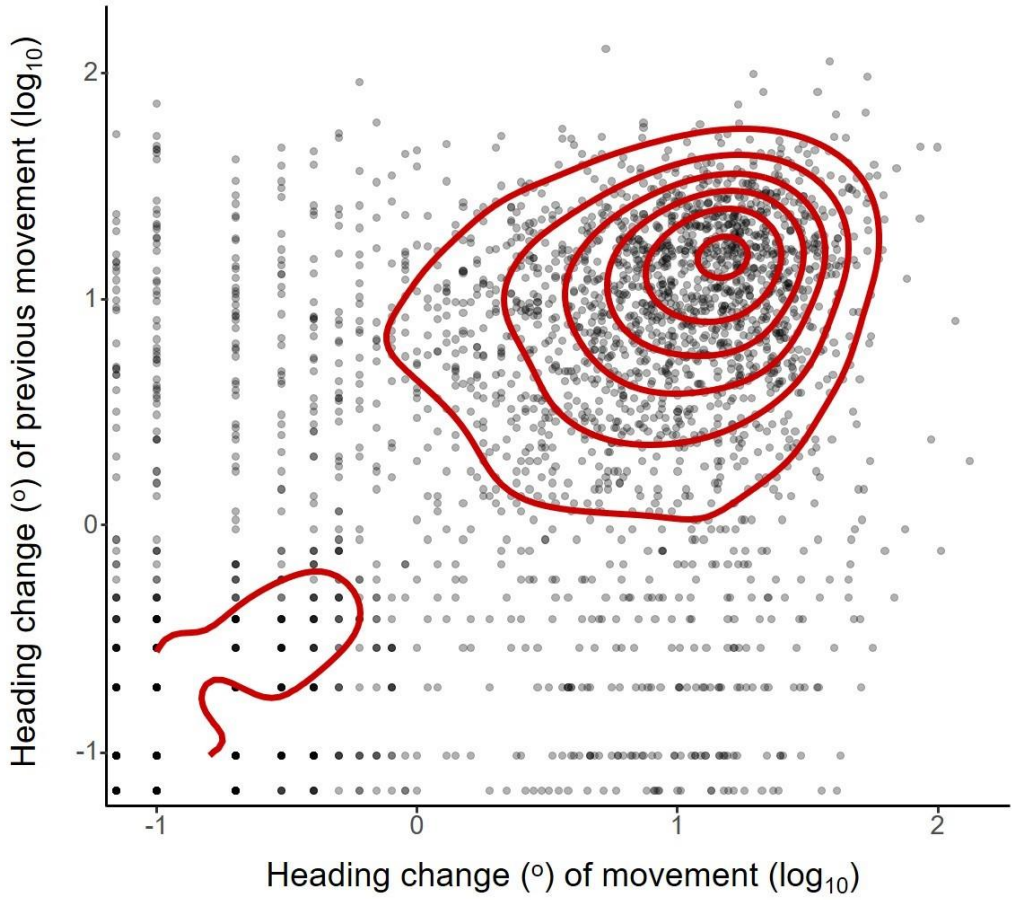

Figure A5.6: The per-movement heading change (movement t_0) against the previous movement's heading change (movement t_{-1}). Both axes are $\log_{10}$ transformed. Contours have a binwidth of 0.01.

Appendix 6

Supplementary Information for Chapter 6 – 'Using biologging to monitor the response of a free-living marine invertebrate to boat noise – a case study with the Maxima clam, *Tridacna maxima*'

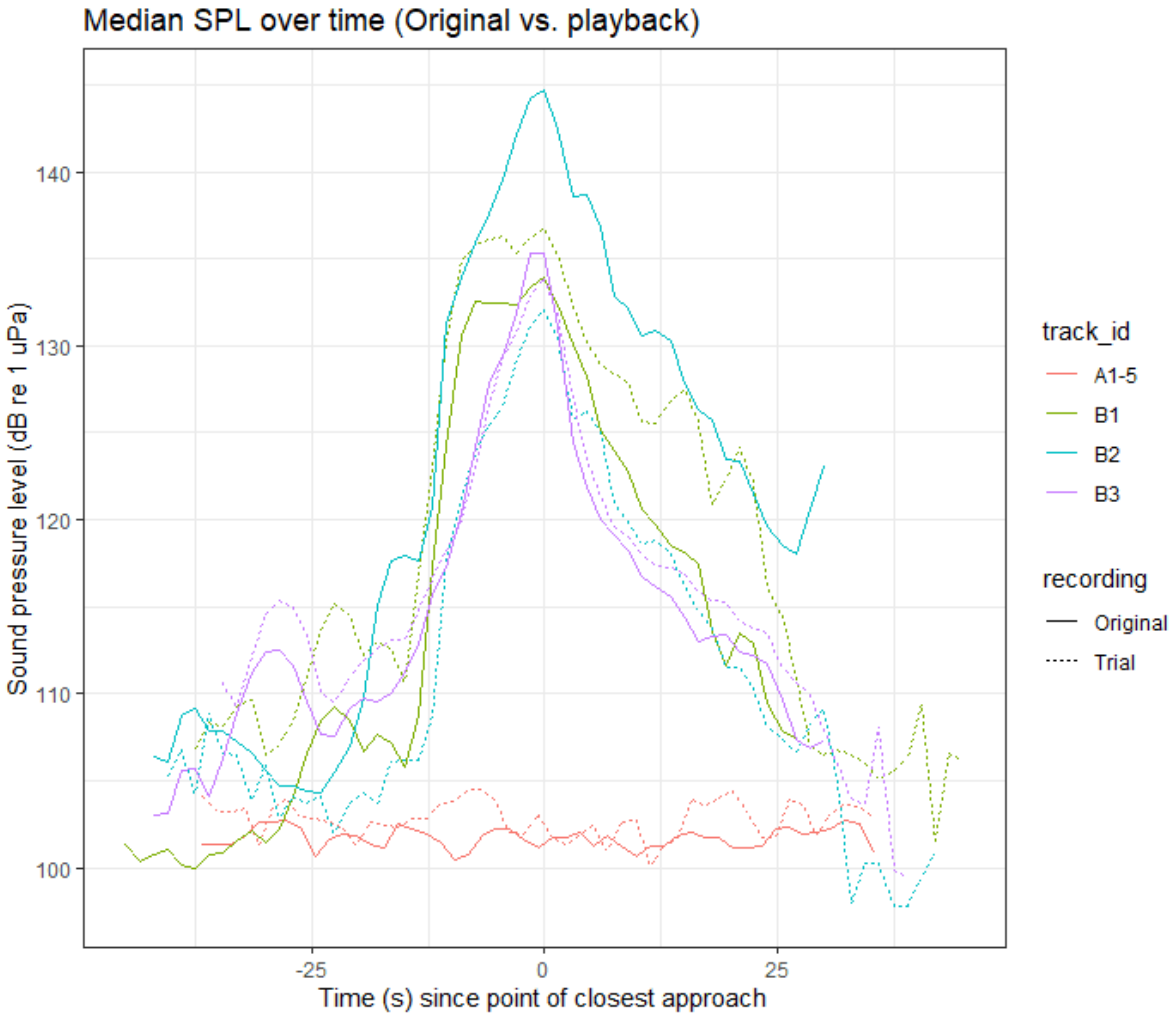

Figure A6.1: Sound pressure level (dB re 1 µPa) over time (3 s segments, 1.5 s overlap) of the original recordings (solid lines) from which the playback tracks were constructed and the median of the recordings of the ambient and boat playbacks used in the experiments. Track ids with prefix 'A' (the flatter lines at the bottom, with lower pressure level) refers to ambient reef recording and playback track, whereas prefix 'B' (the lines with higher pressure level and a

‘spike’ towards the middle) refers to recordings of passes of three different small boats and their playback tracks. This shows that sound pressure level of the playback trial tracks is comparable to that of the original recordings. This figure was made by Jeroen Hubert of Leiden University with permission given for its use here.

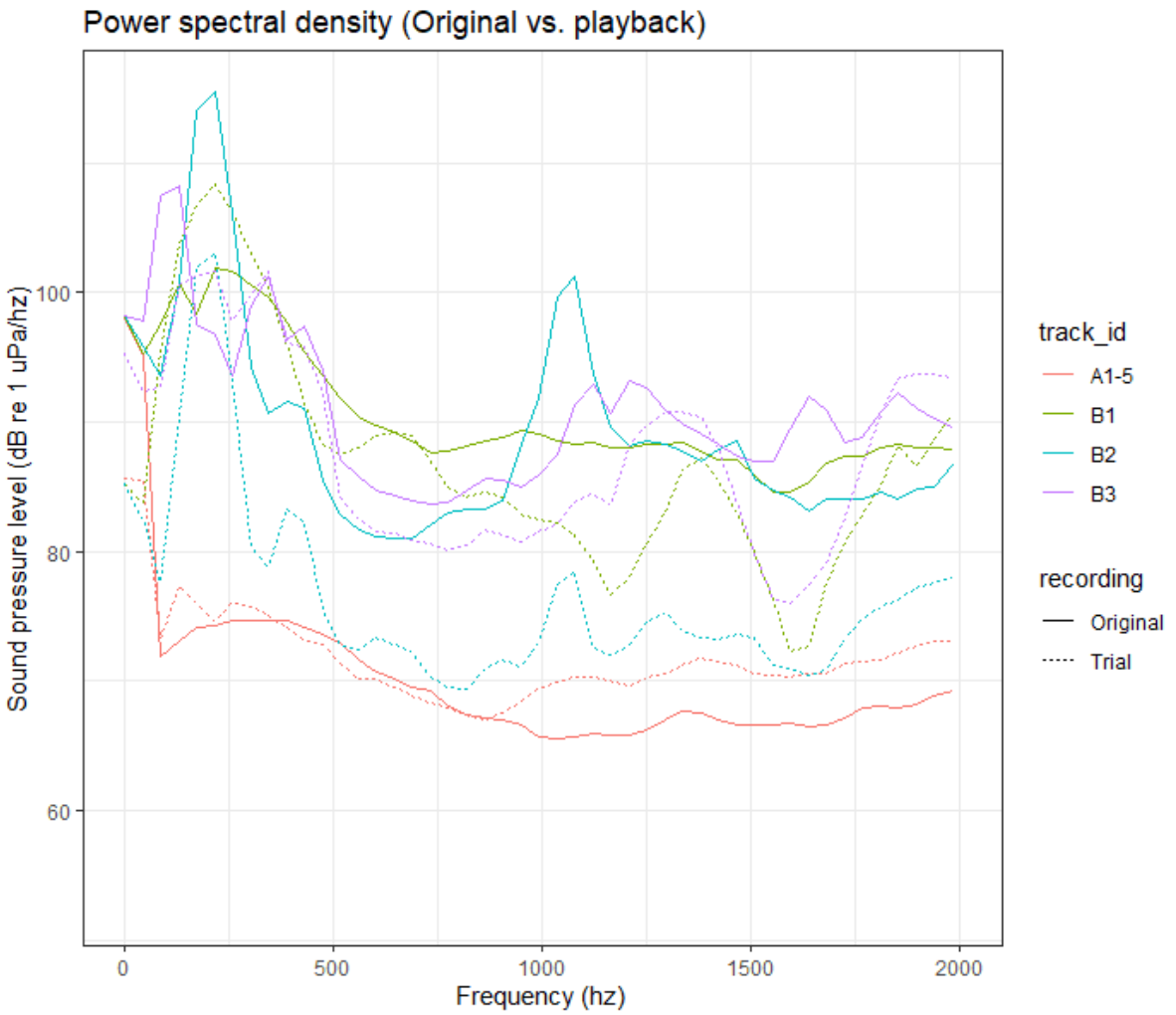

Figure A6.2: Comparisons of power spectral density (PSD) of the original recordings (solid lines) from which the playback tracks were constructed and the median of the recordings of the ambient and boat playbacks (dotted lines) during the actual trials. Track ids with prefix 'A' refers to ambient reef recording and playback track, whereas prefix 'B' refers to recordings of passes of three different small boats and their playback tracks. This figure was made by Jeroen Hubert of Leiden University with permission given for its use here.

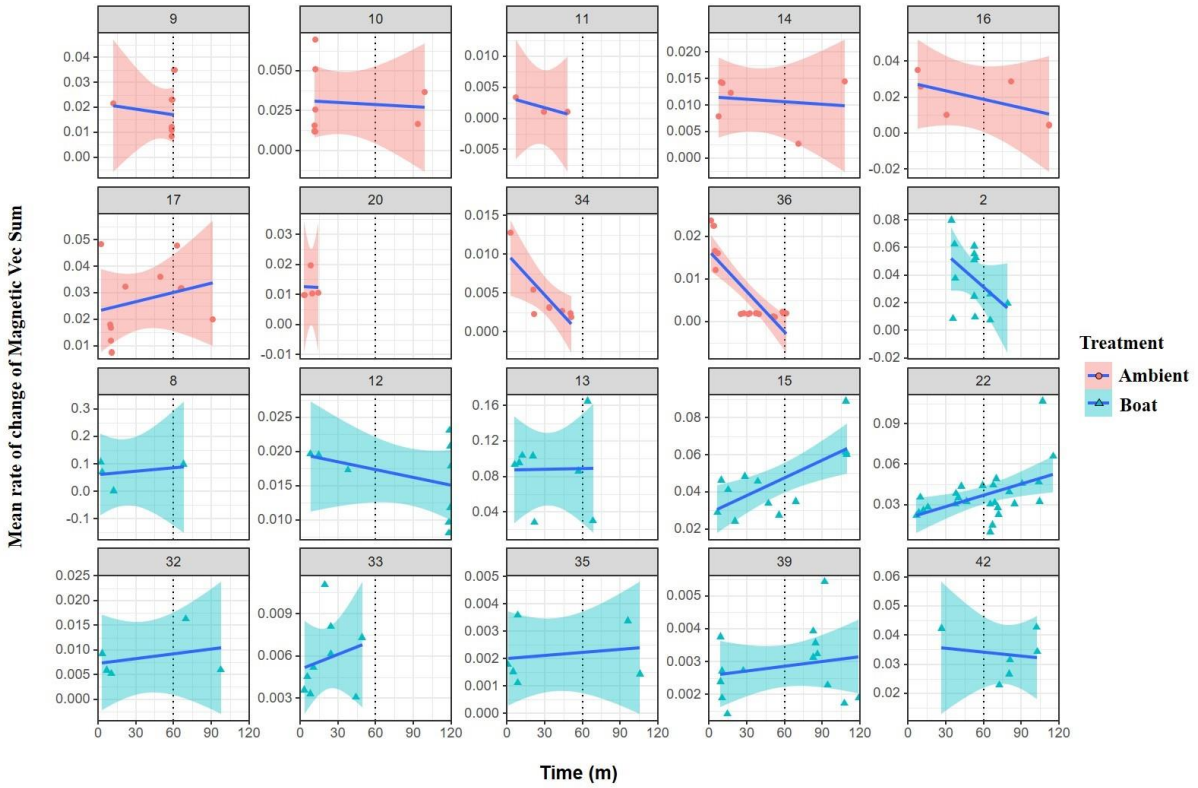

Figure A6.3: The mean rate of change of magnetic vectoral sum (MVS) per closing movement over time (minutes since trial start), per individual (by panel and numbered) and coloured by treatment (ambient noise: red CIs, circular points; boat noise: blue CIs, triangular points). Each individual has been fitted with a linear model trend line and 95% CIs. The vertical dotted line denotes the start of the second hour (when noise treatment either stayed as ambient control noise or switched to boat noise).

Table A6.1: Linear model coefficients for the per-clam relationship between mean Magnetic Vectoral Sum per-movement and time (m) since experiment start, as seen in Chapter 6, Figure 5. 10 clams are excluded here, because 8 did not move at all and 2 only had 2 movements each.

ID	Treatment	Intercept	Slope	R2
9	Ambient	0.30	-0.0007	0.38
10	Ambient	0.38	-0.0007	0.13
11	Ambient	4.27	-0.0003	0.77
14	Ambient	4.23	0.0005	0.34
16	Ambient	0.62	-0.0004	0.33
17	Ambient	0.75	-0.0006	0.24
20	Ambient	0.63	-0.0006	0.18
34	Ambient	4.13	0.0004	0.59
36	Ambient	4.46	-0.005	0.71
2	Boat	0.22	-0.001	0.11
8	Boat	0.82	-0.0007	0.04
12	Boat	0.66	-0.0006	0.67
13	Boat	1.35	-0.007	0.58
15	Boat	1.76	-0.002	0.90
22	Boat	1.21	-0.0005	0.13
32	Boat	4.18	-0.0001	0.11
33	Boat	1.24	0.0009	0.63
35	Boat	4.29	-0.00002	0.74
39	Boat	0.46	-0.000004	0.002
42	Boat	2.20	0.000269	0.17

Bibliography

This section lists all works referred to in this thesis, ordered alphabetically by first author (Harvard system).

Alerstam, T., Hedenström, A., and Åkesson, S., 2003. Long-distance migration: Evolution and determinants. *Oikos*, 103, 247–260.

Alexander, R. M., 2011. Mechanics of Skeleton and Tendons. *In*: Brooks, V. B., ed. *Handbook of Physiology - the nervous system*. Bethesda, MD: American Physiological Society, 17–42.

Amélineau, F., Péron, C., Lescroël, A., Authier, M., Provost, P., and Grémillet, D., 2014. Windscape and tortuosity shape the flight costs of northern gannets. *Journal of Experimental Biology*, 217, 876–885.

An, K. N., Takahashi, K., Harrigan, T. P., and Chao, E. Y., 1984. Determination of muscle orientations and moment arms. *Journal of Biomechanical Engineering*, 106 (3), 280–282.

Anderson, J. M., Clegg, T. M., Véras, L. V. M. V. Q., and Holland, K. N., 2017. Insight into shark magnetic field perception from empirical observations. *Scientific Reports*, 7 (1), 1–15.

Anderson, K. J. and Jetz, W., 2005. The broad-scale ecology of energy expenditure of endotherms. *Ecology Letters*, 8, 310–318.

Anderson, S. D., Chapple, T. K., Jorgensen, S. J., Klimley, A. P., and Block, B. A., 2011. Long-term individual identification and site fidelity of white sharks, Carcharodon carcharias, off California using dorsal fins. *Marine Biology*, 158, 1233–1237.

André, M., Kaifu, K., Solé, M., van der Schaar, M., Akamatsu, T., and Balastegui, A., 2016. Contribution to the Understanding of Particle Motion Perception in Marine Invertebrates. *In*: *Popper A., Hawkins A. (eds) The Effects of Noise on Aquatic Life II. Advances in Experimental Medicine and Biology, vol 875*. New York: Springer.

Andrzejaczek, S., Gleiss, A. C., Lear, K. O., Pattiaratchi, C. B., Chapple, T., and Meekan, M., 2019. Biologging tags reveal links between fine-scale horizontal and vertical movement behaviours in tiger sharks *(Galeocerdo cuvier)*. *Frontiers in Marine Science*, 6 (229).

Arkwright, A. C., Archibald, E., Fahlman, A., Holton, M. D., Luis Crespo-Picazo, J., Cabedo, V. M., Duarte, C. M., Scott, R., Webb, S. L., Gunner, R. M., and Wilson, R. P., 2020. Looking for a fingerprint for animal health: a case study using animal-attached technology on loggerhead turtles. *Frontiers in Ecology and Evolution*, 7 (504).

Bannasch, R., Wilson, R. P., and Culik, B., 1994. Hydrodynamic aspects of design and attachment of a back-mounted device in penguins. *The Journal of Experimental Biology*, 194, 83–96.

Barnothy, M. F. E., 1965. *Biological Effects of Magnetic Fields*. 2nd ed. Plenum, New York: Spring Science and Business Media, LLC.

Baronio, G., Harran, S., and Signoroni, A., 2016. A Critical Analysis of a Hand Orthosis Reverse Engineering and 3D Printing Process. *Applied Bionics and Biomechanics*, 2016.

Bates, D., Maechler, M., Bolker, B., and Walker, S., 2015. Fitting Linear Mixed-Effects Models Using lme4. *Journal of Statistical Software*, 67 (1), 1–48.

Baumgartner, M. F., Hammar, T., and Robbins, J., 2015. Development and assessment of a new dermal attachment for short-term tagging studies of baleen whales. *Methods in Ecology and Evolution*, 6, 289–297.

Bearup, D., Benefer, C. M., Petrovskii, S. V., and Blackshaw, R. P., 2016. Revisiting Brownian motion as a description of animal movement : a comparison to experimental movement data. *Methods in Ecology and Evolution*, 7, 1525–1537.

Berg, Jr, C. J., 1974. A Comparative Ethological Study of Strombid Gastropods. *Behaviour*, 51 (3/4), 274–322.

Bidder, O. R., Walker, J. S., Jones, M. W., Holton, M. D., Urge, P., Scantlebury, D. M., Marks, N. J., and Magowan, E. A., 2015. Step by step : reconstruction of terrestrial animal movement paths by dead-reckoning. *Movement Ecology*, 3 (23), 1–16.

Bissada-Gooding, C. E. and Oxenford, H. A., 2009. Estimating Home Range and Density of a Queen Conch Aggregation Using Acoustic Telemetry and Conventional Tagging. *Proceedings of the 62nd Gulf and Caribbean Fisheries Institute*, 384–389.

Blom, E. L., Kvarnemo, C., Dekhla, I., Schöld, S., Andersson, M. H., Svensson, O., and Amorim, M. C. P., 2019. Continuous but not intermittent noise has a negative impact on mating success in a marine fish with paternal care. *Scientific Reports*, 9 (5494).

Bouyoucos, I. A., Suski, C. D., Mandelman, J. W., and Brooks, E. J., 2017. Effect of weight and frontal area of external telemetry packages on the kinematics, activity levels and swimming performance of small-bodied sharks. *Journal of Fish Biology*, 90, 2097–2110.

Bowlin, M. S., Henningsson, P., Muijres, F. T., Vleugels, R. H. E., Liechti, F., and Hedenström, A., 2010. The effects of geolocator drag and weight on the flight ranges of small migrants. *Methods in Ecology and Evolution*, 1, 398–402.

Boyd, I. L., Frisk, G., Urban, E., Tyack, P., Ausubel, J., Seeyave, S., Cato, D., Southal, B., Weise, M., Andrew, R., Akamatsu, T., Ling, R. D., Erbe, C., Farmer, D., Gentry, R., Gross, T., Hawkins, A., Li, F., Metcalf, K., Miller, J. H., Moretti, D., Rodrigo, C., and Shinke, T., 2011. An international quiet ocean experiment. *Oceanography*, 24 (2), 174–181.

Boyer, D., Ramos-Fernández, G., Miramontes, O., Mateos, J. L., Cocho, H, Larralde, H., Ramos, H., and Rojas, F., 2006. Scale-free foraging by primates emerges from their interaction with a complex environment. *Pro. R. Soc. B*, 273, 1743–1750.

Braun, C. D., Skomal, G. B., and Thorrold, S. R., 2018. Integrating archival tag data and a high-resolution oceanographic model to estimate basking shark (*Cetorhinus maximus*) movements in the western Atlantic. *Frontiers in Marine Science*, 5 (25).

Brewster, L. R., Dale, J. J., Guttridge, T. L., Gruber, S. H., Hansell, A. C., Elliott, M., Cowx,

I. G., Whitney, N. M., and Gleiss, A. C., 2018. Development and application of a machine learning algorithm for classification of elasmobranch behaviour from accelerometry data. *Marine Biology*, 165 (62).

Broell, F., Burnell, C., and Taggart, C. T., 2016. Measuring abnormal movements in free-swimming fish with accelerometers: implications for quantifying tag and parasite load. *Journal of Experimental Biology*, 219, 695–705.

Brown, D. D., Kays, R., Wikelski, M., Wilson, R., and Klimley, A. P., 2013. Observing the unwatchable through acceleration logging of animal behavior. *Animal Biotelemetry*, 1 (20).

Brown, J. H., Gillooly, J. F., Allen, A. P., Savage, V. M., and West, G. B., 2004. Toward a metabolic theory of ecology. *Ecology*, 85 (7), 1771–1789.

Brownscombe, J. W., Wilson, A. D. M., Samson, E., Nowell, L., Cooke, S. J., and Danylchuk, A. J., 2015. Individual differences in activity and habitat selection of juvenile queen conch evaluated using acceleration biologgers. *Endangered Species Research*, 27, 181–188.

Bullock, R. W., Guttridge, T. L., Cowx, I. G., Elliott, M., and Gruber, S. H., 2015. The behaviour and recovery of juvenile lemon sharks *Negaprion brevirostris* in response to external accelerometer tag attachment. *Journal of Fish Biology*, 87, 1342–1354.

Butler, P., Bevan, R., Woakes, A., Croxall, J., and Boyd, I., 1995. The use of data loggers to determine the energetics and physiology of aquatic birds and mammals. *Brazilian Journal of Medical and Biological Research*, 28 (11–12), 1307–17.

Butler, P. J., Green, J. A., Boyd, I. L., and Speakman, J. R., 2004. Measuring metabolic rate in the field: the pros and cons of the doubly labelled water and heart rate methods. *Functional Ecology*, 18, 168–183.

Cabaitan, P. C., Gomez, E. D., and Aliño, P. M., 2008. Effects of coral transplantation and giant clam restocking on the structure of fish communities on degraded patch reefs. *Journal of Experimental Marine Biology and Ecology*, 357, 85–98.

Carroll, A. G., Przeslawski, R., Duncan, A., Gunning, M., and Bruce, B., 2017. A critical review of the potential impacts of marine seismic surveys on fish & invertebrates. *Marine Pollution Bulletin*, 114, 9–24.

Casper, B. M., Smith, M. E., Halvorsen, M. B., Sun, H., Carlson, T. J., and Popper, A. N., 2013. Effects of exposure to pile driving sounds on fish inner ear tissues. *Comparative Biochemistry and Physiology - Part A*, 166, 352–360.

Celi, M., Filiciotto, F., Parrinello, D., Buscaino, G., Damiano, M. A., Cuttitta, A., D'Angelo, S., Mazzola, S., and Vazzana, M., 2013. Physiological and agonistic behavioural response of Procambarus clarkii to an acoustic stimulus. *Journal of Experimental Biology*, 216, 709–718.

Chapman, D. D., Feldheim, K. A., Papastamatiou, Y. P., and Hueter, R. E., 2015. There and Back Again: A Review of Residency and Return Migrations in Sharks, with Implications for Population Structure and Management. *Annual Review of Marine Science*, 7, 547–570.

Chapple, T. K., Gleiss, A. C., Jewell, O. J. D., Wikelski, M., and Block, B. A., 2015. Tracking sharks without teeth: a non-invasive rigid tag attachment for large predatory

sharks. *Animal Biotelemetry*, 3 (14).

Charifi, M., Miserazzi, A., Sow, M., Perrigault, M., Gonzalez, P., Ciret, P., Benomar, S., and Massabuau, J. C., 2018. Noise pollution limits metal bioaccumulation and growth rate in a filter feeder, the Pacific oyster *Magallana gigas*. *PLoS ONE*, 13 (4), e0194174.

Charifi, M., Sow, M., Ciret, P., Benomar, S., and Massabuau, J. C., 2017. The sense of hearing in the Pacific oyster, *Magallana gigas*. *PLoS ONE*, 12 (10), e0185353.

Charrassin, J.-B., Hindell, M., Rintoul, S. R., Roquet, F., Sokolov, S., Biuw, M., Costa, D., Boehme, L., Lovell, P., Coleman, R., Timmermann, R., Meijers, A., Meredith, M., Park, Y.-H., Bailleul, F., Goebel, M., Tremblay, Y., Bost, C.-A., McMahon, C. R., Field, I. C., Fedak, M. A., and Guinet, C., 2008. Southern Ocean frontal structure and sea-ice formation rates revealed by elephant seals. *Proceedings of the National Academy of Sciences*, 105 (33), 11634–11639.

Chia, H. N. and Wu, B. M., 2015. Recent advances in 3D printing of biomaterials. *Journal of Biological Engineering*, 9 (4).

Chivers, L. S., Hatch, S. A., and Elliott, K. H., 2016. Accelerometry reveals an impact of short-term tagging on seabird activity budgets. *The Condor*, 118, 159–168.

Christensen, R. H. B., 2019. ordinal - Regression Models for Ordinal Data. R package version 2019.12-10.

Clements, J. C. and Comeau, L. A., 2019. Use of High-Frequency Noninvasive Electromagnetic Biosensors to Detect Ocean Acidification Effects on Shellfish Behavior. *Journal of Shellfish Research*, 38 (3), 811–818.

Cliffe, R. N., Avey-Arroyo, J. A., Arroyo, F. J., Holton, M. D., and Wilson, R. P., 2014. Mitigating the squash effect: sloths breathe easily upside down. *Biology Letters*, 10 (4), 20140172.

Codling, E. A., Plank, M. J., and Benhamou, S., 2008. Random walk models in biology. *Journal of the Royal Society Interface*, 5, 813–834.

Collins, M. R., Cooke, D. W., Smith, T. I. J., Post, W. C., Russ, D. C., and Walling, D. C., 2002. Evaluation of four methods of transmitter attachment on shortnose sturgeon, *Acipenser brevirostrum*. *Journal of Applied Ichthyology*, 18, 491–494.

Cooke, S. J., 2008. Biotelemetry and biologging in endangered species research and animal conservation: Relevance to regional, national, and IUCN Red List threat assessments. *Endangered Species Research*, 4, 165–185.

Cooke, S. J., Hinch, S. G., Wikelski, M., Andrews, R. D., Kuchel, L. J., Wolcott, T. G., and Butler, P. J., 2004. Biotelemetry: A mechanistic approach to ecology. *Trends in Ecology and Evolution*, 19 (6), 334–343.

Coquereau, L., Jolivet, A., Hégaret, H., and Chauvaud, L., 2016. Short-Term Behavioural Responses of the Great Scallop Pecten maximus Exposed to the Toxic Alga *Alexandrium minutum* Measured by Accelerometry and Passive Acoustics. *PLoS ONE*, 11 (8), e0160935.

Costa, D. P., 1991. Reproductive and foraging energetics of pinnipeds: Implications for life history patterns. *In*: *Renouf D. (eds) The Behaviour of Pinnipeds*. Springer, Dordrecht, 300–344.

Crawley, M. J., 2007. *The R Book*. Chichester, UK: Wiley.

Crossley, S. G. M., Mackintosh, K. A., Wilson, R. P., Lester, L. J., Griffiths, I. W., and McNarry, M. A., 2018. Energy expenditure associated with walking speed and angle of turn in children. *European Journal of Applied Physiology*, 118, 2563–2576.

Daanje, A., 1950. On Locomotory Movements in Birds and the Intention Movements Derived From Them. *Behaviour*, 3 (1), 48–98.

Daniel, T. L. and Tu, M. S., 1999. Animal movement, mechanical tuning and coupled systems. *Journal of Experimental Biology*, 202, 3415–3421.

Dean, B. and Bhushan, B., 2010. Shark-skin surfaces for fluid-drag reduction in turbulent flow: a review. *Philosophical Transactions of the Royal Society A: Mathematical, Physical and Engineering Sciences*, 368, 4775–4806.

Dehaudt, B., Nguyen, M., Vadlamudi, A., and Blumstein, D. T., 2019. Giant clams discriminate threats along a risk gradient and display varying habituation rates to different stimuli. *Ethology*, 125, 392–398.

Dicken, M. L., Booth, A. J., and Smale, M. J., 2006. Preliminary observations of tag shedding, tag reporting, tag wounds, and tag biofouling for raggedtooth sharks (*Carcharias taurus*) tagged off the east coast of South Africa. *ICES Journal of Marine Science*, 63, 1640–1648.

Dickinson, E. R., Stephens, P. A., Marks, N. J., Wilson, R. P., and Scantlebury, D. M., 2020. Best practice for collar deployment of tri - axial accelerometers on a terrestrial quadruped to provide accurate measurement of body acceleration. *Animal Biotelemetry*, 8 (9).

Duarte, C. M., Chapuis, L., Collin, S. P., Costa, D. P., Devassy, R. P., Eguiluz, V. M., Erbe, C., Gordon, T. A. C., Halpern, B. S., Harding, H. R., Havlik, M. N., Meekan, M., Merchant, N. D., Miksis-Olds, J. L., Parsons, M., Predragovic, M., Radford, A. N., Radford, C. A., Simpson, S. D., Slabbekoorn, H., Staaterman, E., Van Opzeeland, I. C., Winderen, J., Zhang, X., and Juanes, F., 2021. The soundscape of the Anthropocene ocean. *Science*, 371 (6529), eaba4658.

Dudley, S. F. J., Anderson-Reade, M. D., Thompson, G. S., and McMullen, P. B., 2000. Concurrent scavenging off a whale carcass by great white sharks, *Carcharodon carcharias*, and tiger sharks, *Galeocerdo cuvier*. *Fishery Bulletin*, 98 (3), 646–649.

Dujon, A. M., Stieglitz, T. C., Amice, E., and Webber, D. M., 2019. Snail leaps and bounds: drivers of the diel movement pattern of a large invertebrate, the caribbean queen conch (*Lobatus gigas*), in a marginal inshore habitat. *Canadian Journal of Zoology*, 97, 436–445.

Duncan, P. F., 2003. Shellfish | Commercially Important Molluscs. *In*: Cabellero, B., ed. *Encyclopedia of Food Sciences and Nutrition (second ed)*. Oxford: Academic Press, 5222–5228.

Edelhoff, H., Signer, J., and Balkenhol, N., 2016. Path segmentation for beginners: An overview of current methods for detecting changes in animal movement patterns. *Movement Ecology*, 4 (21).

Eisenberg, E. and Hill, T. L., 1985. Muscle Contraction and Free Energy Transduction in Biological Systems. *Science*, 227 (4690).

Elfwing, T., Plantman, P., Tedengren, M., and Wijnbladh, E., 2001. Responses to temperature, heavy metal and sediment stress by the giant clam *Tridacna squamosa*. *Marine and Freshwater Behaviour and Physiology*, 34, 239–248.

Elliott, K. H., 2016. Measurement of flying and diving metabolic rate in wild animals: Review and recommendations. *Comparative Biochemistry and Physiology -Part A : Molecular and Integrative Physiology*, 202, 63–77.

Elliott, K. H., Le Vaillant, M., Kato, A., Speakman, J. R., and Ropert-Coudert, Y., 2013. Accelerometry predicts daily energy expenditure in a bird with high activity levels. *Biology Letters*, 9, 20120919.

Ellis, J., Petrovskaya, N., Forbes, E., Walters, K. F. A., and Petrovskii, S., 2020. Movement patterns of the grey field slug (*Deroceras reticulatum*) in an arable field. *Scientific Reports*, 10 (17970), 1–16.

Fehlmann, G. and King, A. J., 2016. Bio-logging. *Current Biology*, 26, R830–R831.

Feldheim, K. A., Gruber, S. H., De Marignac, J. R. C., and Ashley, M. V., 2002. Genetic tagging to determine passive integrated transponder tag loss in lemon sharks. *Journal of Fish Biology*, 61, 1309–1313.

Fernandez-Waid, P., Diez, G., Bidaguren, I., Izagirre, U., Blanco, J. M., and Soto, M., 2019. Morphological Characterization and Hydrodynamic Behavior of Shortfin Mako Shark ([i]Isurus oxyrinchus[/i]) Dorsal Fin Denticles. *Journal of Bionic Engineering*, 16, 730–741.

Field, I. C., Harcourt, R. G., Boehme, L., De Bruyn, P. J. N., Charrassin, J. B., Mcmahon, C. R., Bester, M. N., Fedak, M. A., and Hindell, M. A., 2012. Refining instrument attachment on phocid seals. *Marine Mammal Science*, 28 (3), 325–332.

Filiciotto, F., Vazzana, M., Celi, M., Maccarrone, V., Ceraulo, M., Buffa, G., Stefano, V. Di, Mazzola, S., and Buscaino, G., 2014. Behavioural and biochemical stress responses of Palinurus elephas after exposure to boat noise pollution in tank. *Marine Pollution Bulletin*, 84, 104–114.

Fiore, G., Anderson, E., Garborg, C. S., Murray, M., Johnson, M., Moore, M. J., Howle, L., and Shorter, K. A., 2017. From the track to the ocean: Using flow control to improve marine bio-logging tags for cetaceans. *PLoS ONE*, 12 (2), e0170962.

Fontana, H. de B., Han, S., Sawatsky, A., and Herzog, W., 2018. The mechanics of agonistic muscles. *Journal of Biomechanics*, 79, 15–20.

Fontes, J., Baeyaert, J., Prieto, R., Graca, G., Buyle, F., and Afonso, P., 2017. New non-invasive methods for short-term electronic tagging of pelagic sharks and rays. *Marine Biology*, 165 (34), 2–3.

Fossette, S., Gleiss, A. C., Karpytchev, M., Hays, G. C., Fossette, S., Gleiss, A. C., Chalumeau, J., Bastian, T., Armstrong, C. D., Vandenabeele, S., Karpytchev, M., and Hays, G. C., 2015. Current-Oriented Swimming by Jellyfish and Its Role in Bloom Maintenance. *Current Biology*, 25, 342–347.

Frisk, G. V., 2012. Noiseonomics: The relationship between ambient noise levels in the sea and global economic trends. *Scientific Reports*, 2 (437).

Gazeau, F., Parker, L. M., Comeau, S., Gattuso, J. P., O'Connor, W. A., Martin, S., Pörtner,

H. O., and Ross, P. M., 2013. Impacts of ocean acidification on marine shelled molluscs. *Marine Biology*, 160, 2207–2245.

Gessaman, J. A., 1980. An evaluation of heart rate as an indirect measure of daily energy metabolism of the American kestrel. *Comparative Biochemistry and Physiology -- Part A: Physiology*, 65 (3), 273–289.

Gifford, A., Compagno, L. J. V, Levine, M., and Antoniou, A., 2007. Satellite tracking of whale sharks using tethered tags. *Fisheries Research*, 84, 17–24.

Giomi, F., Barausse, A., Duarte, C. M., Booth, J., Agusti, S., Saderne, V., Anton, A., Daffonchio, D., and Fusi, M., 2019. Oxygen supersaturation protects coastal marine fauna from ocean warming. *Science Advances*, 5, eaax1814.

Gleiss, A. C., Dale, J. J., Holland, K. N., and Wilson, R. P., 2010. Accelerating estimates of activity-specific metabolic rate in fishes: Testing the applicability of acceleration data-loggers. *Journal of Experimental Marine Biology and Ecology*, 385, 85–91.

Gleiss, A. C., Jorgensen, S. J., Liebsch, N., Sala, J. E., Norman, B., Hays, G. C., Quintana, F., Grundy, E., Campagna, C., Trites, A. W., Block, B. A., and Wilson, R. P., 2011. Convergent evolution in locomotory patterns of flying and swimming animals. *Nature Communications*, 2 (352).

Gleiss, A. C., Norman, B., Liebsch, N., Francis, C., and Wilson, R. P., 2009. A new prospect for tagging large free-swimming sharks with motion-sensitive data-loggers. *Fisheries Research*, 97, 11–16.

Gleiss, A. C., Schallert, R. J., Dale, J. J., Wilson, S. G., and Block, B. A., 2019. Direct measurement of swimming and diving kinematics of giant Atlantic bluefin tuna (*Thunnus thynnus*). *Royal Society Open Science*, 6 (190203).

Gleiss, A. C., Wilson, R. P., and Shepard, E. L. C., 2011. Making overall dynamic body acceleration work: on the theory of acceleration as a proxy for energy expenditure. *Methods in Ecology and Evolution*, 2, 23–33.

Godley, B. J., Blumenthal, J. M., Broderick, A. C., Coyne, M. S., Godfrey, M. H., Hawkes, L. A., and Witt, M. J., 2008. Satellite tracking of sea turtles: Where have we been and where do we go next? *Endangered Species Research*, 4, 3–22.

Good, P., 2013. *Permutation Tests: A Practical Guide to Resampling Methods for Testing Hypotheses*. 2nd ed. Springer Science & Business Media.

Green, J. A., 2011. The heart rate method for estimating metabolic rate: Review and recommendations. *Comparative Biochemistry and Physiology - Part A: Molecular and Integrative Physiology*, 158, 287–304.

Green, J. A., Halsey, L. G., Wilson, R. P., and Frappell, P. B., 2009. Estimating energy expenditure of animals using the accelerometry technique: activity, inactivity and comparison with the heart-rate technique. *Journal of Experimental Biology*, 212, 471–482.

Grodzinski, U., Spiegel, O., Korine, C., and Holderied, M. W., 2009. Context-dependent flight speed: Evidence for energetically optimal flight speed in the bat *Pipistrellus kuhlii*? *Journal of Animal Ecology*, 78, 540–548.

Grusha, D. S. and Patterson, M. R., 2005. Quantification of drag and lift imposed by pop-up

satellite archival tags and estimation of the metabolic cost to cownose rays (*Rhinoptera bonasus*). *Fishery Bulletin*, 103, 63–70.

Gubili, C., Johnson, R., Gennari, E., Oosthuizen, W. H., Kotze, D., Meÿer, M., Sims, D. W., Jones, C. S., and Noble, L. R., 2009. Concordance of genetic and fin photo identification in the great white shark, *Carcharodon carcharias*, off Mossel Bay, South Africa. *Marine Biology*, 156, 2199–2207.

Gunner, R. M., Wilson, R. P., Holton, M. D., Scott, R., Hopkins, P., and Duarte, C. M., 2020. A new direction for differentiating animal activity based on measuring angular velocity about the yaw axis. *Ecology and Evolution*, 10, 7872–7886.

Hagen, C. A., Sandercock, B. K., Pitman, J. C., Robel, R. J., and Applegate, R. D., 2006. Radiotelemetry Survival Estimates of Lesser Prairie-Chickens in Kansas: Are There Transmitter Biases? *Wildlife Society Bulletin*, 34 (4), 1064–1069.

Haldane, J., 1926. 'On being the right size'. *Harper's Magazine*, 152.

Hale, J. R., Bouma, J. V., Vadopalas, B., and Friedman, C. S., 2012. Evaluation of Passive Integrated Transponders for Abalone: Tag Placement, Retention, and Effect on Survival. *Journal of Shellfish Research*, 31 (3), 789–794.

Halsey, L. G., 2016. Terrestrial movement energetics: current knowledge and its application to the optimising animal. *The Journal of Experimental Biology*, 219, 1424–1431.

Halsey, L. G., Shepard, E. L. C., Hulston, C. J., Venables, M. C., White, C. R., Jeukendrup, A. E., and Wilson, R. P., 2008. Acceleration versus heart rate for estimating energy expenditure and speed during locomotion in animals: Tests with an easy model species, *Homo sapiens*. *Zoology*, 111, 231–241.

Halsey, L. G., Shepard, E. L. C., Quintana, F., Gomez Laich, A., Green, J. A., and Wilson, R. P., 2009. The relationship between oxygen consumption and body acceleration in a range of species. *Comparative Biochemistry and Physiology - Part A: Molecular and Integrative Physiology*, 152, 197–202.

Halsey, L. G., Shepard, E. L. C., and Wilson, R. P., 2011. Assessing the development and application of the accelerometry technique for estimating energy expenditure. *Comparative Biochemistry and Physiology - Part A: Molecular and Integrative Physiology*, 158, 305–314.

Halsey, L. G. and White, C. R., 2010. Measuring Energetics and Behaviour Using Accelerometry in Cane Toads *Bufo marinus*. *PLoS ONE*, 5 (4), e10170.

Halvorsen, M. B., Casper, B. M., Matthews, F., Carlson, T. J., and Popper, A. N., 2012. Effects of exposure to pile-driving sounds on the lake sturgeon, Nile tilapia and hogchoker. *Proceedings of the Royal Society B: Biological Sciences*, 279, 4705–4714.

Hammerschlag, N., Gallagher, A. J., and Lazarre, D. M., 2011. A review of shark satellite tagging studies. *Journal of Experimental Marine Biology and Ecology*, 398, 1–8.

Harding, H. R., Gordon, T. A. C., Eastcott, E., Simpson, S. D., and Radford, A. N., 2019. Causes and consequences of intraspecific variation in animal responses to anthropogenic noise. *Behavioral Ecology*, 30 (6), 1501–1511.

Harel, R., Horvitz, N., and Nathan, R., 2016. Adult vultures outperform juveniles in challenging thermal soaring conditions. *Scientific Reports*, 6 (27865).

Haulsee, D. E., Fox, D. A., Breece, M. W., Clauss, T. M., and Oliver, J. M., 2016. Implantation and Recovery of Long-Term Archival Transceivers in a Migratory Shark with High Site Fidelity. *PLoS ONE*, 11 (2), e0148617.

Hazekamp, A. A. H., Mayer, R., and Osinga, N., 2010. Flow simulation along a seal: the impact of an external device. *European Journal of Wildlife Research*, 56, 131–140.

Healy, M., Chiaradia, A., Kirkwood, R., and Dann, P., 2004. Balance: a neglected factor when attaching external devices to penguins. *Memoirs of National Institute of Polar Research*, Spec. Issu (58), 179–182.

Heide-Jørgensen, M. P., Nielsen, N. H., Teilmann, J., and Leifsson, P. S., 2017. Long-term tag retention on two species of small cetaceans. *Marine Mammal Science*, 33 (3), 713–725.

Heithaus, M. R., Wirsing, A. J., Dill, L. M., and Heithaus, L. I., 2007. Long-term movements of tiger sharks satellite-tagged in Shark Bay, Western Australia. *Marine Biology*, 151, 1455–1461.

Hof, A. L., 2001. The force resulting from the action of mono- and biarticular muscles in a limb. *Journal of Biomechanics*, 34, 1085–1089.

Holles, S. H., Simpson, S. D., Radford, A. N., Berten, L., and Lecchini, D., 2013. Boat noise disrupts orientation behaviour in a coral reef fish. *Marine Ecology Progress Series*, 485, 295–300.

Holyoak, M., Casagrandi, R. R., Nathan, R., Revilla, E., and Spiegel, O., 2008. Trends and missing parts in the study of movement ecology. *Proceedings of the National Academy of Sciences*, 105 (49), 19060–19065.

Hoolihan, J. P., Luo, J., Abascal, F. J., Campana, S. E., Metrio, G. De, Dewar, H., Domeier, M. L., Howey, L. A., Lutcavage, M. E., Musyl, M. K., Neilson, J. D., Orbesen, E. S., Prince, E. D., and Rooker, J. R., 2011. Evaluating post-release behaviour modification in large pelagic fish deployed with pop-up satellite archival tags, 68 (5), 880–889.

van der Hoop, J. M., Fahlman, A., Hurst, T., Rocho-Levine, J., Shorter, K. A., Petrov, V., and Moore, M. J., 2014. Bottlenose dolphins modify behavior to reduce metabolic effect of tag attachment. *Journal of Experimental Biology*, 217, 4229–4236.

Hoover, A. L., Shillinger, G. L., Swiggs, J., and Bailey, H., 2017. Comparing Acoustic Tag Attachments Designed for Mobile Tracking of Hatchling Sea Turtles. *Frontiers in Marine Science*, 4 (225).

Horne, J. S., Garton, E. O., Krone, S. M., and Lewis, J. S., 2007. Analyzing Animal Movements Using Brownian Bridges. *Ecology*, 88 (9), 2354–2363.

Houghton, J. D. R., Liebsch, N., Doyle, T. K., C, G. A., Lilley, M. K. S., Wilson, R. P., and Hays, G. C., 2009. Harnessing the Sun: Testing a Novel Attachment Method to Record Fine Scale Movements in Ocean Sunfish (*Mola mola*). *In*: Nielsen, J. ., ed. *Tagging and Tracking of Marine Animals with Electronic Devices. Reviews: Methods and Technologies in Fish Biology and Fisheries*. Springer Science+Business Media B.V.

Humphries, N. E., Queiroz, N., Dyer, J. R. M., Pade, N. G., Musyl, M. K., Schaefer, K. M., Fuller, D. W., Brunnschweiler, J. M., Doyle, T. K., Houghton, J. D. R., Hays, G. C., Jones, C. S., Noble, L. R., Wearmouth, V. J., Southall, E. J., and Sims, D. W., 2010. Environmental context explains Lévy and Brownian movement patterns of marine

predators. *Nature*, 465, 1066–1069.

Hutchinson, J., Miller, C., Firtsch, G., and Hildebrandt, T., 2008. The Anatomical Foundation for Multidisciplinary Studies of Animal Limb Function: Examples from Dinosaur and Elephant Limb Imaging Studies. *In*: Endo, H. and R., F., eds. *Digital Imaging and the Transformation of the Anatomical Sciences: Towards a New Morphology*. Berlin: Springer, 22–38.

IMO, 2014. Guidelines for the Reduction of Underwater Noise from Commercial Shipping to Address Adverse Impacts on Marine Life. *International Maritime Organisation, London, England*, 66 (17).

Irschick, D. J. and Hammerschlag, N., 2015. Morphological scaling of body form in four shark species differing in ecology and life history. *Biological Journal of the Linnean Society*, 114, 126–135.

Irvine, M. D., Wells, R. S., and Scott, M. D., 1982. An Evaluation of Techniques for Tagging Small Odontocete Cetaceans. *Fishery Bulletin*, 80 (1), 135–143.

Jacoby, D. M. P., Siriwat, P., Freeman, R., and Carbone, C., 2015. Is the scaling of swim speed in sharks driven by metabolism? *Biology Letters*, 11 (20150781).

Jeanniard-du-Dot, T., Guinet, C., Arnould, J. P. Y., Speakman, J. R., and Trites, A. W., 2017. Accelerometers can measure total and activity-specific energy expenditures in free-ranging marine mammals only if linked to time-activity budgets. *Functional Ecology*, 31, 377–386.

Jepsen, N., Thorstad, E. B., Havn, T., and Lucas, M. C., 2015. The use of external electronic tags on fish: an evaluation of tag retention and tagging effects. *Animal Biotelemetry*, 3 (49).

Jewell, O. J. D., Gleiss, A. C., Jorgensen, S. J., Andrzejaczek, S., Moxley, J. H., Beatty, S. J., Wikelski, M., Block, B. A., and Chapple, T. K., 2019. Cryptic habitat use of white sharks in kelp forest revealed by animal-borne video. *Biology Letters*, 15 (4).

Jewell, O. J. D., Wcisel, M. A., Gennari, E., Towner, A. V., Bester, M. N., Johnson, R. L., and Singh, S., 2011. Effects of smart position only (SPOT) tag deployment on white sharks *Carcharodon carcharias* in South Africa. *PLoS ONE*, 6 (11), e27242.

Johnson, G. C., Karajah, M. T., Mayo, K., Armenta, T. C., and Blumstein, D. T., 2017. The bigger they are the better they taste: size predicts predation risk and anti-predator behavior in giant clams. *Journal of Zoology*, 301, 102–107.

Johnson, M. P. and Tyack, P. L., 2003. A digital acoustic recording tag for measuring the response of marine mammals to sound. *Journal of Oceanic Engineering*, 28 (1), 3–11.

Jones, T. T., Van Houtan, K. S., Bostrom, B. L., Ostafichuk, P., Mikkelsen, J., Tezcan, E., Carey, M., Imlach, B., and Seminoff, J. A., 2013. Calculating the ecological impacts of animal-borne instruments on aquatic organisms. *Methods in Ecology and Evolution*, 4, 1178–1186.

Jou, L., Lin, S., Chen, B., Chen, W., and Liao, C., 2013. Synthesis and measurement of valve activities by an improved online clam-based behavioral monitoring system. *Computers and Electronics in Agriculture*, 90, 106–118.

Kaidarova, A., Khan, M. A., Amara, S., Geraldi, N. R., Karimi, M. A., Shamim, A., Wilson,

R. P., Duarte, C. M., and Kosel, J., 2018. Tunable, Flexible Composite Magnets for Marine Monitoring Applications. *Advanced Engineering Materials*, 20, 1–8.

Kalmijn, A., 1973. Electro-orientation in sharks and rays: theory and experimental evidence. *Scripps Institute of Oceanography*, 73 (39), 1–22.

Kalmijn, A. J., 1982. Electric and magnetic field detection in elasmobranch fishes. *Science*, 218 (4575), 916–918.

Kay, W. P., Naumann, D. S., Bowen, H. J., Withers, S. J., Evans, B. J., Wilson, R. P., Stringell, T. B., Bull, J. C., Hopkins, P. W., and Börger, L., 2019. Minimizing the impact of biologging devices: Using computational fluid dynamics for optimizing tag design and positioning. *Methods in Ecology and Evolution*, 10, 1222–1233.

Kays, R., Crofoot, M. C., Jetz, W., and Wikelski, M., 2015. Terrestrial animal tracking as an eye on life and planet. *Science*, 348 (6240), aaa2478.

Kooyman, G., 1965. Techniques used in measuring diving capacities of Weddell Seals. *Polar Record*, 12 (79), 391–394.

Kunc, H. P., Lyons, G. N., Sigwart, J. D., McLaughlin, K. E., and Houghton, J. D. R., 2014. Anthropogenic noise affects behavior across sensory modalities. *American Naturalist*, 184 (4), 93–100.

Kyte, A., Pass, C., Pemberton, R., Sharman, M., and McKnight, J. C., 2019. A computational fl uid dynamics (CFD) based method for assessing the hydrodynamic impact of animal borne data loggers on host marine mammals. *Marine Mammal Science*, 35, 364–394.

Lear, K. O., Gleiss, A. C., and Whitney, N. M., 2018. Metabolic rates and the energetic cost of external tag attachment in juvenile blacktip sharks *Carcharhinus limbatus*. *Journal of Fish Biology*, 93, 391–395.

Lear, K. O., Poulakis, G. R., Scharer, R. M., Gleiss, A. C., and Whitney, N. M., 2019. Fine-scale behavior and habitat use of the endangered smalltooth sawfish (*Pristis pectinata*): Insights from accelerometry. *Fishery Bulletin*, 117, 348–359.

Lear, K. O. and Whitney, N. M., 2016. Bringing data to the surface: Recovering data loggers for large sample sizes from marine vertebrates. *Animal Biotelemetry*, 4 (12).

Lear, K. O., Whitney, N. M., Brewster, L. R., Morris, J. J., Hueter, R. E., and Gleiss, A. C., 2017. Correlations of metabolic rate and body acceleration in three species of coastal sharks under contrasting temperature regimes. *The Journal of Experimental Biology*, 220, 397–407.

Lecchini, D., Bertucci, F., Gache, C., Khalife, A., Besson, M., Roux, N., Berthe, C., Singh, S., Parmentier, E., Nugues, M. M., Brooker, R. M., Dixson, D. L., and Hédouin, L., 2018. Boat noise prevents soundscape-based habitat selection by coral planulae. *Scientific Reports*, 8 (9283).

Lee, M. A., Nguyen, F. T., Scott, K., Chan, N. Y. L., Bakh, N. A., Jones, K. K., Pham, C., Garcia-salinas, P., Garcia-parraga, D., Fahlman, A., Marco, V., Koman, V. B., Oliver, R. J., Hopkins, L. W., Rubio, C., Wilson, R. P., Meekan, M. G., Duarte, C. M., and Strano, M. S., 2018. Implanted Nanosensors in Marine Organisms for Physiological Biologging: Design, Feasibility, and Species Variability. *ACS Sensors*, 4 (1), 32–43.

Lefevre, S., Watson, S.-A., Munday, P. L., and Nilsson, G. E., 2015. Will jumping snails

prevail? Influence of near-future CO_2, temperature and hypoxia on respiratory performance in the tropical conch Gibberulus gibberulus gibbosus. *Journal of Experimental Biology*, 218, 2991–3001.

Leiva, G. E. and Castilla, J. C., 2002. A review of the world marine gastropod fishery: evolution of catches, management and the Chilean experience. *Reviews in Fish Biology and Fisheries*, 11, 283–300.

Liao, C. M., Jau, S. F., Lin, C. M., Jou, L. J., Liu, C. W., Liao, V. H. C., and Chang, F. J., 2009. Valve movement response of the freshwater clam Corbicula fluminea following exposure to waterborne arsenic. *Ecotoxicology*, 18, 567–576.

Liechti, F., Witvliet, W., Weber, R., and Bachler, E., 2013. First evidence of a 200-day non-stop flight in a bird. *Nature Communications*, 4 (2554), 153–154.

Lifson, N. and McClintock, R., 1966. Theory of use of the turnover rates of body water for measuring energy and material balance. *Journal of Theoretical Biology*, 12, 46–74.

Lighton, J. R. B., 2008. *Measuring metabolic rates: a manual for scientists*. Oxford: Oxford University Press.

Lingham-Soliar, T., 2005. Dorsal fin in the white shark, *Carcharodon carcharias*: A dynamic stabilizer for fast swimming. *Journal of Morphology*, 263, 1–11.

Liu, Y., Battaile, B. C., Trites, A. W., and Zidek, J. V., 2015. Bias correction and uncertainty characterization of Dead-Reckoned paths of marine mammals. *Animal Biotelemetry*, 3 (51).

Livingstone, D. ., de Zwaan, A., and Thompson, R. ., 1981. Aerobic metabolism, octopine production and phosphoarginine as sources of energy in the phasic and catch adductor muscles of the giant scallop placopecten magellanicus during swimming and the subsequent recovery period. *Comparative Biochemistry and Physiology Part B: Comparative Biochemistry*, 70 (1).

Lovvorn, J. R., Croll, D. A., and Liggins, G. A., 1999. Mechanical versus physiological determinants of swimming speeds in diving Brunnich's guillemots. *Journal of Experimental Biology*, 202, 1741–1752.

Lüdecke, D., 2018. ggeffects: Tidy Data Frames of Marginal Effects from Regression Models. [online]. Available from: https://doi.org/10.21105/joss.00772.

Lynch, S. D., Marcek, B. J., Marshall, H. M., Bushnell, P. G., Bernal, D., and Brill, R. W., 2017. The effects of pop-up satellite archival tags (PSATs) on the metabolic rate and swimming kinematics of juvenile sandbar shark *Carcharhinus plumbeus*. *Fisheries Research*, 186, 205–215.

Lyons, G. N., Halsey, L. G., Pope, E. C., Eddington, J. D., and Houghton, J. D. R., 2013. Energy expenditure during activity in the American lobster *Homarus americanus*: Correlations with body acceleration. *Comparative Biochemistry and Physiology - Part A: Molecular and Integrative Physiology*, 166, 278–284.

Malone, P. G. and Dodd, J. R., 1967. Temperature and Salinity Effects on Calcification Rate in Mytilus Edulis and its Paleoecological Implicatons. *Limnology and Oceanography*, 12, 432–436.

Marshall, H., Skomal, G., Ross, P. G., and Bernal, D., 2015. At-vessel and post-release

mortality of the dusky (*Carcharhinus obscurus*) and sandbar (*C . plumbeus*) sharks after longline capture. *Fisheries Research*, 172, 373–384.

Maynard, D. M. and Burke, W., 1971. Maximum tension developed by the posterior adductor muscle of the giant clam, *Tridacna gigas* (Linné). *Comparative Biochemistry and Physiology -- Part A: Physiology*, 38 (A), 339–350.

Mayr, E., 1961. Cause and Effect in Biology. *Science*, 134 (3489), 1501–1506.

McClune, D. W., Marks, N. J., Wilson, R. P., Houghton, J. D. R., Montgomery, I. W., McGowan, N. E., Gormley, E., and Scantlebury, M., 2014. Tri-axial accelerometers quantify behaviour in the Eurasian badger (*Meles meles*): Towards an automated interpretation of field data. *Animal Biotelemetry*, 2 (5).

McDonald, M. A., Hildebrand, J. A., and Wiggins, S. M., 2006. Increases in deep ocean ambient noise in the Northeast Pacific west of San Nicolas Island, California. *The Journal of the Acoustical Society of America*, 120 (2), 711–718.

McMahon, C. R., Autret, E., Houghton, J. D., Lovell, P., Myers, A. E., and Hays, G. C., 2005. Animal borne sensors successfully capture the real-time thermal properties of ocean basins. *Limnology and Oceanography: Methods*, 3, 392–398.

McMahon, C. R., Collier, N., Northfield, J. K., and Glen, F., 2011. Taking the time to assess the effects of remote sensing and tracking. *Animal Welfare*, 20, 515–521.

Mcmahon, T., 1971. Size and Shape in Biology. *Science*, 179 (4079), 1201–1204.

McMahon, T. A., 1975. Using body size to understand the structural design of animals: quadrupedal locomotion. *Journal of Applied Physiology*, 39 (4), 619–627.

Miksis-Olds, J. L. and Tyack, P. L., 2009. Manatee (*Trichechus manatus*) vocalization usage in relation to environmental noise levels. *The Journal of the Acoustical Society of America*, 125 (3), 1806–1815.

Moll, R. J., Millspaugh, J. J., Beringer, J., Sartwell, J., and He, Z., 2007. A new 'view' of ecology and conservation through animal-borne video systems. *Trends in Ecology and Evolution*, 22 (12), 660–668.

Mooney, T. A., Hanlon, R. T., Christensen-Dalsgaard, J., Madsen, P. T., Ketten, D. R., and Nachtigall, P. E., 2010. Sound detection by the longfin squid (*Loligo pealeii*) studied with auditory evoked potentials: Sensitivity to low-frequency particle motion and not pressure. *Journal of Experimental Biology*, 213, 3748–3759.

Van Moorter, B., Bunnefeld, N., Panzacchi, M., Rolandsen, C. M., Solberg, E. J., and Sæther, B. E., 2013. Understanding scales of movement: Animals ride waves and ripples of environmental change. *Journal of Animal Ecology*, 82, 770–780.

Morton, B., 1978. The diurnal rhythm and the processes of feeding and digestion in *Tridacna crocea* (Bivalve: Tridacnidae). *Journal of Zoology, London*, 185, 371–387.

Motta, P., Habegger, M. L., Lang, A., Hueter, R., and Davis, J., 2012. Scale morphology and flexibility in the shortfin mako *Isurus oxyrinchus* and the blacktip shark *Carcharhinus limbatus*. *Journal of Morphology*, 273, 1096–1110.

Mul, E., Blanchet, M. A., Biuw, M., and Rikardsen, A., 2019. Implications of tag positioning and performance on the analysis of cetacean movement. *Animal Biotelemetry*, 7 (11).

Musyl, M. K., Brill, R. W., Curran, D. S., Fragoso, N. M., McNaughton, L. M., Nielsen, A., Kikkawa, B. S., and Moyes, C. D., 2011. Postrelease survival, vertical and horizontal movements, and thermal habitats of five species of pelagic sharks in the central Pacific Ocean. *Fishery Bulletin*, 109 (4), 341–368.

Musyl, M. K., Domeier, M. L., Nasby-Lucas, N., Brill, R. W., McNaughton, L. M., Swimmer, J. Y., Lutcavage, M. S., Wilson, S. G., Galuardi, B., and Liddle, J. B., 2011. Performance of pop-up satellite archival tags. *Marine Ecology Progress Series*, 433, 1–28.

Myers, A. E. and Hays, G. C., 2006. Do leatherback turtles *Dermochelys coriacea* forage during the breeding season? A combination of data-logging devices provide new insights. *Marine Ecology Progress Series*, 322, 259–267.

Myrberg, A. A. and Gruber, S. H., 1974. The Behaviour of the Bonnethead Shark, *Sphyrna tiburo*. *American Society of Ichthyologists and Herpetologists*, 1974 (2), 358–374.

Nagy, K. A., Girard, I. A., and Brown, T. K., 1999. Energetics of Free-Ranging Mammals, Reptiles, and Birds. *Annual Review of Nutrition*, 19, 247–277.

Nakagawa, S. and Schielzeth, H., 2013. A general and simple method for obtaining R^2 from generalized linear mixed-effects models. *Methods in Ecology and Evolution*, 4, 133–142.

Nassar, J. M., Khan, S. M., Velling, S. J., Diaz-gaxiola, A., Shaikh, S. F., Geraldi, N. R., Sevilla, G. A. T., Duarte, C. M., and Hussain, M. M., 2018. Compliant lightweight non-invasive standalone “Marine Skin” tagging system. *npj Flexible Electronics*, 2 (13).

Nathan, R., Getz, W. M., Revilla, E., Holyoak, M., Kadmon, R., Saltz, D., and Smouse, P. E., 2008. A movement ecology paradigm for unifying organismal movement research. *Proceedings of the National Academy of Sciences*, 105 (49), 19052–19059.

Nedelec, S. L., Campbell, J., Radford, A. N., Simpson, S. D., and Merchant, N. D., 2016. Particle motion: the missing link in underwater acoustic ecology. *Methods in Ecology and Evolution*, 7, 836–842.

Neilson, J. D., Loefer, J., Prince, E. D., Royer, F., Calmettes, B., Gaspar, P., Lopez, R., and Andrushchenko, I., 2014. Seasonal distributions and migrations of northwest atlantic Swordfish: Inferences from integration of Pop-Up satellite archival tagging studies. *PLoS ONE*, 9 (11), e112736.

Newcomb, J. M., Lawrence, K. A., and Watson III, W. H., 2004. The influence of light on locomotion in the gastropod *Melibe leonina*. *Mar, Fresh. Behav. Physiol.*, 37 (4), 253–269.

Newell, R. I. E., 2004. Ecosystem influences of natural and cultivated populations of suspension-feeding bivalve molluscs: a review. *Journal of Shellfish Research*, 23, 51–61.

Nickel, B. A., Suraci, J. P., Nisi, A. C., and Wilmers, C. C., 2021. Energetics and fear of humans constrain the spatial ecology of pumas. *Proceedings of the National Academy of Sciences*, 118 (5).

Noar, J. H. and Evans, R. D., 1999. Rare earth magnets in orthodontics: an overview. *British journal of orthodontics*, 26 (1), 29–37.

Noda, T., Kawabata, Y., Arai, N., Mitamura, H., and Watanabe, S., 2014. Animal-mounted gyroscope/accelerometer/magnetometer: In situ measurement of the movement performance of fast-start behaviour in fish. *Journal of Experimental Marine Biology and Ecology*, 451, 55–68.

O'Connell, C. P., Abel, D. C., Rice, P. H., Stroud, E. M., and Simuro, N. C., 2010. Responses of the southern stingray (*Dasyatis americana*) and the nurse shark (*Ginglymostoma cirratum*) to permanent magnets. *Marine and Freshwater Behaviour and Physiology*, 43 (1), 63–73.

Patterson, T. A., Parton, A., Langrock, R., Blackwell, P. G., Thomas, L., and King, R., 2017. Statistical modelling of individual animal movement: an overview of key methods and a discussion of practical challenges. *AStA Advances in Statistical Analysis*, 101, 399–438.

Pavlov, V. V. and Rashad, A. M., 2012. A non-invasive dolphin telemetry tag: Computer design and numerical flow simulation. *Marine Mammal Science*, 28, 16–27.

Pavlov, V. V., Wilson, R. P., and Lucke, K., 2007. A new approach to tag design in dolphin telemetry: Computer simulations to minimise deleterious effects. *Deep-Sea Research Part II: Topical Studies in Oceanography*, 54, 404–414.

Payne, N. L., Gillanders, B. M., Seymour, R. S., Webber, D. M., Snelling, E. P., and Semmens, J. M., 2011. Accelerometry estimates field metabolic rate in giant Australian cuttlefish *Sepia apama* during breeding. *Journal of Animal Ecology*, 80, 422–430.

Payne, N. L., Iosilevskii, G., Barnett, A., Fisher, C., Graham, R. T., Gleiss, A. C., and Watanabe, Y. Y., 2016. Great hammerhead sharks swim on their side to reduce transport costs. *Nature Communications*, 7 (12289).

Perron, F., 1978. Locomotion and shell-righting behaviour in adult and juvenile *Aporrhais occidentalis* (Gastropoda: Strombacea). *Animal Behaviour*, 26, 1023–1028.

Peters, R. C., Eeuwes, L. B. M., and Bretschneider, F., 2007. On the electrodetection threshold of aquatic vertebrates with ampullary or mucous gland electroreceptor organs. *Biological Reviews*, 82, 361–373.

Plank, M. J. and James, A., 2008. Optimal foraging: Lévy pattern or process? *R. Soc. Interface*, 5, 1077–1086.

Poulain, C., Gillikin, D. P., Thébault, J., Munaron, J. M., Bohn, M., Robert, R., Paulet, Y. M., and Lorrain, A., 2015. An evaluation of Mg/Ca, Sr/Ca, and Ba/Ca ratios as environmental proxies in aragonite bivalve shells. *Chemical Geology*, 396, 42–50.

Pratchett, M. S., Cowan, Z. L., Nadler, L. E., Caballes, C. F., Hoey, A. S., Messmer, V., Fletcher, C. S., Westcott, D. A., and Ling, S. D., 2017. Body size and substrate type modulate movement by the western Pacific crown-of-thorns starfish, *Acanthaster solaris*. *PLoS ONE*, 12 (9), e0180805.

Putland, R. L., Merchant, N. D., Farcas, A., and Radford, C. A., 2018. Vessel noise cuts down communication space for vocalizing fish and marine mammals. *Global Change Biology*, 24, 1708–1721.

Qasem, L., Cardew, A., Wilson, A., Griffiths, I., Halsey, L. G., Shepard, E. L. C., Gleiss, A. C., and Wilson, R., 2012. Tri-axial Dynamic Acceleration as a Proxy for Animal Energy Expenditure; Should We Be Summing Values or Calculating the Vector? *PLoS ONE*, 7 (2), e31187.

R Core Team, 2019. *R: A Language and Environment for Statistical Computing*. Vienna, Austria: R Foundation for Statistical Computing.

Randall, J. E., 1964. Contributions to the biology of the Queen Conch, *Strombus gigas*. *Bulletin of Marine Science*, 14 (2), 246–295.

Raposo, E., Buldyrev, S., Luz, M., Viswanathan, G., and Stanley, H., 2009. Lévy flights and random searches. *Journal of Physics A: Mathematical and Theoretical*, 42.

Ren, L., Butler, M., Miller, C., Paxton, H., Schwerda, D., Fischer, M. S., and Hutchinson, J. R., 2008. The movements of limb segments and joints during locomotion in African and Asian elephants. *Journal of Experimental Biology*, 211, 2735–2751.

Resheff, Y. S., Rotics, S., Harel, R., Spiegel, O., and Nathan, R., 2014. AcceleRater: a web application for supervised learning of behavioral modes from acceleration measurements. *Movement Ecology*, 2 (27).

Riisgård, H. U., Lassen, J., and Kittner, C., 2014. Valve-gape response times in mussels (Mytilus edulis) - Effects of laboratory preceding-feeding conditions and in situ tidally induced variation in phytoplankton biomass. *Journal of Shellfish Research*, 25 (3), 901–911.

Ritter, E. K., 2011. Use of sand ripples to enhance chafing in Caribbean reef sharks (*Carcharhinus perezi*) and blacktip sharks (*Carcharhinus limbatus*). *Bulletin of Marine Science*, 87 (3), 413–419.

Ritter, E. K. and Godknecht, A. J., 2000. Agonistic Displays in the Blacktip Shark (*Carcharhinus limbatus*). *Copeia*, 2000 (1), 282–284.

Roberts, L., Cheesman, S., Breithaupt, T., and Elliott, M., 2015. Sensitivity of the mussel *Mytilus edulis* to substrate-borne vibration in relation to anthropogenically generated noise. *Marine Ecology Progress Series*, 538, 185–195.

Roberts, L. and Elliott, M., 2017. Good or bad vibrations? Impacts of anthropogenic vibration on the marine epibenthos. *Science of the Total Environment*, 595, 255–268.

Roberts, R. M., 1989. *Serendipity: Accidental Discoveries in Science*. Wiley.

Robson, A. A., Chauvaud, L., Wilson, R. P., and Halsey, L. G., 2012. Small actions, big costs: the behavioural energetics of a commercially important invertebrate. *Journal of the Royal Society Interface*, 9, 1486–1498.

Robson, A. A., Halsey, L. G., and Chauvaud, L., 2016. Feet, heat and scallops: what is the cost of anthropogenic disturbance in bivalve aquaculture? *Royal Society Open Science*, 3, 150679.

Robson, A. A., de Leaniz, C. G., Wilson, R. P., and Halsey, L. G., 2010. Effect of anthropogenic feeding regimes on activity rhythms of laboratory mussels exposed to natural light. *Hydrobiologia*, 655, 197–204.

Robson, A. A. and Mansfield, R. P., 2014. Overinflated behavioural energetics: using dynamic body acceleration to accurately measure behaviour duration and estimate energy expenditure. *Aquatic Biology*, 21, 121–126.

Robson, A. A., Thomas, G. R., Leaniz, C. G. De, and Wilson, R. P., 2009. Valve gape and exhalant pumping in bivalves : optimization of measurement. *Aquatic Biology*, 6, 191–

200.

Robson, A., Wilson, R., and De Leaniz, C. G., 2007. Mussels flexing their muscles: A new method for quantifying bivalve behaviour. *Marine Biology*, 151, 1195–1204.

Rodgers, G. G., Tenzing, P., and Clark, T. D., 2016. Experimental methods in aquatic respirometry: the importance of mixing devices and accounting for background respiration. *Journal of Fish Biology*, 88, 65–80.

Ropert-Coudert, Y., Kato, A., Baudat, J., Bost, C. A., Le Maho, Y., and Naito, Y., 2001. Feeding strategies of free-ranging Adélie penguins *Pygoscelis adeliae* analysed by multiple data recording. *Polar Biology*, 24, 460–466.

Ropert-Coudert, Y. and Wilson, R., 2005. Trends and perspectives in animal-attached remote sensing. *Frontiers in Ecology and the Environment*, 3 (8), 437–444.

Ropert-coudert, Y., Wilson, R. P., Daunt, F., and Kato, A., 2004. Patterns of energy acquisition by a central place forager : benefits of alternating short and long foraging trips, 15 (5), 824–830.

Ropert-Coudert, Y., Wilson, R. P., Yoda, K., and Kato, A., 2007. Assessing performance constraints in penguins with externally-attached devices. *Marine Ecology Progress Series*, 333, 281–289.

Rossetti, Y. and Cabanac, M., 2006. Light versus temperature: An intersensitivity conflict in a gastropod (*Lymnaea auricularia*). *Journal of Thermal Biology*, 31, 514–520.

Ruiz-Ruiz, P. A., Hinojosa, I. A., Urzua, A., and Urbina, M. A., 2019. Anthropogenic noise disrupts mating behavior and metabolic rate in a marine invertebrate. *Proceedings of Meetings on Acoustics*, 37 (040006).

Rutz, C. and Hays, G. C., 2009. New frontiers in biologging science. *Biology Letters*, 5, 289–292.

Schaeffer, P. J. and Lindstedt, S. L., 2013. How animals move: Comparative lessons on animal locomotion. *Comprehensive Physiology*, 3, 289–314.

Schwartzmann, C., Durrieu, G., Sow, M., Ciret, P., Lazareth, C. E., and Massabuaua, J. C., 2011. In situ giant clam growth rate behavior in relation to temperature: A one-year coupled study of high-frequency noninvasive valvometry and sclerochronology. *Limnology and Oceanography*, 56 (5), 1940–1951.

Seminati, E., Talamas, D. C., Young, M., Twiste, M., Dhokia, V., and Bilzon, J. L. J., 2017. Validity and reliability of a novel 3D scanner for assessment of the shape and volume of amputees' residual limb models. *PLoS ONE*, 12 (9), e0184498.

Shannon, G., McKenna, M. F., Angeloni, L. M., Crooks, K. R., Fristrup, K. M., Brown, E., Warner, K. A., Nelson, M. D., White, C., Briggs, J., McFarland, S., and Wittemyer, G., 2015. A synthesis of two decades of research documenting the effects of noise on wildlife. *Biological Reviews*, 91, 982–1005.

Shepard, E. L. C., Wilson, R. P., Halsey, L. G., Quintana, F., Laich, A. G., Gleiss, A. C., Liebsch, N., Myers, A. E., and Norman, B., 2008. Derivation of body motion via appropriate smoothing of acceleration data. *Aquatic Biology*, 4, 235–241.

Shepard, E. L. C., Wilson, R. P., Liebsch, N., Quintana, F., Gómez Laich, A., and Lucke, K.,

2008. Flexible paddle sheds new light on speed: A novel method for the remote measurement of swim speed in aquatic animals. *Endangered Species Research*, 4, 157–164.

Shepard, E. L. C., Wilson, R. P., Rees, W. G., Grundy, E., Lambertucci, S. A., and Vosper, S. B., 2013. Energy Landscapes Shape Animal Movement Ecology. *The American Naturalist*, 182 (3), 298–312.

Shi, W., Han, Y., Guan, X., Rong, J., Du, X., Zha, S., Tang, Y., and Liu, G., 2019. Anthropogenic Noise Aggravates the Toxicity of Cadmium on Some Physiological Characteristics of the Blood Clam *Tegillarca granosa*. *Frontiers in Physiology*, 10 (377), 1–10.

Shorter, A. K., Murray, M. M., Johnson, M., Moore, M., and Howle, L. E., 2014. Drag of suction cup tags on swimming animals: Modeling and measurement. *Marine Mammal Science*, 30 (2), 726–746.

Simpson, S. D., Meekan, M., Montgomery, J., McCauley, R., and Jeffs, A., 2005. Homeward sound. *Science*, 308 (5719), 221.

Simpson, S. D., Radford, A. N., Nedelec, S. L., Ferrari, M. C. O., Chivers, D. P., McCormick, M. I., and Meekan, M. G., 2016. Anthropogenic noise increases fish mortality by predation. *Nature Communications*, 7 (10544).

Sims, D. W., Humphries, N. E., Bradford, R. W., and Bruce, B. D., 2012. Lévy flight and Brownian search patterns of a free-ranging predator reflect different prey field characteristics. *Journal of Animal Ecology*, 81, 432–442.

Sims, D. W., Southall, E. J., Humphries, N. E., Hays, G. C., Bradshaw, C. J. A., Pitchford, J. W., James, A., Ahmed, M. Z., Brierley, A. S., Hindell, M. A., Morritt, D., Musyl, M. K., Righton, D., Shepard, E. L. C., Wearmouth, V. J., Wilson, R. P., Witt, M. J., and Metcalfe, J. D., 2008. Scaling laws of marine predator search behaviour. *Nature*, 451, 1098–1102.

Sims, D. W., Southall, E. J., Tarling, G. A., and Metcalfe, J. D., 2005. Habitat-specific normal and reverse diel vertical migration in the plankton-feeding basking shark. *Journal of Animal Ecology*, 74, 755–761.

Slabbekoorn, H., 2016. Aiming for Progress in Understanding Underwater Noise Impact on Fish: Complementary Need for Indoor and Outdoor Studies. *Advances in Experimental Medicine and Biology*, 875, 1057–1065.

Smith, L. E. and O'Connell, C. P., 2014. The effects of neodymium-iron-boron permanent magnets on the behaviour of the small spotted catshark (*Scyliorhinus canicula*) and the thornback skate (*Raja clavata*). *Ocean and Coastal Management*, 97, 44–49.

Solan, M., Hauton, C., Godbold, J. A., Wood, C. L., Leighton, T. G., and White, P., 2016. Anthropogenic sources of underwater sound can modify how sediment-dwelling invertebrates mediate ecosystem properties. *Scientific Reports*, 6 (20540).

Soo, P. and Todd, P. A., 2014. The behaviour of giant clams (Bivalvia: Cardiidae: Tridacninae). *Marine Biology*, 161, 2699–2717.

De Soto, N. A., Delorme, N., Atkins, J., Howard, S., Williams, J., and Johnson, M., 2013. Anthropogenic noise causes body malformations and delays development in marine larvae. *Scientific Reports*, 3 (2831).

Speakman, J. R., 2005. Body size, energy metabolism and lifespan. *The Journal of Experimental Biology*, 208, 1717–1730.

Speakman, J. R. and Hambly, C., 2016. Using doubly-labelled water to measure free-living energy expenditure: Some old things to remember and some new things to consider. *Comparative Biochemistry and Physiology - Part A : Molecular and Integrative Physiology*, 202, 3–9.

Spiga, I., Aldred, N., and Caldwell, G. S., 2017. Anthropogenic noise compromises the anti-predator behaviour of the European seabass, *Dicentrarchus labrax* (L.). *Marine Pollution Bulletin*, 122, 297–305.

Stieglitz, T. C. and Dujon, A. M., 2017. A groundwater-fed coastal inlet as habitat for the Caribbean queen conch *Lobatus gigas*-an acoustic telemetry and space use analysis. *Marine Ecology Progress Series*, 571, 139–152.

Sundström, L. F. and Gruber, S. H., 2002. Effects of capture and transmitter attachments on the swimming speed of large juvenile lemon sharks in the wild. *Journal of Fish Biology*, 61, 834–838.

Takagi, T., Tamura, Y., and Weihs, D., 2013. Hydrodynamics and energy-saving swimming techniques of Pacific bluefin tuna. *Journal of Theoretical Biology*, 336, 158–172.

Tan, H. and Wilson, A. M., 2011. Grip and limb force limits to turning performance in competition horses. *Proceedings of the Royal Society B: Biological Sciences*, 278, 2105–2111.

Taylor, G. K., Reynolds, K. V., and Thomas, A. L. R., 2016. Soaring energetics and glide performance in a moving atmosphere. *Philosophical Transactions of the Royal Society B: Biological Sciences*, 371, 20150398.

Technitis, G., Othman, W., Safi, K., and Weibel, R., 2015. From A to B, randomly: a point-to-point random trajectory generator for animal movement. *International Journal of Geographical Information Science*, 29 (6), 912–934.

Tewfik, A. and Guzman, H. M., 2003. Shallow-water distribution and population characteristics of *Strombus gigas* and *S. costatus* (Gastropoda: Strombidae) in Bocas del Toro, Panama. *Journal of Shellfish Research*, 22 (3), 789–794.

Thaxter, C. B., Ross-Smith, V. H., Clark, J. A., Clark, N. A., Conway, G. J., Masden, E. A., Wade, H. M., Leat, E. H. K., Gear, S. C., Marsh, M., Booth, C., Furness, R. W., Votier, S. C., and Burton, N. H. K., 2016. Contrasting effects of GPS device and harness attachment on adult survival of Lesser Black-backed Gulls *Larus fuscus* and Great Skuas *Stercorarius skua*. *Ibis*, 158, 279–290.

Thaxter, C. B., Ross-smith, V. H., Clark, J. A., Clark, N. A., Greg, J., Marsh, M., Leat, E. H. K., Burton, N. H. K., Thaxter, C. B., Ross-smith, V. H., Clark, J. A., Clark, N. A., Greg, J., Marsh, M., Leat, E. H. K., Burton, N. H. K., Thaxter, C. B., Ross-smith, V. H., Clark, J. A., and Clark, N. A., 2015. A trial of three harness attachment methods and their suitability for long-term use on Lesser Black-backed Gulls and Great Skuas. *Ringing & Migration*, 29 (2), 65–76.

Thorstad, E. B., Økland, F., and Heggberget, T. G., 2001. Are long term negative effects from external tags underestimated? Fouling of an externally attached telemetry transmitter. *Journal of Fish Biology*, 59, 1092–1094.

Tomlinson, S., Arnall, S. G., Munn, A., Bradshaw, S. D., Maloney, S. K., Dixon, K. W., and Didham, R. K., 2014. Applications and implications of ecological energetics. *Trends in Ecology and Evolution*, 29 (5), 280–290.

Tözeren, A., 2000. *Human Body Dynamics: Classical Mechanics and Human Movement*. Berlin: Springer.

Tudorache, C., Burgerhout, E., Brittijn, S., and Van Den Thillart, G., 2014. The effect of drag and attachment site of external tags on swimming eels: Experimental quantification and evaluation tool. *PLoS ONE*, 9 (11), e112280.

Vandenabeele, S. P., Grundy, E., Friswell, M. I., Grogan, A., Votier, S. C., and Wilson, R. P., 2014. Excess Baggage for Birds: Inappropriate Placement of Tags on Gannets Changes Flight Patterns. *PLoS ONE*, 9 (3), e92657.

Vandenabeele, S. P., Wilson, R. P., and Grogan, A., 2011. Tags on seabirds: How seriously are instrument-induced behaviours considered? *Animal Welfare*, 20, 559–571.

Vandenabeele, S. P., Wilson, R. P., and Wikelski, M., 2013. New tracking philosophy for birds. *Frontiers in Ecology and the Environment*, 11, 10–12.

Waldbusser, G. G., Bergschneider, H., and Green, M. A., 2010. Size-dependent pH effect on calcification in post-larval hard clam Mercenaria spp. *Marine Ecology Progress Series*, 417, 171–182.

Wale, M. A., Briers, R. A., Hartl, M. G. J., Bryson, D., and Diele, K., 2019. From DNA to ecological performance: Effects of anthropogenic noise on a reef-building mussel. *Science of the Total Environment*, 689, 126–132.

Wale, M. A., Simpson, S. D., and Radford, A. N., 2013. Noise negatively affects foraging and antipredator behaviour in shore crabs. *Animal Behaviour*, 86, 111–118.

Walker, J. S., Jones, M. W., Laramee, R. S., Holton, M. D., Shepard, E. L. C., Williams, H. J., Michael Scantlebury, D., Marks, N. J., Magowan, E. A., Maguire, I. E., Bidder, O. R., Virgilio, A. Di, and Wilson, R. P., 2015. Prying into the intimate secrets of animal lives; software beyond hardware for comprehensive annotation in 'Daily Diary' tags. *Movement Ecology*, 3 (29).

Ward, S., Bishop, C. M., Woakes, A. J., and Butler, P. J., 2002. Heart rate and the rate of oxygen consumption of flying and walking barnacle geese (*Branta leucopsis*) and bar-headed geese (*Anser indicus*). *Journal of Experimental Biology*, 205, 3347–3356.

Watanabe, Y. Y. and Takahashi, A., 2012. Linking animal-borne video to accelerometers reveals prey capture variability. *Proceedings of the National Academy of Sciences*, 110 (6), 2199–2204.

Watanuki, Y., Niizuma, Y., Gabrielsen, G. W., Sato, K., and Naito, Y., 2003. Stroke and glide of wing-propelled divers : deep diving seabirds adjust surge frequency to buoyancy change with depth. *Proceedings of the Royal Society B: Biological Sciences*, 270, 483–488.

Watson, K. P. and Granger, R. A., 1998. Hydrodynamic effect of a satellite transmitter on a juvenile green turtle (Chelonia mydas). *Journal of Experimental Biology*, 201, 2497–2505.

White, C. R., Cassey, P., Schimpf, N. G., Halsey, L. G., Green, J. A., and Portugal, S. J.,

2013. Implantation reduces the negative effects of bio-logging devices on birds. *Journal of Experimental Biology*, 216, 537–542.

Whitmore, B. M., White, C. F., Gleiss, A. C., and Whitney, N. M., 2016. A float-release package for recovering data-loggers from wild sharks. *Journal of Experimental Marine Biology and Ecology*, 475, 49–53.

Whitney, N. M., Pratt, H. L., Pratt, T. C., and Carrier, J. C., 2010. Identifying shark mating behaviour using three-dimensional acceleration loggers. *Endangered Species Research*, 10, 71–82.

Whitney, N. M., White, C. F., Smith, B. J., Cherkiss, M. S., Mazzotti, F. J., and Hart, K. M., 2021. Accelerometry to study fine-scale activity of invasive Burmese pythons (*Python bivittatus*) in the wild. *Animal Biotelemetry*, 9 (2).

Williams, H. J., Holton, M. D., Shepard, E. L. C., Largey, N., Norman, B., Ryan, P. G., Duriez, O., Scantlebury, M., Quintana, F., Magowan, E. A., Marks, N. J., Alagaili, A. N., Bennett, N. C., and Wilson, R. P., 2017. Identification of animal movement patterns using tri-axial magnetometry. *Movement Ecology*, 5 (6).

Williams, H. J., Shepard, E. L. C., Duriez, O., and Lambertucci, S. A., 2015. Can accelerometry be used to distinguish between flight types in soaring birds? *Animal Biotelemetry*, 3 (45).

Williams, T., Kooyman, G., and Croll, D., 1991. The effect of submergence on heart rate and oxygen consumption of swimming seals and sea lions. *Comp Physiol B.*, 260 (6), 637–44.

Wilmers, C. C., Isbell, L. A., Suraci, J. P., and Williams, T. M., 2017. Energetics-informed behavioral states reveal the drive to kill in African leopards. *Ecosphere*, 8 (6), e01850.

Wilson, C. D., Arnott, G., and Elwood, R. W., 2012. Freshwater pearl mussels show plasticity of responses to different predation risks but also show consistent individual differences in responsiveness. *Behavioural Processes*, 89, 299–303.

Wilson, C. D., Arnott, G., Reid, N., and Roberts, D., 2011. The pitfall with PIT tags: marking freshwater bivalves for translocation induces short-term behavioural costs. *Animal Behaviour*, 81, 341–346.

Wilson, R. P., Börger, L., Holton, M. D., Scantlebury, D. M., Gómez-Laich, A., Quintana, F., Rosell, F., Graf, P. M., Williams, H., Gunner, R., Hopkins, L., Marks, N., Geraldi, N. R., Duarte, C. M., Scott, R., Strano, M. S., Robotka, H., Eizaguirre, C., Fahlman, A., and Shepard, E. L. C., 2020. Estimates for energy expenditure in free-living animals using acceleration proxies: A reappraisal. *Journal of Animal Ecology*, 89, 161–172.

Wilson, R. P., Grant, W. S., and Duffy, D. C., 1986. Recording Devices on Free-Ranging Marine Animals : Does Measurement Affect Foraging Performance? *Ecology*, 67 (4), 1091–1093.

Wilson, R. P., Griffiths, I. W., Legg, P. A., Friswell, M. I., Bidder, O. R., Halsey, L. G., Lambertucci, S. A., and Shepard, E. L. C., 2013. Turn costs change the value of animal search paths. *Ecology Letters*, 16 (9), 1145–1150.

Wilson, R. P., Holton, M. D., di Virgilio, A., Williams, H., Shepard, E. L. C., Lambertucci, S., Quintana, F., Sala, J. E., Balaji, B., Lee, E. S., Srivastava, M., Scantlebury, D. M., and Duarte, C. M., 2018. Give the machine a hand: A Boolean time-based decision-tree

template for rapidly finding animal behaviours in multisensor data. *Methods in Ecology and Evolution*, 9, 2206–2215.

Wilson, R. P., Holton, M. D., Walker, J. S., Shepard, E. L. C., Scantlebury, D. M., Wilson, V. L., Wilson, G. I., Tysse, B., Gravenor, M., Ciancio, J., McNarry, M. A., Mackintosh, K. A., Qasem, L., Rosell, F., Graf, P. M., Quintana, F., Gomez-Laich, A., Sala, J. E., Mulvenna, C. C., Marks, N. J., and Jones, M. W., 2016. A spherical-plot solution to linking acceleration metrics with animal performance, state, behaviour and lifestyle. *Movement Ecology*, 4 (22).

Wilson, R. P., Holton, M., Wilson, V. L., Gunner, R., Tysse, B., Wilson, G. I., Quintana, F., Duarte, C., and Scantlebury, D. M., 2019. Towards informed metrics for examining the role of human-induced animal responses in tag studies on wild animals. *Integrative Zoology*, 14 (1), 17–29.

Wilson, R. P. and Liebsch, N., 2003. Up-beat motion in swinging limbs: New insights into assessing movement in free-living aquatic vertebrates. *Marine Biology*, 142, 537–547.

Wilson, R. P., Liebsch, N., Davies, I. M., Quintana, F., Weimerskirch, H., Storch, S., Lucke, K., Siebert, U., Zankl, S., Muller, G., Zimmer, I., Scolaro, A., Campagna, C., Plotz, J., Bornemann, H., Teilmann, J., and McMahon, C. R., 2007. All at sea with animal tracks ; methodological and analytical solutions for the resolution of movement. *Deep-Sea Research Part II*, 54, 193–210.

Wilson, R. P. and McMahon, C. R., 2006. Measuring devices on wild animals: What constitutes acceptable practice? *Frontiers in Ecology and the Environment*, 4 (3), 147–154.

Wilson, R. P., Neate, A., Holton, M. D., Shepard, E. L. C., Scantlebury, D. M., Lambertucci, S. A., di Virgilio, A., Crooks, E., Mulvenna, C., and Marks, N., 2018. Luck in Food Finding Affects Individual Performance and Population Trajectories. *Current Biology*, 28, 3871–3877.

Wilson, R. P., Quintana, F., and Hobson, V. J., 2012. Construction of energy landscapes can clarify the movement and distribution of foraging animals. *Proceedings of the Royal Society of Biology*, 279, 975–980.

Wilson, R. P., Shepard, E. L. C., and Liebsch, N., 2008. Prying into the intimate details of animal lives: use of a daily diary on animals. *Endangered Species Research*, 3, 123–137.

Wilson, R. P., Steinfurth, A., Ropert-Coudert, Y., Kato, A., and Kurita, M., 2002. Lip-reading in remote subjects: an attempt to quantify and separate ingestion, breathing and vocalisation in free-living animals using penguins as a model. *Marine Biology*, 140, 17–27.

Wilson, R. P., White, C. R., Quintana, F., Halsey, L. G., Liebsch, N., Martin, G. R., and Butler, P. J., 2006. Moving towards acceleration for estimates of activity-specific metabolic rate in free-living animals: The case of the cormorant. *Journal of Animal Ecology*, 75, 1081–1090.

Wilson, R. P. and Wilson, M., 1989. Tape: A Package-Attachment Technique for Penguins. *Wildlife Society Bulletin*, 17 (1), 77–79.

Wilson, R., Reuter, P., and Wahl, M., 2005. Muscling in on mussels: New insights into bivalve behaviour using vertebrate remote-sensing technology. *Marine Biology*, 147,

1165–1172.

Woakes AJ, Butler, P., and Bevan, R., 1995. Implantable data logging system for heart rate and body temperature: its application to the estimation of field metabolic rates in Antarctic predators. *Med Biol Eng Comput.*, 33 (2), 145–51.

Wright, S., Metcalfe, J. D., Hetherington, S., and Wilson, R., 2014. Estimating activity-specific energy expenditure in a teleost fish, using accelerometer loggers. *Marine Ecology Progress Series*, 496, 19–32.

Yoda, K., Naito, Y., Sato, K., Takahashi, A., Nishikawa, J., Ropert-Coudert, Y., Kurita, M., and Le Maho, Y., 2001. A new technique for monitoring the behaviour of free-ranging Adelie penguins. *The Journal of Experimental Biology*, 204, 685–690.

Zenone, A., Ciancio, J. E., Badalamenti, F., Buffa, G., D'Anna, G., Pipitone, C., and Giacalone, M. V., 2020. Influence of light, food and predator presence on the activity pattern of the European spiny lobster *Palinurus elephas*: An investigation using tri-axial accelerometers. *Ecological Indicators*, 113, 106174.

Zuur, A. F., Ieno, E. N., Walker, N. J., Saveliev, A. A., and Smith, G. M., 2009. *Mixed Effects Models and Extensions in Ecology with R*. New York: Springer-Verlag.